

**Characterizing the microtubule-associated  
function of the B1-type cyclins in *Arabidopsis  
thaliana* and towards live cell imaging of meiosis  
in *A. lyrata* and *A. arenosa***

Dissertation with the aim of achieving a doctoral degree  
at the faculty of Mathematics, Informatics and Natural Sciences

Department of Biology  
University of Hamburg

submitted by  
Mariana Romeiro Motta

2022 in Hamburg, Germany



Supervisor: Prof. Dr. Arp Schnittger

First Examiner: Prof. Dr. Arp Schnittger

Second Examiner: Dr. Magdalena Weingartner

Date of oral defense: 01.04.2022



# Index

|   |           |
|---|-----------|
| <b>Abstract</b> .....   | <b>5</b>  |
| <b>Zusammenfassung</b> .....  | <b>7</b>  |
| <b>General introduction</b> .....   | <b>9</b>  |
| <b>1. The cell cycle: lifetime of a cell</b> .....  | <b>9</b>  |
| <b>2. Cyclins and cyclin-dependent kinases</b> .....  | <b>10</b> |
| 2.1. A- and B-type cyclins.....   | 15        |
| <b>3. Overview of mitosis</b> .....   | <b>17</b> |
| <b>4. Overview of mitotic microtubule arrays</b> .....  | <b>17</b> |
| <b>5. Microtubule-associated proteins (MAPs) and their role in microtubule array assembly</b>   | <b>20</b> |
| 5.1. Regulation of preprophase band dynamics .....  | 21        |
| 5.2. Control of spindle microtubules.....   | 22        |
| 5.3. Organization of the phragmoplast.....  | 23        |
| <b>6. The control of microtubule dynamics by plus-end binding proteins</b> .....  | <b>24</b> |
| 6.1. Plus-end binding proteins .....  | 25        |
| <b>7. The regulation of mitotic microtubule arrays by cyclins and CDKs</b> .....  | <b>26</b> |
| <b>8. References</b> .....  | <b>27</b> |
| <b>Thesis summary</b> .....   | <b>33</b> |
| <b>Chapter 1. B1-type cyclins control microtubule organization during cell division in <i>Arabidopsis</i> (published in EMBO reports)</b> ..... | <b>35</b> |
| <b>Chapter 2. Investigating the role of CYCB1-dependent regulation of microtubule arrays</b> .....  | <b>61</b> |
| <b>2.1. Introduction</b> .....  | <b>63</b> |
| 2.1.1. Microtubule nucleation in the absence of a centrosome .....  | 63        |
| 2.1.2. The role of the $\gamma$ TuRC in microtubule nucleation .....  | 64        |
| 2.1.3. The augmin complex: a conserved role in enabling microtubule-based microtubule nucleation .....  | 66        |
| <b>Research aim</b> .....   | <b>72</b> |
| <b>2.2. Results</b> .....   | <b>73</b> |

|  |            |
|--|------------|
| 2.2.1. Mutating the consensus CDK phosphorylation site in GIP1 does not visibly alter its function .....   | 73         |
| 2.2.2. A dephosphomutant version of EDE1 does not rescue <i>ede1-1</i> 's spindle architecture and growth under microtubule-destabilizing conditions ..... | 79         |
| <b>2.3. Discussion .....</b>   | <b>85</b>  |
| 2.3.1. The CYCB1 group is a conserved regulator of mitosis and microtubule organization.....   | 85         |
| 2.3.2. The regulation of microtubule-associated proteins of the $\gamma$ TuRC by phosphorylation.....  | 86         |
| 2.3.3. Phospho-regulation of microtubule-associated proteins of the augmin complex .....   | 88         |
| 2.3.4. The CYCB1 group likely regulates a plethora of substrates in <i>A. thaliana</i> .....   | 90         |
| <b>2.4. Appendix.....</b>  | <b>92</b>  |
| <b>2.5. References .....</b>   | <b>95</b>  |
| <br>   |            |
| <b>Chapter 3. Towards live cell imaging of meiosis in <i>Arabidopsis lyrata</i> and <i>Arabidopsis arenosa</i> auto- and allopolyploids .....</b>          | <b>101</b> |
| <br>   |            |
| <b>3.1. Introduction .....</b>   | <b>103</b> |
| 3.1.1. Overview of meiosis .....   | 103        |
| 3.1.2. The axial element and the synaptonemal complex.....   | 105        |
| 3.1.3. The stepwise removal of cohesion in meiosis .....   | 106        |
| 3.1.4. The challenge for chromosome segregation in polyploid meiosis .....   | 108        |
| 3.1.5. The adaptations to polyploid meiosis.....   | 109        |
| 3.1.6. <i>A. lyrata</i> and <i>A. arenosa</i> : outcrossing relatives of <i>A. thaliana</i> as models for auto- and allopolyploidy .....                   | 111        |
| 3.1.7. State of the art of <i>A. lyrata</i> and <i>A. arenosa</i> transformation .....   | 112        |
| <b>Research aim.....</b>   | <b>113</b> |
| <br>   |            |
| <b>3.2. Results .....</b>  | <b>114</b> |
| 3.2.1. Cloning of reporter constructs .....  | 114        |
| 3.2.2. Cloning of CRISPR-Cas9 constructs.....  | 116        |
| 3.2.3. Floral dipping of <i>A. lyrata</i> and <i>A. arenosa</i> .....  | 117        |
| <br>   |            |
| <b>3.3. Discussion .....</b>   | <b>123</b> |
| 3.3.1. Self-incompatibility: a challenge for studies in <i>A. lyrata</i> and <i>A. arenosa</i> .....   | 123        |
| 3.3.2. Selecting a specific <i>A. lyrata</i> promoter could promote expression of the microtubule reporter construct in meiocytes.....                     | 123        |
| 3.3.3. A low transformation efficiency can be associated with the plant ecotype .....  | 124        |
| 3.3.4. Progression of meiosis in auto- and allopolyploids .....  | 125        |
| 3.3.5. Outlook.....  | 125        |
| <br>   |            |
| <b>3.4. References .....</b>   | <b>127</b> |

|  |            |
|--|------------|
| <b>Material and Methods .....</b>  | <b>131</b> |
| <b>1. Plant methods.....</b>   | <b>131</b> |
| 1.1. Plant growth conditions.....  | 131        |
| 1.2. Floral dipping of <i>A. thaliana</i> .....  | 131        |
| 1.3. DNA extraction and genotyping of mutant plants .....                                  | 131        |
| 1.4. Flow cytometry assay.....   | 133        |
| 1.5. Endosperm nuclei proliferation analysis.....  | 133        |
| 1.6. Root growth assays .....  | 133        |
| <b>2. Cloning methods .....</b>  | <b>134</b> |
| 2.1. Amplification of genomic and coding sequence fragments.....                           | 134        |
| 2.2. Classical restriction-based cloning .....   | 135        |
| 2.3. Gateway cloning.....  | 136        |
| 2.4. Seamless ligation cloning extract (SLiCE) .....                                       | 137        |
| <b>3. Microbiological methods.....</b>   | <b>137</b> |
| 3.1. Heat shock transformation of <i>Escherichia coli</i> chemically competent cells ..... | 137        |
| 3.2. Heat shock transformation of <i>Agrobacterium tumefaciens</i> .....                   | 138        |
| 3.3. Heat shock transformation of <i>Saccharomyces cerevisiae</i> .....                    | 138        |
| 3.4. Yeast two-hybrid .....  | 139        |
| <b>4. Biochemical methods .....</b>  | <b>140</b> |
| 4.1. SDS-PAGE .....  | 140        |
| 4.2. Coomassie Brilliant Blue (CBB) staining and destaining.....                           | 140        |
| 4.3. Western blotting .....  | 140        |
| 4.4. Protein expression .....  | 141        |
| 4.5. Cell lysis and protein purification.....  | 141        |
| 4.6. <i>In vitro</i> kinase assays.....  | 142        |
| <b>5. Resources table.....</b>   | <b>143</b> |
| 5.1. General resources table .....   | 143        |
| 5.2. Resources table from Chapter 2 .....  | 144        |
| 5.3. Resources table from Chapter 3 .....  | 146        |
| <b>6. References .....</b>   | <b>148</b> |
| <b>Publications and presentations.....</b>   | <b>149</b> |
| <b>Eidesstattliche Versicherung/Declaration On Oath .....</b>                              | <b>150</b> |
| <b>Declaration of contributions .....</b>  | <b>151</b> |
| <b>Confirmation of correct English.....</b>  | <b>152</b> |

**Acknowledgments.....153**



## Abstract

In mitosis, a precise duplication and equal distribution of the genomic DNA between daughter cells is essential for genome stability and growth. For such a precise division, eukaryotes make use of a set of cytoskeletal arrays, which are composed mainly of microtubule filaments. Because plant cells cannot move as opposed to animal cells, plants rely on a precise cell division site determination for organ growth and patterning. Accordingly, plants have developed specific microtubule-based structures for cell divisions, such as the preprophase band (PPB) and the phragmoplast. The PPB is a band of microtubules that forms before division at the cell cortex around the equator of the nucleus. It is known to mark the periphery of the division plane and anchor proteins that remain there throughout cell division, acting as fiducial markers. The spindle, which appears after the PPB has disassembled and the nuclear envelope has broken down, is essential for accurate sister chromatid segregation. After sister chromatids have been segregated, the phragmoplast forms, which guides accurate membrane and cell wall formation between the two daughter nuclei, ensuring a successful cell division.

The progression of the cell cycle is tightly regulated by cyclins and cyclin-dependent kinases (CDKs). They act together to phosphorylate a plethora of substrates, with specificity provided by both the cyclin and CDK partner. Phosphorylation can promote rapid changes in protein activity, which is in accordance with the significant changes in microtubule conformation throughout cell division. Here, in the first chapter, I have characterized the function of the five-member CYCLIN B1 group in *Arabidopsis thaliana*. I show that the function of B1-type cyclins is highly redundant and tissue-dependent. Interestingly, mutants for B1-type cyclin members have compromised microtubule arrays, including misplaced and double PPBs, as well as chromosome laggards in metaphase and abnormal phragmoplasts. I further reveal that B1-type cyclins, especially together with CDKB2;2, can phosphorylate a key microtubule nucleation factor *in vitro*, MOZART1/GIP1. Accordingly, I show that GIP1 mislocalizes in a B1-type cyclin mutant background.

In the second chapter, I explore in detail the function of B1-type cyclin-dependent phosphorylation of two microtubule-associated proteins. First, I test the function of MOZART1/GIP1 phosphorylation by generating two GIP1 versions with residues that cannot be phosphorylated (alanine) in a *gip1 gip2* background and analyzing the phenotype of these plants. Second, being unable to detect a clear phenotype in these

GIP1 versions in *gip1 gip2*, I also test the function of phosphorylation of another microtubule-associated protein, namely ENDOSPERM DEFECTIVE 1 (EDE1). EDE1 is an essential member of the augmin complex in mitosis and promotes branched microtubule-dependent microtubule nucleation. After mutating eight EDE1 residues into alanine and introducing this construct in a mutant *ede1-1* background, I detected a clear impact on spindle architecture and dynamics compared to the wild-type EDE1 in an *ede1-1* background. Hence, I was able to find a direct link between cyclin-CDK-dependent phosphorylation and microtubule array regulation in mitosis.

In sexually-reproducing organisms, a special cell division called meiosis takes place. Meiosis, unlike mitosis, is reductional and key for gamete formation. Since chromosomes must pair to segregate equally during meiosis I, polyploids, i.e., organisms that possess three or more chromosome sets, have an extra challenge to produce balanced gametes. Surprisingly, established polyploids have evolved to possess stable meiosis and accurate chromosome segregation. In the third chapter, I describe an attempt of using the outcrossing *A. lyrata* and *A. arenosa* species as models for polyploid meiosis. Following meiotic cell divisions live in these species, similar to what has been recently achieved in *A. thaliana*, could provide us key insights into meiotic adaptations to polyploidy. However, generating reporter lines in those plants was a challenge and I describe my attempts in this thesis.

## Zusammenfassung

In der Mitose ist eine präzise Verdopplung und gleichmäßige Verteilung der genomischen DNA zwischen den Tochterzellen für die Stabilität des Genoms und das Wachstum unerlässlich. Für eine solche präzise Teilung nutzen Eukaryoten eine Reihe von Zytoskelettanordnungen, die hauptsächlich aus Mikrotubuli-Filamenten bestehen. Da sich Pflanzenzellen im Gegensatz zu tierischen Zellen nicht bewegen können, sind sie für das Wachstum und die Strukturierung von Organen auf eine präzise Bestimmung der Zellteilungsstelle angewiesen. Dementsprechend haben Pflanzen spezifische Mikrotubuli-basierte Strukturen für die Zellteilung entwickelt, wie das Präprophasenband (PPB) und den Phragmoplast. Das PPB ist ein Band aus Mikrotubuli, welches sich vor der Teilung an der Zellrinde (Pellicula) um den Äquator des Zellkerns bildet. Es markiert die Peripherie der Teilungsebene und verankert Proteine, die während der gesamten Zellteilung dort verbleiben und als Referenzmarker dienen. Die Spindel, die nach dem Abbau der PPB und dem Zerfall der Kernhülle entsteht, ist für die genaue Segregation der Schwesterchromatiden unerlässlich. Nach der Segregation der Schwesterchromatiden bildet sich der Phragmoplast, der die korrekte Membran- und Zellwandbildung zwischen den beiden Tochterkernen leitet und so eine erfolgreiche Zellteilung gewährleistet.

Der Ablauf des Zellzyklus wird durch Cycline und Cyclin-abhängige Kinasen (CDKs) streng reguliert. Sie wirken zusammen und phosphorylieren eine Vielzahl von Substraten, wobei die Spezifität sowohl durch das Cyclin als auch durch den CDK-Partner gewährleistet wird. Die Phosphorylierung kann zu schnellen Veränderungen der Proteinaktivität führen, was mit den erheblichen Veränderungen der Mikrotubuli-Konformation während der Zellteilung in Einklang steht. Im ersten Kapitel habe ich die Funktion der CYCLIN B1-Gruppe in *Arabidopsis thaliana* charakterisiert, welche aus fünf Mitgliedern besteht. Ich zeige, dass die Funktion der B1-Typ-Cycline hochgradig redundant und gewebeabhängig ist. Mutanten in Cyclinen des B1-Typs weisen beeinträchtigte Mikrotubuli-Anordnungen auf, darunter fehlplatzierte und doppelte PPBs, sowie Nachzüglerchromosome in der Metaphase und abnorme Phragmoplasten. Ich zeige außerdem, dass B1-Cycline, insbesondere zusammen mit CDKB2;2, einen wichtigen Mikrotubuli-Nukleationsfaktor, MOZART1/GIP1, *in vitro* phosphorylieren können. Dementsprechend zeige ich, dass GIP1 in einem Mutantenhintergrund des B1-Typ-Cyclins fehllokalisiert ist.

Im zweiten Kapitel untersuche ich im Detail die Funktion der B1-Typ-Cyclin-abhängigen Phosphorylierung von zwei Mikrotubuli assoziierten Proteinen. Zunächst teste ich die Funktion der MOZART1/GIP1-Phosphorylierung, indem ich zwei GIP1-Versionen mit Resten, die nicht phosphoryliert werden können (Alanin), in einem *gip1 gip2*-Hintergrund erzeugte und den Phänotyp dieser Pflanzen analysierte. Da ich bei diesen GIP1-Versionen in *gip1 gip2* keinen eindeutigen Phänotyp feststellen konnte, habe ich außerdem die Funktion der Phosphorylierung eines anderen Mikrotubuli-Proteins, nämlich ENDOSPERM DEFECTIVE 1 (EDE1), untersucht. EDE1 ist ein wesentliches Mitglied des Augmin-Komplexes in der Mitose und fördert die von verzweigten Mikrotubuli abhängige Mikrotubuli-Nukleation. Nachdem ich acht EDE1-Reste zu Alanin mutiert und dieses Konstrukt in einen mutierten *ede1-1*-Hintergrund eingebracht hatte, konnte ich im Vergleich zum Wildtyp-EDE1 in einem *ede1-1*-Hintergrund deutliche Auswirkungen auf die Spindelarchitektur und -dynamik feststellen. Somit konnte ich eine direkte Verbindung zwischen der Cyclin-CDK-abhängigen Phosphorylierung und der Regulierung der Mikrotubuli-Anordnung in der Mitose feststellen.

Bei sich sexuell fortpflanzenden Organismen findet eine spezielle Zellteilung statt, die Meiose. Im Gegensatz zur Mitose ist die Meiose reduktiv und entscheidend für die Bildung der Gameten. Da sich die Chromosomen während der Meiose I paarweise und gleichmäßig teilen müssen, ist es für Polyploide, d. h. Organismen mit drei oder mehr Chromosomensätzen, eine besondere Herausforderung, ausgewogene Gameten zu erzeugen. Überraschenderweise haben sich etablierte Polyploide so entwickelt, dass sie eine stabile Meiose und eine genaue Chromosomentrennung aufweisen. Im dritten Kapitel beschreibe ich einen Versuch, die sich auskreuzenden Arten *A. lyrata* und *A. arenosa* als Modelle für die polyploide Meiose zu verwenden. Wenn man die meiotischen Zellteilungen bei diesen Arten live verfolgt, ähnlich wie es kürzlich bei *A. thaliana* gelungen ist, könnte man wichtige Erkenntnisse über die meiotischen Anpassungen an die Polyploidie gewinnen. Die Erzeugung von Reporterlinien in diesen Pflanzen war jedoch eine Herausforderung, und ich beschreibe meine Versuche in dieser Arbeit.

# General introduction

## 1. The cell cycle: lifetime of a cell

Eukaryotes rely on a series of events to duplicate and subsequently faithfully segregate their genetic material. This series of events is the so-called cell cycle that is typically divided into four stages: G1, S, G2, and M (Fig 1A; Harashima *et al*, 2013; Wijnker & Schnittger, 2013). During the S phase, the DNA is duplicated. During G1 and G2, which separate S from M phase and therefore are called Gap1 (G1) and Gap2 (G2), cells were shown to grow. Finally, during M phase, which stands for mitosis, the sister chromatids get separated equally into two daughter nuclei. Mitosis is often followed by cytokinesis, which is the division of the original cell into two compartments with one nucleus each. However, there are a few exceptions to this order of events (Fig 1B-C). For instance, *Arabidopsis* endosperm development (Berger *et al*, 2006) starts with several rounds of mitosis without cytokinesis, leading to the formation of the syncytial endosperm, while cell walls are formed only later to then generate the cellular endosperm.

The cell cycle has three known major checkpoints: at G1/S, when DNA is checked for any damage; at G2/M, when cells must ensure that the DNA has been properly duplicated; and at the metaphase-anaphase transition, when the spindle assembly checkpoint (SAC) monitors if the kinetochores of the sister chromatids are properly attached to spindle microtubules.

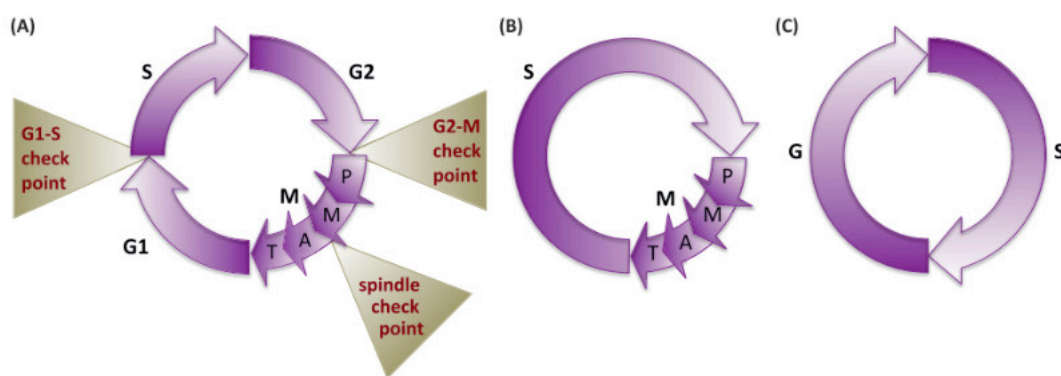


**Figure 1: The eukaryotic cell cycle.** The figure was taken from Harashima *et al*, 2013.

A. In a typical meristematic cell, G1, S, G2, and M phases can be distinguished. The three main checkpoints are the G1/S and G2/M checkpoints as well as the spindle assembly checkpoint during mitosis.

B. In rapidly dividing early embryos, one or more gap phases can be skipped.

C. Differentiated cells often undergo duplication of the DNA material without an ensuing cell division, which is called an endocycle and generates polyploid cells. P, prophase; M, metaphase; A, anaphase; and T, telophase.

## 2. Cyclins and cyclin-dependent kinases

At the heart of cell cycle regulation lie cyclins and cyclin-dependent kinases (CDKs; Fig 2-4). Cyclins (Fig 2), as the name suggests, are expressed in a cyclic, phase-specific manner and promote the progression of the cell cycle together with their CDK counterparts (Fig 3). Cyclins are often classified according to their expression timing; for example, as G1/S, S- or M-phase cyclins (Morgan, 2007).

While in budding yeast only 22 cyclins have been found (Andrews & Measday, 1998), plants have evolved to possess an astonishing number of cyclins. For instance, there are at least 50 putative cyclin-encoding genes in *Arabidopsis thaliana* (Fig 2; Wang *et al*, 2004; Shimotohno *et al*, 2021). This variety of cyclin genes is presumed to account for developmental plasticity in space and time in response to environmental cues (Shimotohno *et al*, 2021).

Cyclins often contain a region with 250 conserved amino acids that constitute the so-called cyclin core, which has two domains named Cyclin\_N and Cyclin\_C (Fig 2; Wang *et al*, 2004). The Cyclin\_N domain (also called cyclin box) is approximately 100-amino-acid long, contains the CDK binding site and is found in all known cyclins. The Cyclin\_C domain, however, is less conserved. Another domain that is commonly found in cyclins is the Destruction box (or D-box). The D-box is a nine-residue motif that is responsible for cyclin proteolysis by the 26S proteasome in a ubiquitin-dependent manner.

Since there is a large number of plant cyclins, a nomenclature based on sequence homology was established (Fig 2; Renaudin *et al*, 1996). Sequence homology is a good starting point to infer individual cyclin roles, although it is not a guarantee of similar function.

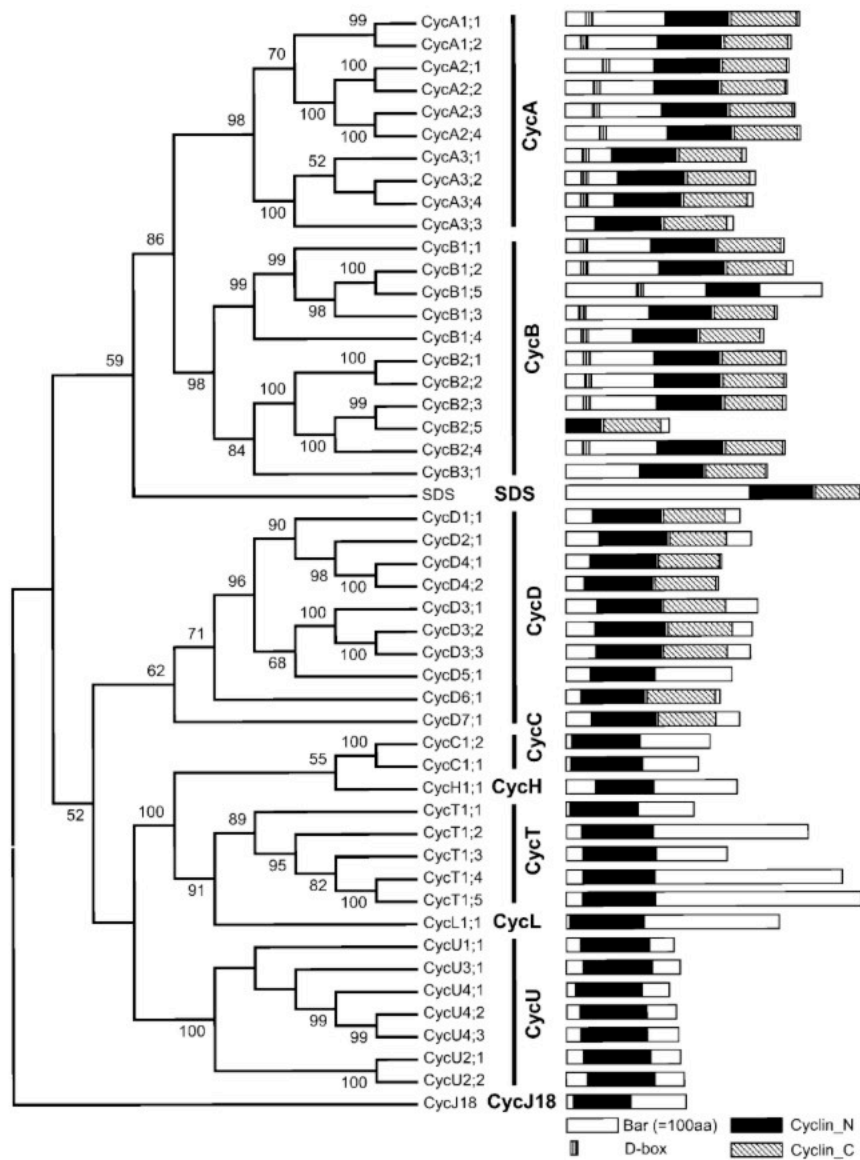


**Figure 2. Phylogenetic tree of 49 *Arabidopsis* cyclin-encoding genes with domain information.** Taken from Wang *et al*, 2004.

Almost all of the A-, B-, D- and SDS-type cyclins contain both the N- and C-terminal cyclin domains (Cyclin\_N and Cyclin\_C respectively); the other cyclin families lack the C-terminal domain. The D-box was identified in nine A- and nine B-cyclins. One of the original 50 putative cyclin-encoding genes lacks the Cyclin\_N domain and therefore was not included in the phylogenetic tree.

The D-type cyclins are the main G1/S group and amount to ten genes in *Arabidopsis* (CYCD1;1, CYCD2;1, CYCD3;1, CYCD3;2, CYCD3;3, CYCD4;1, CYCD4;2, CYCD5;1, CYCD6;1, and CYCD7;1). They were suggested to control both the decision to pursue a cell nuclear division and the responses to internal and environmental cues during G1 (Cockcroft *et al*, 2000). CYCD-CDKA complexes are the key actors in phosphorylating RETINOBLASTOMA-RELATED 1 (RBR1) and, thus, releasing the transcription of genes

by E2F transcription factors, which triggers entry into and progression through the S phase (Fig 4; Boniotti & Gutierrez, 2001). Some A-type cyclins, specifically CYCA3;1 and CYCA3;2, may also play a role at this stage since their expression starts at late G1 and continues until mid M phase (Shimotohno *et al*, 2021; Takahashi *et al*, 2010). However, most A-type and B-type cyclins are mainly considered mitotic cyclins (Bulankova *et al*, 2013; Takahashi *et al*, 2010; Motta *et al*, 2021) that are expressed from G2 onwards and promote the transition from G2 to M. There are ten A-type cyclin genes in *Arabidopsis* (CYCA1;1, CYCA1;2, CYCA2;1, CYCA2;2, CYCA2;3, CYCA2;4, CYCA3;1, CYCA3;2, CYCA3;3 and CYCA3;4). B1-type cyclins have four members (CYCB1;1, CYCB1;2, CYCB1;3 and CYCB1;4), similarly to B2-type cyclins (CYCB2;1, CYCB2;2, CYCB2;3 and CYCB2;4), while the B3-type family has only one member (CYCB3;1), which is expressed in both mitosis and meiosis (Sofroni *et al*, 2020; Bulankova *et al*, 2013).

At G2, CYCA/B/D-CDKA/B complexes promote the phosphorylation of Activator-MYBs and Repressor-MYBs, which causes the stabilization and degradation of those substrates respectively (Fig 4). Activator-MYBs, in turn, will then activate the expression of mitotic genes (Fig 4; Shimotohno *et al*, 2021). It is important to mention that the exact expression pattern and biological role of the individual cyclin members is, at the moment, far from being completely understood, i.e., the identification and mode of regulation of specific CDK targets has not been extensively studied.

On the CDK side, plants have eight families, including CDKA to CDKG (Fig 3) and the CDK-like kinase (CLK) group. The A-type CDK (CDKA) and B-type CDK (CDKB) groups play major roles in the regulation of the cell cycle (Vandepoele *et al*, 2002). The A-type CDKs possess the typical PSTAIRE motif, which is important for binding to cyclins and is conserved in yeast and mammals, whereas *Arabidopsis* B-type CDKs have modified motifs, either PPTALRE, PSTTLRE or PPTTLRE (Vandepoele *et al*, 2002). Moreover, B-type CDKs are plant-specific.



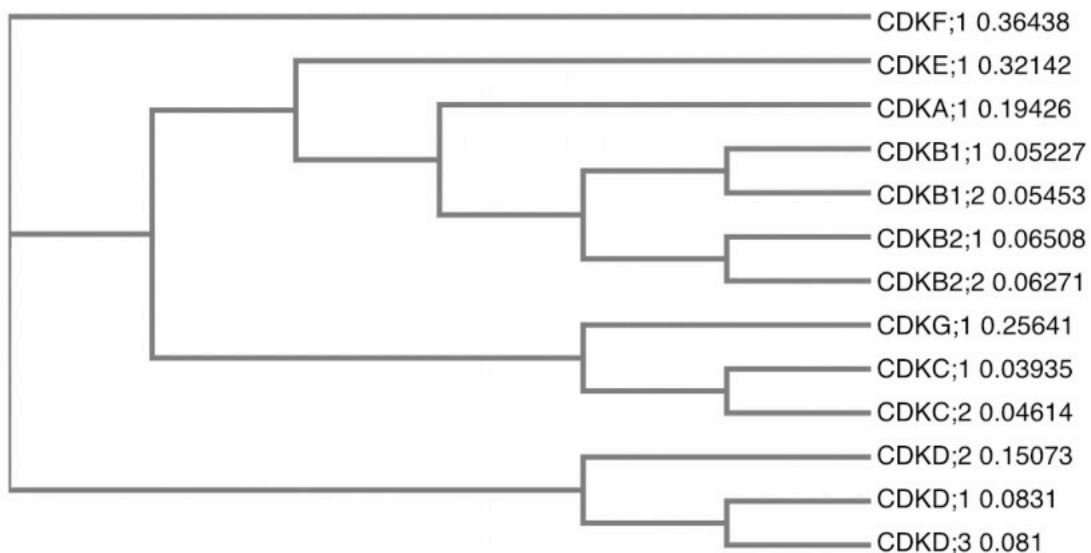


**Figure 3. A phylogenetic tree of the main *Arabidopsis thaliana* CDKA to CDKG members.**

The alignment of the CDK protein sequences was performed with Clustal Omega (<https://www.ebi.ac.uk/Tools/msa/clustalo/>). Sequence distance measurements are shown next to the protein names.

In *Arabidopsis*, the A-type CDK (*CDKA;1*) transcript levels are present throughout the cell cycle, although the activity itself peaks at G1/S and G2/M. On the other hand, transcripts from B-type CDKs (*CDKB1;1*, *CDKB1;2*, *CDKB2;1* and *CDKB2;2*) vary in expression pattern. For instance, *CDKB1* transcripts accumulate from S to M phase, while *CDKB2* are expressed from G2 to M.

The regulation of CDK activity in plants is considerably different from that of metazoans. This is exemplified by the differences between the regulation of *CDKA;1* in *Arabidopsis*, which is considered the central cell cycle regulator in plants (Nowack *et al*, 2012), and the analogous animal Cdk1. In metazoans, Cdk1-cyclin B complexes are inhibited by phosphorylation of the residues Thr14 and Tyr15 in the P-loop by certain kinases, e.g. WEE1, while phosphorylation at the T-loop is required for CDK activation (Morgan, 1997). Phosphorylation of the T-loop in *CDKA;1* from *Arabidopsis* has been confirmed to be necessary for protein function (Dissmeyer *et al*, 2007), whereas P-loop dephosphorylation does not seem to be critical (Dissmeyer *et al*, 2009). Additionally, in metazoans, removal of the inhibitory phosphorylation at residues Thr14 and Tyr15 is performed by Cdc25, whereas, in plants, there is no Cdc25 homolog with an equivalent function (Dissmeyer *et al*, 2010, 2009). Finally, the WEE1 kinase in *Arabidopsis* seems not to be essential under normal conditions but to function in response to DNA damage

controlling S-phase progression rather than controlling mitosis (De Schutter *et al*, 2007; Cools *et al*, 2011).

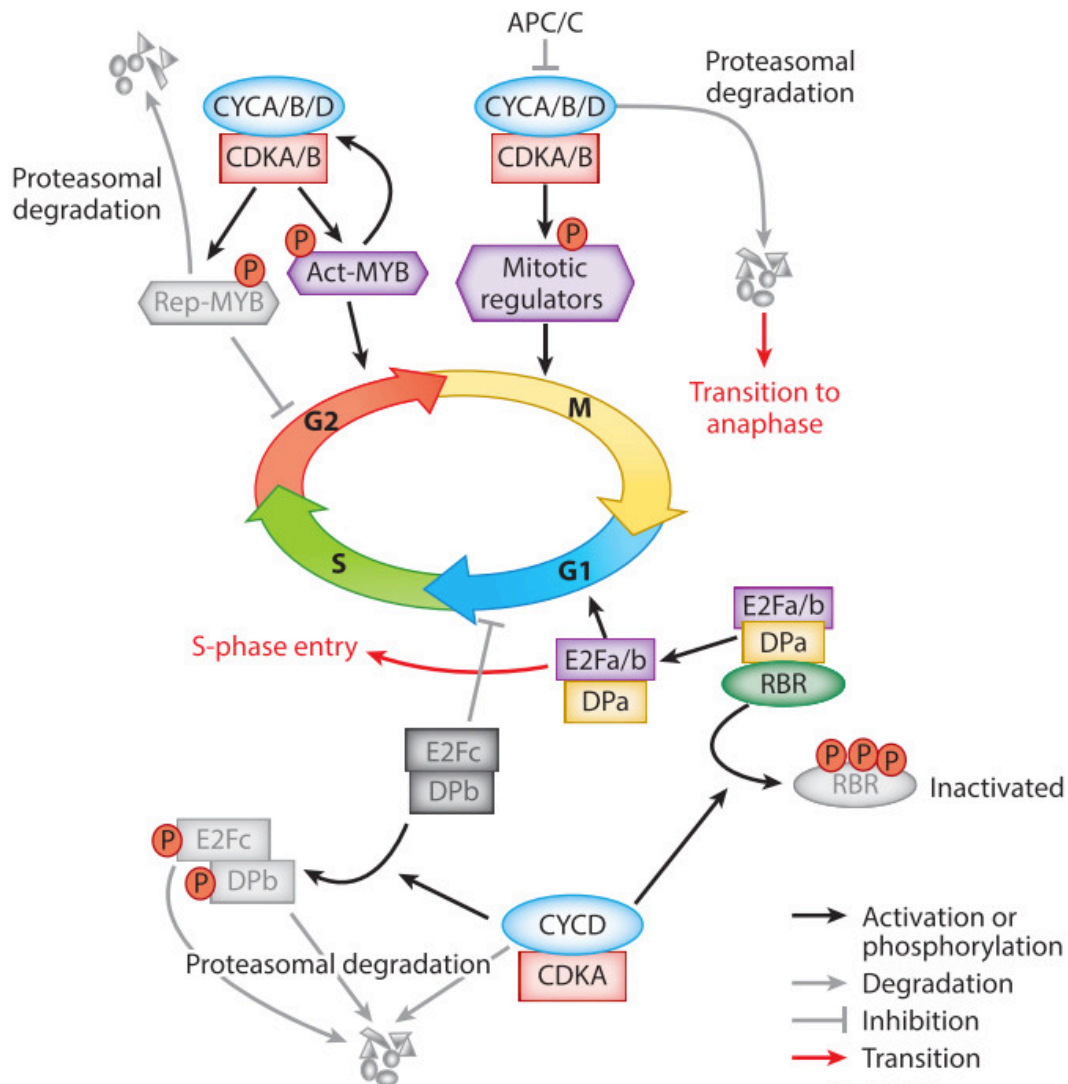


**Figure 4. Cell cycle regulation by cyclin-CDK complexes in plants.** This figure was modified from Shimotohno *et al*, 2021.

CYCD-CDKA complexes are responsible for the phosphorylation of RBR, which displaces it from E2Fa/b-DPa heterodimers and enables the transcription of S-phase-specific genes. Simultaneously, CYCD-CDKA complexes phosphorylate E2Fc and DPb, which repress the expression of S-phase genes. Tagged by phosphorylation, E2Fc and DPb are ubiquitinated and degraded by the proteasome. At G2, CYCA, CYCB, and CYCD interact with CDKA and CDKB members, promoting phosphorylation and activation of Activator-MYBs as well as phosphorylation and destabilization of Repressor-MYBs. The activation of Activator-MYBs, in turn, promotes the expression of G2/M genes, including mitotic cyclins. CYCA/B/D-CDKA/B complexes can phosphorylate specific substrates and promote progression through mitosis. The APC/C is then responsible for the degradation of mitotic cyclins and subsequent exit from mitosis.

It has been suggested that CDK activity oscillates throughout the cell cycle (Fig 5; Wijnker & Schnittger, 2013). It presumably increases progressively, beginning in G1 when DNA is licensed to replicate and followed by DNA replication in S phase. The activity reaches its peak at mitosis before the activation of the Anaphase-Promoting Complex/Cyclosome (APC/C) and separation of the sister chromatids. At this point, CDK activity potentially drops down to base levels after the APC/C has promoted ubiquitination of the key mitotic cyclins and subsequent degradation by the 26S proteasome.

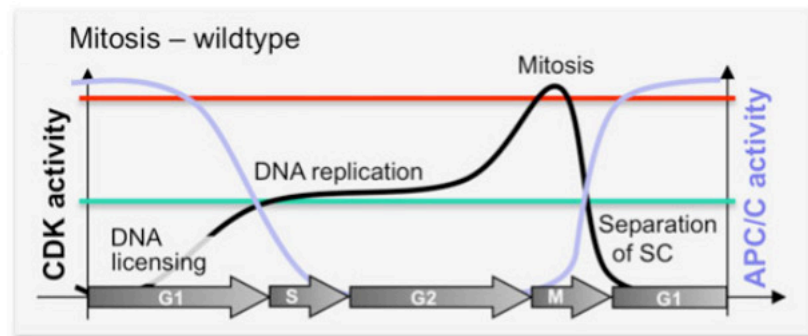


**Figure 5. A hypothetical model for CDK activity oscillation throughout mitosis.** This figure was modified from Wijnker & Schnittger, 2013.

In mitotic cell divisions, CDK activity presumably rises progressively from G1 until it peaks at mitosis, followed by a sharp drop in activity caused by the degradation of mitotic factors, e.g., cyclins, by the APC/C.

## 2.1. A- and B-type cyclins

There are 19 described A- and B-type cyclins in total. Single A- and B-type cyclin mutants do not usually display a strong mutant phenotype, which suggests that there is a high level of redundancy between the different cyclin members. One of the exceptions to this is *CYCA1;2/TAM*, which is known to be important for the transition from meiosis I to meiosis II. Accordingly, *cyca1;2/tam* mutants exit meiosis prematurely and produce diploid spores (d'Erfurth *et al*, 2010). *CYCA1;2* is also expressed in mitosis (Bulankova *et al*, 2013), although its function in this division has not been clarified.

A2-type cyclins are highly expressed in proliferative tissues (Vanneste *et al*, 2011). Accordingly, a loss-of-function mutation in the four A2-cyclins strongly slows down post-embryonic development. Furthermore, mutating only three out of the four A2-cyclin members already impacts growth, as for instance seen in a decreased root length and reduced seed set. *CYCA2;3* has been shown to form a complex with *CDKB1;1* to drive

mitosis and prevent endocycle onset (Boudolf *et al*, 2009). Interestingly, *CYCA2;1* and *CYCA2;2* have also been described to be expressed in meiosis, although their exact meiotic function remains to be studied (Bulankova *et al*, 2013). Finally, the triple *cyca2;2 cyca2;3 cyca2;4* mutant has been shown to have problems in meiotic chromosome condensation and segregation, although the reporter lines for the *CYCA2;3* and *CYCA2;4* members have not been detected in meiosis.

A3-type cyclins have a complex pattern of expression: reporter lines for *CYCA3;1*, *CYCA3;2* and *CYCA3;4* have been detected in the nucleus of root and shoot mitotic cells, whereas *CYCA3;2*, *CYCA3;3* and *CYCA3;4* reporter lines were also active in meiosis (Bulankova *et al*, 2013). Hence, *CYCA3;3* is the only A3-type cyclin that is meiosis-specific. Plants overexpressing *CYCA3;4* contain small leaves and no stomata; hence, the levels of this cyclin have to be precisely regulated in an APC-dependent manner for proper organ formation (Willems *et al*, 2020).

B1-type cyclins are strictly mitotic and have been linked to DNA damage response, where they promote homology-dependent DNA repair (Schnittger & De Veylder, 2018; Weimer *et al*, 2016). *CYCB1;1* is activated upon DNA damage in a SOG1-dependent manner (SOG1 is an analogous transcription factor to p53 from animals). Furthermore, RADIATION SENSITIVE 51 (RAD51), which is one of the main actors in homology-dependent DNA repair, was shown to be a substrate of CYCB1-CDKB1 complexes. In this thesis, the role of the B1-type cyclins in microtubule organization was explored in detail.

B2-type cyclins have also been shown to be strictly mitotic and expressed in the cytoplasm (Bulankova *et al*, 2013). Their specific role in mitosis is, at the moment, not understood.

Finally, the sole B3-type cyclin member *CYCB3;1* has been shown to be present in both mitosis and meiosis and to associate with spindle microtubules (Bulankova *et al*, 2013; Sofroni *et al*, 2020). Mutants in *CYCB3;1* are fully fertile and do not present any obvious growth defects, but *cycb3;1* roots grow shorter in comparison to wildtype on media containing the microtubule-disrupting drug oryzalin (Sofroni *et al*, 2020). Moreover, it has been shown that *CYCB3;1* has a function in the timing and accuracy of cell wall formation (Bulankova *et al*, 2013).

### 3. Overview of mitosis

After faithful duplication of the DNA in S phase, cells enter G<sub>2</sub>. If the G<sub>2</sub>/M checkpoint is satisfied and no DNA damage is present, mitosis takes place (Fig 6). In prophase, DNA progressively condenses. Nuclear envelope breakdown (NEB) marks the beginning of prometaphase. At metaphase, DNA condensation has reached its peak and chromosomes are visible in the metaphase plate, with their kinetochores attached to spindle fibers in a bipolar manner. At anaphase, sister chromatids are segregated into two opposing poles (that will later turn into two daughter cells) by the spindle. At telophase, chromosomes decondense and the nuclear envelope reforms, giving rise to the nascent daughter nuclei. Finally, cytokinesis happens and two daughter cells are formed by the activity of a structure called the phragmoplast (see below, Pines & Rieder, 2001). For details about meiosis, the cell division that is necessary for gamete formation, see Chapter 3.

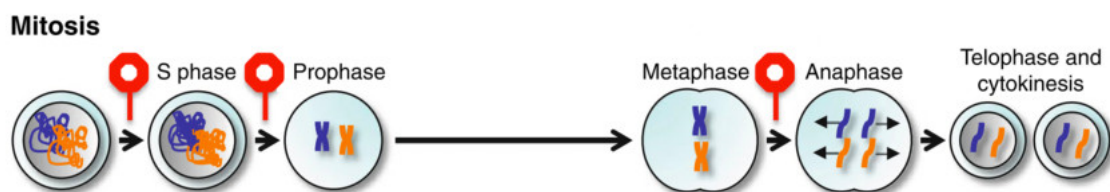


**Figure 6. An overview of mitotic progression in plants.** This figure was modified from Wijnker & Schnittger, 2013.

In the figure, the three major cell cycle checkpoints are represented by red octagons, from left to right: G<sub>1</sub>/S, G<sub>2</sub>/M, and the SAC. At prophase, there is visible condensation of the DNA. At metaphase, DNA is at its maximum condensation state and chromosomes are aligned at the metaphase plate. In anaphase, sister chromatids are pulled towards two opposing poles. In telophase, DNA decondenses and the nuclear envelope reforms. Often, telophase is followed by cytokinesis when a cell wall and plasma membrane form to separate the two daughter nuclei into two different cells.

### 4. Overview of mitotic microtubule arrays

Since plant cells are largely immobile in comparison to metazoan cells, cell division fulfills not only a developmental task but also is central in adaptation to environmental cues. Key to the execution of cell divisions are the mitotic microtubule arrays (Fig 7), which in plants are mainly represented by the preprophase band, the spindle and the phragmoplast. The preprophase band (PPB; Fig 7A) is a plant-specific band of

microtubules that forms at the cell periphery around the cell nucleus in G2 and remains until the prophase of mitosis. It serves as a positional cue for the precise orientation of the future cell wall and is thought to function by anchoring of proteins involved in cell division site determination. However, it is not present in meiotic, endosperm and gametophytic divisions. It was originally thought that the PPB is essential for cell division site determination, but recent studies have revealed that, in PPB-devoid mutants, no completely aberrant cell divisions are observed (see below; Schaefer *et al*, 2017). Hence, the PPB is a non-essential tool to ensure a higher degree of robustness with respect to cell division site selection in plants.

Following the disassembly of the PPB and NEB, the spindle (Fig 7C) starts to form from a population of microtubules that were localized around the nucleus. Its primary function is to separate sister chromatids equally into two new nuclei. In animal cells, centrosomes are crucial during spindle assembly and are the main microtubule generation site as well as the main microtubule organizing center at this stage (Yamada & Goshima, 2017). Animal spindles are fusiform and exhibit two clear poles, since the microtubules remain associated with centrosomes. In plants, in the absence of centrosomes, there is a large accumulation of microtubules around the nucleus in prophase, as mentioned above, which develop into the so-called prometaphase spindle or prospindle. Upon NEB, microtubules rapidly assemble into a barrel-shaped spindle with multiple mini-poles.

After NEB, two other mechanisms are present for microtubule generation in both plants and animals: chromosome-mediated nucleation and microtubule-dependent microtubule nucleation. Since flowering plants do not possess centrosomes, spindle microtubules are highly dependent on the so-called branched microtubule-dependent microtubule nucleation, which is mainly performed in an augmin-dependent manner (Lee & Liu, 2019; Yamada & Goshima, 2017; for details see below in Chapter 2). Indeed, knocking down subunits of the augmin complex in moss reduced the number of spindle microtubules by approximately 50%, showing the importance of this complex for microtubule generation in plant spindles (Nakaoka *et al*, 2012). Essentially three populations of microtubules can be distinguished in mitotic spindles at metaphase: astral microtubules that are produced from spindle poles and are directed towards the cell cortex; interpolar microtubules that meet in the spindle midzone; and kinetochore fibers that are attached to chromosomes (Fig 7C). In anaphase, the spindle elongates as the sister chromatids are pulled apart.

At the anaphase to telophase transition, the phragmoplast forms (Fig 7E and 8; Lee & Liu, 2019; Smertenko *et al*, 2018). Like the PPB, the phragmoplast is plant-specific and

contains a microtubule array that serves as a highway for vesicles originating at the Golgi apparatus and fusing at the plane of cell division to form and enlarge the cell plate between the two daughter nuclei. It has a characteristic bipolar orientation with two sets of highly bundled and cross-linked anti-parallel microtubules. The formation of the cell plate starts in the center and progresses towards the cortex. Accordingly, the phragmoplast expands in time towards the cell cortex (leading zone) and, hence, microtubules present in the central region with a maturely assembled cell plate depolymerize (lagging zone).

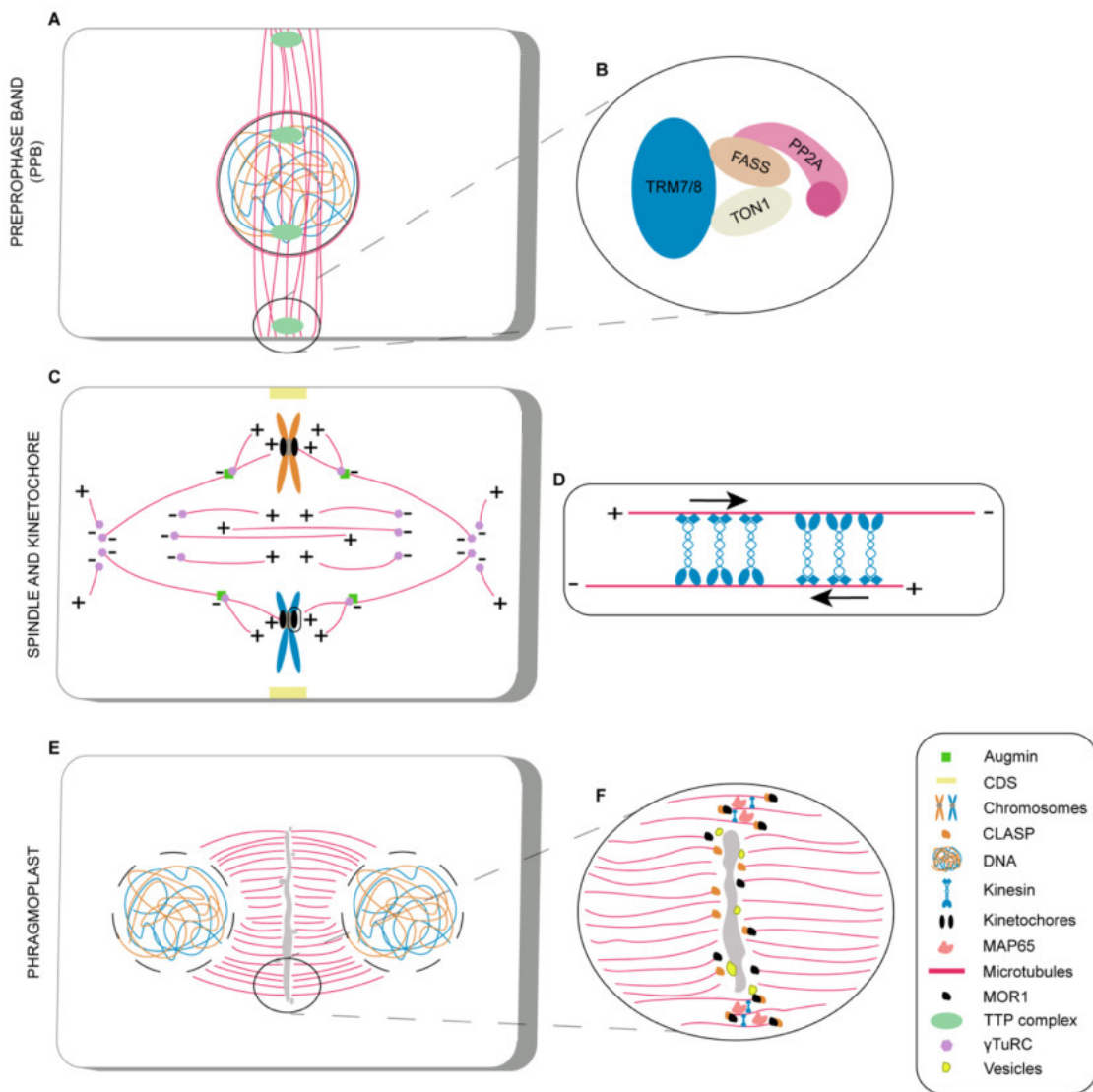


**Figure 7. An overview of the mitotic microtubule arrays.** This figure was modified from Motta & Schnittger, 2021.

A. The PPB, which is a thick band of microtubules that forms at the cell periphery around the equator of the nucleus, is assembled at G2 and remains until prophase, marking the future cell division site.

B. The components of the TTP complex (TRM7/8, FASS, TON1, and PP2A) are associated with the PPB.

C. The spindle begins its formation at prometaphase and reaches its maximum conformation right before anaphase. The kinetochore is a multiprotein structure that attaches the sister chromatids to spindle microtubules. At least three types of microtubule populations can be clearly distinguished at the spindle stage: astral and interpolar microtubules as well as kinetochore fibers. Astral microtubules originate at the spindle poles and grow towards the cell cortex; interpolar microtubules overlap in the central spindle in an anti-parallel manner; and kinetochore fibers attach to chromosomes. Spindle microtubules are mainly generated by the  $\gamma$ TuRC, which is a microtubule-nucleating complex. The augmin complex is essential for microtubule-dependent microtubule nucleation in a branched fashion.

D. Spindle microtubules are tightly regulated by the action of kinesins. They are for example responsible for an anti-parallel sliding of interpolar microtubules.

E. The phragmoplast microtubules are a scaffolding structure for Golgi-originated vesicle fusion in the nascent cell wall region.

F. Important factors for phragmoplast function and structure are represented. CLASP is a known microtubule stabilizer. MAP65 is responsible for cross-linking anti-parallel microtubules. MOR1 is a conserved plus-end binding protein that is involved in regulating microtubule dynamics.

CDS, cortical division site.

## **5. Microtubule-associated proteins (MAPs) and their role in microtubule array assembly**

The structure of the mitotic microtubule arrays is finetuned by a diverse set of regulators on a smaller or bigger scale. Here in section 1.5, I focus on the function of kinesins in forming robust microtubule arrays by controlling the dynamics and interaction of microtubules. In the next section (1.6), I will zoom in on the regulation at the single-microtubule level, discussing what is known about plus- and minus-end binding proteins.

An important class of regulators of the microtubule arrays is the kinesin family (Fig 7D and 8). Kinesins are motor proteins that can move along microtubules to either carry some cargo, to link to other microtubules or to regulate microtubule dynamics (Nebenführ & Dixit, 2018). In plants, based on homology in the amino acid sequence of the motor domain, there are 14 kinesin families (Lawrence *et al*, 2004). Additionally, kinesins can be classified as plus- or minus-end directed. Plus-end directed kinesins often generate, for instance, forces that allow elongation of the spindle, while minus-end directed kinesins mostly reduce the spindle length.



## 5.1. Regulation of preprophase band dynamics

Results from research on *Arabidopsis thaliana* show that the TTP complex (Fig 7B), which is composed of TONNEAU1 (TON1), TONNEAU2/FASS (TON2/FASS), PROTEIN PHOSPHATASE A (PP2A), and the TRM (TON1 RECRUITING MOTIF) proteins is a key regulator of microtubule arrays, especially the PPB (Azimzadeh *et al*, 2008; Schaefer *et al*, 2017; Drevensek *et al*, 2012). In this complex, TON1, FASS, and the TRM proteins interact in a triangular manner, while PP2A interacts with FASS and provides enzymatic activity to the complex (Fig 7B). The TRM proteins are presumably the targeting factors of the complex to microtubules.

In *ton1* and *ton2/fass* mutants, not only the PPB but also the cortical microtubules are affected (Azimzadeh *et al*, 2008; Drevensek *et al*, 2012). Cortical microtubules are present in interphase and are important for cell wall deposition in growing cells. Due to this broader role of the *TON* genes, the function of the PPB could, until recently, not be properly dissected from the general microtubule regulation. Finally, the isolation of *trm6/trm7/trm8* mutants, which are completely devoid of PPBs and present no problems in the cortical arrays, allowed the conclusion that PPBs are not essential for cell division site determination *per se* (Schaefer *et al*, 2017). In these mutants, mitotic parameters, such as spindle positioning, cell volume between daughter cells, and cell division angle, were not significantly changed on average, but there was a great increase in the variance of these parameters (Schaefer *et al*, 2017). Therefore, the PPB is now seen as a tool for fine-tuning the selection of the site of cell division.

The PPB disassembles before NEB and, hence, the positional information must be stored by other structures. Indeed, the kinesin-12 family members POK1 and POK2 are well known for retaining information on the cortical division site where the PPB was once localized (Fig 8; Lipka *et al*, 2014; Herrmann *et al*, 2018). They presumably function as a scaffold for PPB marker proteins, since the *pok1 pok2* double mutant exhibits loss of cortical division site characteristics, as judged by the absence of TANGLED and the Ran GTPase regulatory protein RanGAP1 at that site in metaphase. Recently, an additional role for POK2 in stabilizing the phragmoplast midzone by interacting with MAP65-3 (see below) has been uncovered (Herrmann *et al*, 2018).

## 5.2. Control of spindle microtubules

The prospindle is the population of microtubules that localizes on the nuclear envelope in a bipolar fashion preceding NEB. After NEB, this population of microtubules reorganizes for the generation of the prometaphase and metaphase spindle. New microtubules are rapidly generated in a branched manner from existing microtubules, which is highly regulated by the function of the augmin complex (see Chapter 2 for details) and the Targeting Protein for Xklp2 (TPX2; Lee *et al*, 2017; Petry *et al*, 2013).

TPX2 is regarded as a crucial regulator of mitosis since it mediates the interaction of several proteins with the spindle. For instance, in vertebrates, it is critical to the regulation of the kinase AURORA A, which phosphorylates many MAPs and is crucial for spindle formation and dynamics. In addition, TPX2 promotes spindle- and chromosome-induced microtubule nucleation (Alfaro-Aco *et al*, 2017). The TPX2 family in plants has expanded in comparison to metazoans to contain, in addition to the canonical TPX2, eight TPX-LIKE PROTEINs (TPXLs), of which TPXL2 and TPXL3 have been characterized (Vos *et al*, 2008; Boruc *et al*, 2019). TPX2 and TPXL2 were found to be redundant and non-essential for plants, while a mutation in TPXL3 is lethal in a homozygous state in the embryo (Boruc *et al*, 2019).

Four kinesin family members have been implicated in spindle regulation: KRP125c, ATK1, ATK5, and KINESIN-12E. First, midzone spindle microtubules are presumably stabilized and cross-linked by KRP125c, a plus-end directed kinesin-5 (Bannigan *et al*, 2007). ATK1 and ATK5 are kinesin-14 minus-end directed motors that also localize to the spindle. Mutants for ATK1 exhibit spindles with multiple poles in both mitosis and meiosis and have problems with chromosome segregation in male meiosis (Marcus *et al*, 2003). The reason why mitotic chromosome segregation is unaffected in the *atk1* mutants is unclear, but it could be due to a redundancy of ATK1 with other kinesin members in mitosis. In addition, ATK1 is hypothesized to be important for microtubule translocation to the spindle poles. Mutants for ATK5 have abnormally broad spindles and this kinesin has been implicated in the search and capture of interpolar antiparallel microtubules as well as in cross-linking of microtubules in the spindle midzone and at the spindle poles (Ambrose *et al*, 2005; Ambrose & Cyr, 2007). Recently, it has been found that KINESIN-12E is also relevant for spindle structure and dynamics (Herrmann *et al*, 2020). Mutants for this kinesin member have a delay in spindle formation and shorter spindles than the wildtype.

### 5.3. Organization of the phragmoplast

The phragmoplast (Fig 7E and 7F) is a complex structure that also requires a precise orchestration of microtubule dynamics, i.e., polymerization, depolymerization, stabilization, bundling, cross-linking, and nucleation (for details on microtubule dynamics see the next section; Smertenko *et al*, 2018).

Several kinesins have been identified to play a role in phragmoplast structure (Fig 8). The kinesin-12 family members PAKRP1 (Kinesin12A) and PAKRP2 (Kinesin12B) are known to stabilize antiparallel microtubules in the phragmoplast midzone (Lee *et al*, 2007; Pan *et al*, 2004). NACK1 and NACK2 are kinesin-7 members that are important for a MAP kinase cascade that ultimately destabilizes the phragmoplast midzone by phosphorylation of MAP65 in the lagging phragmoplast zone (Tanaka *et al*, 2004; Nishihama *et al*, 2002). Last, KCBP, a kinesin-14 member, helps to guide the leading phragmoplast zone towards the cortex by pulling on microtubules protruding into the periphery (Buschmann *et al*, 2015).

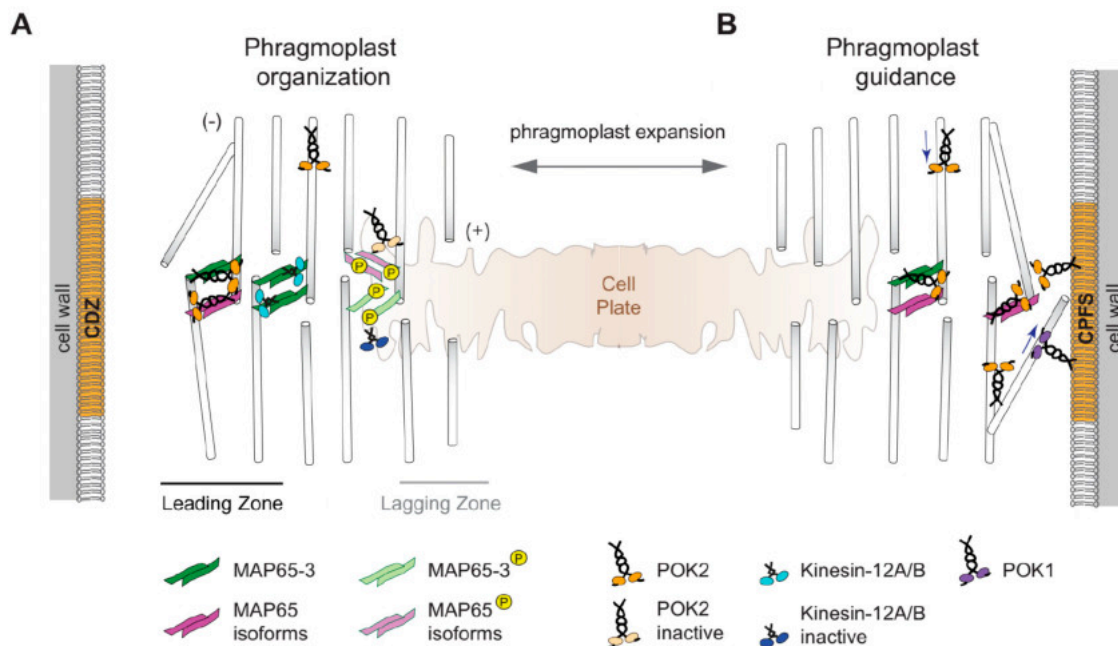


**Figure 8. The *Arabidopsis* kinesin-12 members play important roles in phragmoplast formation and dynamics.** The figure was taken from Müller & Livanos, 2019.

A. The phragmoplast contains two groups of anti-parallel microtubules with plus-ends partially overlapping in the phragmoplast midzone. Microtubules polymerize in the leading zone and depolymerize in the lagging zone. Plus-end directed kinesins (PAKRP1/Kinesin12A, PAKRP2/Kinesin12B and POK2/Kinesin12D) interact with MAP65-3 and other MAP65 isoforms, mediating their localization to the phragmoplast midzone. MAP65 members, in turn, promote

phragmoplast stability and expansion. Phosphorylated MAP65 is unable to bind microtubules. The regulation of kinesin-12 activity in the midzone is currently uncharacterized.

B. As cytokinesis progresses, peripheral microtubules extend towards the cell cortex. POK1/Kinesin12C and POK2/Kinesin12D, localized at the CDZ, probably interact with these microtubule filaments and move towards their plus ends (blue arrow). With that, the phragmoplast and cell plate are placed in a median region of the CDZ called CPFS.

CDZ, cortical division zone. CPFS, cell plate fusion site.

Another class of important regulators of the phragmoplast structure is the MICROTUBULE-ASSOCIATED PROTEIN 65 (MAP65; Fig 7F and 8) family of proteins, which is responsible for cross-linking anti-parallel microtubules by generating 25-30 nm bridges between them and which also potentially stabilizes microtubules (Smertenko *et al*, 2018). There are currently four *MAP65* genes characterized: *MAP65-1*, *MAP65-2*, *MAP65-3*, and *MAP65-4*. *MAP65-1* and *MAP65-2* seem to be redundantly involved in axial growth. However, their function seems to be non-essential since the double null mutant has similar growth to the wildtype (Sasabe *et al*, 2011; Lucas & Shaw, 2012). On the other hand, *MAP65-3* seems to be the main player: it is predominantly expressed in dividing cells and its knockout mutant exhibits around 40% abortion frequency in cytokinesis (Ho *et al*, 2012). However, this number suggests that MAP65-3's function can partially be replaced by other microtubule bundling factors. Indeed, a mutation in both *MAP65-3* and *MAP65-4* is lethal (Li *et al*, 2017). Moreover, introducing an additional copy of *MAP65-4* in the *map65-3* mutant almost completely restored plant growth, indicating that the final amount of MAP65 is critical for proper phragmoplast function (Li *et al*, 2017).

## 6. The control of microtubule dynamics by plus-end binding proteins

Microtubules are highly dynamic structures, since  $\alpha$ - and  $\beta$ -tubulin heterodimers can be added at both ends of microtubule filaments. However, the rate of growth and shrinkage at both ends is not equal. In fact, microtubules have a plus-end, that grows more rapidly, and a minus-end, that is less dynamic and is initially where microtubules are nucleated (see Chapter 2 for details on the  $\gamma$ -tubulin nucleating complex). In the next subsection, I will discuss some of the known plus-end MAPs in plants. In animals, also a class of minus-end targeting proteins has been described, but these are not conserved in plants (Akhmanova & Hoogenraad, 2015)

## 6.1. Plus-end binding proteins

Plus-end tracking proteins (+TIPs) are known to localize to microtubule growing ends to regulate their interactive properties and dynamics. A well-known class of +TIPs is END-BINDING 1 (EB1; Komaki *et al*, 2010). In *Arabidopsis*, there are three members: EB1a, EB1b and EB1c. All three members were found to decorate mitotic microtubule arrays. EB1a and EB1b decorate the growing plus-ends, whereas EB1c has a slightly different localization pattern and decorates spindle microtubules along their length. Furthermore, mutants for *EB1c* often have collapsed or tilted spindles and phragmoplasts. Generally, EB1 is regarded to promote microtubule growth, although there are contradictory reports on the precise function of the protein. For instance, Molines *et al*, 2020 have reported that the mammalian EB1 from mouse seems to promote microtubule growth *in vitro*, while EB1b from *Arabidopsis* seems to rather stabilize microtubules.

XMAP215 and CLASP are +TIPs that were initially characterized in animal cells. However, their plant counterparts are known to associate with the full microtubule structure (Kawamura *et al*, 2006; Ambrose *et al*, 2007). MOR1 (MICROTUBULE ORGANIZATION 1; Fig 7F), which is the single member of the XMAP215 family in *Arabidopsis*, is an indispensable protein that has a role in a range of microtubule arrays, including the PPB, spindle and phragmoplast (Kawamura *et al*, 2006). It has been revealed that *mor1* mutants exhibit a reduction in both microtubule growth and shrinkage rates at plus ends (Kawamura & Wasteneys, 2008). CLASP (CLIP-Associated Protein; Fig 7F) is known to stabilize microtubules and has an important role in the formation of cortical microtubule arrays as well as the PPB, spindle and phragmoplast in *Arabidopsis* (Ambrose *et al*, 2007). CLASP is slightly enriched at microtubule plus-ends rather than showing a comet-like localization pattern as seen for other +TIPs. Interestingly, the binding of CLASP to the sides of microtubules seems to be important for the interaction of microtubules with the cell cortex (Ambrose & Wasteneys, 2008).

SPIRAL (SPR) is a plant-specific MAP family with six members in *Arabidopsis* that have been described as +TIPs. SPR1, for instance, localizes to cortical microtubules as well as the PPB, spindle and the phragmoplast (Sedbrook *et al*, 2004). Its localization is described to be concentrated at the growing microtubule plus-ends; however, SPR1 might bind microtubules indirectly since co-sedimentation assays failed to recover the protein (Sedbrook *et al*, 2004). Interestingly, SPR2, another member of the SPIRAL family, has been recently shown to regulate microtubule plus- and minus-ends in an

opposing manner; SPR2 binds and stabilizes minus-ends, while it also promotes destabilization of plus-ends (Fan *et al*, 2018).

## 7. The regulation of mitotic microtubule arrays by cyclins and CDKs

The assembly and dynamics of the mitotic microtubule arrays must be tightly in sync with the cell cycle, since events in mitosis are highly dependent on each other. For instance, cytokinesis must only happen after the chromatids have been properly separated into two daughter nuclei. Hence, it is tempting to speculate that cyclins and CDKs may be involved in the regulation of the mitotic microtubule arrays. Consistent with such a regulatory role, many of these proteins have been found to localize at microtubule arrays, e.g., CYCB3;1 at the spindle in male meiosis (Sofroni *et al*, 2020); CDKA;1 at the PPB, spindle and phragmoplast in *Arabidopsis* BY-2 cells (Boruc *et al*, 2010); and CYCB1;2 in the PPB and spindle in maize (Mews *et al*, 1997).

However, if and how cyclin-CKD complexes regulate microtubule arrays remains largely unexplored, albeit preliminary results indicate multiple routes of control. The phosphorylation of MAP65-1 by CDKs, for instance, has been shown to decrease its ability to bind microtubules *in vitro* (Fig 8; Smertenko *et al*, 2006). The kinesin NACK1 is another example, as its phosphorylation by CDKs in early mitosis, i.e., prophase and metaphase, inhibits the activation of a signaling cascade that promotes cytokinesis. Finally, ENDOSPERM DEFECTIVE 1 (EDE1), which is a member of the augmin complex (see chapter 2 for details), has also been shown to be phosphorylated *in vitro* (Pignocchi *et al*, 2009), but the function of this phosphorylation is still unknown.

Hence, an in-depth analysis of CDK-dependent phosphorylation of MAPs will likely shed light on how major changes in the plant cytoskeleton are coupled to the cell cycle.

## 8. References

- Akhmanova A & Hoogenraad CC (2015) Microtubule minus-end-targeting proteins. *Curr Biol* 25: R162–R171
- Alfaro-Aco R, Thawani A & Petry S (2017) Structural analysis of the role of TPX2 in branching microtubule nucleation. *J Cell Biol* 216: 983–997
- Ambrose JC & Cyr R (2007) The kinesin ATK5 functions in early spindle assembly in Arabidopsis. *Plant Cell* 19: 226–236
- Ambrose JC, Li W, Marcus A, Ma H & Cyr R (2005) A Minus-End-directed Kinesin with Plus-End Tracking Protein Activity Is Involved in Spindle Morphogenesis. *Mol Biol Cell* 16: 1584–1592
- Ambrose JC, Shoji T, Kotzer AM, Pighin JA & Wasteneys GO (2007) The Arabidopsis *CLASP* gene encodes a microtubule-associated protein involved in cell expansion and division. *Plant Cell* 19: 2763–2775
- Ambrose JC & Wasteneys GO (2008) CLASP Modulates Microtubule-Cortex Interaction during Self-Organization of Acentrosomal Microtubules. *Mol Biol Cell* 19: 4730–4737
- Andrews B & Measday V (1998) The cyclin family of budding yeast: abundant use of a good idea. *Trends Genet* 14: 66–72
- Azimzadeh J, Nacry P, Christodoulidou A, Drevensek S, Camilleri C, Amiour N, Parcy F, Pastuglia M & Bouchez D (2008) Arabidopsis TONNEAU1 proteins are essential for preprophase band formation and interact with centrin. *Plant Cell* 20: 2146–2159
- Bannigan A, Scheible WR, Lukowitz W, Fagerstrom C, Wadsworth P, Somerville C & Baskin TI (2007) A conserved role for kinesin-5 in plant mitosis. *J Cell Sci* 120: 2819–2827
- Berger F, Grini PE & Schnittger A (2006) Endosperm: an integrator of seed growth and development. *Curr Opin Plant Biol* 9: 664–670
- Boniotti MB & Gutierrez C (2001) A cell-cycle-regulated kinase activity phosphorylates plant retinoblastoma protein and contains, in Arabidopsis, a CDKA/cyclin D complex. *Plant J* 28: 341–350
- Boruc J, Deng X, Mylle E, Besbrugge N, Van Durme M, Demidov D, Tomaščíková ED, Tan TRC, Vandorpe M, Eeckhout D, *et al* (2019) TPX2-LIKE PROTEIN3 is the primary activator of  $\alpha$ -aurora kinases and is essential for embryogenesis. *Plant Physiol* 180: 1389–1405
- Boruc J, Mylle E, Duda M, de Clercq R, Rombauts S, Geelen D, Hilson P, Inzé D, van Damme D & Russinova E (2010) Systematic localization of the Arabidopsis core

- cell cycle proteins reveals novel cell division complexes. *Plant Physiol* 152: 553–565
- Boudolf V, Lammens T, Boruc J, van Leene J, van den Daele H, Maes S, van Isterdael G, Russinova E, Kondorosi E, Witters E, *et al* (2009) CDKB1;1 forms a functional complex with CYCA2;3 to suppress endocycle onset. *Plant Physiol* 150: 1482–1493
- Bulankova P, Akimcheva S, Fellner N & Riha K (2013) Identification of Arabidopsis Meiotic Cyclins Reveals Functional Diversification among Plant Cyclin Genes. *PLoS Genet* 9: 1–11
- Buschmann H, Dols J, Kopischke S, Peña EJ, Andrade-Navarro MA, Heinlein M, Szymanski DB, Zachgo S, Doonan JH & Lloyd CW (2015) Arabidopsis KCBP interacts with AIR9 but stays in the cortical division zone throughout mitosis via its MYTH4-FERM domain. *J Cell Sci* 128: 2033–2046
- Cockcroft CE, Den Boer BGW, Healy JMS & Murray JAH (2000) Cyclin D control of growth rate in plants. *Nature* 405: 575–579
- Cools T, Iantcheva A, Weimer AK, Boens S, Takahashi N, Maes S, van den Daele H, van Isterdael G, Schnittger A & de Veylder L (2011) The *Arabidopsis thaliana* checkpoint kinase WEE1 protects against premature vascular differentiation during replication stress. *Plant Cell* 23: 1435–1448
- d'Erfurth I, Cromer L, Jolivet S, Girard C, Horlow C, Sun Y, To JPC, Berchowitz LE, Copenhaver GP & Mercier R (2010) The CYCLIN-A CYCA1;2/TAM is required for the meiosis I to meiosis II transition and cooperates with OSD1 for the prophase to first meiotic division transition. *PLoS Genet* 6: 1–12
- Dissmeyer N, Nowack MK, Pusch S, Stals H, Inzé D, Grini PE & Schnittger A (2007) T-loop phosphorylation of Arabidopsis CDKA;1 is required for its function and can be partially substituted by an aspartate residue. *Plant Cell* 19: 972–985
- Dissmeyer N, Weimer AK, Pusch S, de Schutter K, Kamei CLA, Nowack MK, Novak B, Duan GL, Zhu YG, de Veylder L, *et al* (2009) Control of cell proliferation, organ growth, and DNA damage response operate independently of dephosphorylation of the Arabidopsis Cdk1 Homolog CDKA;1. *Plant Cell* 21: 3641–3654
- Dissmeyer N, Weimer AK, de Veylder L, Novak B & Schnittger A (2010) The regulatory network of cell cycle progression is fundamentally different in plants versus yeast or metazoans. *Plant Signal Behav* 5: 1613–1618
- Drevensek S, Goussot M, Duroc Y, Christodoulidou A, Steyaert S, Schaefer E, Duvernois E, Grandjean O, Vantard M, Bouchez D, *et al* (2012) The Arabidopsis TRM1-TON1 interaction reveals a recruitment network common to plant cortical microtubule arrays and eukaryotic centrosomes. *Plant Cell* 24: 178–191



- Fan Y, Burkart GM & Dixit R (2018) The Arabidopsis SPIRAL2 Protein Targets and Stabilizes Microtubule Minus Ends. *Curr Biol* 28: 987–994
- Harashima H, Dissmeyer N & Schnittger A (2013) Cell cycle control across the eukaryotic kingdom. *Trends Cell Biol* 23: 345–356
- Herrmann A, Livanos P, Lipka E, Gadeyne A, Hauser M, Van Damme D & Müller S (2018) Dual localized kinesin-12 POK 2 plays multiple roles during cell division and interacts with MAP65-3. *EMBO Rep* 19: 1–16
- Herrmann A, Livanos P, Zimmermann S, Berendzen K, Rohr L, Lipka E & Müller S (2020) KINESIN-12E regulates metaphase spindle flux and helps control spindle size in Arabidopsis. *Plant Cell*: 1–17
- Ho CMK, Lee YRJ, Kiyama LD, Dinesh-Kumar SP & Liu B (2012) Arabidopsis microtubule-associated protein MAP65-3 cross-links antiparallel microtubules toward their plus ends in the phragmoplast via its distinct C-Terminal microtubule binding domain. *Plant Cell* 24: 2071–2085
- Kawamura E, Himmelspach R, Rashbrooke MC, Whittington AT, Gale KR, Collings DA & Wasteneys GO (2006) MICROTUBULE ORGANIZATION 1 regulates structure and function of microtubule arrays during mitosis and cytokinesis in the Arabidopsis root. *Plant Physiol* 140: 102–114
- Kawamura E & Wasteneys GO (2008) MOR1, the *Arabidopsis thaliana* homologue of *Xenopus* MAP215, promotes rapid growth and shrinkage, and suppresses the pausing of microtubules in vivo. *J Cell Sci* 121: 4114–4123
- Komaki S, Abe T, Coutuer S, Inzé D, Russinova E & Hashimoto T (2010) Nuclear-localized subtype of end-binding 1 protein regulates spindle organization in Arabidopsis. *J Cell Sci* 123: 451–459
- Lawrence CJ, Dawe RK, Christie KR, Cleveland DW, Dawson SC, Endow SA, Goldstein LSB, Goodson H V., Hirokawa N, Howard J, *et al* (2004) A standardized kinesin nomenclature. *J Cell Biol* 167: 19–22
- Lee YRJ, Hiwatashi Y, Hotta T, Xie T, Doonan JH & Liu B (2017) The Mitotic Function of Augmin Is Dependent on Its Microtubule-Associated Protein Subunit EDE1 in *Arabidopsis thaliana*. *Curr Biol* 27: 3891–3897
- Lee YRJ, Li Y & Liu B (2007) Two Arabidopsis phragmoplast-associated kinesins play a critical role in cytokinesis during male gametogenesis. *Plant Cell* 19: 2595–2605
- Lee YRJ & Liu B (2019) Microtubule nucleation for the assembly of acentrosomal microtubule arrays in plant cells. *New Phytol* 222: 1705–1718
- Li H, Sun B, Sasabe M, Deng X, Machida Y, Lin H, Julie Lee YR & Liu B (2017) Arabidopsis MAP65-4 plays a role in phragmoplast microtubule organization and marks the cortical cell division site. *New Phytol* 215: 187–201

- Lipka E, Gadeyne A, Stöckle D, Zimmermann S, De Jaeger G, Ehrhardt DW, Kirik V, Van Damme D & Müller S (2014) The phragmoplast-orienting kinesin-12 class proteins translate the positional information of the preprophase band to establish the cortical division zone in *Arabidopsis thaliana*. *Plant Cell* 26: 2617–2632
- Lucas JR & Shaw SL (2012) MAP65-1 and MAP65-2 promote cell proliferation and axial growth in Arabidopsis roots. *Plant J* 71: 454–463
- Marcus AI, Li W, Ma H & Cyr RJ (2003) A Kinesin Mutant with an Atypical Bipolar Spindle Undergoes Normal Mitosis. *Mol Biol Cell* 14: 1717–1726
- Mews M, Sek FJ, Moore R, Volkmann D, Gunning BES & John PCL (1997) Mitotic cyclin distribution during maize cell division: Implications for the sequence diversity and function of cyclins in plants. *Protoplasma* 200: 128–145
- Molines AT, Molines AT, Stoppin-Mellet V, Arnal I, Coquelle FM & Coquelle FM (2020) Plant and mouse EB1 proteins have opposite intrinsic properties on the dynamic instability of microtubules. *BMC Res Notes* 13: 4–9
- Morgan DO (1997) Cyclin-dependent kinases: engines, clocks, and microprocessors. *Annu Rev Cell Dev Biol* 13: 261–291
- Morgan DO (2007) *The Cell Cycle: Principles of Control* London: New Science Press Ltd
- Motta MR & Schnittger A (2021) A microtubule perspective on plant cell division. *Curr Biol* 31: R547–R552
- Motta MR, Zhao A, Pastuglia M, Belcram K, Komaki M, Harashima H, Komaki S, Bulankova P, Heese M, Riha K, *et al* (2021) B1-type cyclins control microtubule organization during cell division in Arabidopsis. *bioRxiv*
- Müller S & Livanos P (2019) Plant kinesin-12: Localization heterogeneity and functional implications. *Int J Mol Sci* 20: 1–12
- Nakaoka Y, Miki T, Fujioka R, Uehara R, Tomioka A, Obuse C, Kubo M, Hiwatashi Y & Goshima G (2012) An inducible RNA interference system in *Physcomitrella patens* reveals a dominant role of augmin in phragmoplast microtubule generation. *Plant Cell* 24: 1478–1493
- Nebenführ A & Dixit R (2018) Kinesins and Myosins: Molecular Motors that Coordinate Cellular Functions in Plants. *Annu Rev Plant Biol* 69: 329–361
- Nishihama R, Soyano T, Ishikawa M, Araki S, Tanaka H, Asada T, Irie K, Ito M, Terada M, Banno H, *et al* (2002) Expansion of the cell plate in plant cytokinesis requires a kinesin-like protein/MAPKKK complex. *Cell* 109: 87–99
- Nowack MK, Harashima H, Dissmeyer N, Zhao X, Bouyer D, Weimer AK, De Winter F, Yang F & Schnittger A (2012) Genetic Framework of Cyclin-Dependent Kinase Function in Arabidopsis. *Dev Cell* 22: 1030–1040

- Pan R, Lee YRJ & Liu B (2004) Localization of two homologous Arabidopsis kinesin-related proteins in the phragmoplast. *Planta* 220: 156–164
- Petry S, Groen AC, Ishihara K, Mitchison TJ & Vale RD (2013) Branching microtubule nucleation in *Xenopus* egg extracts mediated by augmin and TPX2. *Cell* 152: 768–777
- Pignocchi C, Minns GE, Nesi N, Koumproglou R, Kitsios G, Benning C, Lloyd CW, Doonan JH & Hills MJ (2009) Endosperm Defective1 is a novel microtubule-associated protein essential for seed development in Arabidopsis. *Plant Cell* 21: 90–105
- Pines J & Rieder CL (2001) Re-staging mitosis: A contemporary view of mitotic progression. *Nat Cell Biol* 3: E3–E6
- Renaudin JP, Doonan JH, Freeman D, Hashimoto J, Hirt H, Inzé D, Jacobs T, Kouchi H, Rouzé P, Sauter M, *et al* (1996) Plant cyclins: A unified nomenclature for plant A-, B- and D-type cyclins based on sequence organization. *Plant Mol Biol* 32: 1003–1018
- Sasabe M, Kosetsu K, Hidaka M, Murase A & Machida Y (2011) Arabidopsis thaliana MAP65-1 and MAP65-2 function redundantly with MAP65-3/PLEIADE in cytokinesis downstream of MPK4. *Plant Signal Behav* 6: 743–747
- Schaefer E, Belcram K, Uyttewaal M, Duroc Y, Goussot M, Legland D, Laruelle E, De Tauzia-Moreau ML, Pastuglia M & Bouchez D (2017) The preprophase band of microtubules controls the robustness of division orientation in plants. *Science* 356: 186–189
- Schnittger A & De Veylder L (2018) The Dual Face of Cyclin B1. *Trends Plant Sci* 23: 475–478
- De Schutter K, Joubès J, Cools T, Verkest A, Corellou F, Babiychuk E, Van Der Schueren E, Beeckman T, Kushnir ST, Inzé D, *et al* (2007) Arabidopsis WEE1 kinase controls cell cycle arrest in response to activation of the DNA integrity checkpoint. *Plant Cell* 19: 211–225
- Sedbrook JC, Ehrhardt DW, Fisher SE, Scheible WR & Somerville CR (2004) The Arabidopsis *SKU6/SPIRAL 1* gene encodes a plus end-localized microtubule-interacting protein involved in directional cell expansion. *Plant Cell* 16: 1506–1520
- Shimotohno A, Aki SS, Takahashi N & Umeda M (2021) Regulation of the Plant Cell Cycle in Response to Hormones and the Environment. *Annu Rev Plant Biol* 72: 273–296
- Smertenko A, Hewitt SL, Jacques CN, Kacprzyk R, Liu Y, Marcec MJ, Moyo L, Ogden A, Oung HM, Schmidt S, *et al* (2018) Phragmoplast microtubule dynamics - A game of zones. *J Cell Sci* 131: 1–11

- Smertenko AP, Chang HY, Sonobe S, Fenyk SI, Weingartner M, Bögre L & Hussey PJ (2006) Control of the AtMAP65-1 interaction with microtubules through the cell cycle. *J Cell Sci* 119: 3227–3237
- Sofroni K, Takatsuka H, Yang C, Dissmeyer N, Komaki S, Hamamura Y, Böttger L, Umeda M & Schnittger A (2020) CDKD-dependent activation of CDKA<sub>1</sub> controls microtubule dynamics and cytokinesis during meiosis. *J Cell Biol* 219: 1–21
- Takahashi I, Kojima S, Sakaguchi N, Umeda-Hara C & Umeda M (2010) Two Arabidopsis cyclin A3s possess G1 cyclin-like features. *Plant Cell Rep* 29: 307–315
- Tanaka H, Ishikawa M, Kitamura S, Takahashi Y, Soyano T, Machida C & Machida Y (2004) The *AtNACK1/HINKEL* and *STUD/TETRASPORE/AtNACK2* genes, which encode functionally redundant kinesins, are essential for cytokinesis in Arabidopsis. *Genes to Cells* 9: 1199–1211
- Vandepoele K, Raes J, De Veylder L, Rouzé P, Rombauts S & Inzé D (2002) Genome-wide analysis of core cell cycle genes in Arabidopsis. *Plant Cell* 14: 903–916
- Vanneste S, Coppens F, Lee E, Donner TJ, Xie Z, Van Isterdael G, Dhondt S, De Winter F, De Rybel B, Vuylsteke M, *et al* (2011) Developmental regulation of CYCA2s contributes to tissue-specific proliferation in Arabidopsis. *EMBO J* 30: 3430–3441
- Vos JW, Pieuchot L, Evrard JL, Janski N, Bergdoll M, De Ronde D, Perez LH, Sardon T, Vernos I & Schmit AC (2008) The plant TPX2 protein regulates prospindle assembly before nuclear envelope breakdown. *Plant Cell* 20: 2783–2797
- Wang G, Kong H, Sun Y, Zhang X, Zhang W, Altman N, DePamphilis CW & Ma H (2004) Genome-wide analysis of the cyclin family in Arabidopsis and comparative phylogenetic analysis of plant cyclin-like proteins. *Plant Physiol* 135: 1084–1099
- Weimer AK, Biedermann S, Harashima H, Roodbarkelari F, Takahashi N, Foreman J, Guan Y, Pochon G, Heese M, Van Damme D, *et al* (2016) The plant-specific CDKB1-CYCB1 complex mediates homologous recombination repair in Arabidopsis. *EMBO J* 35: 2068–2086
- Wijnker E & Schnittger A (2013) Control of the meiotic cell division program in plants. *Plant Reprod* 26: 143–158
- Willems A, Heyman J, Eekhout T, Achon I, Pedroza-Garcia JA, Zhu T, Li L, Vercauteren I, Van den Daele H, van de Cotte B, *et al* (2020) The cyclin CYCA3;4 is a postprophase target of the APC/CCCS52A2 E3-ligase controlling formative cell divisions in Arabidopsis. *Plant Cell* 32: 2979–2996
- Yamada M & Goshima G (2017) Mitotic spindle assembly in land plants: Molecules and mechanisms. *Biology (Basel)* 6: 1–20

## Thesis summary

In chapter 1, I present the characterization of the microtubule-associated function of the B1-type cyclins in *Arabidopsis thaliana*. This work is published in EMBO Reports. By using multiple mutant combinations, I show that CYCB1;2 is the most important B1-type cyclin for microtubule organization. Nevertheless, the function of the B1-type cyclins highly overlaps and is tissue-specific. For instance, I show CYCB1;2 to be crucial for endosperm divisions, acting together with CYCB1;1 and CYCB1;3. In sporophytic divisions, CYCB1;1 and CYCB1;2 act together, as judged by overall growth of the double *cycb1;1 cycb1;2* mutant combination. When gametophytic divisions are studied in detail, CYCB1;1, CYCB1;2 and CYCB1;4 appear essential for female gametophyte development, whereas CYCB1;2 and CYCB1;3 take over in male gametophyte development.

In chapter 2, I explore in detail the role of CYCB1-mediated phosphorylation of two MAPs, GIP1 and EDE1. GIP1 is an essential member of the main microtubule-nucleation complex  $\gamma$ TuRC, whereas EDE1 is an essential member of the augmin complex in G2/M. By mutating predicted phosphorylated residues of these proteins into an amino acid that cannot be phosphorylated (alanine), I show that the phosphorylation of EDE1 is crucial for its function. A protein version of EDE1 with eight residues mutated into alanine is not able to rescue the *ede1-1* mutant phenotype under microtubule-destabilizing conditions and produces spindles with altered architecture in this *ede1-1* background.

In chapter 3, I present the results of a project I have developed in diploid and tetraploid *Arabidopsis lyrata* and *Arabidopsis arenosa*. By using these out-crossing wild relatives of *Arabidopsis thaliana*, I tried to establish a model for the study of meiosis in auto- and allopolyploids. The initial idea was to follow meiosis in whole anthers by imaging meiotic protein reporters together with a microtubule reporter. However, the two species have shown to be resistant to *Agrobacterium*-mediated plant transformation and, therefore, the project was not fully carried out. Nevertheless, I present the results I obtained and discuss how the transformation of these species could be improved.



## **Chapter 1. B1-type cyclins control microtubule organization during cell division in *Arabidopsis* (published in EMBO reports)**

The following manuscript has been published in EMBO reports on the 9<sup>th</sup> of December of 2021 and is currently online with the following digital object identifier (DOI):  
10.15252/embr.202153995.









While I have performed most of the experiments and carried out manuscript writing and most of the data evaluation together with my supervisor Prof. Dr. Arp Schnittger, the following experiments or resources were provided by co-authors:

- Figures 3 and 4 were made based on female and male gametophytic analyses kindly performed by Dr. Xin' Ai Zhao
- Figures 5 and 6 were made based on root whole mount immunolocalization studies kindly performed by Katia Belcram and Dr. Martine Pastuglia and were analyzed with the help of Dr. David Bouchez
- Figure 7A-C was made based on *in vitro* kinase assays performed by Dr. Hirofumi Harashima
- The GFP-GIP1 reporter lines in Col-0 and *cycb1;1 cycb1;2* backgrounds used in figure 7D were made by Dr. Shinichiro Komaki
- Figure EV1 was prepared based on data provided by Dr. Petra Bulankova and Dr. Karel Riha
- Figure EV2 was prepared using images provided by Dr. Manoj Kumar
- Table 2 was prepared with allele transmission data kindly provided by Dr. Xin' Ai Zhao





# B1-type cyclins control microtubule organization during cell division in *Arabidopsis*

Mariana Romeiro Motta<sup>1</sup> , Xin'AI Zhao<sup>1,2</sup> , Martine Pastuglia<sup>3</sup>, Katia Belcram<sup>3</sup> , Farshad Roodbarkelari<sup>4</sup>, Maki Komaki<sup>1</sup>, Hirofumi Harashima<sup>5,†</sup>, Shinichiro Komaki<sup>1,6</sup> , Manoj Kumar<sup>7</sup>, Petra Bulankova<sup>8</sup> , Maren Heese<sup>1</sup> , Karel Riha<sup>9</sup> , David Bouchez<sup>3</sup> & Arp Schnittger<sup>1,\*</sup> 

## Abstract

Flowering plants contain a large number of cyclin families, each containing multiple members, most of which have not been characterized to date. Here, we analyzed the role of the B1 subclass of mitotic cyclins in cell cycle control during *Arabidopsis* development. While we reveal *CYCB1;5* to be a pseudogene, the remaining four members were found to be expressed in dividing cells. Mutant analyses showed a complex pattern of overlapping, development-specific requirements of B1-type cyclins with *CYCB1;2* playing a central role. The double mutant *cycb1;1 cycb1;2* is severely compromised in growth, yet viable beyond the seedling stage, hence representing a unique opportunity to study the function of B1-type cyclin activity at the organismic level. Immunolocalization of microtubules in *cycb1;1 cycb1;2* and treating mutants with the microtubule drug oryzalin revealed a key role of B1-type cyclins in orchestrating mitotic microtubule networks. Subsequently, we identified the GAMMA-TUBULIN COMPLEX PROTEIN 3-INTERACTING PROTEIN 1 (GIP1/MOZART) as an *in vitro* substrate of B1-type cyclin complexes and further genetic analyses support a potential role in the regulation of GIP1 by *CYCB1s*.

**Keywords** CDK; *CYCB1*; endosperm; microtubule nucleation; mitosis

**Subject Categories** Cell Cycle; Plant Biology

**DOI** 10.15252/embr.202153995 | Received 16 September 2021 | Revised 11 October 2021 | Accepted 14 October 2021 | Published online 9 December 2021

**EMBO Reports (2022) 23: e53995**

## Introduction

A highly elaborated control system guides cells through mitosis during which chromosomes are separated and distributed to the

newly forming daughter cells. Cyclin-dependent kinase (CDK)-cyclin complexes stand in the center of this control system (Morgan, 1997; Lindqvist *et al.*, 2009). In animals, Cdk1 together with B-type cyclins are an essential part of the so-called mitosis promoting factor (MPF) complex that phosphorylates a plethora of mitotic substrates including nuclear structure proteins, such as Lamin A and B, and chromosome segregation proteins, such as the spindle assembly factor TPX2 (Blethrow *et al.*, 2008). MPF activity is kept low prior to mitotic entry by excluding Cyclin B1 (CycB1) from the nucleus (Hagting *et al.*, 1998; Toyoshima *et al.*, 1998; Yang *et al.*, 1998). In addition, Cdk1-cyclin B complexes are inhibited by phosphorylation on two inhibitory residues, Thr14 and Tyr15 (or the homologous amino acids in the P-loop of the respective Cdk) by the action of Wee1 and/or Myt1 kinases (O'Farrell, 2001). After a threshold concentration of Cdk1-CycB1 is reached, CycB1 accumulates in the nucleus and the Cdk-CycB1 complex becomes activated by a group of dual-specificity Cdc25 phosphatases that remove the inhibitory phosphorylation from the P-loop of the kinase. Due to a negative feedback wiring with Wee1 and a positive feedback with Cdc25 (Tyson & Novak, 2001), Cdk1-cyclin activity levels rise rapidly and promote entry and progression through mitosis, including the separation of the duplicated centrosomes (spindle pole body in yeast) as a key step to generate a bipolar spindle (Lacey *et al.*, 1999; Haase *et al.*, 2001). Finally, to complete mitosis and promote cytokinesis, Cdk1-cyclin B levels have to drop. This is accomplished by the degradation of cyclin B mediated by the Anaphase Promoting Complex/Cyclosome (APC/C) (Nakayama & Nakayama, 2005).

While a wealth of information about the execution of mitosis exists in animals and yeast, information is still scarce in plants. Notably, flowering plants appear to regulate mitosis differently from yeast and animals. First of all, flowering plants do not contain centrosomes and it is still not fully understood how the mitotic

1 Department of Developmental Biology, University of Hamburg, Hamburg, Germany  
 2 Centre for Organismal Studies Heidelberg, University of Heidelberg, Heidelberg, Germany  
 3 Institute Jean-Pierre Bourgin, INRAE, AgroParisTech, Université Paris-Saclay, Versailles, France  
 4 BIOS Centre for Biological Signaling Studies, University of Freiburg, Freiburg, Germany  
 5 RIKEN Center for Sustainable Resource Science, Yokohama, Japan  
 6 Nara Institute of Science and Technology, Nara, Japan  
 7 Amity Institute of Genome Engineering, Amity University Uttar Pradesh, Sector 125, Noida, India  
 8 VIB-Ugent Center for Plant Systems Biology, Gent, Belgium  
 9 Central European Institute of Technology, Masaryk University, Brno, Czech Republic  
 \*Corresponding author. Tel: +49 40 428 16 502; Fax: +49 40 428 16 503; E-mail: arp.schnittger@uni-hamburg.de  
 †Present address: Solution Research Laboratory, AS ONE Corporation, Kawasaki, Japan

spindle is organized, although many microtubule-regulating components are conserved (Yamada & Goshima, 2017). Next, *Arabidopsis* WEE1 kinase was shown to prevent premature cell differentiation in S phase after DNA damage rather than functioning in mitotic control (De Schutter *et al*, 2007; Cools *et al*, 2011). Moreover, *Arabidopsis* does not contain a functional Cdc25 homolog, thus one of the most central control loops of the animal cell cycle is absent at least in this plant (Dissmeyer *et al*, 2009, 2010).

Another difference in mitotic regulation between plants and animals appears at the level of cyclins. In animals, D-type cyclins control entry into the S phase (G1 cyclins), while cyclin A controls the S phase as well as early mitotic events, and B-type cyclins control mitosis (Riabowol *et al*, 1989; Furuno *et al*, 1999). In contrast, functional studies and expression analyses have revealed that members of all three cyclin classes, that is, cyclin A, B, and D, are involved in the control of mitosis in plants (Schnittger *et al*, 2002; Menges *et al*, 2005; Dewitte *et al*, 2007; Boudolf *et al*, 2009; Vanneste *et al*, 2011). While there are only a few members in each cyclin family in metazoans, plant cyclin families are large, which makes functional studies challenging. For instance, as opposed to 3 B-type cyclins in mammals (CycB1, CycB2, and CycB3) and 2 in *Drosophila* (CycB1 and CycB3), there are 11 predicted B-type cyclins divided into three subgroups (B1, B2, and B3) in *Arabidopsis* that are all equally distant from animal B-type cyclins, that is, *Arabidopsis* B1-type cyclins are closer related to B2 and B3 from *Arabidopsis* than to any B-type cyclin from animals (Doerner *et al*, 1996; Vandepoele *et al*, 2002; Wang *et al*, 2004). This classification is currently only based on sequence similarities and for B-type cyclins, as for most other cyclins in plants, the biological role is far from being understood.

Here, we present a functional analysis of the largest class of B-type cyclins in *Arabidopsis*, that is, the five-member B1 group. We reveal a central role for *CYCB1;2* that is backed up by one or more of the other B1-type cyclins in a tissue-dependent manner. Unlike *CycB1* mutants in mouse (Brandeis *et al*, 1998), *Arabidopsis cycb1;1 cycb1;2* double mutants are viable, presenting a unique opportunity to study cyclin B function at an organismic level. This allowed us to reveal the organization of mitotic microtubules as the main function of B1-type cyclins in *Arabidopsis*, a finding supported by *in vitro* kinase assays that indicated that GIP1/MOZART, a key factor of microtubule organization, is a substrate of CDK-CYCB1 complexes.

## Results

### ***CYCB1;1*, *CYCB1;2*, and *CYCB1;3* are redundantly required for endosperm proliferation**

To start the characterization of B1-type cyclins, we first determined their expression pattern. To this end, we used previously generated promoter reporter lines comprising *GFP* fused to the N-terminal part of the respective cyclin (*CYCB1;1* to *CYCB1;4*), including the destruction box (Weimer *et al*, 2016). For *CYCB1;5*, since different annotations exist for this gene, we generated three different reporter constructs, each reaching to the different predicted transcriptional start sites. One upstream of the first ATG, one upstream of the second ATG, and the third one including the first and second upstream regions. However, in none of these *CYCB1;5* reporter lines

a signal could be detected. Therefore, we next analyzed the expression of *CYCB1;5* by qRT-PCR. Sequencing of the amplified products showed the existence of many different *CYCB1;5* cDNAs that exhibited exon skipping, intron retention, and use of internal polyadenylation sites (Fig EV1A–C), consistent with the lack of reliable transcriptional support for *CYCB1;5* in public depositories (The Arabidopsis Information Resource, TAIR). Taken together with data from previous studies (Bulankova *et al*, 2013) and the fact that many *Arabidopsis* accessions have accumulated several point mutations and even deletions in *CYCB1;5* (The Arabidopsis Information Resource, TAIR), we concluded that *CYCB1;5* is a pseudogene. In the following study, we therefore concentrated on the analysis of *CYCB1;1* through *CYCB1;4*.

The expression of the four B1-type cyclins has been previously described in a patchy pattern in regions with high cell proliferation activity, such as in the roots (Weimer *et al*, 2016). Hence, these cyclins seem to be true mitotically expressed genes. Furthermore, previous genome-wide expression studies have detected that the transcripts of all three B1-type cyclins *CYCB1;1*, *CYCB1;2*, and *CYCB1;3* are overrepresented in the developing endosperm (Day *et al*, 2008). In agreement, we found that the promoter reporter constructs for *CYCB1;1*, *CYCB1;2*, and *CYCB1;3* but not *CYCB1;4* were expressed during endosperm development (Fig EV2A).

To assess the individual biological role of B1-type cyclins, we then analyzed previously isolated null mutants for all four B1-type cyclins (Weimer *et al*, 2016). However, none of the single mutants showed an obvious deviation from the wild type under normal growth conditions, as for instance seen in root growth (Fig 1A) and seed viability (Fig 1F) in comparison to the wild type. This finding was consistent with former observations (Weimer *et al*, 2016). Since *CYCB1;1*, *CYCB1;2*, and *CYCB1;3* reporters have similar enrichment in the proliferating endosperm (Fig EV2A), and *CYCB1;1*, *CYCB1;2*, *CYCB1;3*, and *CYCB1;4* have a similar expression pattern in the roots, we reasoned that the B1-type cyclins might control mitotic divisions redundantly. Therefore, we also generated and analyzed all six possible double mutant combinations. The growth of the *cycb1;1 cycb1;2* double mutant was severely reduced (Fig 1B–D; for detailed characterization see below), while the size and morphology of the other double mutants were at a first look indistinguishable from the wild type.

An analysis of the siliques in the double mutants revealed that *cycb1;1 cycb1;3*, *cycb1;1 cycb1;4*, and *cycb1;3 cycb1;4* did not have a reduced seed set. In contrast, *cycb1;1 cycb1;2* and *cycb1;2 cycb1;3* had on average approximately half of the seeds aborted (Fig 1E and G;  $52.0\% \pm 13.5\%$ ,  $n = 3$  biological replicates, 550 seeds in total, for *cycb1;1 cycb1;2* and  $51.3\% \pm 7.2\%$ ,  $n = 3$  biological replicates, 769 seeds in total, for *cycb1;2 cycb1;3* vs.  $4.0\% \pm 3.2\%$ ,  $n = 3$  biological replicates, 821 seeds in total, for wild type, Col-0;  $P < 0.0001$  for both comparisons). The appearance of the aborted seeds varied in size and color (Fig 1E). Some seeds lacked the typical green color of a maturing embryo and looked transparent while others appeared brown and shriveled; in some cases, unfertilized or aborted ovules were visible.

To investigate the cause of this seed abortion, we collected, fixed and cleared seeds 3 days after pollination (DAP) (Fig 2). Since endosperm nuclei exhibit a strong autofluorescence, we were able to assess seed development quantitatively by using confocal laser scanning microscopy. In wild-type *Arabidopsis* seeds, a fertilized

central cell will undergo seven to eight cycles of free nuclear divisions leading to an estimated total of more than 200 nuclei in the endosperm of 3-day-old seeds (Boisnard-Lorig et al, 2001). In our analysis, the general morphology of the seeds at the single mutant level seemed unchanged in comparison to the wild type (Fig 2A). However, counting the number of endosperm nuclei 3 DAP in these

seeds displayed a strong reduction in endosperm divisions in the *cycb1;2* mutant (Fig 2C;  $94.1 \pm 55.4$  endosperm nuclei per seed,  $n = 30$ ) in comparison to the wild type (Col-0,  $175.2 \pm 43.6$ ,  $n = 30$ ;  $P < 0.0001$ ).

At the double mutant level, the general morphology of *cycb1;1 cycb1;2* and *cycb1;2 cycb1;3* seeds appeared abnormal 3 DAP

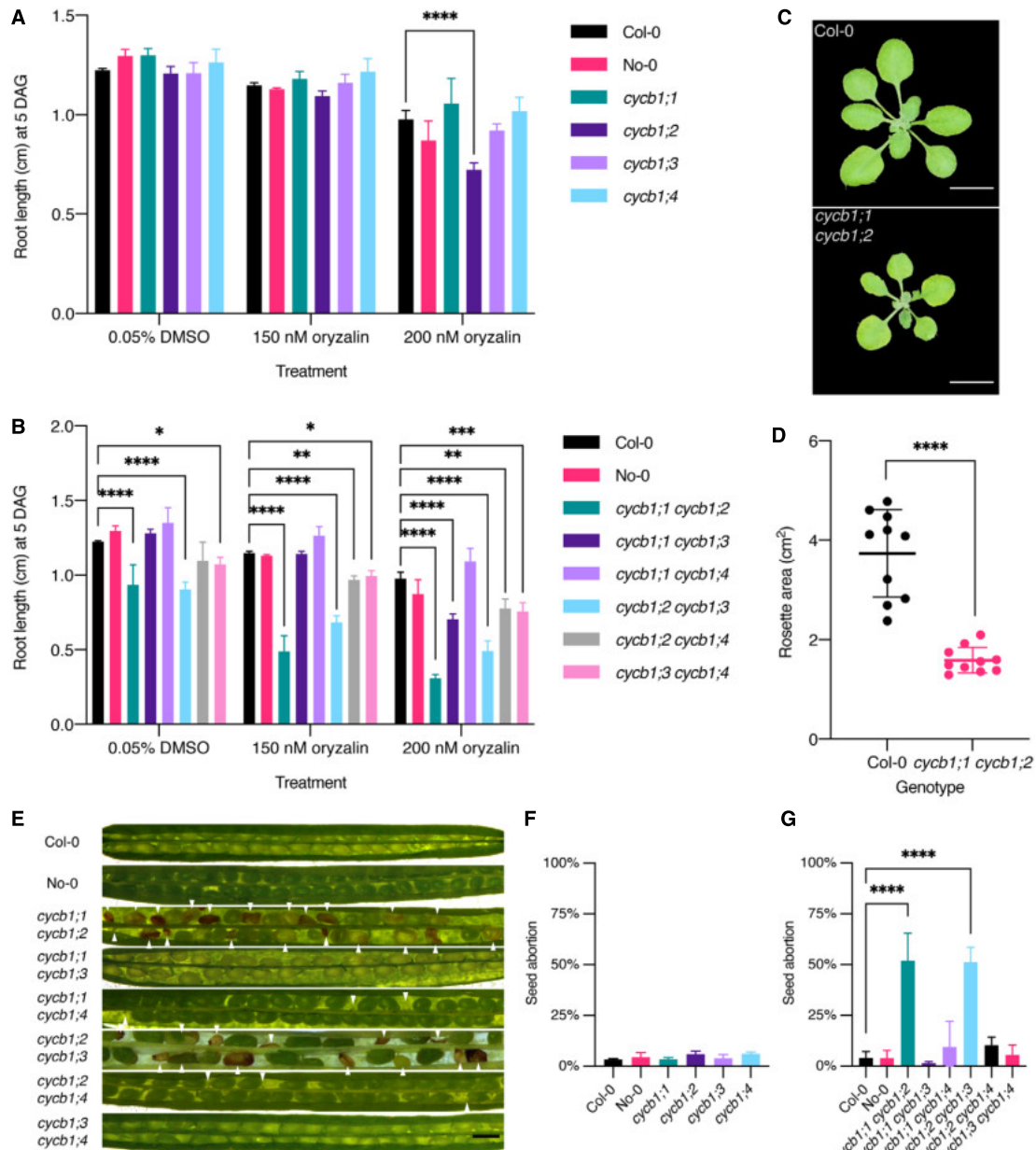


Figure 1.

**Figure 1. *cycb1;1 cycb1;2* mutants show decreased root growth and shoot development as well as higher seed abortion.**

- A, B Quantification of oryzalin root growth assays in single (A) and double (B) mutants. DAG, days after germination. Graphs show mean  $\pm$  SD of three biological replicates with at least 10 plants per genotype per replicate. Asterisks indicate a significant difference in root length in a two-way ANOVA followed by Tukey's multiple comparisons test (\* $P < 0.05$ , \*\* $P < 0.01$ , \*\*\* $P < 0.001$  and \*\*\*\* $P < 0.0001$ ).
- C Rosette pictures of 20-day-old Col-0 and *cycb1;1 cycb1;2*. Scale bar: 1 cm.
- D Quantification of the rosette area using total leaf surface in Col-0 and *cycb1;1 cycb1;2*. Graph represents the single rosette area values and the horizontal lines indicate the mean value  $\pm$  SD,  $n = 10$  plants per genotype. Asterisks indicate a significant difference in rosette area using an unpaired t-test,  $t = 7.421$ ,  $df = 18$  (\*\*\*\* $P < 0.0001$ ).
- E Silique pictures of *cycb1* double mutant combinations. White arrowheads indicate aborted ovules and seeds. Scale bars: 500  $\mu$ m.
- F, G Quantification of aborted seeds in single (F) and double (G) mutants. Graphs represent the average seed abortion rate per plant  $\pm$  SD of three biological replicates,  $n = 550$ – $1,029$  seeds analyzed per genotype. Asterisks indicate significant differences in seed abortion rate in an ordinary one-way ANOVA test, followed by a Dunnett's multiple comparisons test (\*\*\*\* $P < 0.0001$ ).

(Fig 2B). The endosperm nuclei number at this time point was dramatically reduced with only  $6 \pm 3$  in *cycb1;1 cycb1;2* ( $n = 26$ ) and  $28 \pm 9$  in *cycb1;2 cycb1;3* ( $n = 30$ ) in relation to  $77 \pm 19.3$  in the wild type (Fig 2D; Col-0,  $n = 30$ ;  $P < 0.0001$  for both comparisons). Moreover, the nuclei appeared to be extremely enlarged in *cycb1;1 cycb1;2* and *cycb1;2 cycb1;3* (Fig 2B; magenta arrowheads), and in *cycb1;2 cycb1;3* atypical agglomerates of micro-sized nuclei were seen (Fig 2B; green arrowheads). The strong accumulation of a reporter gene when expressed from the *CYCB1;1*, *CYCB1;2*, and *CYCB1;3* promoters in the seeds of these two double mutants consistently revealed enlarged nuclei which appeared, on the basis of reporter activity, to be halted at G2/M (Fig EV2B and C). The double mutant *cycb1;2 cycb1;4* also showed a decrease in endosperm nuclei number ( $33.4 \pm 12.87$ ,  $n = 30$ ) in relation to the wild type ( $P < 0.0001$ ), yet not as extensive as in the *cycb1;1 cycb1;2* and *cycb1;2 cycb1;3* double mutants and no major morphological abnormalities were identified, which could be explained by our observation that *CYCB1;4* was never expressed in the developing endosperm, consistent with the non-enrichment of the transcript in this tissue as shown in Day *et al*, 2008, and therefore *CYCB1;4* might not play a major role in endosperm divisions.

Taken together, we conclude that *CYCB1;2* is of major importance for the free nuclear divisions during endosperm development and acts redundantly with *CYCB1;1* and *CYCB1;3*.

#### **CYCB1;1, CYCB1;2, and CYCB1;4 together control female gametophyte development**

Up to this point, we did not find a clear role for *CYCB1;4*, suggesting even higher levels of redundancy among the B1-type cyclins or, alternatively, an overlapping function with other B-type cyclins in *Arabidopsis*. To clarify the relative contribution of the four *CYCB1* genes to development, we decided to investigate the role of the *CYCB1* group in detail by first constructing the triple *cycb1;1<sup>-/-</sup> cycb1;3<sup>-/-</sup> cycb1;4<sup>-/-</sup>* mutant. Notably, this triple mutant was not different from the wild type as, for instance, judged by overall growth, seed viability (Fig 3D), pollen development, and pollen viability (Fig 4C and E). This finding further underlined the paramount role of *CYCB1;2* among the B1-type cyclins. This result also indicated that *CYCB1;4*, if functionally relevant, may have a redundant role with either one or both of the two pairs *CYCB1;1 CYCB1;2* and *CYCB1;2 CYCB1;3*. To test this, we generated the triple and quadruple mutant combinations *cycb1;1<sup>-/-</sup> cycb1;2<sup>-/-</sup> cycb1;4<sup>-/-</sup>* and *cycb1;1<sup>-/-</sup> cycb1;2<sup>-/-</sup> cycb1;3<sup>-/-</sup> cycb1;4<sup>-/-</sup>*. While overall growth of the triple and quadruple mutant combinations (note that

at least one B1 gene is not homozygous mutant in these combinations) was similar to the wild-type, we found a strong reduction in fertility as siliques contained approximately 43% ( $\pm 0.4\%$ ,  $n = 3$  biological replicates, 500 seeds;  $P < 0.0001$ ) and 48% ( $\pm 2.1\%$ ,  $n = 3$  biological replicates, 579 seeds;  $P < 0.0001$ ) of aborting or unfertilized ovules and/or aborting seeds for *cycb1;1<sup>-/-</sup> cycb1;2<sup>-/-</sup> cycb1;4<sup>-/-</sup>* and *cycb1;1<sup>-/-</sup> cycb1;2<sup>-/-</sup> cycb1;3<sup>-/-</sup> cycb1;4<sup>-/-</sup>*, respectively, in comparison to the wild type (Fig 3D and E;  $0.8\% \pm 0.9\%$ ,  $n = 3$  biological replicates, 487 seeds). This abortion rate suggested a female gametophytic defect and we, therefore, analyzed embryo sac development in the mutants.

In wild-type *Arabidopsis* plants, an embryo sac develops from a megaspore that is released after meiosis (Drews & Yadegari, 2002). Every megaspore undergoes three rounds of nuclear divisions resulting in an eight-celled embryo sac that subsequently cellularizes. The two centrally located polar nuclei then fuse to generate the central cell nucleus while the three antipodal cells that lay at the opposite side of the egg cell undergo programmed cell death, resulting in a four-celled mature embryo sac that consists of a large, homodiploid central cell and an egg cell (red arrowheads; Fig 3A, Col-0) and two synergids that flank the egg cell (not shown). While this stereotypic wild-type developmental pattern was not significantly altered in *cycb1;1<sup>-/-</sup> cycb1;2<sup>-/-</sup>* double mutant combinations, consistent with the full transmission of the mutant allele through the female gametophyte (Table 1), we found embryo sacs from *cycb1;1<sup>-/-</sup> cycb1;2<sup>-/-</sup> cycb1;4<sup>-/-</sup>* and *cycb1;1<sup>-/-</sup> cycb1;2<sup>-/-</sup> cycb1;3<sup>-/-</sup> cycb1;4<sup>-/-</sup>* mutant combinations with only one, two, or four nuclei that did not show any sign of cellularization (Fig 3A); in addition, fuzzy embryo sacs were present in 30 and 27% of the cases, respectively, likely indicating degenerating tissues, which is consistent with an early arrest of gametophytic development. In total, 46% ( $n = 459$  embryo sacs analyzed) and 44.7% ( $n = 445$ ) of embryo sacs from plants of the *cycb1;1<sup>-/-</sup> cycb1;2<sup>-/-</sup> cycb1;4<sup>-/-</sup>* and *cycb1;1<sup>-/-</sup> cycb1;2<sup>-/-</sup> cycb1;3<sup>-/-</sup> cycb1;4<sup>-/-</sup>* combinations, respectively, were abnormal, in comparison to 6.2% ( $n = 210$ ) in the wild type ( $P < 0.0001$ ) and 6.8% in the *cycb1;1<sup>-/-</sup> cycb1;3<sup>-/-</sup> cycb1;4<sup>-/-</sup>* triple mutant (Fig 3B;  $P < 0.0001$ ). The observation that the triple *cycb1;1<sup>-/-</sup> cycb1;2<sup>-/-</sup> cycb1;4<sup>-/-</sup>* and quadruple *cycb1;1<sup>-/-</sup> cycb1;2<sup>-/-</sup> cycb1;3<sup>-/-</sup> cycb1;4<sup>-/-</sup>* mutants displayed a similar number of mutant embryo sacs (Fig 3B) suggests that *CYCB1;3* is not required, at least at this triple mutant level, for the divisions of the female gametophyte.

To assess the functionality of these embryo sacs, we pollinated the quadruple mutant combination with pollen from wild-type plants (Fig 3C). Supporting a female gametophytic defect, we observed a similar proportion of unfertilized and/or arrested

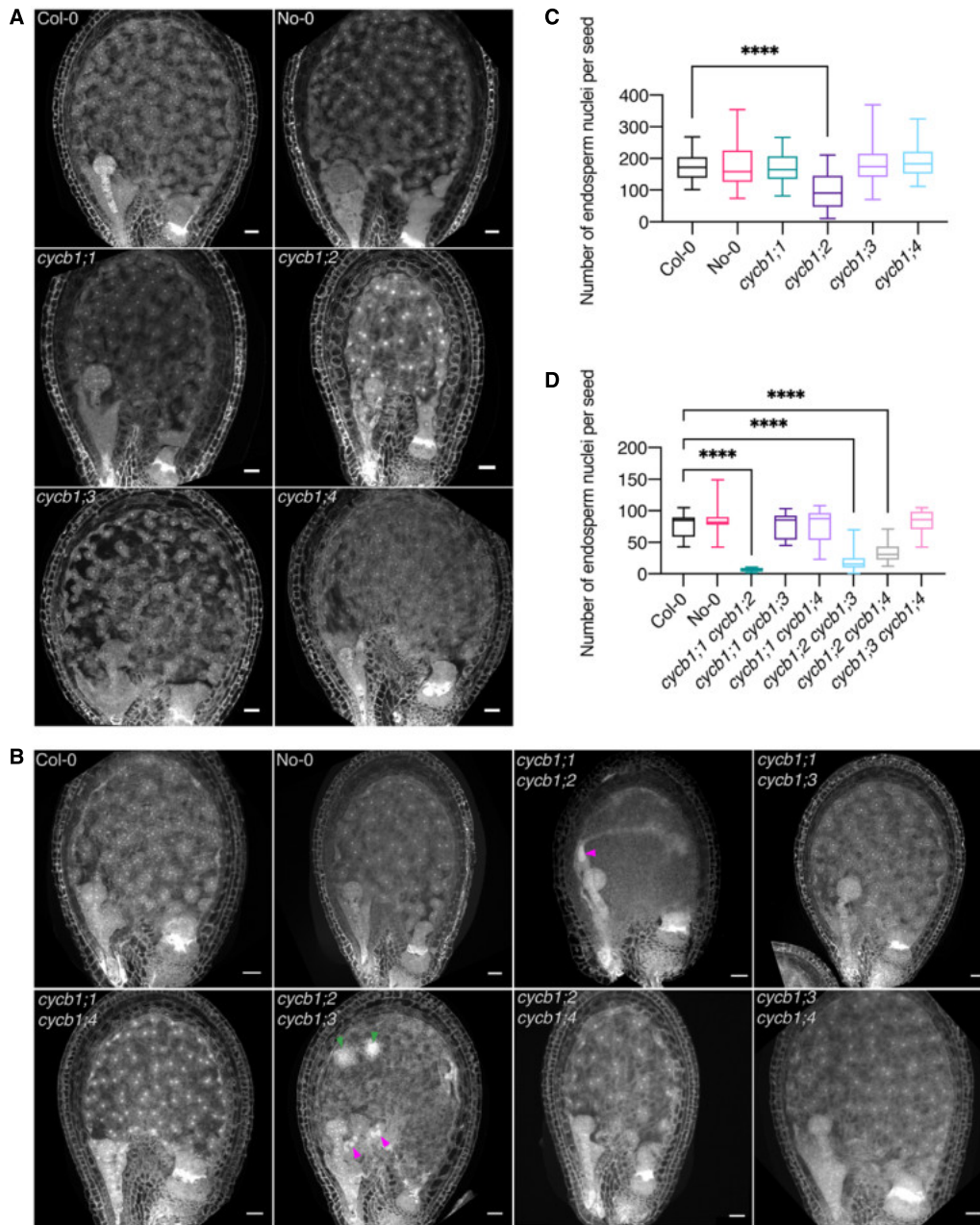


**Figure 2. CYCB1 mutations delay endosperm proliferation.**

A, B Confocal microscopy images of seeds 3 DAP. Endosperm and embryo morphology in *cycb1* single (A) and double (B) mutants. Magenta arrowheads indicate enlarged endosperm nuclei, while green arrowheads indicate atypical agglomerates of endosperm nuclei. Scale bars: 25  $\mu$ m.  
 C, D Quantification of endosperm nuclei in *cycb1* single (C) and double (D) mutants. Boxes and whiskers represent min to max values with the median indicated as a central horizontal line,  $n = 26\text{--}30$  seeds per genotype. Asterisks show significant differences in the number of endosperm nuclei per seed in a Kruskal–Wallis test followed by Dunn’s multiple comparisons test (\*\*\*\* $P < 0.0001$ ).

embryo sacs in these crosses 3 DAP (44.3%,  $n = 684$  seeds) in comparison to control crosses in which wild-type plants were used as a female parent fertilized with wild-type pollen (0.7% arrested embryo sacs,  $n = 597$ ). In reciprocal control crosses with pollen from mutant plants onto stigmas of wild-type plants, embryo and endosperm were formed in the developing seeds (seed

abortion = 2.9%,  $n = 902$  seeds). Thus, CYCB1;4, next to CYCB1;1 and CYCB1;2 appears to be required for embryo sac development. This was corroborated by analyzing the transmission of the *cycb1;2* and *cycb1;3* mutant alleles in reciprocal crosses of wild-type plants with the quadruple *cycb1;1<sup>-/-</sup> cycb1;2<sup>+/-</sup> cycb1;3<sup>+/-</sup> cycb1;4<sup>-/-</sup>* mutant. As expected, transmission of *cycb1;2* was abolished through

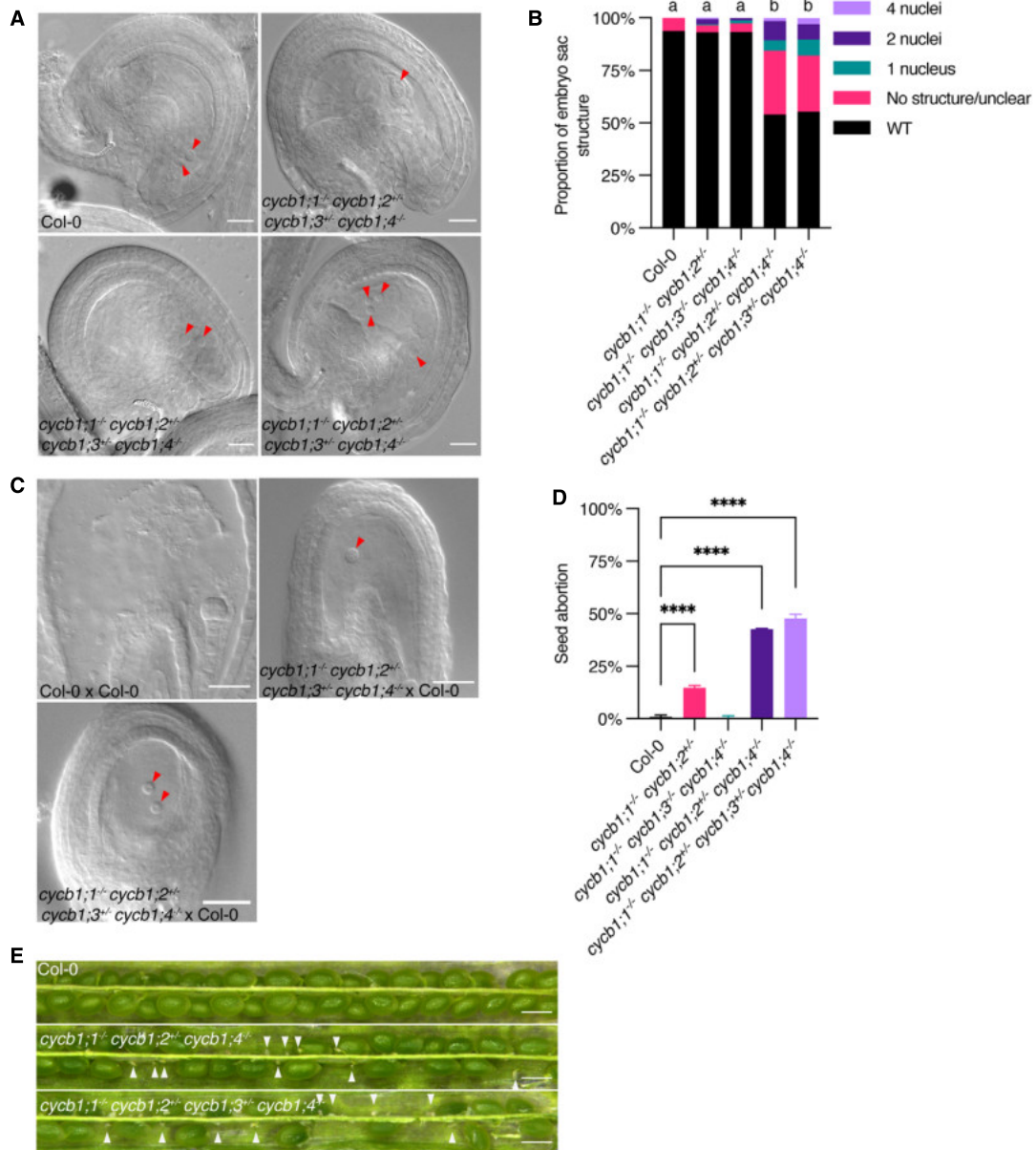


Figure 3.

**Figure 3. Embryo sac development is controlled by CYCB1 members.**

- A DIC images of abnormal embryo sacs in *cycb1* mutant combinations. Red arrowheads indicate the visible nuclei in Col-0 embryo sacs (central and egg cells) and the corresponding structures in the quadruple *cycb1;1<sup>-/-</sup> cycb1;2<sup>+/-</sup> cycb1;3<sup>+/-</sup> cycb1;4<sup>-/-</sup>* mutant. Scale bars: 20  $\mu$ m.
- B Quantification of the different abnormal embryo sac structures in *cycb1* mutant combinations ( $n = 202$ – $459$  embryo sacs per genotype). Different letters indicate significant differences in the proportion of abnormal embryo sacs in a Chi-squared test followed by the Marascuilo procedure to identify significant pairwise comparisons. WT, wild type.
- C DIC images of embryo sacs 3 DAP with wild-type pollen (female  $\times$  male). Red arrowheads indicate the visible embryo sac nuclei in the crosses with the quadruple *cycb1;1<sup>-/-</sup> cycb1;2<sup>+/-</sup> cycb1;3<sup>+/-</sup> cycb1;4<sup>-/-</sup>* mutant as a female donor, while the control Col-0  $\times$  Col-0 cross exhibits a developing embryo. Scale bars: 20  $\mu$ m.
- D Quantification of seed abortion in different *cycb1* mutant combinations. Graph represents the average seed abortion rate per plant  $\pm$  SD of three biological replicates,  $n = 463$ – $579$  seeds analyzed per genotype. Asterisks indicate significant differences in seed abortion rate in an ordinary one-way ANOVA test, followed by a Dunnett's multiple comparisons test (\*\*\*\* $P < 0.0001$ ).
- E Silique pictures of *cycb1* triple and quadruple mutants. White arrowheads indicate early aborted ovules. Scale bars: 500  $\mu$ m.

the female gametophyte (0%) and the efficiency in transmission was clearly reduced through the male gametophyte (70.8%) (Table 2), while the *cycb1;3* allele could be transmitted without an obvious reduction in efficiency through the females (92.7%).

Interestingly, the requirement of the B1-type cyclins was different on the male side. Pollen develops from microspores through two consecutive divisions resulting in a tricellular grain that harbors two sperms next to one vegetative cell (McCormick, 2004) (Fig 4). We observed that both the *cycb1;2* as well as the *cycb1;3* mutant alleles were not fully transmitted through pollen in a cross of *cycb1;1<sup>-/-</sup> cycb1;2<sup>+/-</sup> cycb1;3<sup>+/-</sup> cycb1;4<sup>-/-</sup>* with wild type plants (Table 2; 70.8 and 30.2% transmission efficiency, respectively), indicating that all four B1-type cyclins contribute to the mitotic divisions of the developing pollen grain. Consistent with the reduced transmission, we also found pollen grains in mature anthers of *cycb1;1<sup>-/-</sup> cycb1;2<sup>+/-</sup> cycb1;4<sup>-/-</sup>* and *cycb1;1<sup>-/-</sup> cycb1;2<sup>+/-</sup> cycb1;3<sup>+/-</sup> cycb1;4<sup>-/-</sup>* mutant combinations that comprised, instead of three, only two or sometimes even one cell (Fig 4A–C). Accordingly, differential staining of aborted and non-aborted pollen showed an increased pollen abortion in the triple and quadruple mutants (Fig 4D and E) to 8.9% ( $n = 403$  pollen grains analyzed) and 14.1% ( $n = 467$ ), respectively, in relation to the wild type (Col-0, 0.5%,  $n = 404$ ;  $P < 0.0001$ ).

Taken together, CYCB1;2 is also the most important B1-type cyclin during gametophyte development. CYCB1;3 appears to have only a minor role during female gametophyte development where instead CYCB1;4 acts together with CYCB1;1 and CYCB1;2. Remarkably, after fertilization the requirement changes, as presented above, and CYCB1;3 instead of CYCB1;4 is necessary for endosperm development.

#### Root growth under microtubule-destabilizing conditions underlines the redundant role of CYCB1;1, CYCB1;2, and CYCB1;3 in regulating the cytoskeleton

Considering the severe reduction of growth in *cycb1;1 cycb1;2* mutants (Fig 1; see above) and to explore the role of CYCB1;2 and the other B1-type cyclins in controlling the microtubule cytoskeleton, we next analyzed the growth of B1-type cyclin mutants on medium containing the microtubule poison oryzalin. The rationale is that a minor defect in the mutants could become more prominent if the microtubule cytoskeleton is already slightly compromised. To that end, we compared the root growth of *cycb1* single and double mutants in  $\frac{1}{2}$  MS medium containing 150 or 200 nM oryzalin (Fig 1A and B, respectively; Figs EV3A–C and EV4A–C). As shown

above, under control conditions (0.05% DMSO), the single *cycb1* mutants had similar root growth to the wild type (Fig 1A). Once oryzalin was applied at 200 nM, *cycb1;2* grew significantly less ( $0.7 \pm 0.03$  cm,  $n = 3$  biological replicates with at least 10 plants each) when compared to the wild type (Col-0,  $1.0 \pm 0.04$  cm,  $n = 3$ ;  $P < 0.0001$ ).

At the double mutant level, some combinations already showed a significantly shorter root even in control conditions (Fig 1B), such as *cycb1;1 cycb1;2* ( $0.9 \pm 0.1$  cm,  $n = 3$ ;  $P < 0.0001$ ) and *cycb1;2 cycb1;3* ( $0.9 \pm 0.05$  cm,  $n = 3$ ;  $P < 0.0001$ ) in comparison to the wild type (Col-0,  $1.2 \pm 0.009$  cm,  $n = 3$ ). When 150 nM oryzalin was applied, the growth of Col-0 was reduced by approximately 6%, while *cycb1;1 cycb1;2* had a reduction of almost 50% in growth and *cycb1;2 cycb1;3* had a reduction of around 24%. As the concentration of oryzalin increased to 200 nM oryzalin, the difference in growth between Col-0 and other double mutants, such as *cycb1;2 cycb1;4* and *cycb1;3 cycb1;4*, became more pronounced. However, most strikingly, *cycb1;1 cycb1;3* mutants, which so far had shown no specific phenotype and no reduction in shoot or root growth, grew significantly shorter at 200 nM oryzalin ( $0.7 \pm 0.04$  cm,  $n = 3$ ) in comparison to the wild type (Col-0,  $1.0 \pm 0.04$  cm,  $n = 3$ ;  $P < 0.0001$ ).

Collectively, a major function of all four B1-type cyclins seems to be regulating the microtubule cytoskeleton.

#### CYCB1;1 and CYCB1;2 control the organization of different microtubule arrays in the roots

Following our finding that *cycb1;1 cycb1;2* and *cycb1;2 cycb1;3* mutants have a severe reduction in root growth both in control and especially in microtubule-depolymerizing conditions, we performed whole mount immunolocalization studies against  $\alpha$ -tubulin and KNOLLE, which is a G2/M and cell plate marker (Figs 5 and 6). By analyzing mitotic divisions in the roots of these double mutants, a more detailed picture of cell division appeared.

Preceding a mitotic division, a band of microtubules that encircles the nucleus at the equatorial plane, the so-called preprophase band (PPB), will form at the site of the future division plane. The PPB functions as a positional cue and anchoring site for proteins involved in the cell division site determination and by that contributes to the robustness of cell divisions (Schaefer et al, 2017). Following nuclear envelope breakdown, the barrel-shaped acentrosomal spindle that is responsible for separating the chromosomes forms. After proper bipolar kinetochore-microtubule attachments

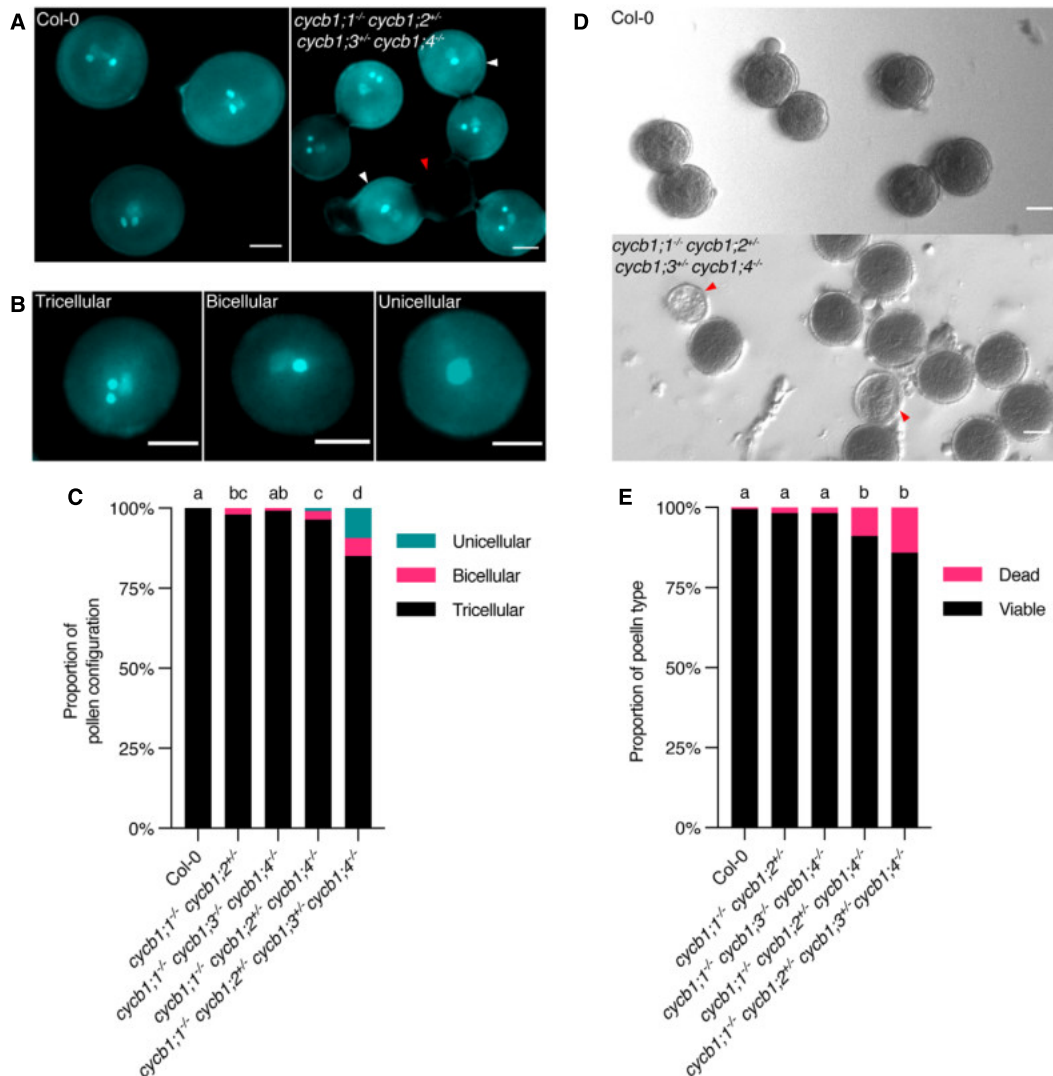


**Figure 4. Pollen development is affected by mutations in the CYCB1 group.**

A, B DAPI staining of pollen in *cycb1* mutants, including pollen configurations found in *cycb1;1<sup>-/-</sup> cycb1;2<sup>+/-</sup> cycb1;3<sup>+/-</sup> cycb1;4<sup>-/-</sup>* mutants (B). Scale bars: 5  $\mu$ m.  
 C Quantification of DAPI-stained pollen configurations in different *cycb1* mutant combinations,  $n = 420$ –616 pollen grains per genotype. Different letters indicate significant differences in the proportion of abnormal pollen (uni- and bicellular) in a Chi-squared test followed by the Marascuilo procedure to identify significant pairwise comparisons.  
 D Alexander staining of mature pollen indicating pollen viability. Scale bars: 5  $\mu$ m.  
 E Quantification of Alexander stained pollen viability,  $n = 403$ –498 pollen grains per genotype. Different letters indicate significant differences in the proportion of dead pollen in a Chi-squared test followed by the Marascuilo procedure to identify significant pairwise comparisons.

Data information: Red arrowheads indicate dead pollen, while white arrowheads indicate bicellular pollen.

occur and enough tension is sensed, sister chromatids are pulled toward opposing poles. Next, the phragmoplast, which is a bipolar microtubule structure that expands in time toward the cell cortex, forms. The phragmoplast is a scaffold for cell wall formation on

which vesicles are transported toward the microtubule-devoid midzone, where a growing cell plate is located.

As the cell progresses from G2 toward mitosis, the nuclear surface becomes a prominent site of microtubule nucleation. In *cycb1;1*



**Table 1. Transmission efficiency of the *cycb1;1* and *cycb1;3* mutant alleles in reciprocal crosses of a triple mutant with wild type.**

| Parental genotypes (female x male)  | Mutant allele  |                | Number of seeds (n) |
|---|----------------|----------------|---------------------|
|   | <i>cycb1;1</i> | <i>cycb1;3</i> |                     |
| <i>cycb1;1</i> <sup>-/-</sup> <i>cycb1;2</i> <sup>-/-</sup> <i>cycb1;3</i> <sup>-/-</sup> × Col-0 | 92%            | 98%            | 94                  |
| Col-0 × <i>cycb1;1</i> <sup>-/-</sup> <i>cycb1;2</i> <sup>-/-</sup> <i>cycb1;3</i> <sup>-/-</sup> | 106%           | 100%           | 90                  |

A transmission efficiency of 100% indicates full transmission of the mutant allele; that is, 50% of the genotyped F1 seedlings are heterozygous. A transmission efficiency may be higher than 100% if one of the two alleles is transmitted in a reduced manner, conversely making the other allele overrepresented. A z-test for one proportion was performed to test whether the observed transmission frequencies differ from expected values and the significance level was corrected for multiple comparisons using Bonferroni. Asterisks indicate significant differences from expected values. Primers used for genotyping are listed in Table EV1.

**Table 2. Transmission efficiency of the *cycb1;2* and *cycb1;3* mutant alleles in reciprocal crosses of a quadruple mutant with wild type.**

| Parental genotypes (female × male)  | Mutant allele  |                | Number of seeds (n) |
|---|----------------|----------------|---------------------|
|   | <i>cycb1;2</i> | <i>cycb1;3</i> |                     |
| <i>cycb1;1</i> <sup>-/-</sup> <i>cycb1;2</i> <sup>-/-</sup><br><i>cycb1;3</i> <sup>-/-</sup> <i>cycb1;4</i> <sup>-/-</sup><br>× Col-0 | 0%****         | 92.7%****      | 192                 |
| Col-0 × <i>cycb1;1</i> <sup>-/-</sup><br><i>cycb1;2</i> <sup>-/-</sup> <i>cycb1;3</i> <sup>-/-</sup><br><i>cycb1;4</i> <sup>-/-</sup> | 70.84%****     | 30.2%****      | 192                 |

A transmission efficiency of 100% indicates full transmission of the mutant allele, that is, 50% of the genotyped F1 seedlings are heterozygous. A transmission efficiency may be higher than 100% if one of the two alleles is transmitted in a reduced manner, conversely making the other allele overrepresented. A z-test for one proportion was performed to test if the observed transmission frequencies differ from expected values and the significance level was corrected for multiple comparisons using Bonferroni. Asterisks indicate significant differences from expected values (\*\*\*\**P* < 0.0001). Primers used for genotyping are listed in Table EV1.

*cycb1;2* and *cycb1;2 cycb1;3* mutants, at the PPB stage, we observed an increase in perinuclear microtubules, with an average of 18.3% PPBs with prominent microtubules in Col-0 versus 34 and 30% in *cycb1;1 cycb1;2* and *cycb1;2 cycb1;3*, respectively (Fig 5B and E). Either *cycb1* mutations induce an early accumulation of perinuclear microtubules or else the “mature” PPB stage, that is, with perinuclear microtubules, lasts longer in the *cycb1* mutants, and cells have trouble progressing into mitosis. In the stele and pericycle cells of the *cycb1;1 cycb1;2* double mutant, we also observed cells harboring double PPBs and cells with misplaced PPBs, that is, PPBs that did not align properly at the equatorial plane of the nucleus. These double and misplaced PPBs were rarely seen in Col-0 wild-type plants; we found 6.50% double PPBs in *cycb1;1 cycb1;2* in

comparison to 0.22% in wild type (*P* < 0.0001) and 6.21% misplaced PPBs in comparison to 2.38% in wild type (*P* = 0.009; Fig 5A and D).

At the spindle stage, irregular chromosome configurations were observed in *cycb1;1 cycb1;2*, with a significantly larger number of metaphase and anaphase spindles with chromosome laggards (Fig 5C and F). Although the number of spindles with lagging chromosomes in *cycb1;2 cycb1;3* was not significantly larger than in the wild type, the impairment seen in those mutants in chromosome alignment was much more severe than that of the wild-type plants, that is, chromosomes were seen far away from the metaphase plate. Finally, abnormal phragmoplasts were observed in the two double mutant combinations, including fragmented phragmoplasts, deformed phragmoplasts around abnormally shaped nuclei, and daughter cells with incompletely separated nuclei (*P* < 0.0001; Fig 6A and B). These abnormal phragmoplasts were likely a consequence of the irregular chromosome alignment and segregation seen in metaphase and anaphase. In short, all microtubule arrays were affected in the double mutants to a smaller or larger degree.

Next, we analyzed the proportion of cells at PPB, spindle, and phragmoplast stages per root (Fig 6C). A significantly larger proportion of cells in both prospindle and early spindle stages were observed in *cycb1;1 cycb1;2* and *cycb1;2 cycb1;3* mutants (*P* < 0.0001), which indicates that these stages are delayed in those mutants. The phragmoplast stage is proportionally shorter in the *cycb1;1 cycb1;2* mutant, although this could be a direct consequence of the extended spindle stage since, if the proportions of some stages increase, the others decrease automatically. Accordingly, a flow cytometrical analysis revealed that *cycb1;1 cycb1;2* mutants have a higher proportion of 4C, 8C, and 16C nuclei in comparison to the wild type (Fig EV5), which is an indication that these mutants have longer G2 and/or M phases. An increase in polyploid cells could have two, not mutually excluding, reasons. First, a failure to

**Figure 5. The double *cycb1;1 cycb1;2* mutant has abnormal microtubule arrays.**

- A–C Co-immunolocalization against tubulin (magenta) and KNOLLE (green) in root meristematic cells. Nuclei were counterstained with DAPI for the DNA (cyan). White arrowheads indicate laggards in the metaphase stage. Scale bars: 5 μm.
- D Quantification of wild-type (WT), double, and misplaced PPBs. Different letters indicate significant differences in the proportions of the different arrays per category in a Chi-squared test followed by the Marascuilo procedure to identify significant pairwise comparisons. Ten roots were analyzed per genotype.
- E Quantification of PPBs with prominent perinuclear microtubules (MTs). Boxes and whiskers represent min to max values with the median indicated as a central horizontal line, *n* = 10 roots per genotype. Asterisks show significant differences in the percentage of PPBs with prominent perinuclear microtubules per root in an ANOVA test followed by Dunnett's multiple comparisons test (\*\**P* < 0.01 and \*\*\*\**P* < 0.0001).
- F Quantification of spindles with lagging chromosomes. Boxes and whiskers represent min to max values with the median indicated as a central horizontal line, *n* = 10 roots per genotype. Asterisks show significant differences in the percentage of spindles with lagging chromosomes per root in a Kruskal–Wallis test followed by Dunn's multiple comparisons test (\*\**P* < 0.01 and ns, non-significant).

Source data are available online for this figure.

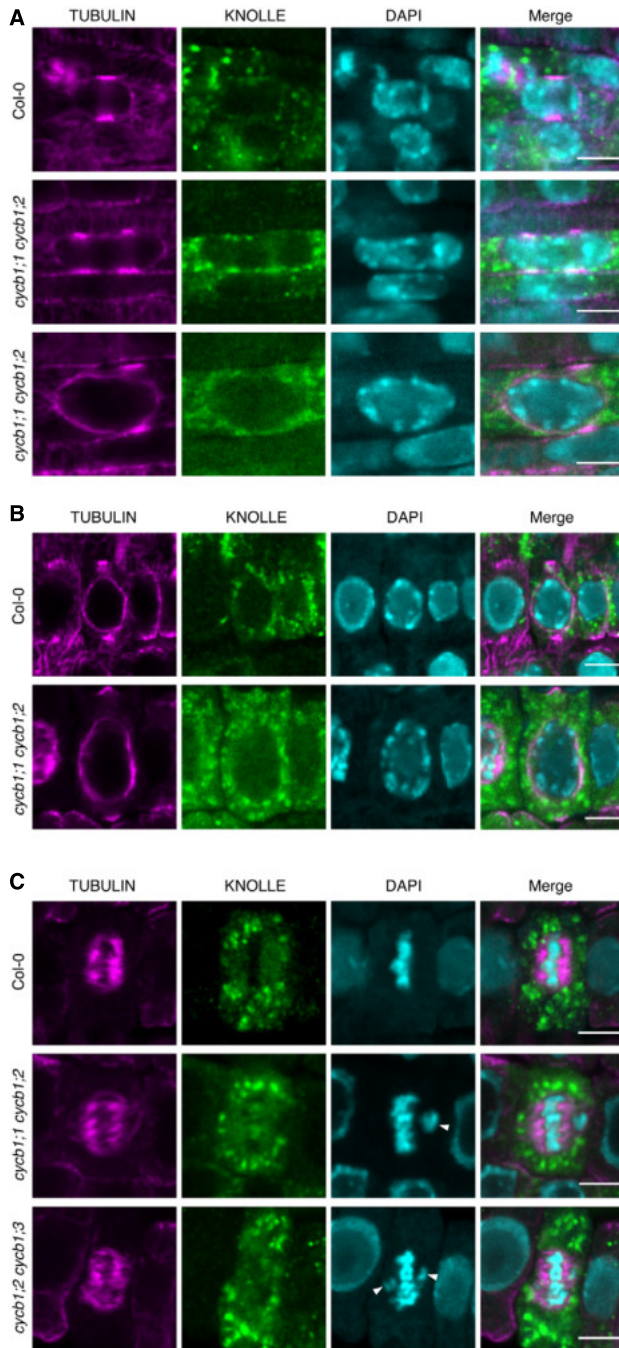
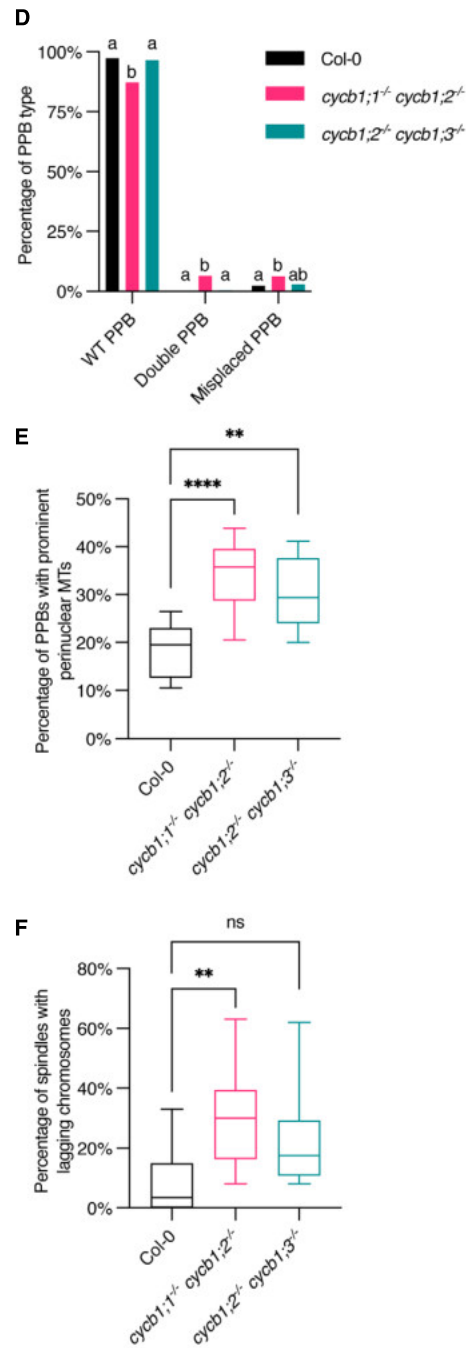
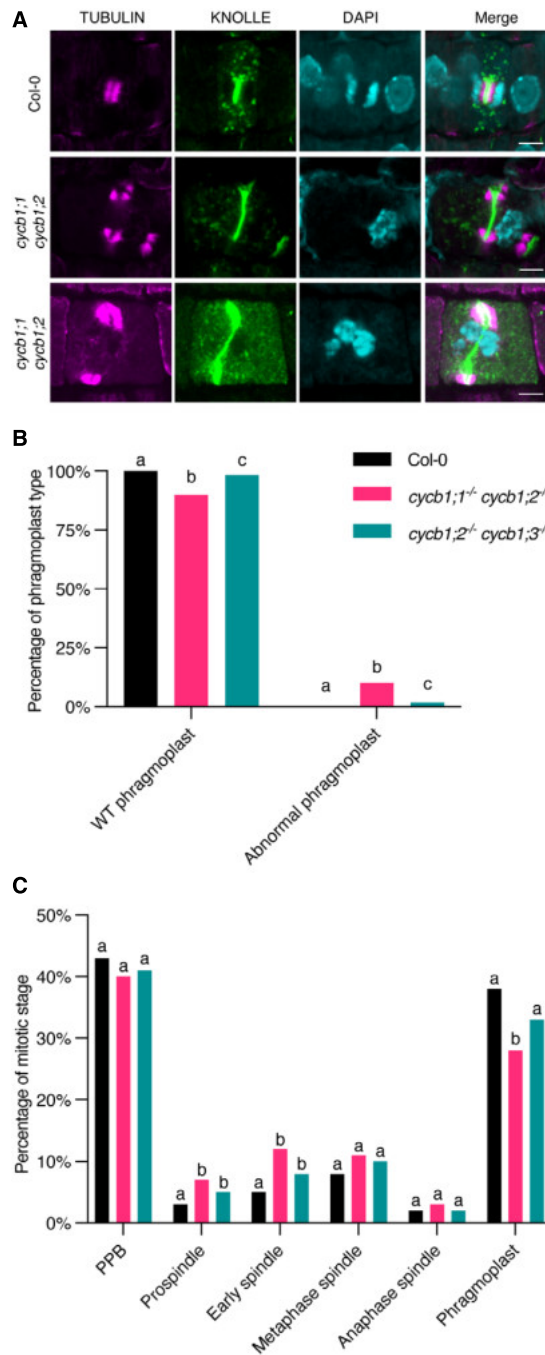


Figure 5.





**Figure 6. Both *cycb1;1 cycb1;2* and *cycb1;2 cycb1;3* have abnormal phragmoplasts and extended spindle stages.**

A Co-immunolocalization against tubulin (magenta) and KNOLLE (green) in root meristematic cells. Nuclei were counterstained with DAPI for the DNA (cyan). Scale bars: 5  $\mu$ m.

B Quantification of wild-type (WT) and abnormal phragmoplasts. Different letters indicate significant differences in the proportions of the different arrays per category in a Chi-squared test followed by the Marascuilo procedure to identify significant pairwise comparisons. Ten roots were analyzed per genotype.

C Quantification of the different mitotic stages in roots of the different genotypes. Different letters indicate significant differences in the proportions of the different arrays per category in a Chi-squared test followed by the Marascuilo procedure to identify significant pairwise comparisons. Ten roots were analyzed per genotype.

Source data are available online for this figure.

were observed, suggesting the formation of aneuploidies as a result of irregular mitotic divisions in this genotype.

In summary, CYCB1;1 and CYCB1;2 seem to be both redundantly required for robust root mitotic divisions under normal conditions, with CYCB1;3 playing a secondary role.

#### The CYCB1 group forms active complexes mainly together with CDKB2;2 and can phosphorylate a MAP

Previous studies have shown that all B1-type cyclins can interact with all five major cell cycle CDKs from *Arabidopsis*, that is, CDKA;1, CDKB1;1, CDKB1;2, CDKB2;1, and CDKB2;2 (Van Leene *et al.*, 2010). However, when we assessed the biochemical activity of all four B1-type cyclins with CDKA;1, CDKB1;1, and CDKB2;2, as representative members of the major cell cycle CDKs, in comparative *in vitro* kinase assays against Histone H1, a well-known, generic CDK substrate (Harashima & Schnittger, 2012), a more complex pattern appeared (Fig 7A and C). As a general principle, all four B1-type cyclins build the most active complexes with CDKB2;2, which is strictly expressed in mitosis. CYCB1;1 and CYCB1;4 showed overall the highest activity levels with CDKB2;2, followed by CYCB1;2 with CDKB2;2, while the CYCB1;3-CDKB2;2 pair was the least active among the CYCB1-CDKB2 complexes. Although much less than in complex with CDKB2;2, CYCB1;1, CYCB1;2, and CYCB1;4 could also phosphorylate Histone H1 together with CDKB1;1, but little to no activity was found in complexes with CDKA;1. In contrast, we could not detect any activity of CYCB1;3-CDKB1;1 complexes, while CYCB1;3 with CDKA;1 was almost as active as CYCB1;3-CDKB2;2 pairs.

The abnormal microtubule pattern observed in *cycb1;1 cycb1;2* mutants was reminiscent of the defects observed in microtubule binding and organizing protein mutants, such as in *gip1 gip2* double mutants (Janski *et al.*, 2012; Nakamura *et al.*, 2012), which are homologs of MOZART1 in animals. The *gip1 gip2* double knock-down mutant displays growth defects, sterility, defective microtubule arrays, and spindles with irregular polarity, which is linked to chromosome laggards in metaphase and anaphase and aneuploidy (Janski *et al.*, 2012). Additionally, the  $\gamma$ -tubulin *tubg1 tubg2* mutants display similar aberrant female and male gametophytes, with abnormal embryo sacs and reduced pollen nuclei number (Pastuglia *et al.*, 2006). This suggested that CDK complexes containing B1-type cyclins might phosphorylate the GIPs and/or other

undergo cytokinesis. Second, a compromised division program leading to premature exit from proliferation and entry into differentiation accompanied by endoreplication. In addition, broader peaks

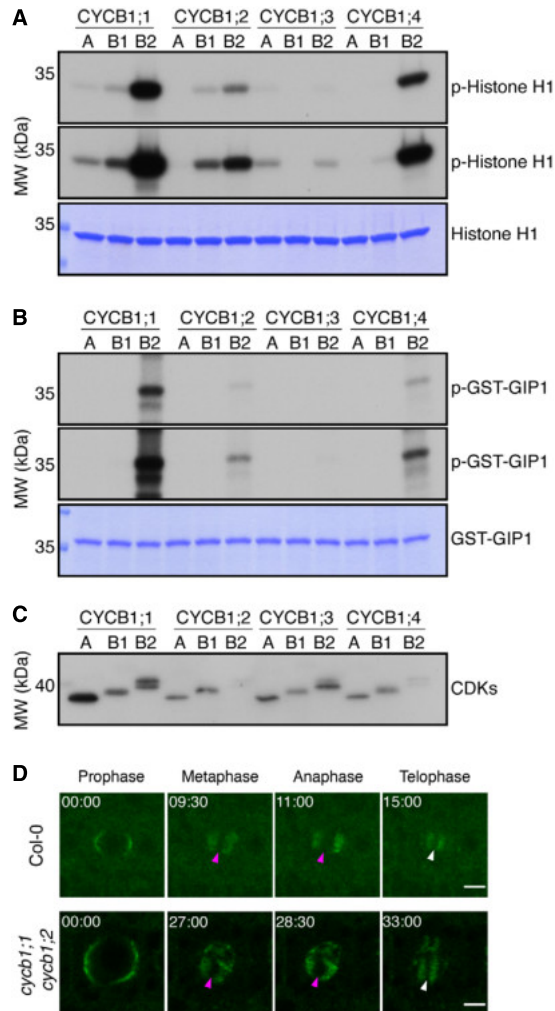


**Figure 7. CYCB1-CDKB2 complexes are the most active and are able to phosphorylate a MT-nucleation factor.**

A Kinase assays against Histone H1. Top and middle panels indicate shorter and longer exposures, respectively, of the same kinase assays. Bottom panel is a CBB staining of Histone H1 showing equal loading of the protein. A: CDKA;1, B1: CDKB1;1, B2: CDKB2;2.

B Kinase assays against GIP1. Top and middle panels indicate shorter and longer exposures, respectively, of the same kinase assays. Bottom panel is a CBB staining of GIP1 showing equal loading of the protein. A: CDKA;1, B1: CDKB1;1, B2: CDKB2;2.

C Western blot against StrepIII-tagged proteins to show loaded amounts of the CDKs. A: CDKA;1, B1: CDKB1;1, B2: CDKB2;2. Double CDKB2;2 bands are likely due to a truncation of the expressed protein.

D Time lapse of confocal microscope pictures of root meristematic cells tagged with GFP-GIP1 in Col-0 (top panel) and *cycb1;1 cycb1;2* (bottom panel). GIP1 localizes at the nuclear polar caps, followed by co-localization with microtubules at the spindle and phragmoplast arrays. In *cycb1;1 cycb1;2* double mutants, GIP1 exhibited an abnormal localization, being found at the spindle (magenta arrowheads) and phragmoplast (white arrowheads) midzones, which are normally devoid of the protein. Scale bars: 5  $\mu$ m.

whether the missing triple mutant was due to a gametophytic and/or embryonic defect, we performed reciprocal crosses with *gip1<sup>-/-</sup> cycb1;1<sup>-/-</sup> cycb1;2<sup>+/-</sup>* and *gip2<sup>-/-</sup> cycb1;1<sup>-/-</sup> cycb1;2<sup>+/-</sup>* as male and female donors with Col-0 (Table 4). With the exception of a reduced transmission efficiency of *cycb1;2* through the female gametophyte of approximately 65% in *gip2<sup>-/-</sup> cycb1;1<sup>-/-</sup> cycb1;2<sup>+/-</sup>* crosses with the wild type, we observed that both *gip1 cycb1;1 cycb1;2* and *gip2 cycb1;1 cycb1;2* gametes were largely viable and transmitted through both the female and male sides. This indicated that the triple *gip2<sup>-/-</sup> cycb1;1<sup>-/-</sup> cycb1;2<sup>-/-</sup>* mutation is embryo lethal.

Based on the results of our segregation analysis and reciprocal crosses (Tables 3 and 4), the assumption that GIP1 and GIP2 are completely interchangeable is challenged. It seems likely that GIP1 but not GIP2 is regulated by a CYCB1-dependent process. Thus, we generated a 2,849-bp genomic *GFP-GIP1* reporter in order to follow protein localization in the *cycb1;1 cycb1;2* mutant background (Fig 7D). We reasoned that, if GIP1 is indeed modulated by the CYCB1-CDK complexes, protein localization would be impaired in a *cycb1* mutant background. A cause–consequence relationship, however, is hard to establish, since defective microtubule structures as a consequence of other faulty pathways might also result in mislocalization of GIP1.

GIP1 is a microtubule nucleation factor and mainly localizes to microtubule minus ends across mitosis. At prophase, it localizes at the nuclear surface. At metaphase and anaphase, it is directed to the two spindle poles, co-localizing with microtubule minus ends. At telophase, it localizes at the two opposing sides of the phragmoplast, directing microtubule nucleation toward the midzone. With some degree of variation between divisions, GFP-GIP1 localization differed greatly in *cycb1;1 cycb1;2* mutants in comparison to the wild type. In some cases, GFP-GIP1 was found to remain in the spindle midzone (Fig 7D; magenta arrowheads) during metaphase in abnormal mitotic divisions. The resulting phragmoplast, which is normally devoid of GIP1 in its midzone (Fig 7D; white arrowheads), also contained remaining GIP1. The duration of these abnormal mitotic divisions in the double mutant was also around double the time of the wild-type divisions (Fig 7D). Thus, we conclude that B1-

microtubule-organizing proteins. Indeed, GIP1 but not GIP2 contains a consensus CDK phosphorylation site at position T67. Therefore, we expressed GIP1 in bacteria and subjected it to *in vitro* kinase assays with all four CYCB1 members each paired with either CDKA;1, CDKB1;1, or CDKB2;2. High activity levels against GIP1 were found for CYCB1;1, CYCB1;2, and CYCB1;4 (Fig 7B and C). However, these B1-type cyclins phosphorylated GIP1 only in combination with CDKB2;2, highlighting the importance of both the cyclin and the CDK partner for substrate recognition in plants and further emphasizing B2-type CDKs as the most important partners of the cyclin B1 group.

Following the finding that GIP1 is phosphorylated by CYCB1-CDKB2;2 complexes, we decided to generate triple *gip1 cycb1;1 cycb1;2* and *gip2 cycb1;1 cycb1;2* mutants. However, we were never able to isolate *gip2 cycb1;1 cycb1;2* mutants (Table 3). To address

**Table 3. Distortion of *cycb1;2* segregation in a *gip2*<sup>-/-</sup> *cycb1;1*<sup>-/-</sup> *cycb1;2*<sup>+/-</sup> background.**

| Genotype (selfed)  | Genotype of progeny           |                               |                               | Number of seeds (n) |
|--|-------------------------------|-------------------------------|-------------------------------|---------------------|
|  | <i>cycb1;2</i> <sup>+/-</sup> | <i>cycb1;2</i> <sup>-/-</sup> | <i>cycb1;2</i> <sup>-/-</sup> |                     |
| <i>cycb1;1</i> <sup>-/-</sup> <i>cycb1;2</i> <sup>+/-</sup>                            | 25.26%                        | 65.26%                        | 9.47%**                       | 95                  |
| <i>gip1</i> <sup>-/-</sup> <i>cycb1;1</i> <sup>-/-</sup> <i>cycb1;2</i> <sup>+/-</sup> | 31.25%                        | 64.58%                        | 4.17%****                     | 96                  |
| <i>gip2</i> <sup>-/-</sup> <i>cycb1;1</i> <sup>-/-</sup> <i>cycb1;2</i> <sup>+/-</sup> | 34.55%                        | 65.44%                        | 0%****                        | 191                 |
| Expected Mendelian   | 25%                           | 50%                           | 25%                           | -                   |

The expected Mendelian segregation reflects the proportion of F1 seedlings with the respective genotypes if the mutant alleles promote no deleterious effects. A z-test for one proportion was performed to test if the observed homozygous mutant frequencies differ from the expected Mendelian value and the significance level was corrected for multiple comparisons using Bonferroni. Asterisks indicate significant differences from the expected value (25%) (\*\**P* < 0.01, \*\*\*\**P* < 0.0001). Primers used for genotyping are listed in Table EV1.

**Table 4. Transmission efficiency of the *cycb1;2* mutant allele in reciprocal crosses of *gip1*<sup>-/-</sup> *cycb1;1*<sup>-/-</sup> *cycb1;2*<sup>+/-</sup> and *gip2*<sup>-/-</sup> *cycb1;1*<sup>-/-</sup> *cycb1;2*<sup>+/-</sup> with wild type.**

| Parental genotypes (female × male)   | Allele    |                | Number of seeds (n) |
|--|-----------|----------------|---------------------|
|  | Wild-type | <i>cycb1;2</i> |                     |
| Col-0 × <i>gip1</i> <sup>-/-</sup> <i>cycb1;1</i> <sup>-/-</sup> <i>cycb1;2</i> <sup>+/-</sup> | 93.62%    | 106.38%        | 94                  |
| Col-0 × <i>gip2</i> <sup>-/-</sup> <i>cycb1;1</i> <sup>-/-</sup> <i>cycb1;2</i> <sup>+/-</sup> | 111.36%   | 88.64%****     | 88                  |
| <i>gip1</i> <sup>-/-</sup> <i>cycb1;1</i> <sup>-/-</sup> <i>cycb1;2</i> <sup>+/-</sup> × Col-0 | 112.36%   | 87.64%****     | 89                  |
| <i>gip2</i> <sup>-/-</sup> <i>cycb1;1</i> <sup>-/-</sup> <i>cycb1;2</i> <sup>+/-</sup> × Col-0 | 134.78%   | 65.22%****     | 92                  |

A transmission efficiency of 100% indicates full transmission of the mutant allele, that is, 50% of the genotyped F1 seedlings are heterozygous. A transmission efficiency may be higher than 100% if one of the two alleles is transmitted in a reduced manner, conversely making the other allele overrepresented. A z-test for one proportion was performed to test if the observed transmission frequencies differ from expected values and the significance level was corrected for multiple comparisons using Bonferroni. Asterisks indicate significant differences from expected values (\*\*\*\**P* < 0.0001). Primers used for genotyping are listed in Table EV1.

type cyclins and in particular CYCB1;2 might control microtubule organization through the regulation of GIP1 and more likely through several additional substrates.

## Discussion

Angiosperms have undergone an extensive expansion of the cyclin family in comparison to yeast and mammals, containing for instance a total of 10 different cyclin families with more than 50 protein-encoding cyclin genes in *Arabidopsis* (Wang et al, 2004; Jia et al, 2014). For most of these genes, functional information is still lacking. Although genetic dissection of such an enlarged number of cyclin members may be more challenging and require the construction of multiple mutant combinations, it also provides an opportunity to study the function of these cyclins in compromised, yet viable mutant combinations of redundantly acting genes. In contrast, mutants for the CycB1 in mice, for example, are not viable and die *in utero* making its analysis, especially at the developmental level, challenging (Brandeis et al, 1998). Here, we have functionally dissected the group of B1-type cyclins and created various double

and multiple mutant combinations. In particular the combination of *cycb1;1* and *cycb1;2* proved to be a valuable tool to study the function of this class of cyclins.

### Endosperm—a demanding structure

During plant development, many different cell cycle programs are executed (Jakoby & Schnittger, 2004). One of the most particular proliferation modes are the free nuclear divisions during endosperm proliferation (Berger et al, 2006). Despite its importance for seed growth and embryo nutrition, there is currently very little known about the cell cycle machinery that drives these free nuclear divisions. Laser dissection microscopy-based transcriptional profiling of *Arabidopsis* endosperm revealed that B1-type cyclins are among the most prominently expressed cell cycle regulators in this tissue (Day et al, 2008). Consistently, we found that nuclear divisions are reduced in *cycb1;2* single mutants and aberrant mitotic divisions appear in *cycb1;1 cycb1;2* and *cycb1;2 cycb1;3* double mutants. Correspondingly, seed development defects were reported as an effect of silencing cyclin B1 expression in rice (Guo et al, 2010).

Strikingly, the phenotypes of *cycb1;1 cycb1;2* and *cycb1;2 cycb1;3* double mutant endosperm closely resemble the defects seen in mutants for ENDOSPERM DEFECTIVE 1 (EDE1), a plant-specific microtubule-binding protein (Pignocchi et al, 2009). EDE1 contains short CDK consensus phosphorylation sites (S/T-P) and so far has not been identified in CDK substrate searches in *Arabidopsis* (Pusch et al, 2012; Harashima et al, 2016). However, EDE1 could be phosphorylated by human Cdk complexes in *in vitro* kinase assays and it is known that short CDK consensus sites are sufficient to be phosphorylated by CDK/cyclin complexes (Ubersax et al, 2003; Pignocchi & Doonan, 2011). Interestingly, many cytoskeletal components are highly expressed in proliferating endosperm tissue and the free nuclear divisions might be very sensitive to alterations in cytoskeleton function, providing a possible reason why these divisions are apparently more sensitive to the loss of CYCB1 function (Day et al, 2009). Endosperm development in *Arabidopsis* might thus advance as a model system to study cell biological questions. However, endosperm is difficult to access, since it is buried in maternal structures, such as the seed coat and the silique. Therefore, morphological analyses always require mechanical preparation steps. In this light, the identification of *cycb1;1 cycb1;2* homozygous double mutants represents a unique tool to investigate the control of mitosis in roots or other much more easily accessible plant tissues than gametophytes.

### B1-type cyclins and the control of microtubule nucleation

Microtubules nucleate from ring-shaped complexes that contain  $\gamma$ -tubulin, and a family of related proteins called  $\gamma$ -tubulin complex proteins (GCPs). The composition of  $\gamma$ -tubulin ring complexes ( $\gamma$ TURC) varies between organisms: budding yeast contains only the  $\gamma$ -tubulin small complex ( $\gamma$ TUSC), with two molecules of  $\gamma$ -tubulin, and one each of GCP2 and GCP3 (Vinh *et al.*, 2002). On the other hand, animal nucleating complexes are made of multiple copies of the  $\gamma$ TUSC plus GCP4, GCP5, and GCP6, as well as other non-GCP constituents, such as GIP1/MOZART1, MOZART2, and NEDD1, which is a localization factor (Tovey & Conduit, 2018). In plants,  $\gamma$ -tubulin complexes contain all GCP subunits, the GIP1/MOZART1 protein, and a NEDD1 homolog (Lee & Liu, 2019).

The dynamic assembly and disassembly of the microtubule network generally runs in parallel with the cell cycle and, for example, even strong defects in microtubule arrays, for example, lack of the PPB formation (Schaefer *et al.*, 2017), do not block the cell cycle. However, rearrangements of the microtubule cytoskeleton in plant cells are obviously coupled with the cell cycle. Specific microtubule arrays accompany each stage of the cell cycle, either in interphase (the interphase cortical microtubule array), in pre-mitosis (the PPB), or in mitosis (spindle and phragmoplast). Moreover, several observations indicate a tight—at least temporal—coordination of both cycles. For instance, the PPB is formed in the late G2-prophase in somatic tissues. Rapid PPB dismantling precisely coincides with nuclear envelope breakdown and entry into metaphase. Prospindle and spindle formation also takes place at precise stages of the cell cycle. Likewise, the phragmoplast is precisely initiated at telophase from remnants of the spindle. However, very little is currently known about the molecular mechanisms of how this coordination is achieved. Interestingly, several cell cycle regulators including CDKA;1 have been identified at microtubule arrays such as the PPB, spindle, and phragmoplast (Boruc *et al.*, 2010). Our finding that GIP1/MOZART1 is phosphorylated by CDKB2-CYCB1 complexes offers a potential mechanism of how the cell cycle might orchestrate microtubule assembly. Interestingly, double PPBs and asymmetric PPBs, as we report here to be present in *cycb1;1 cycb1;2* mutants, have also been described in a *gip1 gip2* double knockdown mutant previously, further strengthening that CYCB1 controls the cytoskeleton via regulation of the  $\gamma$ TURC complex components (Janski *et al.*, 2012). The exact mechanism by which this regulation happens, including if phosphorylation of GIP1 at T67 plays an important role and if there is indeed a differential phosphorylation regulation of GIP1 and GIP2, remains to be explored.

Moreover, other factors of the  $\gamma$ TURC have also been found to be phosphorylated in animals and yeast. For instance, all core units of the  $\gamma$ TURC ( $\gamma$ -tubulin, GCP2-GCP6, GCP-WD, and GCP8/MOZART2), but GIP1/MOZART1, have been found to be phosphorylated in mammals (Teixidó-Travesa *et al.*, 2012). In particular, CDKs were shown to phosphorylate  $\gamma$ TURC components including  $\gamma$ -tubulin and others in yeast and Nedd1 in humans (Zhang *et al.*, 2009; Keck *et al.*, 2011). However, the functional importance of these phosphorylation sites is not understood and an analysis of microtubule dynamics in animals is complicated due to the lethality of core cell cycle regulators such as Cdk1 or CycB1 (Brandeis *et al.*, 1998; Santamaría *et al.*, 2007).

In plants, all of the core  $\gamma$ TURC components (GIP1, GCP2, GCP3, GCP4, GCP5a, GCP5b, NEDD1, and  $\gamma$ -tubulin 1 as well as  $\gamma$ -tubulin 2), but GIP2, have at least one CDK consensus phosphorylation site, and for NEDD1 and GCP4 as well as GCP5a a phosphorylated Ser/Thr in a consensus CDK site has been deposited in the PhosPhAt database (<http://phosphat.uni-hohenheim.de>). In addition, CYCB1;3 has been found to bind to GCP3 and  $\gamma$ -tubulin 1 (Van Leene *et al.*, 2010). Thus, the regulation of the  $\gamma$ TURC complex by CYCB1s likely goes even beyond the phosphorylation of GIP1 reported here.

### The CYCB1 group has an evolutionarily conserved role in microtubule networks

Mammalian CycB1 is mainly cytoplasmic in interphase, rapidly accumulates in the nucleus at the end of prophase, and associates with the mitotic apparatus in the course of mitosis, that is, chromatin, microtubules, kinetochores, and centrosomes (Toyoshima *et al.*, 1998; Yang *et al.*, 1998; Hagting *et al.*, 1999; Bentley *et al.*, 2007). Loss of the CycB1 function in mice results in very early embryo lethality (Brandeis *et al.*, 1998). In contrast, mammalian cyclin B2 (CycB2) localizes mostly to the Golgi apparatus in both interphase and metaphase and CycB2 knockout mice are viable (Jackman *et al.*, 1995; Brandeis *et al.*, 1998; Draviam *et al.*, 2001). However, knocking down both CycB1 and CycB2 in HeLa cells showed a redundant function for both cyclins (Soni *et al.*, 2008). Cyclin B3 is only poorly expressed in mitotic cells, but its mRNA is readily observed in both male and female meiosis (Lozano *et al.*, 2002; Nguyen *et al.*, 2002).

Interestingly, CycB1 in mammals localizes to the outer plate of the kinetochore at prometaphase and later on to the spindle poles following microtubule attachment to kinetochores (Bentley *et al.*, 2007; Chen *et al.*, 2008). Reduction of CycB1 by the use of RNA interference results in the irregular attachment of kinetochores to microtubules, chromosome alignment defects and delays anaphase (Chen *et al.*, 2008), which is reminiscent of the chromosome alignment and segregation problems in addition to the extended spindle stages we found in *cycb1;1 cycb1;2* mutants.

In contrast to many other eukaryotes, the setup of interphasic and mitotic microtubule networks in flowering plants is not driven by microtubule-organizing centers containing centrioles/basal bodies. Instead, it has been proposed that mitotic microtubule networks nucleate from chromatin. Consistent with a role in microtubule nucleation, CYCB1;1 and CYCB1;2 have been found to be present mainly at chromatin during mitosis, while CYCB1;3 is localized to both chromatin and cytoplasm and CYCB1;4 is localized mainly in the cytoplasm as well as in the region of the cytoplasm that co-localizes with the mitotic spindle (Bulankova *et al.*, 2013). Thus, although the CYCB1 group in *Arabidopsis* appears from a general point of view to regulate the mitotic microtubule network similarly to CycB1 in mammals, the localization of B1-type cyclins is different in both species, indicating that the work of B-type cyclins in different species is differently distributed among its members.

Remarkably, and in contrast to CycB1 localization in mammals, CYCB1;1, CYCB1;2, and CYCB1;3 were not found at the mitotic spindle. We cannot rule out at the moment that B1-type cyclins do not have a function in further organizing the mitotic spindle. However, it seems likely that other, yet to be characterized subgroups of mitotic cyclins, in particular the B2 and B3 group, might play a key

role here especially since a recent analysis of *CYCB3;1* found that this cyclin is localized to the spindle, at least in meiosis (Sofroni *et al.*, 2020). With this, it will be exciting to have eventually a complete view on B-type cyclin function in *Arabidopsis*.

## Materials and Methods

### Plant material and growth conditions

The accessions Columbia (Col-0) and Nossen (No-0) were used as wild type controls. The single *cycb1;1*, *cycb1;2*, *cycb1;3*, and *cycb1;4* mutants were previously described and characterized (Weimer *et al.*, 2016). The *cycb1;3* T-DNA insertion is in a No-0 background. The *gip1* (GABL\_213D01) and *gip2* (FLAG\_36406) mutants were also previously characterized (Janski *et al.*, 2012). Genotyping primers are listed in Table EV1.

*Arabidopsis thaliana* seeds were sown on half-strength ( $\frac{1}{2}$ ) Murashige and Skoog (MS) medium (basal salt mixture, Duchefa Biochemie) containing 0.5% sucrose and 0.8% plant agar (Duchefa Biochemie) at pH 5.8. Seeds were either sterilized with chlorine gas or by liquid sterilization. For the liquid sterilization, a 2% bleach, 0.05% Triton X-100 solution was applied for 5 min, followed by three washing steps with sterile distilled water and the addition of 0.05% agarose. Stratification of the seeds on plates was performed at 4°C for 2–3 days in the dark. Plants were initially grown *in vitro* at 22°C in a 16-h light regime and subsequently transferred to soil with a 16-h light/21°C and 8-h/18°C dark regime with 60% humidity.

### Quantitative PCR

Total RNA was isolated from plant tissues using the RNeasy Plant Mini Kit (Qiagen). Dnase (TaKaRa) treatment was performed to avoid DNA contamination and RNA concentration was measured using a Nanodrop ND-1000 instrument. A total of 3.5  $\mu$ g of total RNA was reverse transcribed using SuperScript<sup>®</sup> III reverse transcriptase kit (Invitrogen). An additional step of Rnase H treatment at 37°C for 20 min was performed to eliminate the remaining RNA. The cDNA was further purified and concentrated by using QIAquick PCR Purification Kit (Qiagen) and the concentration was determined by Nanodrop ND-1000 instrument. Finally, using cDNA as the template, qPCR was performed on a Light-cycler LC480 instrument (Roche) as per the manufacturer's instructions.

### Plasmid construction and plant transformation

To analyze the expression of the *CYCB1* group in seeds, we used previously generated promoter reporter lines for *CYCB1;1* to *CYCB1;4* fused at the N-terminus to GFP (Weimer *et al.*, 2016).

To generate a *PRO<sub>GIP1</sub>:GFP:GIP1* construct, a 2,849-bp genomic region including the native promoter and terminator was amplified by PCR and integrated into a *pENTR-D-TOPO* vector. A *SmaI* restriction site was introduced before the first ATG codon of the *GIP1* CDS. After linearization of the construct by restriction digest with *SmaI*, a ligation with *GFP* was performed, followed by LR reaction with the destination vector *pGWBS01*. The constructs were transformed in *Arabidopsis thaliana* by floral dipping.

### Flow cytometry assay

Ten 7-day-old seedlings per genotype were chopped with a new razorblade in homogenization buffer (45 mM MgCl<sub>2</sub>, 20 mM MOPS, 30 mM sodium citrate, 0.1% Triton X-100, pH 7.0), followed by filtration through a 15- $\mu$ m nylon mesh. After that, propidium iodide (Sigma) and Rnase A (Sigma) were added to final concentrations of 50  $\mu$ g/ml and 10  $\mu$ g/ml, respectively. Samples were left on ice for 5 min and then analyzed in a S3e Cell Sorter (Bio-Rad) with a laser excitation at 488 nm. The scatterplots were analyzed and processed using the FlowJo software.

### Endosperm nuclei proliferation analysis

Flower buds were initially emasculated before the visible maturation and release of pollen. Emasculated flowers were then hand pollinated with pollen from the same genotype after 2–3 days. After 3 days, siliques were dissected and fixed in a solution of 4% glutaraldehyde in 12.5 mM cacodylate buffer, pH 6.8, followed by vacuum application for 20 min and storage at 4°C overnight. The following day, individual seeds were mounted on microscope slides containing a clearing 1:8:2 glycerol:chloral hydrate:water solution and stored at 4°C overnight. Imaging was performed with a Zeiss LSM 780 or 880 confocal microscope with excitation at 488 nm and detection between 498 and 586 nm and Z-stacks were analyzed using the Fiji software.

### Pollen staining

To identify single nuclei in mature pollen, pollen grains were released into a DAPI staining solution (2.5  $\mu$ g/ml DAPI, 0.01% Tween, 5% dimethyl sulfoxide, 50 mM Na phosphate buffer, pH 7.2) and incubated at 4°C overnight. Pollen viability was analyzed by mounting pollen as previously described (Alexander, 1969). Imaging was performed with a Zeiss Axioimager.

### Embryo sac analysis

Mature ovules and developing seeds were prepared from siliques before and 3 days after fertilization, respectively, mounted on microscope slides on a clearing 1:8:2 glycerol:chloral hydrate:distilled water solution and kept at 4°C overnight before analysis as previously described (Nowack *et al.*, 2006). Differential Interference Contrast (DIC) imaging was performed on a Zeiss Axioimager.

### Microtubule cytoskeleton dynamics in roots

Meristematic cell divisions in the root were observed in 5–7 day-old seedlings under a layer of  $\frac{1}{2}$  MS medium using a Leica TCS SP8 inverted confocal microscope.

### Immunostaining

Roots of 4-day-old *Arabidopsis* seedlings were fixed in 4% paraformaldehyde and 0.1% Triton X-100 in  $\frac{1}{2}$  MTSB buffer (25 mM PIPES, 2.5 mM MgSO<sub>4</sub>, 2.5 mM EGTA, pH 6.9) for 1 h under vacuum, then rinsed in PBS 1X for 10 min. Samples were then permeabilized in ethanol for 10 min and rehydrated in PBS for

10 min. Cell walls were digested using the following buffer for 1 h: 2 mM MES pH 5, 0.20% driselase and 0.15% macerozyme. Tissues were hybridized overnight at room temperature with the B-5-1-2 monoclonal anti- $\alpha$ -tubulin (Sigma) and the anti-KNOLLE antibody (kind gift of G. Jürgens, University of Tübingen, Germany; Lauber *et al.*, 1997). The next day, tissues were washed for 15 min in PBS, 50 mM glycine, incubated with secondary antibodies (Alexa Fluor 555 goat anti-rabbit for KNOLLE antibody and Alexa Fluor 488 goat anti-mouse for the tubulin antibody) overnight and washed again in PBS, 50 mM glycine, and DAPI 20 ng/ml. Tissues were mounted in VECTASHIELD and DAPI and viewed using an SP8 confocal laser microscope (Leica Microsystems). Samples were excited sequentially at 405 nm (DAPI), 488 nm (@TUB/Alexa Fluor 488), and 561 nm (@KNOLLE/Alexa Fluor 555), with an emission band of 420–450 nm (DAPI), 495–545 nm (Alexa Fluor 488), and 560–610 nm (Alexa Fluor 555) using a PMT for DAPI imaging, and hybrid detectors for MT and KNOLLE imaging. All stacks have been imaged using the same zoom (x 1.60) with a pixel size xyz of 200 nm × 200 nm × 500 nm. KNOLLE is particularly useful when mutants do not form a PPB to unambiguously identify cells at the G2/M stage, although this was not the case in our study.

A blind counting was set up to count mitotic MT arrays seen in 10 roots of each genotype. The “Cell counter” plugin was used to count the occurrence of MT arrays within each root stack (<https://imagej.nih.gov/ij/plugins/cell-counter.html>).

#### Protein expression and purification and *in vitro* kinase assays

Purified GIP1 was kindly donated by Nicolas Baumberger (IBMP, Strasbourg). *GIP1* CDS was cloned into the *pGEX-2TK* vector (GE Healthcare; courtesy of Etienne Herzog) and transformed into the BL21(DE3) *E. coli* strain. An overnight culture cultivated at 37°C was used to inoculate an expression culture at an OD<sub>600</sub> of 0.1. The expression culture was grown at 37°C and 250 rpm until it reached an OD<sub>600</sub> of 0.6. Afterwards, 0.5 mM IPTG was added and the growth continued at 37°C for 6 h. Cells were collected by centrifugation at 5,000 g for 15 min and the pellet resuspended in 50 mM Tris pH 8, 300 mM NaCl, 5% glycerol, 5 mM EDTA, 0.1% Tween 20. Cells were lysed by sonication and the lysate clarified by centrifugation at 10,000 g for 20 min at 4°C. GST-GIP was purified by passage onto a glutathione-sepharose GSTrap HP 1 ml column (GE Healthcare) with 50 mM Tris pH 7.5, 10 mM MgCl<sub>2</sub>, 100 mM NaCl as an equilibration/washing buffer and 50 mM Tris pH 7.5, 10 mM MgCl<sub>2</sub>, 100 mM NaCl plus 10 mM reduced glutathione as an elution buffer. Elution fractions were analyzed on polyacrylamide gel and concentrated by ultrafiltration before being frozen and stored at –80°C. Histone H1<sup>0</sup> was purchased from NEB. *In vitro* kinase assays were performed as described previously (Harashima & Schnittger, 2012).

#### Oryzalin root growth assays

Plants were sown on ½ MS medium containing either 0.05% DMSO as a control or oryzalin. 100 mM oryzalin stock solutions were prepared in DMSO and stored at –20°C and further diluted to a final concentration of 150 nM or 200 nM for the root assays. Root growth was recorded daily up until 5 days after germination, when plates were scanned, and root length was subsequently measured using

the Fiji software. Three biological replicates with at least 10 plants per genotype were performed. The mean root length of each individual experiment was determined and again averaged.

#### Statistical analysis

The employed statistical tests are indicated in the figure legends. Statistical tests were performed using the GraphPad Prism 9 software and the XLSTAT plugin for Microsoft Excel. The distribution of the measured values was tested beforehand, for example, by the Anderson–Darling test. If the distribution was significantly different from a normal distribution, a non-parametric test was employed. Significance levels are  $P \geq 0.05$  (ns),  $P < 0.05$  (\*),  $P < 0.01$  (\*\*),  $P < 0.001$  (\*\*\*),  $P < 0.0001$  (\*\*\*\*). In the case of the Chi-squared test followed by the Marascuilo procedure, significant pairwise comparisons are indicated by letters.

#### Data availability

This study includes no data deposited in external repositories.

**Expanded View** for this article is available online.

#### Acknowledgments

This work was supported by a grant from the Ohsumi Frontier Science Foundation to S.K., a fellowship from the International Graduate School in Genetics and Functional Genomics, University of Cologne to M.Ku., by the Ministry of Education, Youth, and Sports of the Czech Republic, European Regional Development Fund–Project REMAP (grant CZ.02.1.01/0.0/0.0/15\_003/0000479) to K.R., by the Human Frontier Science Program to D.B. and A.S., and by a grant from the Deutsche Forschungsgemeinschaft (SCHN 736/2-2) to A.S. Open access funding enabled and organized by Projekt DEAL.

#### Author contributions

MM, XZ, MP, FR, HH, SK, MH, and AS designed the research; MM, XZ, MP, KB, FR, MKo, HH, SK, MKU, and PB performed the experiments; MM, XZ, and MP performed the statistical analysis; MM, XZ, MP, KB, FR, MKo, HH, SK, MKU, PB, MH, KR, DB, and AS analyzed and discussed the data; DB, KR, and AS provided material and reagents, MM and AS wrote the article; MM, XZ, MP, FR, MKo, HH, SK, MKU, PB, MH, KR, DB, and AS revised and approved the article.

#### Conflict of interest

The authors declare that they have no conflict of interest.

#### References

- Alexander MP (1969) Differential staining of aborted and nonaborted pollen. *Biotech Histochem* 44: 117–122
- Bentley AM, Normand G, Hoyt J, King RW (2007) Distinct sequence elements of Cyclin B1 promote localization to chromatin, centrosomes, and kinetochores during mitosis. *Mol Biol Cell* 18: 4847–4858
- Berger F, Grini PE, Schnittger A (2006) Endosperm: an integrator of seed growth and development. *Curr Opin Plant Biol* 9: 664–670
- Blethrow JD, Glavy JS, Morgan DO, Shokat KM (2008) Covalent capture of kinase-specific phosphopeptides reveals Cdk1-cyclin B substrates. *Proc Natl Acad Sci U S A* 105: 1442–1447



- Boisnard-Lorig C, Colon-Carmona A, Bauch M, Hodge S, Doerner P, Bancharel E, Dumas C, Haseloff J, Berger F (2001) Dynamic analyses of the expression of the histone: YFP fusion protein in *Arabidopsis* show that syncytial endosperm is divided in mitotic domains. *Plant Cell* 13: 495–509
- Boruc J, Mylle E, Duda M, de Clercq R, Rombauts S, Geelen D, Hilson P, Inzé D, van Damme D, Russinova E (2010) Systematic localization of the *Arabidopsis* core cell cycle proteins reveals novel cell division complexes. *Plant Physiol* 152: 553–565
- Boudolf V, Lammens T, Boruc J, Van Leene J, Van Den Daele H, Maes S, Van Isterdael G, Russinova E, Kondorosi E, Witters E et al (2009) CDKB1;1 forms a functional complex with CYCA2;3 to suppress endocycle onset. *Plant Physiol* 150: 1482–1493
- Brandeis M, Rosewell I, Carrington M, Crompton T, Jacobs MA, Kirk J, Gannon J, Hunt T (1998) Cyclin B2-null mice develop normally and are fertile whereas cyclin B1-null mice die in utero. *Proc Natl Acad Sci U S A* 95: 4344–4349
- Bulankova P, Akimcheva S, Fellner N, Riha K (2013) Identification of *Arabidopsis* meiotic cyclins reveals functional diversification among plant cyclin genes. *PLoS Genet* 9: e1003508
- Chen Q, Zhang X, Jiang Q, Clarke PR, Zhang C (2008) Cyclin B1 is localized to unattached kinetochores and contributes to efficient microtubule attachment and proper chromosome alignment during mitosis. *Cell Res* 18: 268–280
- Cools T, Iantcheva A, Weimer AK, Boens S, Takahashi N, Maes S, van den Daele H, van Isterdael G, Schnittger A, de Veylder L (2011) The *Arabidopsis thaliana* checkpoint kinase WEE1 protects against premature vascular differentiation during replication stress. *Plant Cell* 23: 1435–1448
- Day RC, Herridge RP, Ambrose BA, Macknight RC (2008) Transcriptome analysis of proliferating *Arabidopsis* endosperm reveals biological implications for the control of syncytial division, cytokinin signaling, and gene expression regulation. *Plant Physiol* 148: 1964–1984
- Day RC, Müller S, Macknight RC (2009) Identification of cytoskeleton-associated genes expressed during *Arabidopsis* syncytial endosperm development. *Plant Signal Behav* 4: 883–886
- Dewitte W, Scofield S, Alcasabas AA, Maughan SC, Menges M, Braun N, Collins C, Nieuwland J, Prinsen E, Sundaresan V et al (2007) *Arabidopsis* CYCD3 D-type cyclins link cell proliferation and endocycles and are rate-limiting for cytokinin responses. *Proc Natl Acad Sci U S A* 104: 14537–14542
- Dissmeyer N, Weimer AK, Pusch S, de Schutter K, Kamei CLA, Nowack MK, Novak B, Duan GL, Zhu YG, de Veylder L et al (2009) Control of cell proliferation, organ growth, and DNA damage response operate independently of dephosphorylation of the *Arabidopsis* Cdk1 Homolog CDKA;1. *Plant Cell* 21: 3641–3654
- Dissmeyer N, Weimer AK, de Veylder L, Novak B, Schnittger A (2010) The regulatory network of cell cycle progression is fundamentally different in plants versus yeast or metazoans. *Plant Signal Behav* 5: 1613–1618
- Doerner P, Jørgensen JE, You R, Steppuhn J, Lamb C (1996) Control of root growth and development by cyclin expression. *Nature* 380: 520–523
- Draviam VM, Orrechia S, Lowe M, Pardi R, Pines J (2001) The localization of human cyclins B1 and B2 determines CDK1 substrate specificity and neither enzyme requires MEK to disassemble the Golgi apparatus. *J Cell Biol* 152: 945–958
- Drews GN, Yadegari R (2002) Development and function of the angiosperm female gametophyte. *Annu Rev Genet* 36: 99–124
- Furuno N, Den EN, Pines J (1999) Human cyclin A is required for mitosis until mid prophase. *J Cell Biol* 147: 295–306
- Guo J, Wang F, Song J, Sun W, Zhang XS (2010) The expression of Orysa; CycB1;1 is essential for endosperm formation and causes embryo enlargement in rice. *Planta* 231: 293–303
- Haase SB, Winey M, Reed SI (2001) Multi-step control of spindle pole body duplication by cyclin-dependent kinase. *Nat Cell Biol* 3: 38–42
- Hagting A, Jackman M, Simpson K, Pines J (1999) Translocation of cyclin B1 to the nucleus at prophase requires a phosphorylation-dependent nuclear import signal. *Curr Biol* 9: 680–689
- Hagting A, Karlsson C, Clute P, Jackman M, Pines J (1998) MPF localization is controlled by nuclear export. *EMBO J* 17: 4127–4138
- Harashima H, Dissmeyer N, Hammann P, Nomura Y, Kramer K, Nakagami H, Schnittger A (2016) Modulation of plant growth *in vivo* and identification of kinase substrates using an analog-sensitive variant of CYCLIN-DEPENDENT KINASE A;1. *BMC Plant Biol* 16: 1–19
- Harashima H, Schnittger A (2012) Robust reconstitution of active cell-cycle control complexes from co-expressed proteins in bacteria. *Plant Methods* 8: 1–9
- Jackman M, Firth M, Pines J (1995) Human cyclins B1 and B2 are localized to strikingly different structures: B1 to microtubules, B2 primarily to the Golgi apparatus. *EMBO J* 14: 1646–1654
- Jakoby M, Schnittger A (2004) Cell cycle and differentiation. *Curr Opin Plant Biol* 7: 661–669
- Janski N, Masoud K, Batzenschlager M, Herzog E, Evrard JL, Houlné G, Bourge M, Chaboué ME, Schmit AC (2012) The GCP3-interacting proteins GIP1 and GIP2 are required for  $\gamma$ -tubulin complex protein localization, spindle integrity, and chromosomal stability. *Plant Cell* 24: 1171–1187
- Jia RD, Guo CC, Xu GX, Shan HY, Kong HZ (2014) Evolution of the cyclin gene family in plants. *J Syst Evol* 52: 651–659
- Keck JM, Jones MH, Wong CCL, Binkley J, Chen D, Jaspersen SL, Holinger EP, Xu T, Niepel M, Rout MP et al (2011) A cell cycle phosphoproteome of the yeast centrosome. *Science* 332: 1557–1562
- Lacey KR, Jackson PK, Stearns T (1999) Cyclin-dependent kinase control of centrosome duplication. *Proc Natl Acad Sci U S A* 96: 2817–2822
- Lauber MH, Waizenegger I, Steinmann T, Schwarz H, Mayer U, Hwang I, Lukowitz W, Jürgens G (1997) The *Arabidopsis* KNOLLE protein is a cytokinesis-specific syntaxin. *J Cell Biol* 139: 1485–1493
- Lee YR, Liu B (2019) Microtubule nucleation for the assembly of acentrosomal microtubule arrays in plant cells. *New Phytol* 222: 1705–1718
- Van Leene J, Hollunder J, Eeckhout D, Persiau G, Van De Slijke E, Stals H, Van Isterdael G, Verkest A, Neiryck S, Buffel Y, et al (2010) Targeted interactomics reveals a complex core cell cycle machinery in *Arabidopsis thaliana*. *Mol Syst Biol* 6: 397
- Lindqvist A, Rodríguez-Bravo V, Medema RH (2009) The decision to enter mitosis: feedback and redundancy in the mitotic entry network. *J Cell Biol* 185: 193–202
- Lozano JC, Schatt P, Peaucellier G, Picard A, Perret E, Arnould C (2002) Molecular cloning, gene localization, and structure of human cyclin B3. *Biochem Biophys Res Commun* 291: 406–413
- McCormick S (2004) Control of male gametophyte development. *Plant Cell* 16: 142–154
- Menges M, De Jager SM, Gruitsem W, Murray JAH (2005) Global analysis of the core cell cycle regulators of *Arabidopsis* identifies novel genes, reveals multiple and highly specific profiles of expression and provides a coherent model for plant cell cycle control. *Plant J* 41: 546–566
- Morgan DO (1997) Cyclin-dependent kinases: engines, clocks, and microprocessors. *Annu Rev Cell Dev Biol* 13: 261–291

- Nakamura M, Yagi N, Kato T, Fujita S, Kawashima N, Ehrhardt DW, Hashimoto T (2012) *Arabidopsis* GCP3-interacting protein 1/MOZART 1 is an integral component of the  $\gamma$ -tubulin-containing microtubule nucleating complex. *Plant J* 71: 216–225
- Nakayama KI, Nakayama K (2005) Regulation of the cell cycle by SCF-type ubiquitin ligases. *Semin Cell Dev Biol* 16: 323–333
- Nguyen TB, Manova K, Capodice P, Lindon C, Bottega S, Wang XY, Refik-Rogers J, Pines J, Wolgemuth DJ, Koff A (2002) Characterization and expression of mammalian cyclin B3, a prepachytene meiotic cyclin. *J Biol Chem* 277: 41960–41969
- Nowack MK, Grini PE, Jakoby MJ, Lafos M, Koncz C, Schnittger A (2006) A positive signal from the fertilization of the egg cell sets off endosperm proliferation in angiosperm embryogenesis. *Nat Genet* 38: 63–67
- O'Farrell PH (2001) Triggering the all-or-nothing switch into mitosis. *Trends Cell Biol* 11: 512–519
- Pastuglia M, Azimzadeh J, Goussot M, Camilleri C, Belcram K, Evrand JL, Schmit AC, Guerche P, Bouchez D (2006)  $\gamma$ -tubulin is essential for microtubule organization and development of *Arabidopsis*. *Plant Cell* 18: 1412–1425
- Pignocchi C, Doonan JH (2011) Interaction of a 14-3-3 protein with the plant microtubule-associated protein EDE1. *Ann Bot* 107: 1103–1109
- Pignocchi C, Minns GE, Nesi N, Koumproglou R, Kitsios G, Benning C, Lloyd CW, Doonan JH, Hills MJ (2009) Endosperm Defective1 is a novel microtubule-associated protein essential for seed development in *Arabidopsis*. *Plant Cell* 21: 90–105
- Pusch S, Harashima H, Schnittger A (2012) Identification of kinase substrates by bimolecular complementation assays. *Plant J* 70: 348–356
- Riabowol K, Draetta G, Brizuela L, Vandre D, Beach D (1989) The cdc2 kinase is a nuclear protein that is essential for mitosis in mammalian cells. *Cell* 57: 393–401
- Santamaría D, Barrière C, Cerqueira A, Hunt S, Tardy C, Newton K, Cáceres JF, Dubus P, Malumbres M, Barbacid M (2007) Cdk1 is sufficient to drive the mammalian cell cycle. *Nature* 448: 811–815
- Schaefer E, Belcram K, Uyttewaal M, Duroc Y, Goussot M, Legland D, Laruelle E, De Tauzia-Moreau ML, Pastuglia M, Bouchez D (2017) The preprophase band of microtubules controls the robustness of division orientation in plants. *Science* 356: 186–189
- Schnittger A, Schöbinger U, Bouyer D, Weinl C, Stierhof YD, Hülkamp M (2002) Ectopic D-type cyclin expression induces not only DNA replication but also cell division in *Arabidopsis* trichomes. *Proc Natl Acad Sci U S A* 99: 6410–6415
- De Schutter K, Joubès J, Cools T, Verkest A, Corellou F, Babiychuk E, Van Der Schueren E, Beekman T, Kushnir ST, Inzé D et al (2007) *Arabidopsis* WEE1 kinase controls cell cycle arrest in response to activation of the DNA integrity checkpoint. *Plant Cell* 19: 211–225
- Sofroni K, Takatsuka H, Yang C, Dissmeyer N, Komaki S, Hamamura Y, Böttger L, Umeda M, Schnittger A (2020) CDK-dependent activation of CDKA1 controls microtubule dynamics and cytokinesis during meiosis. *J Cell Biol* 219: 1–21
- Soni DV, Sramkoski RM, Lam M, Stefan T, Jacobberger JW (2008) Cyclin B1 is rate limiting but not essential for mitotic entry and progression in mammalian somatic cells. *Cell Cycle* 7: 1285–1300
- Teixidó-Travesa N, Roig J, Lüders J (2012) The where, when and how of microtubule nucleation - one ring to rule them all. *J Cell Sci* 125: 4445–4456
- Tovey CA, Conduit PT (2018) Microtubule nucleation by  $\gamma$ -tubulin complexes and beyond. *Essays Biochem* 62: 765–780
- Toyoshima F, Moriguchi T, Wada A, Fukuda M, Nishida E (1998) Nuclear export of cyclin B1 and its possible role in the DNA damage-induced G2 checkpoint. *EMBO J* 17: 2728–2735
- Tyson JJ, Novak B (2001) Regulation of the eukaryotic cell cycle: molecular antagonism, hysteresis, and irreversible transitions. *J Theor Biol* 210: 249–263
- Ubersax JA, Woodbury EL, Quang PN, Paraz M, Blethrow JD, Shah K, Shokat KM, Morgan DO (2003) Targets of the cyclin-dependent kinase Cdk1. *Nature* 425: 859–864
- Vandepoel K, Raes J, De Veylder L, Rouzé P, Rombauts S, Inzé D (2002) Genome-wide analysis of core cell cycle genes in *Arabidopsis*. *Plant Cell* 14: 903–916
- Vanneste S, Coppens F, Lee E, Donner TJ, Xie Z, Van Isterdael G, Dhondt S, De Winter F, De Rybel B, Vuylsteke M et al (2011) Developmental regulation of CYCA2s contributes to tissue-specific proliferation in *Arabidopsis*. *EMBO J* 30: 3430–3441
- Vinh DBN, Kern JW, Hancock WO, Howard J, Davis TN (2002) Reconstitution and characterization of budding yeast  $\gamma$ -tubulin complex. *Mol Biol Cell* 13: 1144–1157
- Wang G, Kong H, Sun Y, Zhang X, Zhang W, Altman N, DePamphilis CW, Ma H (2004) Genome-wide analysis of the cyclin family in *Arabidopsis* and comparative phylogenetic analysis of plant cyclin-like proteins. *Plant Physiol* 135: 1084–1099
- Weimer AK, Biedermann S, Harashima H, Roodbarkelari F, Takahashi N, Foreman J, Guan Y, Pochon G, Heese M, Van Damme D et al (2016) The plant-specific CDKB1-CYCB1 complex mediates homologous recombination repair in *Arabidopsis*. *EMBO J* 35: 2068–2086
- Yamada M, Goshima G (2017) Mitotic spindle assembly in land plants: molecules and mechanisms. *Biology* 6: 6
- Yang J, Bardes ESG, Moore JD, Brennan J, Powers MA, Kornbluth S (1998) Control of Cyclin B1 localization through regulated binding of the nuclear export factor CRM1. *Genes Dev* 12: 2131–2143
- Zhang X, Chen Q, Feng J, Hou J, Yang F, Liu J, Jiang Q, Zhang C (2009) Sequential phosphorylation of Nedd1 by Cdk1 and Plk1 is required for targeting of the  $\gamma$ TuRC to the centrosome. *J Cell Sci* 122: 2240–2251



**License:** This is an open access article under the terms of the Creative Commons Attribution-NonCommercial-NoDerivs License, which permits use and distribution in any medium, provided the original work is properly cited, the use is non-commercial and no modifications or adaptations are made.

### Expanded View Figures

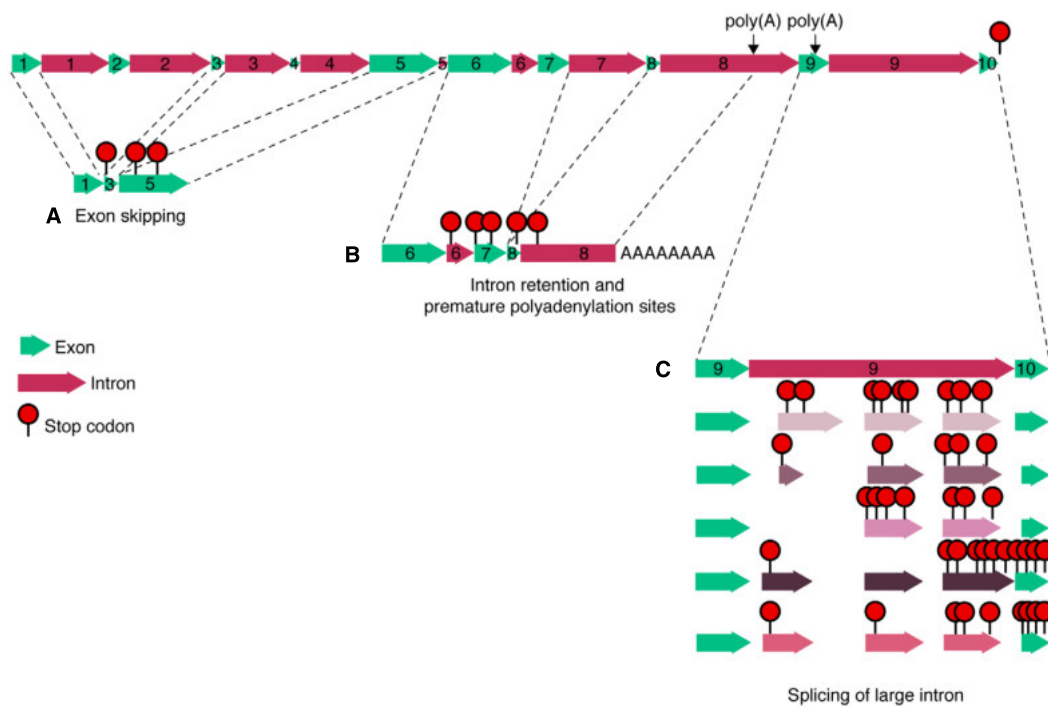


**Figure EV1. *CYCB1;5* is a pseudogene.**

A–C The predicted gene structure of *CYCB1;5*, including the observed cDNAs with exon skipping (A), intron retention and premature polyadenylation sites (B), and alternative splicing of a large intron (C).

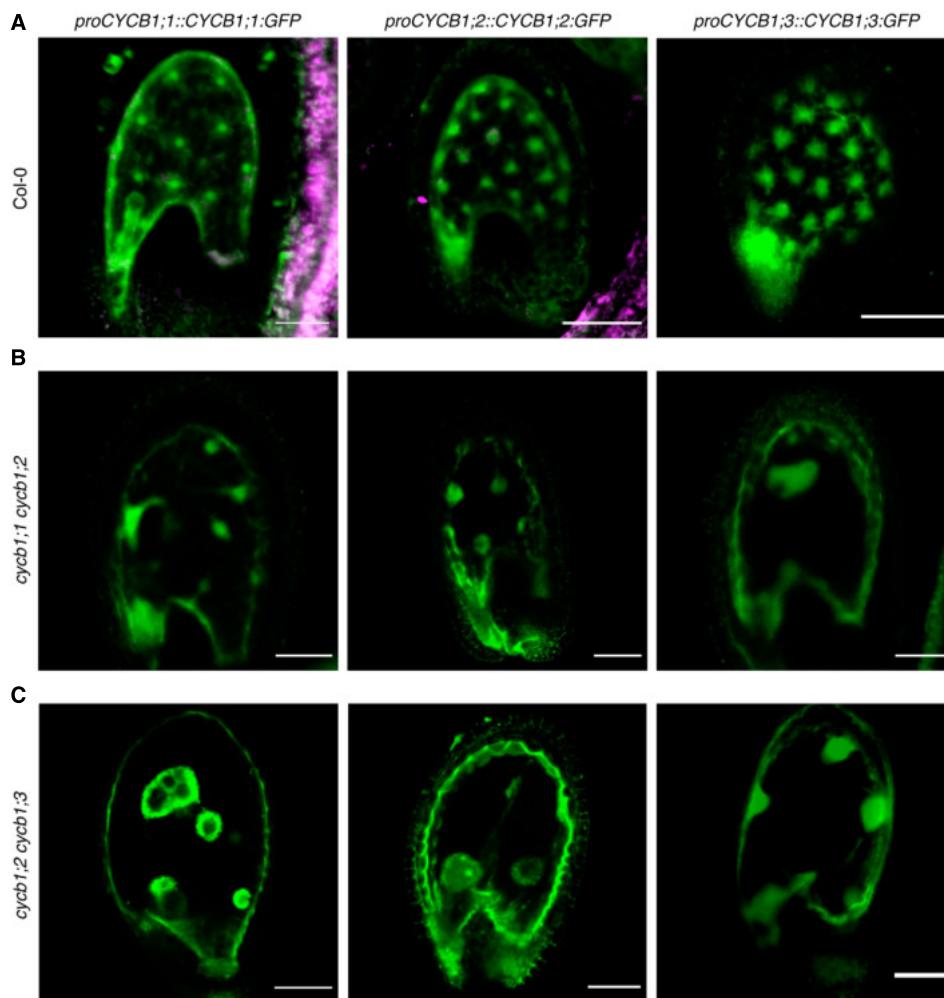


**Figure EV2. *CYCB1;1*, *CYCB1;2*, and *CYCB1;3* but not *CYCB1;4* are expressed during seed development.**

A–C Confocal microscope pictures of seeds expressing either *proCYCB1;1::GFP*, *proCYCB1;2::GFP* or *proCYCB1;3::GFP* in Col-0 (A), *cycb1;1 cycb1;2* (B), or *cycb1;2 cycb1;3* (C). Scale bars: 30  $\mu$ m.

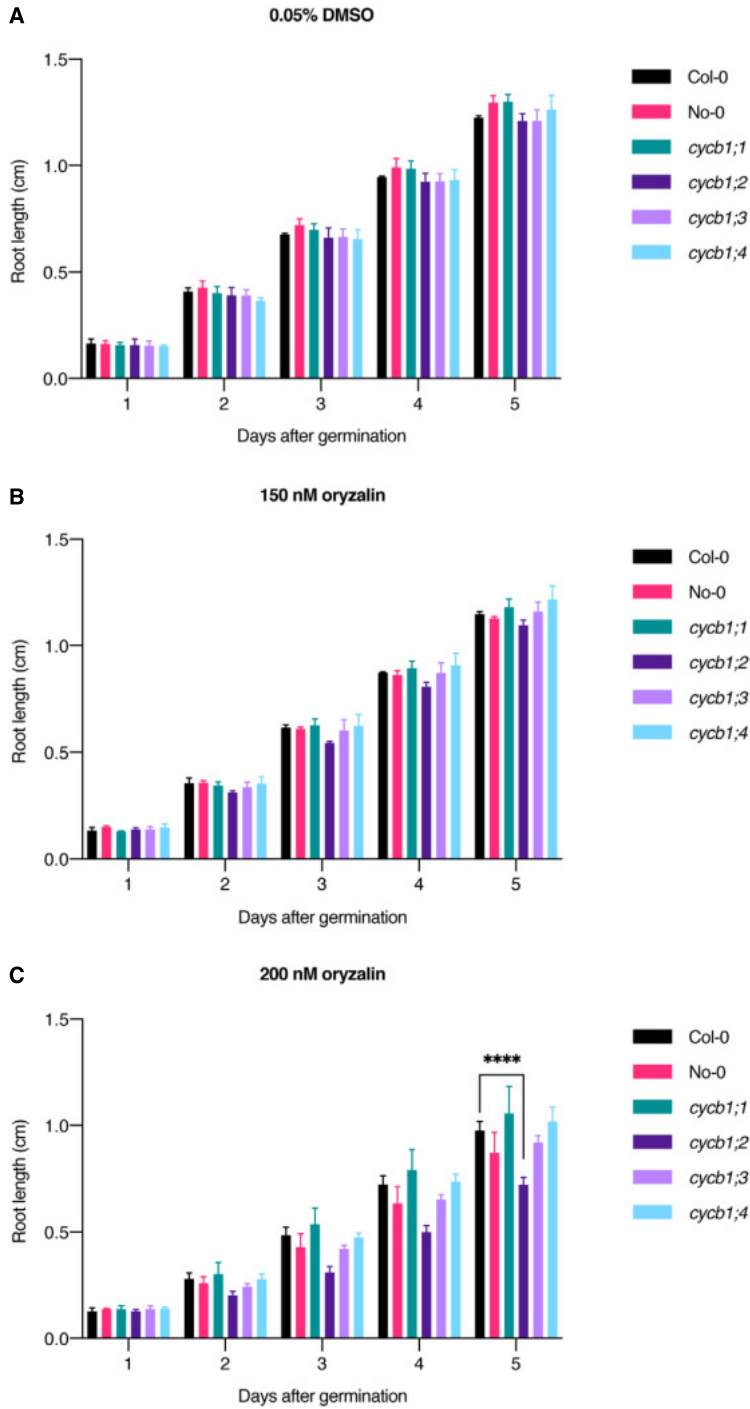


**Figure EV3. Oryzalin root growth assays across time in *cycb1* single mutants.**

A–C Quantification of root length in a control condition (A), 150 nM oryzalin (B) and 200 nM oryzalin (C). Graphs show mean ± SD of three biological replicates with at least 10 plants per genotype per replicate. Asterisks indicate a significant difference in root length in a two-way ANOVA followed by Tukey's multiple comparisons test (\*\*\*\*p < 0.0001).

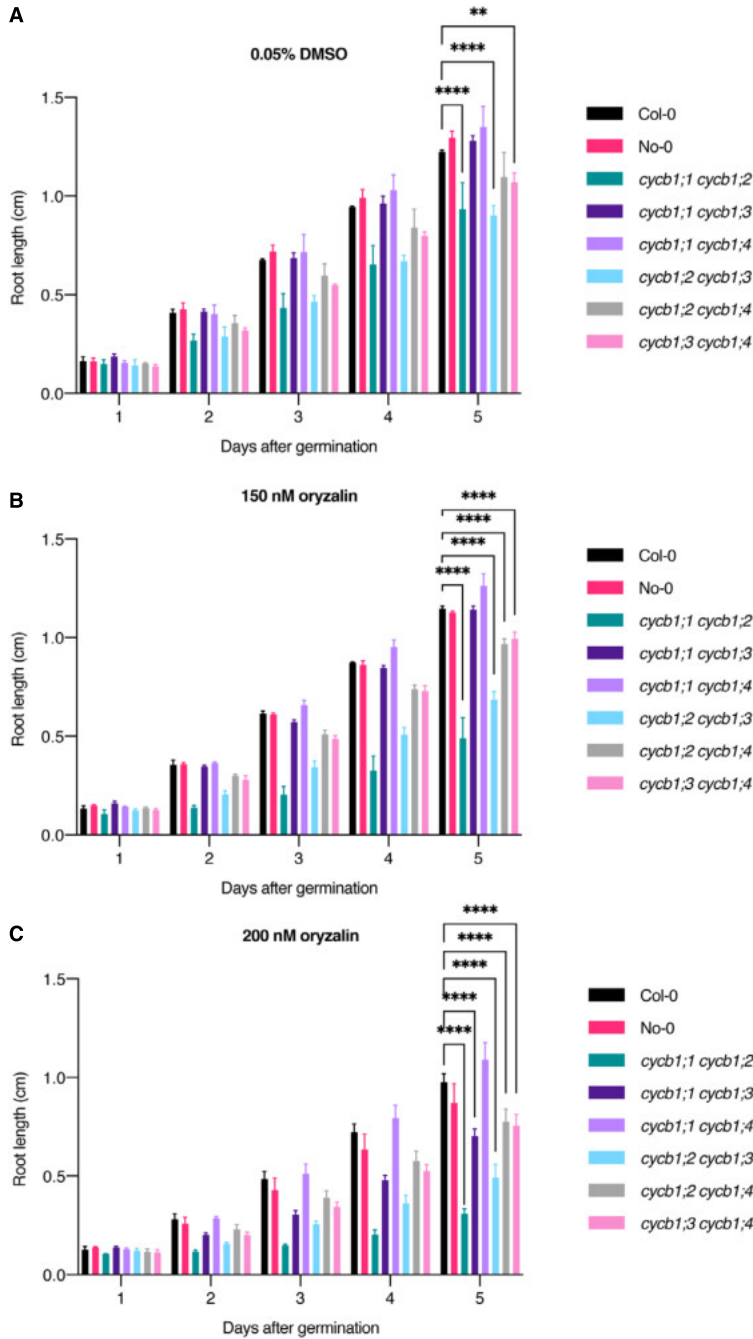


**Figure EV4. Oryzalin root growth assays across time in *cycb1* double mutants.**

A–C Quantification of root length in a control condition (A), 150 nM oryzalin (B), and 200 nM oryzalin (C). Graphs show mean  $\pm$  SD of three biological replicates with at least 10 plants per genotype per replicate. Asterisks indicate a significant difference in root length in a two-way ANOVA followed by Tukey's multiple comparisons test (\*\* $P < 0.01$  and \*\*\*\* $P < 0.0001$ ).

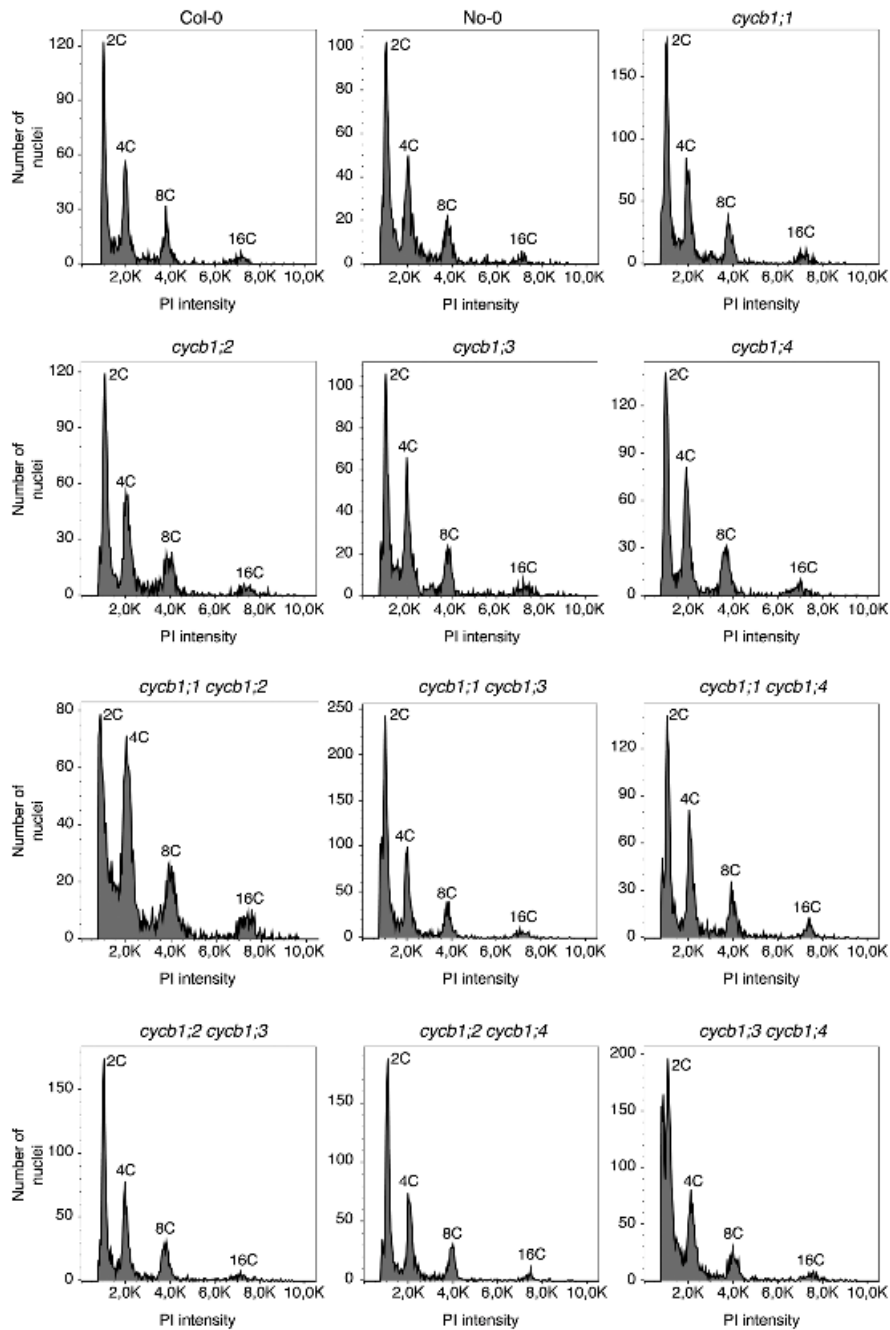


**Figure EV5. Ploidy analysis of young seedlings of the single and double mutants.**

Flow cytometrical quantification of the different nuclear ploidy levels, as indicated by propidium iodide (PI) intensity. Single (top rows) and double (bottom rows) mutants have been analyzed. The individual genotypes are indicated on the top of each graph. Each peak has been labeled according to the expected nuclear content (2C, 4C, 8C or 16C).





## **Chapter 2. Investigating the role of CYCB1-dependent regulation of microtubule arrays**



## 2.1. Introduction

### 2.1.1. Microtubule nucleation in the absence of a centrosome

Microtubules are dynamic structures with a plus- and a minus-end. The plus-end is the dynamic one, switching rapidly between phases of growth and shrinkage, while the minus-end is more stable and is the end where the microtubule is initially nucleated (Fig 1; Goodson & Jonasson 2018). The nucleation of microtubules in animals and fungi is concentrated in distinct microtubule organizing centers (MTOCs; Paz & Lüders, 2018), a prominent example being the centrosome, where most of the main microtubule nucleator  $\gamma$ -tubulin Ring Complex ( $\gamma$ TuRC) is localized. In flowering plants, however, there is no centrosome and the localization of nucleation events of microtubules is more flexible (Fig 1A-D; Lee & Liu, 2019).

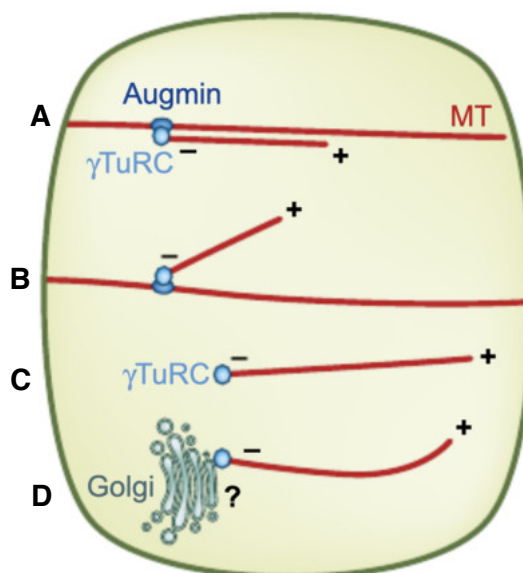


**Figure 1. Microtubule nucleation in the plant cell.** The figure was adapted from Lee & Liu, 2019.

- A, B. Microtubule nucleation can take place in the plant cell in a microtubule-dependent manner by means of the augmin complex, that enables binding of the  $\gamma$ TuRC to existing microtubules. This microtubule-dependent microtubule nucleation can be parallel (A) or branched (B).
- C. Nucleation can also happen *de novo* and requires only the activity of the  $\gamma$ TuRC.
- D. The  $\gamma$ TuRC can nucleate new microtubules from membranous organelles, e.g., the Golgi apparatus, although this mechanism has not been confirmed in plants.

### 2.1.2. The role of the $\gamma$ TuRC in microtubule nucleation

The  $\gamma$ TuRC is regarded as the most important factor in microtubule nucleation, i.e., the formation of a new microtubule seed onto which polymerization of  $\alpha$ - and  $\beta$ -tubulin heterodimers can happen. In other words, it serves as a docking station onto which new microtubules can assemble. It is important to mention, however, that the knockdown of  $\gamma$ -tubulin does not completely abolish microtubule assembly and, hence, other mechanisms for microtubule nucleation are likely in place (Paz & Lüders, 2018). In fact, microtubules can assemble spontaneously *in vitro*, although the composition of such spontaneous microtubules slightly varies when compared to  $\gamma$ TuRC-assembled microtubules, i.e.,  $\gamma$ TuRC-assembled microtubules have consistently 13 protofilaments, while spontaneously assembled microtubules have between 13 and 15 protofilaments (Paz & Lüders, 2018). Furthermore, in human colon cancer cells, depletion of CLASP1 or TPX2 (see general introduction for detailed function) significantly delayed the assembly of microtubules in the absence of  $\gamma$ -tubulin (Tsuchiya & Goshima, 2021). Hence, many MAPs are likely playing a secondary role in microtubule nucleation that is independent of  $\gamma$ -tubulin.

The vertebrate  $\gamma$ TuRC has been intensely studied, which has recently led to detailed information about the complex's composition and structure (Consolati *et al*, 2020; Wieczorek *et al*, 2020; Liu *et al*, 2020). The  $\gamma$ TuRC is assembled from a gamma-tubulin complex protein (GCP) scaffold containing GCP2 to GCP6 subunits – five copies of GCP2, five copies of GCP3, two copies of GCP4, one copy of GCP5 and one copy of GCP6 (Fig 2; Liu *et al*, 2021). Each GCP binds to one molecule of  $\gamma$ -tubulin through its C-terminal gamma-tubulin ring protein 2 motif (Liu *et al*, 2021).

Additional components of the  $\gamma$ TuRC include NEDD1 and MOZART1 (MZT1), which are considered to be less central to  $\gamma$ TuRC function and instead take part in assembly, targeting and activation of the complex (Farache *et al*, 2018). NEDD1 is a WD40 repeat protein that is known to be important for targeting the  $\gamma$ TuRC to centrosomes and the mitotic spindle, as well as promoting microtubule polymerization in the centrosomes in interphase and in the spindle during mitosis (Manning *et al*, 2010; Manning & Kumar, 2007). MZT1 is an essential member of the  $\gamma$ TuRC that interacts mainly with GCP3 and promotes what has been called an “interaction-competent” state of GCP3 *in vitro* in fission yeast, meaning that it prevents aggregation of  $\gamma$ -tubulin small complexes (comprised of  $\gamma$ -tubulin, GCP2 and GCP3; Leong *et al*, 2019). The specific function of

MZT1 across different organisms, although essential, has been a matter of debate. For instance, RNA interference experiments against MZT1 in human cells showed a pronounced impairment of  $\gamma$ TuRC function. The specific mechanism behind these results, however, have differed depending on the type of cell that was used (Cota *et al*, 2017; Lin *et al*, 2016; Hutchins *et al*, 2010).

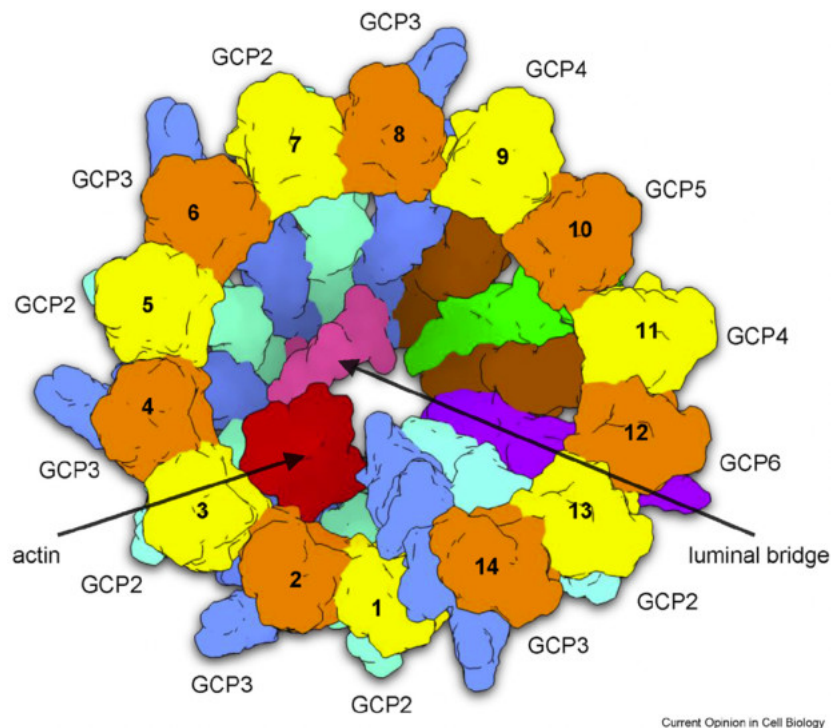


**Figure 2. A schematic picture of the vertebrate  $\gamma$ TuRC.** The figure was taken from Liu *et al*, 2021.

Top view of a *Xenopus levis*  $\gamma$ TuRC. Actin was also found to interact with the  $\gamma$ TuRC. Color code: yellow/orange:  $\gamma$ -tubulin; cyan: GCP2; blue: GCP3; brown: GCP4; green: GCP5; purple: GCP6; red: actin; and pink: luminal bridge.

Most of the plant counterparts of the  $\gamma$ TuRC components have been identified and characterized in *A. thaliana*, such as NEDD1, GCP2, GCP3, GCP4, GCP6 and MZT1 (Zeng *et al*, 2009; Seltzer *et al*, 2007; Kong *et al*, 2010; Miao *et al*, 2019; Nakamura *et al*, 2012; Janski *et al*, 2012).

NEDD1 seems to have an essential and conserved function in *Arabidopsis*, since a T-DNA insertion mutation can only be kept in a heterozygous state (Zeng *et al*, 2009). MZT1 in plants is represented by two homologs that are called GCP3-Interacting Protein 1 and 2 (GIP1 and GIP2; Nakamura *et al*, 2012; Janski *et al*, 2012). GIP1 and GIP2 are

highly redundant, i.e., the single knockout mutants are viable, while the double *gip1 gip2* mutant is embryonic lethal (Nakamura *et al*, 2012).

### 2.1.3. The augmin complex: a conserved role in enabling microtubule-based microtubule nucleation

The augmin complex is highly conserved in eukaryotes and is mainly responsible for microtubule-dependent microtubule nucleation (Fig 3A and 3B; Tian & Kong, 2019). It is composed of eight members and electron microscopy has revealed a flexible Y-shaped structure in humans (Fig 4; Hsia *et al*, 2014). In *Xenopus levis*, two functional modules of the augmin complex have been identified: one module (tetramer-II) is necessary for microtubule binding, while the other one interacts with the  $\gamma$ TuRC (tetramer-III; Song *et al*, 2018). Both *X. levis* tetramers fit together into a similar Y shape to what has been described for the human augmin complex.

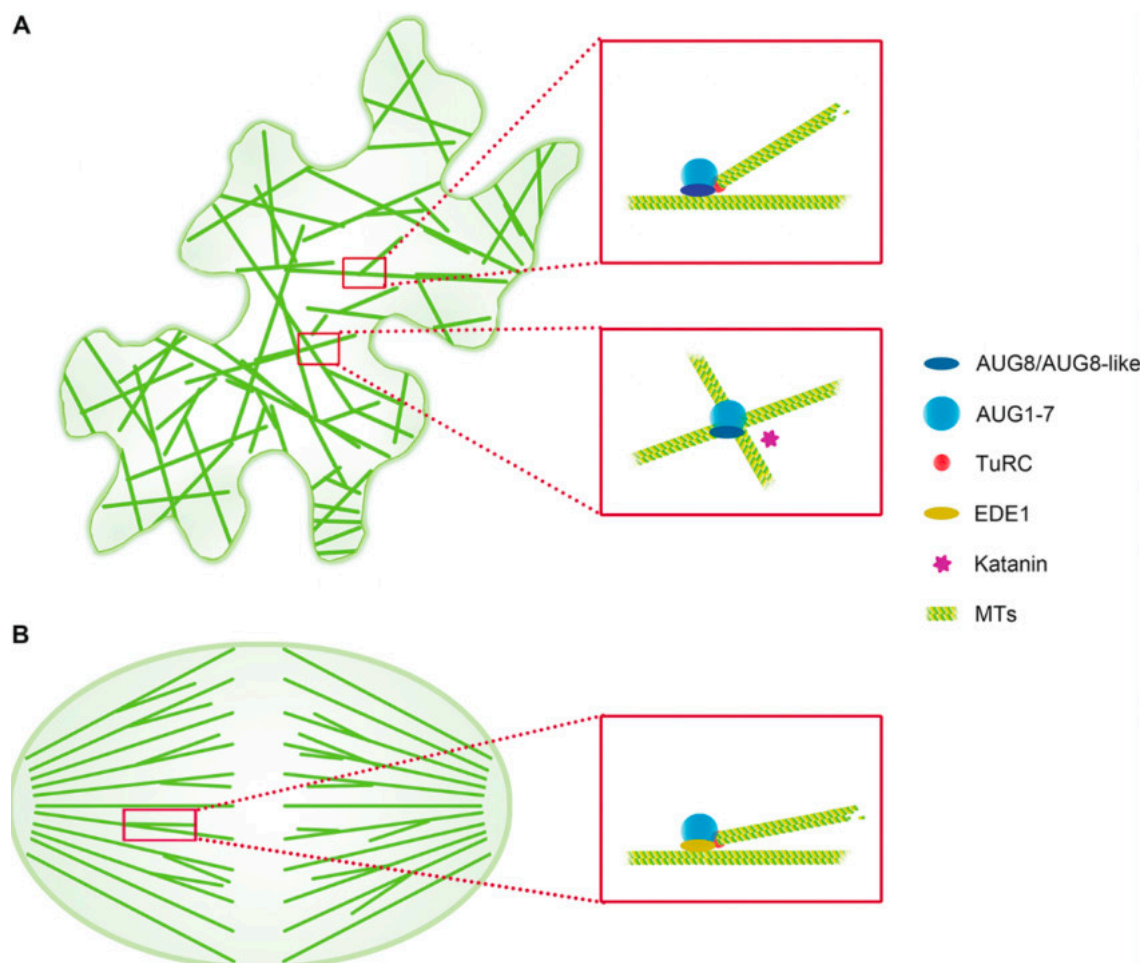


**Figure 3. Role of the augmin complex in interphasic and mitotic plant cells.** The figure was taken from Tian & Kong, 2019.

A. In interphase, microtubules are nucleated from the side wall of existent microtubules through the interaction of the AUG8/AUG8-like microtubule-binding subunit of the augmin complex with those structures. Microtubule crossovers (in detail) are stabilized by the action of the augmin complex that antagonizes the microtubule-severing complex katanin.

B. In mitosis, EDE1 takes over the action of AUG8/AUG8-like and promotes the interaction of the augmin complex with the walls of existent microtubules for microtubule-dependent microtubule nucleation.

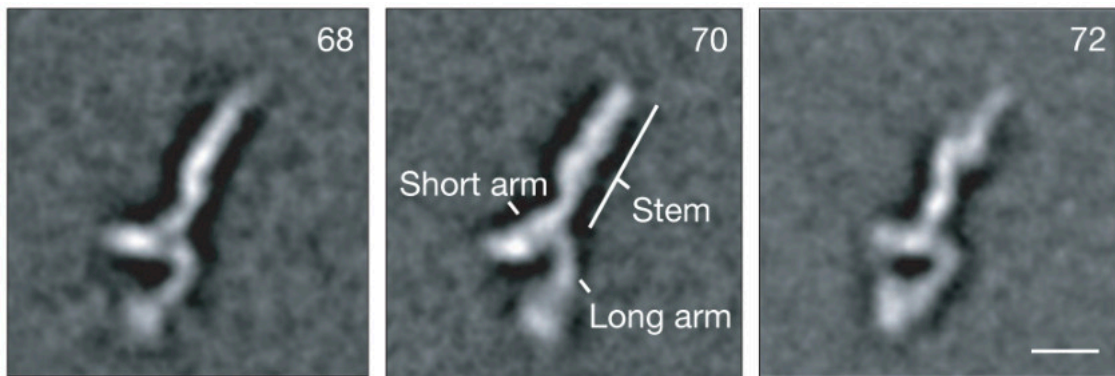


**Figure 4. The Y-shaped structure of the human augmin complex.** The figure was taken from Hsia *et al*, 2014.

The human augmin complex has been studied by electron microscopy, revealing a flexible Y-shaped structure with three different main conformations (seen in the figure;  $N = 68, 70$  and  $72$  for each class accordingly). The main features of the complex are indicated in the figure, with a short and long arm and a stem.

In humans, the augmin complex is composed of HAUS1-8, with the microtubule-binding component being HAUS8/Hice1 (Wu *et al*, 2008; Johmura *et al*, 2011). In plants, there are also eight main members: AUG1-8, with AUG8 being represented by several isoforms (Fig 3). AUG8 and its isoforms (from here on referred to as AUG8-like) represent the so-called nine-member QWRF family (Fig 5; Albrecht *et al*, 2010) and constitute individually the plant microtubule-binding component of the augmin complex. An essential homolog of AUG8 (QWRF8) is EDE1 (QWRF5), which is plant-specific since there is little sequence conservation with other animal augmin components and also a member of the QWRF family (Lee *et al*, 2017; Hotta *et al*, 2012). EDE1 replaces the function of AUG8/AUG8-like in G2/M – AUG8 cannot fulfil the function of EDE1 in that stage (Lee *et al*, 2017). EDE1 and AUG8 (and likely AUG8-like) interact with AUG6 to form a functional augmin complex (Lee *et al*, 2017).

Furthermore, an alignment of the amino acid sequence of human HAUS8 and the plant QWRF family members reveals little conservation in sequence between the plant microtubule-binding components and their respective human counterpart at the N-terminus, suggesting that plants likely evolved a specific regulation and/or structure of the augmin complex (Fig 5). HAUS8 is known to have a microtubule-binding domain between amino acids 1 and 140, but this sequence shows little conservation when, for instance, it is compared to EDE1 (Fig 5; Wu *et al*, 2008). The C-terminus of the QWRF and HAUS8 proteins, however, is highly conserved and is likely important for interaction with other augmin components and complex establishment. Indeed, in humans, HAUS8 has been shown to interact with HAUS6 via its C-terminus (Hsia *et al*, 2014). In *A. thaliana*, EDE1's C-terminal amino acids 237 to 341 are also sufficient for interaction with AUG6, as shown by yeast two-hybrid experiments (Muzaffer Emre Gül, master's thesis).

Although knockout mutants for EDE1 are not viable, a partial loss-of-function *ede1-1* allele has been extensively used to study EDE1 function (Lee *et al*, 2017; Pignocchi *et al*, 2009). This mutant has a generally normal growth, but affected seed endosperm development, retarded root growth and extremely elongated spindle arrays in mitosis (Lee *et al*, 2017; Pignocchi *et al*, 2009).

A related factor and antagonist of augmin function is the katanin complex. It is comprised of the p60 AAA ATPase catalytic subunit and the p80 regulatory subunit (McNally & Roll-Mecak, 2018). This complex is necessary to sever microtubules after branched microtubule-dependent microtubule nucleation to generate free microtubules (Nakamura *et al*, 2010) or at microtubule junctions (the above-mentioned crossovers) to promote amplification and reorganization of cortical microtubules (Lindeboom *et al*, 2013).

Recently, a function of augmin at microtubule crossovers has been uncovered in plants: augmin antagonizes the microtubule-severing katanin and thus stabilizes microtubule crossovers rather than triggering microtubule nucleation at those sites (Wang *et al*, 2018). Hence, many questions remain and the augmin complex might play diverse roles apart from branched microtubule nucleation.



```

sp | Q9BT25 | HAUS8_HUMAN | ----- | 0
sp | Q8S8I1 | QWRF3_ARATH | ----- | 0
sp | Q80588 | EDE1_ARATH | MEARIGRSM EHPSTPAINAPA----- PVP P P P S T R R P R - V R E V S S R F M S P 43
sp | Q5BPM6 | QWRF6_ARATH | MEA----- K T S G P K Q I Q P S T ----- P A P P P S T R R P R - V R E V S S R F M S P 37
sp | Q1PE51 | QWRF7_ARATH | ----- | 0
sp | F4INP9 | QWRF4_ARATH | - M Q V G S K K A S M G K Q Q S V S D A T S P - R P P L A P S E K N N V G S V T R R A R - T M E V S S R Y R S P 54
sp | Q95UH5 | AUG8_ARATH | ----- M D V A T D T T - R R R L L P S D K N N A V V A T R R P R - T M E V S S R Y R S P 39
sp | F4K4M0 | QWRF9_ARATH | ----- M T A A T I S P S F N A N - V K Q N K P P S F P S E - S S N R R P K - T R D V A S R Y L G G 43
sp | Q8GXD9 | SC03_ARATH | - M V - - - A A I P Q G A A I S N T D S K N P P P R D R Q D K P Q L T A N N G G L Q R R P R A A K N V P S R Y L S P 54
sp | Q94AI1 | QWRF2_ARATH | ----- M V A A A I S T T D P R N P P - - - R D R P Q S L T N N G G Q - R R P R - G K Q V P S R Y L S P 43

sp | Q9BT25 | HAUS8_HUMAN | ----- | 0
sp | Q8S8I1 | QWRF3_ARATH | ----- | 0
sp | Q80588 | EDE1_ARATH | I S S S S S S S S S S A G D ----- L H Q L T S N S P R - H H ----- H Q - 72
sp | Q5BPM6 | QWRF6_ARATH | V T S S - - - S S S A G D ----- L H S L T C N S P K - Q H ----- H L Q 62
sp | Q1PE51 | QWRF7_ARATH | ----- | 0
sp | F4INP9 | QWRF4_ARATH | T P T K T R - - - - - R C - P S P I V T R T A P S S S S P E - - - - - 77
sp | Q95UH5 | AUG8_ARATH | T P T K N G - - - - - R C - P S P S V T R P T V S S S S Q - - - - - 62
sp | F4K4M0 | QWRF9_ARATH | T S S F F H Q - - - - - S S P K R C - Q S P I V T R P V T P S - - - - - 68
sp | Q8GXD9 | SC03_ARATH | S P S H S T T T T T T T - - - - - A T S T S T S S S S S V I L R S S K R Y P S P - L L S - R T T N S A S N L V Y P T 105
sp | Q94AI1 | QWRF2_ARATH | S P S H S V S S T T T T T T T T T T S S S S S S S S A I L R T S K R Y P S P S P L L S R S T T N S A S N S K T P 103

sp | Q9BT25 | HAUS8_HUMAN | ----- | 0
sp | Q8S8I1 | QWRF3_ARATH | ----- M K S C E H E L L K T R R G K S 16
sp | Q80588 | EDE1_ARATH | - H Q N Q R S T S A Q R M R R Q L K M Q E - - - - - G D E N - R P S E T - A - - - - - 102
sp | Q5BPM6 | QWRF6_ARATH | H H Q I Q R S V S A Q R L R R Q L K M A D - - - - - G D E N - R S S E T A A - - - - - 94
sp | Q1PE51 | QWRF7_ARATH | ----- | 0
sp | F4INP9 | QWRF4_ARATH | S F - L K R A V S A E R N R - - - - - G P S T P T P V S D V L V D L P V S S R R L S T G R L P E S L W P S T M - - - - - 127
sp | Q95UH5 | AUG8_ARATH | S V A A K R A V S A E R K R P S T P S P T S P T P I R D L S I D L P A S S R R L S T G R L P E S L W P S T M - - - - - 118
sp | F4K4M0 | QWRF9_ARATH | S V A T N R P Q S T P R R - - - - - E S L D - - - - - R R E V S K A E R M L L T S G - - - - - 100
sp | Q8GXD9 | SC03_ARATH | S S L P K R S Q S V D R R R P S A V S D - T - - - - - R T E M S A A T K M L I T S T - - - - - 141
sp | Q94AI1 | QWRF2_ARATH | S L L P K R S Q S V D R R R P S A V S V T V - - - - - G T E M S A A T K M L I T S T - - - - - 140

sp | Q9BT25 | HAUS8_HUMAN | ----- | 0
sp | Q8S8I1 | QWRF3_ARATH | R E V S S R F L S S - - - - - P - - - - - S A S S S P N R R N 37
sp | Q80588 | EDE1_ARATH | R S L D S P F P L Q Q V D G G - - - - - K N - - - - - P - - - - - K Q 122
sp | Q5BPM6 | QWRF6_ARATH | R S L D S P F T L S Q S R K S - - - - - S K - - - - - P - - - - - 112
sp | Q1PE51 | QWRF7_ARATH | ----- | 0
sp | F4INP9 | QWRF4_ARATH | R S L S V S F Q S D S V S V P V S K K E K P L V T S S T D R T L R P S S S N I A H K Q S E T T S V T R K Q T P E R K R 187
sp | Q95UH5 | AUG8_ARATH | R S L S V S F Q S D S V S V P V S K K E R P V S S S S G D R T L R P S - S N I A Q K H K A E T T S V S R K P T P E R K R 177
sp | F4K4M0 | QWRF9_ARATH | R S L F A S F Q A D S F T P G T L E R R K T T S S A - - - - - T I S K S G - - - - - 132
sp | Q8GXD9 | SC03_ARATH | R S L S V S F Q G E A F S F P I S K K K E T - A T P - - - - - V S H R K C T P E R R R 178
sp | Q94AI1 | QWRF2_ARATH | R S L S V S F Q G E A F S L P I S K K K E T T S T P - - - - - V S H R K S T P E R R R 178

sp | Q9BT25 | HAUS8_HUMAN | ----- | 0
sp | Q8S8I1 | QWRF3_ARATH | S T S N - - - S S R D D - Q N N G V K G H L G L - - - - - K K H D R M S D G T R V - C - F G L P N Q S S I E V - - - - - D T K 85
sp | Q80588 | EDE1_ARATH | - H I R S K P L K E N G H R L D T P T T A M L P P P S R - - - - - S R L N Q - - - - - Q R L L T A S A A 163
sp | Q5BPM6 | QWRF6_ARATH | - - - - - S H L K P L N E N S H R L E T P T P M V P P P P S R - - - - - S R L S Q - - - - - Q R L P T A - 149
sp | Q1PE51 | QWRF7_ARATH | ----- | 4
sp | F4INP9 | QWRF4_ARATH | S P L K G K N V S P G Q S E N S K P M D G S H S M L I P P Q H R W S G R I R G N - - - - - R S F D L G D K A 236
sp | Q95UH5 | AUG8_ARATH | S P L K G K N N V S D L S E N S K P V D G P H S R L I - E Q H R W P S R I G G K - - - - - I T S N S L N R S L D L G D K A 232
sp | F4K4M0 | QWRF9_ARATH | - - - - - G G K Q E K L K - - - - - L S D Q W P R S L Q P S C - - - - - L S S R S V D F T D T R 165
sp | Q8GXD9 | SC03_ARATH | A T - - - - - P V R D Q R E N S K P V - - - - - D Q Q L W P G A S R R G S S E S V V P N S L S R S V D S D S D D 224
sp | Q94AI1 | QWRF2_ARATH | S T - - - - - P V R D Q R E N S K P V - - - - - D Q Q R W P G A S R R G N S E S V V P N S L S R S L D C G S D R 224

sp | Q9BT25 | HAUS8_HUMAN | ----- | 0
sp | Q8S8I1 | QWRF3_ARATH | E N R M P S P W I N D - - - - - E D N V I L P G R F S V D E C A L Y - - - - - R A S S R R N S C - 123
sp | Q80588 | EDE1_ARATH | T R L L R S S G - - - - - 171
sp | Q5BPM6 | QWRF6_ARATH | T R L L Q L S G - - - - - 157
sp | Q1PE51 | QWRF7_ARATH | G R R L R P P S P N N - - - - - N R S R T I S S S I S L P V S L N A S L S S T - S S S S S S P S N S S - 51
sp | F4INP9 | QWRF4_ARATH | V R R - - - - - V S L P L S N K S S R H K - - - - - K S S S D I T R L - 261
sp | Q95UH5 | AUG8_ARATH | S R G I P T S G P G M G P S L R R - - - - - M S L P L S S S S R P L H - - - - - K T S S N T S S Y G 272
sp | F4K4M0 | QWRF9_ARATH | K K L I G S G N G V A R - A L Q D S M V S N R P V S - - - - - R E - - - - - 192
sp | Q8GXD9 | SC03_ARATH | G R K L G S G F V G R S - M L Q H S - - - - - Q S S R V S G D R L N L G F V G D G M L E M R D E N K A R Q S T H P R L A 280
sp | Q94AI1 | QWRF2_ARATH | G - K L G S G F V G R S - M L H N S M I D E S P R V S V N G R L S L D L G G R D E Y L D I G D D I Q R R - - P N N G L T 280

sp | Q9BT25 | HAUS8_HUMAN | ----- | 31
sp | Q8S8I1 | QWRF3_ARATH | S L L Y E S F N D E T D S E L S D V S - - - - - C - - - - - A S S L S T N - - - - - R S S W N H K P G 159
sp | Q80588 | EDE1_ARATH | - I S L S S T D - G E E D N N N R E I F K S N G P D L L P - T - - - - - I - R - - - - - T Q - - - - - 204
sp | Q5BPM6 | QWRF6_ARATH | - I S A C Y E K E - G I I - N I Q E K P K S N G S D Q F P - T - - - - - L S C R - - - - - T H - - - - - 190
sp | Q1PE51 | QWRF7_ARATH | K R V M I T R S Q - S T - - - - - T R S S R P I G S S D S K S G E - N I P A R N S A S R S Q E I N N G R S R E S - - 101
sp | F4INP9 | QWRF4_ARATH | - - - - - F S C Y D N - - - - - G - R L E V S S T T S E D S S - - - - - S T E - S L - - - - - K H F S T S S - 294
sp | Q95UH5 | AUG8_ARATH | G L V S P T K S - - - - - E - D N N I A R T S G A Q R L L - - - - - S A G - S L D - - - - - R A T L A T A - 308
sp | F4K4M0 | QWRF9_ARATH | - - - - - R I T S V D - L E T E - - - - - S V S S G S N G R G K M L P A - R G N V V K A R - - - - - V S - - - - - 228
sp | Q8GXD9 | SC03_ARATH | S S V S C D F T A - S D T D - - - - - S V S S G S T N G A H E C G S G - - - - - E V S K T R - S L P R N G M A S T K F W Q E T - - 331
sp | Q94AI1 | QWRF2_ARATH | S S V S C D F T A - S D T D - - - - - S V S S G S T N G V Q E C G S G V N G E I S K S K - S L P R N I M A S A R F W Q E T - 334

```

```

sp|Q9BT25|HAUS8_HUMAN  GRVIESRYLQYEKKTQK-APAGD-----GSQTRGKMSGGRRKSSLLQKS  75
sp|Q8S8I1|QWRF3_ARATH  IKVSSKYLHDLTAKPKSGNNKTKLRS-----QDSSQRTNSSKGIEN-RLQRN  205
sp|080588|EDE1_ARATH    A-----KAFNTPTASP-----LSRSLSSD-----  223
sp|Q5BPM6|QWRF6_ARATH  ---L-----KVFNNPVPSS-----LNRSVSSP-----  209
sp|Q1PE51|QWRF7_ARATH  ---FARYL-----EQTRGSPRSNA-----SS  120
sp|F4INP9|QWRF4_ARATH  ---LPRLLHPMSAPGSRRTASPSR-----SSFSSSS  SS-----NSRGMSS-----  328
sp|Q9SUH5|AUG8_ARATH    ---VARLHPLPAPGSRPASPSPR-----TSFLLSSS  SISRGMSTSRGVS-----PS  349
sp|F4K4M0|QWRF9_ARATH  ---QDRLEP-----SSHGLRKISVDSSVLS-----PKEANLSSSPRGTSS-----I  265
sp|Q8GXD9|SCO3_ARATH    ---NSRLRRMQDPGSPQCSPPSSRISSISSKFSQSKRFSSDSPLTSSPRGMT-----S  381
sp|Q94AI1|QWRF2_ARATH  ---NSRLRRLQDPGSPSSPGLKTSISSKFGLSKRFSSDAVPLSSPRGMA-----S  384

sp|Q9BT25|HAUS8_HUMAN  KAD-----SSGVGKGDQLQST-L-----LEGHGTAPPDLDLSAINDKSIIVK  115
sp|Q8S8I1|QWRF3_ARATH  NSVSRVYGSMSQWALSPGRSLDTQAV-----TVPSKSLKPPRG-KGVGK  248
sp|080588|EDE1_ARATH    -----DASMFDRVR-A-----SLSLKNVGVL  243
sp|Q5BPM6|QWRF6_ARATH  -----SSSCN-VR-E-----S-SSFSRLGL  226
sp|Q1PE51|QWRF7_ARATH  RGVKPGASSPSAWALSPGRLSTMKTPLSSSAPTTSMC---MTPPESPVSKAKIRSGGGG  176
sp|F4INP9|QWRF4_ARATH  ---PSRGGVSPMRGLSPV-----GNRSLVRSSTPPSRGVSPSRIRQTAQS  369
sp|Q9SUH5|AUG8_ARATH  ---RGLSPSRGLSPTRGLSPRGLSP-----SRGTNTSCFARPSTPPSRGISPSRIRQTTTS  403
sp|F4K4M0|QWRF9_ARATH  ---ARGLSPSREVVP-----P-----RGVSPSDRMSPLRVSSL---  296
sp|Q8GXD9|SCO3_ARATH    ---PIRGA-TRPASPSKLWAT-----A-----TSAPARTSSSPSRVNRNGVSE  419
sp|Q94AI1|QWRF2_ARATH  ---PVRGSAIRSASPSKLWAT-----T-----TSSPARALSSPSRARNGVSD  423

sp|Q9BT25|HAUS8_HUMAN  TPQLA---KTISKKPESTSFSA---PRKKS PDLSE---AMEMMESQTLTLLTLLSVKMENN  166
sp|Q8S8I1|QWRF3_ARATH  LINLGFDFFRSKNKSS---PFTS---PLKPKTCDTESAHLKLMNRLQLQWRFVNARACDV  303
sp|080588|EDE1_ARATH    S-----LPPVAPNSKIQADTKKQKALGQQADVHSLKLLHNRYLQWRFANANAQV  294
sp|Q5BPM6|QWRF6_ARATH  P-----LPPMAPK---VPADTKKQKRVTEQLQEDVHSLKLLHNRYLQWRFANANAQV  275
sp|Q1PE51|QWRF7_ARATH  ---AVAGVLYKTFM---AQKKVSPVQEEYHFRIFQNRLLQWRFVNARTEAT  222
sp|F4INP9|QWRF4_ARATH  ---SSTNTSVLSFIADVKKGKKA-TYIEDVHQLRLLYNRYSQWRFANARAEGV  418
sp|Q9SUH5|AUG8_ARATH  ---TQSSTTTSLVLSFITDVKKGKKA-SYIEDVHQLRLLHNRYLQWRFANARAQV  454
sp|F4K4M0|QWRF9_ARATH  ---SKNTPLIPIHFAVD-GKEKIRDNQVADAHLLRLLHSLRLLQWRFANARNAV  345
sp|Q8GXD9|SCO3_ARATH    QM---NAYNRT-LPSILCFADIRRGKIGEDRVMDAHLRLLYRDLQWRFANARADST  474
sp|Q94AI1|QWRF2_ARATH  QM---NAYNRNNTPSILSFSADIRRGKIGEDRVMDAHLRLLYRDLQWRFVNARADST  479

sp|Q9BT25|HAUS8_HUMAN  LAEFERRAEKNLLIMCKEKEKLLQKKAHELKRRLLSQRKRELADVLDQIEMLSPFEEVA  226
sp|Q8S8I1|QWRF3_ARATH  NKNVASQEKNLQLCAWDTLTKLNNLVLQERIKLQKKNLEMKNYVFLSQVKKHLEAWEDME  363
sp|080588|EDE1_ARATH    TQSQKAQAERMFYSLGLKMSLESDSVQRKRRIEQLHLQRVKAVTEIVESQTPSLEQWAVLE  354
sp|Q5BPM6|QWRF6_ARATH  TQTHKTQTETMIHSFGSKISELHDSVQRKRRIEQLRLLKTKALLAITESQTPCLEQWSAIE  335
sp|Q1PE51|QWRF7_ARATH  MANLKINVEDQLFWVWLRYYKMRNYVVENLIEIQRLRQDIKRVREVLSQLMPLLNQWESKID  282
sp|F4INP9|QWRF4_ARATH  SYVQSLIAKETLYNVVWHASIDLRDLVTTQRICLQQLKLEIKLRSILNDQMVCLQWAMVE  478
sp|Q9SUH5|AUG8_ARATH  MYIQRLTSEETLFNVVWHASIDLDHVTQRIGLQQLKLEIKLNSLNDQMVCLQWAMVE  514
sp|F4K4M0|QWRF9_ARATH  ISSQKMRREERLYNAWRSISNLYNSVSMKRIEMOHLKQNLKLSILNMOMGHLEEWLVID  405
sp|Q8GXD9|SCO3_ARATH    LMVQRLSAEKILWNAWVSISELRHSVTLKRKIKLLMRQKLLKASILKEQMCYLEEWSLLD  534
sp|Q94AI1|QWRF2_ARATH  VMVQRLNAEKNLWNAWVSISELRHSVTLKRKIKLLLRQKLLKASILRGMGLFEWWSLLD  539

sp|Q9BT25|HAUS8_HUMAN  TRFKEQYRTFATALDTRHELVPVRSIHLEGDGQQLLDALQHELVTTQRLLGELDV---GDS  284
sp|Q8S8I1|QWRF3_ARATH  IQHLSLSSLIIRDLSLHVSRLPLKE-----GAKVNLSEAVSIIKNAEAVDAIISTVDDY  418
sp|080588|EDE1_ARATH    DEFSTSLLETTEALLNASLRLPLDS-----KIKVETKELAEALVVASKSMGIVQNIQNL  409
sp|Q5BPM6|QWRF6_ARATH  EEYSTSVSQTIQAFSNASLRLPLDG-----DIMVDSKQLGDLVAASKIVDGITQNVGNY  390
sp|Q1PE51|QWRF7_ARATH  AKNSEALSCLTRKLHALSVRLPLVH-----GATIDMVSIIHEEMVIAIEVMDIEIDVIFK  337
sp|F4INP9|QWRF4_ARATH  REHISSLAGAIGDLEANTLRLPLAG-----GTKADLGLSKLAMSSALDVMQSMGSSISWL  533
sp|Q9SUH5|AUG8_ARATH  RDHVSSLVGAISDLEANTLRLPATG-----GTKADTESLKAAMSSALDVMQAMGSSISWL  569
sp|F4K4M0|QWRF9_ARATH  RNYMGSLVGAEEALKGSTLCLPVDC-----GAMVNVQSVKDATCSAVDVMQAMASSICLL  460
sp|Q8GXD9|SCO3_ARATH    RNHSNLSGATEALKASTLRLPVSG-----KAVVDIQDLKHAVSSAVDVMHAMVSSIFSL  589
sp|Q94AI1|QWRF2_ARATH  RDHSSSLSGATESLKASTLRLPIVG-----KTVVDIQDLKHAVSSAVDVMQAMSSIFSL  594

sp|Q9BT25|HAUS8_HUMAN  -EENVQVLDLLELKDVTAKKDLERRSFAQVLELSAEASKEAALANQEVW-----  334
sp|Q8S8I1|QWRF3_ARATH  APTMEGIVPLASQLAEVVVQEKLMLEKCHDLLRMISELEMQERSLKCCFLIQHKQTFDNT  478
sp|080588|EDE1_ARATH    VPKTQEMETLMSELARVSGIEKASVEDCRVALLKTHSSQMEECYLRSQLIQHQKCHQOQE  469
sp|Q5BPM6|QWRF6_ARATH  MPKAKEMESLSELTRVARSERSLTENCVALLKTOASQVNLSSLHKLKNVL-----  442
sp|Q1PE51|QWRF7_ARATH  LPRVEIILYELTELIGMFNQELLYFEEMDESLLSIPLFTAKESSLRVHILQKTEEQR---  394
sp|F4INP9|QWRF4_ARATH  HSQMEEMNKLVSDLAVIAKTENFLLDKCNLLASTAVMEIEERSLKTHLIQKKQEEVVRD  593
sp|Q9SUH5|AUG8_ARATH  LSKVEEMNIMVTELAVVVTKESSMQGKCEDLLASTAIMQIEECSLRTHLIQRREEG-ED  628
sp|F4K4M0|QWRF9_ARATH  LPKVGKISSLAELGRVNAKDEGMLDVCRDLLNTISALQVTECSLRTQVTQLQ-----  513
sp|Q8GXD9|SCO3_ARATH    TSKVEMNSVMAEMVNTIGKEVLLQCGFLTRVAAMQVTDCSMKTHIIQLSRL-----  644
sp|Q94AI1|QWRF2_ARATH  TSKVDEMNSVMVETVNTAKEKVVLLERCQGCLSRVAAMQVTDCSMKTHIIQLSRIPIITSS  654

sp|Q9BT25|HAUS8_HUMAN  -EETQGMAPPSPRWYFNQDSACRESGGAPKNTPLSEDDNPGASSAPAQATFISPSSEDFSSS  393
sp|Q8S8I1|QWRF3_ARATH  LLKH-----  482
sp|080588|EDE1_ARATH    CTTSV-----  474
sp|Q5BPM6|QWRF6_ARATH  -----  442
sp|Q1PE51|QWRF7_ARATH  -----  394
sp|F4INP9|QWRF4_ARATH  DAESSPLPLSKFQWP-----  609
sp|Q9SUH5|AUG8_ARATH  AETPPPLPLSKFPWP-----  644
sp|F4K4M0|QWRF9_ARATH  -----  513
sp|Q8GXD9|SCO3_ARATH  -----  644
sp|Q94AI1|QWRF2_ARATH  L---TPQL-----  659

```

|                       |       |       |       |       |       |       |       |       |       |       |       |       |       |       |     |
|-----------------------|-------|-------|-------|-------|-------|-------|-------|-------|-------|-------|-------|-------|-------|-------|-----|
| sp Q9BT25 HAUS8_HUMAN | SQA   | E     | V     | P     | P     | S     | L     | R     | S     | G     | R     | D     | L     | S     | 410 |
| sp Q8S8I1 QWRF3_ARATH | ----- | ----- | ----- | ----- | ----- | ----- | ----- | ----- | ----- | ----- | ----- | ----- | ----- | ----- | 482 |
| sp O80588 EDE1_ARATH  | ----- | ----- | ----- | ----- | ----- | ----- | ----- | ----- | ----- | ----- | ----- | ----- | ----- | ----- | 474 |
| sp Q5BPM6 QWRF6_ARATH | ----- | ----- | ----- | ----- | ----- | ----- | ----- | ----- | ----- | ----- | ----- | ----- | ----- | ----- | 442 |
| sp Q1PE51 QWRF7_ARATH | ----- | ----- | ----- | ----- | ----- | ----- | ----- | ----- | ----- | ----- | ----- | ----- | ----- | ----- | 394 |
| sp F4INP9 QWRF4_ARATH | ----- | ----- | ----- | ----- | ----- | ----- | ----- | ----- | ----- | ----- | ----- | ----- | ----- | ----- | 609 |
| sp Q9SUH5 AUG8_ARATH  | ----- | ----- | ----- | ----- | ----- | ----- | ----- | ----- | ----- | ----- | ----- | ----- | ----- | ----- | 644 |
| sp F4K4M0 QWRF9_ARATH | ----- | ----- | ----- | ----- | ----- | ----- | ----- | ----- | ----- | ----- | ----- | ----- | ----- | ----- | 513 |
| sp Q8GXD9 SCO3_ARATH  | ----- | ----- | ----- | ----- | ----- | ----- | ----- | ----- | ----- | ----- | ----- | ----- | ----- | ----- | 644 |
| sp Q94AI1 QWRF2_ARATH | ----- | ----- | ----- | ----- | ----- | ----- | ----- | ----- | ----- | ----- | ----- | ----- | ----- | ----- | 659 |

**Figure 5. An alignment of the protein sequences of the human HAUS8 and *A. thaliana* QWRF family members, including AUG8 (QWRF8) and EDE1 (QWRF5).**

The alignment of the protein sequences was performed with Clustal Omega (<https://www.ebi.ac.uk/Tools/msa/clustalo/>). In red, small and hydrophobic amino acids, including aromatic residues except tyrosine; in blue, acidic amino acids; in magenta, basic amino acids except histidine; in green, amino acids with hydroxyl, sulfhydryl and amine groups and glycine; and, in grey, unusual amino acids are represented. An asterisk indicates residues which are fully conserved; a colon indicates conservation between groups of strongly similar properties; and a period indicates conservation between groups of weakly similar properties.

## Research aim

As previously described, CYCB1 members are known to control microtubule organization in *A. thaliana* (Chapter 1; Motta *et al*, 2021). However, the mechanism by which CYCB1-mediated phosphorylation is responsible for microtubule organization is largely uncharacterized. Hence, in this part of my project, I tested the role of phosphorylation of two MAPs, GIP1 and EDE1, by CYCB1-CDKB2;2 complexes.

First, GIP1 had already been identified as a substrate of CYCB1-CDKB2;2 complexes (Chapter 1; Motta *et al*, 2021), although the exact position and function of its phosphorylation was not studied. Here, I identified the amino acids phosphorylated *in vitro* and tested the functionality of two dephosphomutant combinations by analyzing the general phenotype of plants carrying these mutations and the ability of the respective mutant protein to interact with its  $\gamma$ TuRC partner.

Next, EDE1 was chosen as a possible target of CYCB1-CDKB2;2 complexes because of the remarkable similarity between *cycb1;1 cycb1;2* and *ede1-1* mutant seed development. Indeed, EDE1 was found to be phosphorylated at several sites. A dephosphomutant of EDE1 was generated and its function in general plant growth, root mitotic divisions and spindle architecture was tested, revealing a potential role of the CYCB1 group in regulation of microtubule-dependent microtubule nucleation.

## 2.2. Results

### 2.2.1. Mutating the consensus CDK phosphorylation site in GIP1 does not visibly alter its function

GIP1 was previously confirmed to be a substrate of CYCB1-CDKB2;2 complexes in *in vitro* kinase assays (Motta *et al*, 2021). Therefore, we created a reporter to follow its localization in mitosis (GFP-GIP1; Motta *et al*, 2021) and to conduct analyses of protein function.

GIP1 contains a single consensus CDK phosphorylation site (T67; Fig 6 and 7). GIP2, its close homolog, does not possess a CDK phosphorylation site; in turn, an aspartate is seen at the C-terminus in a similar position (D67; Fig 6 and 8). To analyze if phosphorylation of T67 is relevant for GIP1 function, I mutated this amino acid into an Alanine (Ala), which is an amino acid that cannot be phosphorylated (from now on referred to as GIP1<sup>T67A</sup>), and introduced this construct into the *gip1 gip2* double mutant (Fig 9).

```

sp|Q9M0N8|GIP1_ARATH      MDEEASRTARESELELVFRMSNILD TGLDRHTLSVLIALCDLGVNPEALATVVKELRRESI 60
sp|Q9C9T3|GIP2_ARATH      MNQEAAETARESELELVFRMSNILE TGLDRHTLSVLIALCDIGLNPEALATLVKELRRDSA 60
*!::**!.*****:*****:*****:*****:*****:*****:*****:*****:
                                     *

sp|Q9M0N8|GIP1_ARATH      PDSVTTTPSIH 71
sp|Q9C9T3|GIP2_ARATH      TTTTTVD---- 67
                                     !.*.

```

#### Figure 6. Comparison of the protein sequences of GIP1 and GIP2.

The alignment of the protein sequences was performed with Clustal Omega (<https://www.ebi.ac.uk/Tools/msa/clustalo/>). In red, small and hydrophobic amino acids, including aromatic residues except tyrosine; in blue, acidic amino acids; in magenta, basic amino acids except histidine; in green, amino acids with hydroxyl, sulfhydryl and amine groups and glycine; and, in grey, unusual amino acids are represented. An asterisk indicates residues which are fully conserved; a colon indicates conservation between groups of strongly similar properties; and a period indicates conservation between groups of weakly similar properties.

As judged by pollen viability (Fig 9A), seed abortion (Fig 9B) and root growth over time (Fig 9C), a GFP-GIP1<sup>T67A</sup> construct fully rescued the mutant phenotype. Therefore, I wondered if another site was the actual phosphorylation target. To test for this possibility, I cloned, expressed and purified HisGST-GIP1 and HisGST-GIP2 protein fusions and submitted them to *in vitro* kinase assays together with CYCB1-CDKB2;2 complexes (Fig

10A-D and Table S1). Mass spectrometry was then performed to identify the position of the phosphorylated amino acids (Fig 7 and 8; Table S1).

MDEEASRTARESLELVFRMSNILD TGLDRHTLSVLIALCDLGVNPEALATVVKELRRRES  
IPDSVITPSIH\*

**Figure 7. Phosphorylation sites identified in GIP1 in *in vitro* kinase assays performed with CYCB1-CDKB2;2 complexes by mass spectrometry.**

Amino acids that were identified as potential phosphorylation sites *in vitro* are indicated in bold and underlined. The consensus S/T-P CDK phosphorylation site is colored in magenta, while the other non-proline directed phosphorylation sites are indicated in green. The identification of the phosphorylation sites was obtained in collaboration with the Nakagami group at the Max Planck Institute for Plant Breeding Research and analyzed by Dr. Sara Stolze, who analyzed *in vitro* kinase assays performed by me.

MNQEAAETARESLELVFRMSNILETGLDRHTLSVLIALCDIGLNPEALATLVKELRRDS  
ATTTTTVD\*

**Figure 8. The protein sequence of GIP2.**

GIP2 does not contain a minimal consensus CDK phosphorylation site. Conversely, there is a negatively charged amino acid at the end of its C-terminus (represented in bold; D67).

GIP2, as predicted, was not phosphorylated in these *in vitro* kinase assays. For GIP1, on the other hand, phosphorylated peptides could be identified, and, indeed, T67 was found to be the most likely phosphorylation target, as revealed by the MaxQuant software which uses an algorithm to predict localization of the phosphosites (Fig 7; Table S1). However, since T67 is preceded by two additional threonines, I wondered if these might become targets of CDK phosphorylation in case the consensus site is not available, a phenomenon that is known as compensatory phosphorylation (Bauer *et al*, 2003). Additionally, it is often difficult to predict the exact location of phosphorylation sites in a peptide, especially when several amino acids are phosphorylated in the same peptide fragment (Dephoure *et al*, 2013). Indeed, mapping of these phosphosites did not completely rule out phosphorylation of T65 and T66. Thus, I proceeded to test the other two threonines (T65 and T66) of GIP1 *in vivo*. To that end, I generated a construct with T65, T66 and T67 each mutated into an Ala, which will from now on be referred to as GFP-GIP1<sup>T65A;T66A;T67A</sup>.

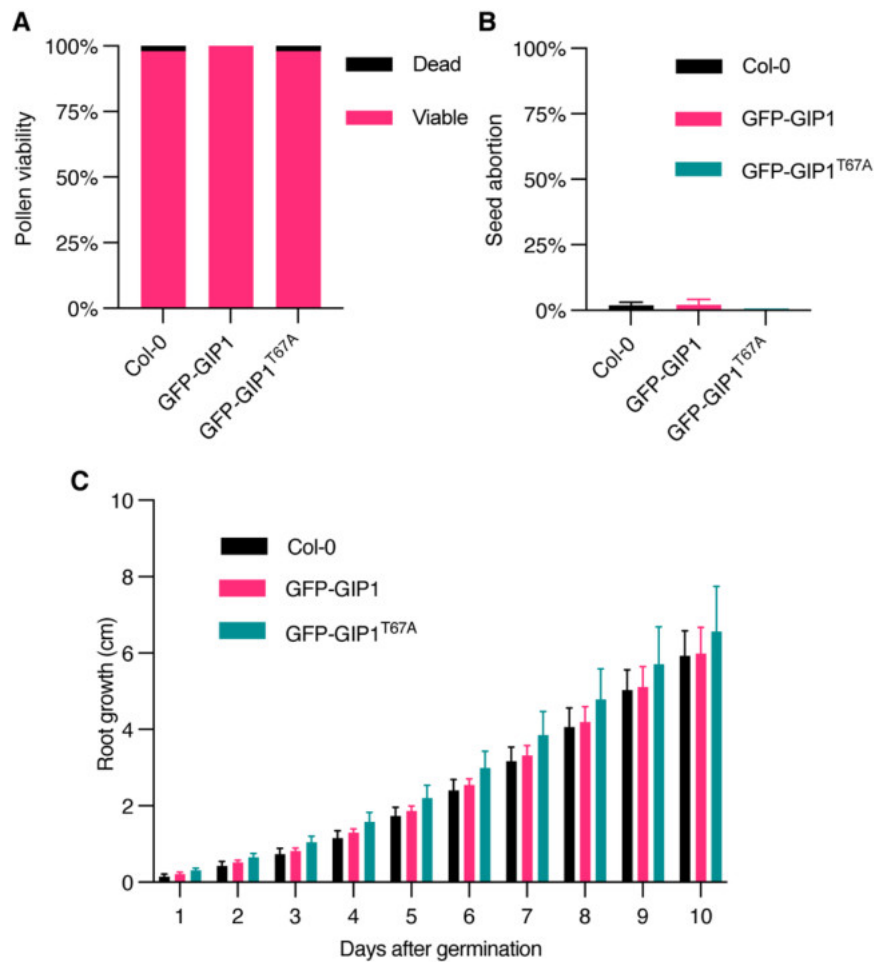


**Figure 9. GIP1<sup>T67A</sup> does not display significant changes in protein function compared to GIP1.**

A. Pollen viability assessed by Peterson staining in wildtype and *gip1 gip2* double mutants rescued by either GFP-GIP1 or GFP-GIP1<sup>T67A</sup>,  $n = 226 - 402$  pollen grains analyzed per genotype.

B. Quantification of seed abortion in wildtype and *gip1 gip2* double mutants rescued by either GFP-GIP1 or GFP-GIP1<sup>T67A</sup>. Graph represents mean seed abortion values per plant  $\pm$  SD from two biological replicates,  $n = 528 - 605$  seeds in total analyzed per genotype.

C. Root growth on  $\frac{1}{2}$  MS plates over time in wildtype and *gip1 gip2* double mutants rescued by either GFP-GIP1 or GFP-GIP1<sup>T67A</sup>. Graph represents mean root length value  $\pm$  SD of one biological replicate with  $n = 14 - 19$  plants per genotype. The GFP-GIP1 and GFP-GIP1<sup>T67A</sup> in *gip1 gip2* lines were generated by Dr. Shinichiro Komaki.

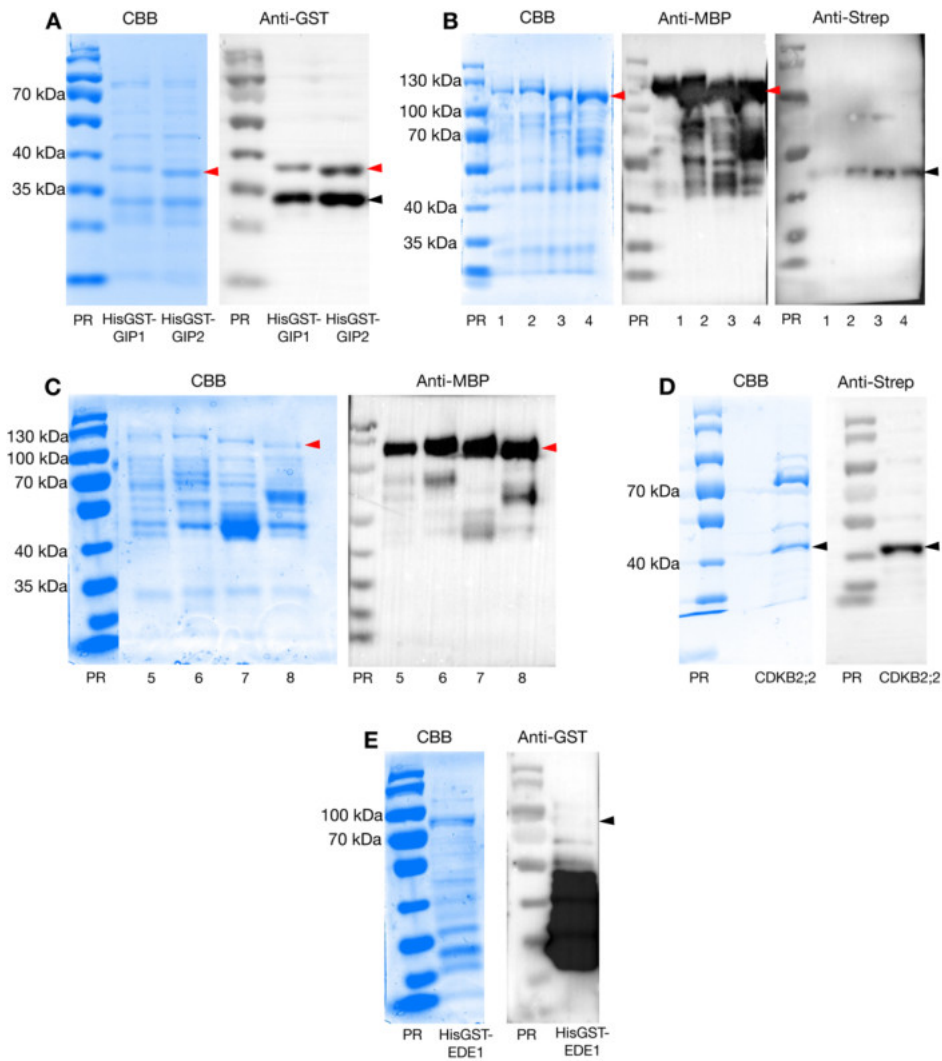


**Figure 10. Purified proteins for *in vitro* kinase assays.**

A. Purified HisGST-GIP1 and HisGST-GIP2 proteins (expected to be 36.3 kDa and 35.9 kDa respectively). Red arrowheads indicate proteins at expected molecular weight, while a black arrowhead indicates free GST.

B. Purified CYCB1-CDKB2;2 complexes. 1 = CYCB1;1-CDKB2;2, 2 = CYCB1;2-CDKB2;2, 3 = CYCB1;3-CDKB2;2 and 4 = CYCB1;4-CDKB2;2. Single HisMBP-CYCB1;1 is expected at 91.6 kDa, HisMBP-CYCB1;2 at 92.9 kDa, HisMBP-CYCB1;3 at 89.4 kDa and HisMBP-CYCB1;4 at 86.7 kDa. Red arrowheads indicate expected size of CYCB1 members. Black arrowhead indicates expected size of Strep-CDKB2;2 (39.9 kDa).

C. Purified single HisMBP-CYCB1 proteins. 5 = HisMBP-CYCB1;1, 6 = HisMBP-CYCB1;2, 7 = HisMBP-CYCB1;3 and 8 = HisMBP-CYCB1;4 (see above for expected sizes). Red arrowheads indicate expected size of CYCB1 members.

D. Purified single Strep-CDKB2;2 (see above for expected size). A black arrowhead indicates protein at expected size.

E. Purified HisGST-EDE1 (expected to be 81.1 kDa). Black arrowhead indicates approximate expected protein size.



Data information: PR = PageRuler Prestained protein ladder, CBB = Coomassie brilliant blue staining. The HisMBP-CYCB1;1 to HisMBP-CYCB1;4 and StrepIII-CDKB2;2 proteins were produced using plasmids generated by Dr. Hirofumi Harashima.

The GFP-GIP1<sup>T65A;T66A;T67A</sup> construct was also able to fully rescue a double *gip1 gip2* mutant (Fig 11A-D). I tested two independent insertion lines for both GFP-GIP1 and GFP-GIP1<sup>T65A;T66A;T67A</sup> in the *gip1 gip2* background and judged root growth on control and microtubule-destabilizing conditions (Fig 11A), seed abortion (Fig 11B and 11C) and pollen viability (Fig 11D). In all of these experiments, the triple dephosphomutant in the *gip1 gip2* background showed a similar behavior to the wildtype (Col-0) in both lines analyzed.

Next, I tested the ability of a GIP1<sup>T65A;T66A;T67A</sup> protein to interact with GCP3, which is its direct interacting partner in the  $\gamma$ TuRC complex (Fig 12). In a yeast two-hybrid assay, I detected a positive interaction of both GIP1 and its mutated GIP1<sup>T65A;T66A;T67A</sup> version with GCP3. Based on these results, it is likely that the regulation of GIP1 by the CYCB1 group is more complicated than I initially hypothesized. Thus, I started studying other substrates that are likely regulated by CYCB1-CDK complexes.

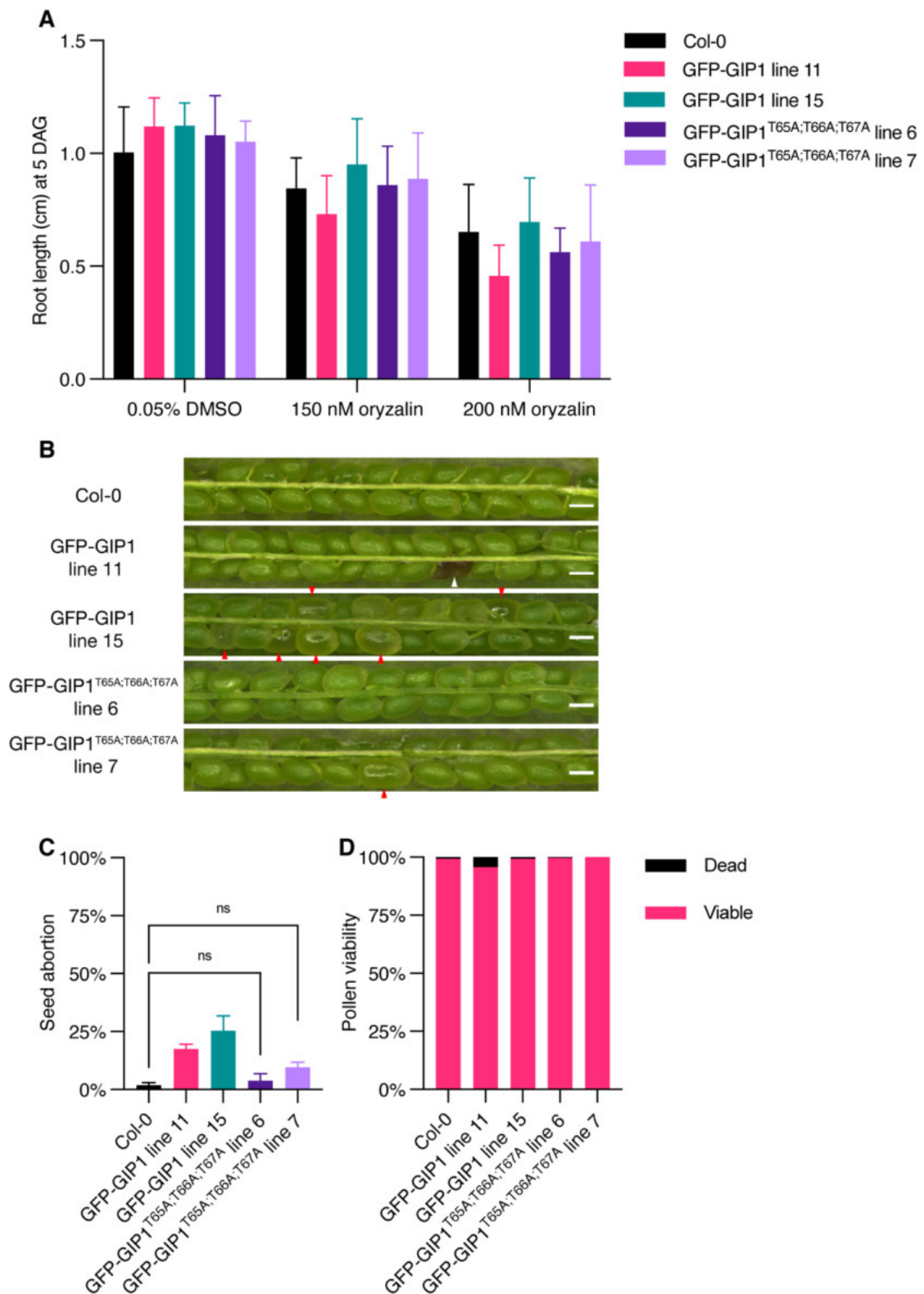


**Figure 11. Double *gip1 gip2* mutants rescued by GFP-GIP1<sup>T65A;T66A;T67A</sup> do not display significant changes in phenotype compared to *gip1 gip2* mutants rescued by GFP-GIP1.**

A. Root growth on 0.05% DMSO (control), 150 nM and 200 nM oryzalin plates in wildtype and *gip1 gip2* double mutants rescued by either GFP-GIP1 or GFP-GIP1<sup>T65A;T66A;T67A</sup>. Three experiments were performed independently with at least 10 seedlings per genotype. The mean

root length value 5 DAG was calculated individually for each experiment. These mean values were then averaged and plotted with  $\pm$  SD. DAG = days after germination.

B. Dissected siliques of wildtype and *gip1 gip2* double mutants rescued by either GFP-GIP1 or GFP-GIP1<sup>T65A;T66A;T67A</sup>. Red arrowheads indicate enlarged transparent seeds, which are likely defective in the development of the embryo. White arrowheads indicate late aborted seeds, with a typical dark appearance. Scale bars = 500  $\mu$ m.

C. Quantification of seed abortion in wildtype and *gip1 gip2* double mutants rescued by either GFP-GIP1 or GFP-GIP1<sup>T65A;T66A;T67A</sup>. Graph represents mean seed abortion values per plant  $\pm$  SD from three biological replicates in the case of Col-0, GFP-GIP1 line 11, GFP-GIP1 line 15 and GFP-GIP1<sup>T65A;T66A;T67A</sup> line 7, and two biological replicates in the case of GFP-GIP1<sup>T65A;T66A;T67A</sup> line 6,  $n = 433 - 1005$  seeds in total analyzed per genotype. An ordinary one-way ANOVA was performed followed by a Tukey's multiple comparisons test (ns = non-significant).

D. Pollen viability assessed by Peterson staining in wildtype and *gip1 gip2* double mutants rescued by either GFP-GIP1 or GFP-GIP1<sup>T65A;T66A;T67A</sup>,  $n = 205 - 303$  pollen grains analyzed per genotype. The GFP-GIP1 in *gip1 gip2* lines were generated by Dr. Shinichiro Komaki.

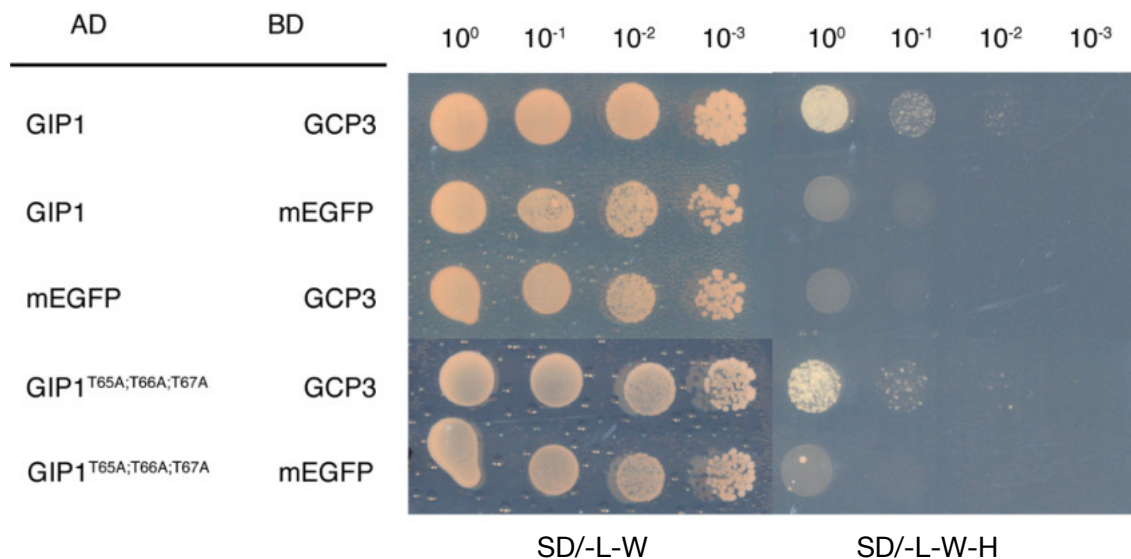


**Figure 12. A substitution of amino acids T65, T66 and T67 from GIP1 into alanine does not affect its interaction with GCP3.** The yeast two-hybrid was performed by Muzaffer Emre Gül during his master's thesis under my supervision. AD = activation domain, BD = binding domain. Yeast plates were incubated for 5 days.

### 2.2.2. A dephosphomutant version of EDE1 does not rescue *ede1-1*'s spindle architecture and growth under microtubule-destabilizing conditions

The weak Endosperm DEfective 1 (EDE1) mutant *ede1-1* (Pignocchi *et al*, 2009; Lee *et al*, 2017) exhibits an endosperm mutant phenotype that is highly reminiscent of the *cyb1;1 cyb1;2* endosperm failure (Motta *et al*, 2021). Thus, I hypothesized that this

protein might be regulated by CYCB1-CDK complexes. To test that, I expressed, purified and submitted a HisGST-EDE1 fusion to *in vitro* kinase assays (Fig 10B-E and Table S1). A total of 19 sites were identified to possibly be phosphorylated by CYCB1-CDKB2;2 complexes (Fig 13). As mentioned above, mapping of phosphorylation sites involves some degree of uncertainty and the location of the phosphosites is identified with a certain probability (Table S1).

MEARIGRSMEHP**ST**PAINAPAPVPPP**STR**RRPRVREVSSRFM**SP**ISSSSSSSSSSSAGD  
 LHQL**TS**NSPRHHHQHQNRSTSAQRMRRQLKMQEGDENRP**SET**ARSLD**SP**PFPLQQ  
 VDGGKNPKQHIRSKPLKENGHRLD**IP**T**IA**MLPPPSRSRLNQQRLTA**SA**ATRLLRSS  
 GISLSSSTDGEEDNNNREIFKSNGPDLLPTIRTQAKAFN**IP**T**AS**PLSRSLSSDDA**SM**FR  
 DVRASLSLKNVGLSLPPVAPNSKIQADTKKQKALGQQADVHSLKLLHNRYLQWRF  
 ANANAEVKTQSQAQAERMFYSLGLKMSSESDSVQRKRIELQHLQRVKAVTEIVESQ  
**IP**SLEQWAVLEDEFSTSLLETTEALLNASLRLPLDSKIKVETKELAEALVVASKSMEGIV  
 QNIGNLVPKTQEMETLMSELARVSGIEKASVEDCRVALLKTHSSQMEECYLRSQLIQH  
 QKKCHQQECTTSV\*

**Figure 13. Phosphorylation sites identified in EDE1 by *in vitro* kinase assays performed with CYCB1-CDKB2;2 complexes followed by mass spectrometry.**

Amino acids that were likely phosphorylated are indicated in bold and underlined. Consensus S/T-P CDK phosphorylation sites are indicated in magenta, while the other non-proline directed phosphorylation sites are indicated in green. Consensus S/T-P sites that were not identified in the *in vitro* kinase assays are underlined and in orange. The identification of the phosphorylation sites was obtained in collaboration with the Nakagami group at the Max Planck Institute for Plant Breeding Research and analyzed by Dr. Sara Stolze, who analyzed *in vitro* kinase assays performed by me.

To test the relevance of these sites *in vivo*, I generated a *GFP-EDE1* construct by making use of a 3,322 bp genomic fragment including 832 bp of promoter region and 503 bp of terminator sequence of *EDE1*. The GFP tag was inserted at the N-terminus just before the start codon. After generating this *GFP-EDE1* reporter construct, I decided to mutate eight S/T sites into Ala and will from now on refer to this mutant as EDE1<sup>8A</sup> (Fig 14). This dephosphomutant includes mutations in all the seven consensus S/T-P sites of EDE1's N-terminus as well as one Serine (S13) right next to the consensus T14 site. Since HAUS8, the human AUG8 homologue, has a microtubule binding domain between amino acids 1 and 140 at the N-terminus, it was likely that these phosphosites at the N-terminus of EDE1 would be involved in microtubule binding activity. The *GFP-EDE1*<sup>8A</sup>

dephosphomutant was then introduced into the *ede1-1* background and the phenotype of these mutants was checked in detail.



**Figure 14. The mutated S/T sites in EDE1<sup>8A</sup>**

Amino acids that were identified as phosphorylated in the *in vitro* kinase assays are represented in black. The T210 site was not identified by mass spectrometry and is therefore represented in gray. T14, S42, S66, S107, T138, T210 and S214 are all located in a minimal S/T-P CDK phosphorylation consensus site.

In the following root growth experiments, I tested three lines each for GFP-EDE1 and GFP-EDE1<sup>8A</sup> in the *ede1-1* mutant background. Under control conditions, the *ede1-1* mutants have a similar root growth to wildtype plants (when a delayed germination time is taken into account) and this was generally unchanged in the GFP-EDE1 and GFP-EDE1<sup>8A</sup> lines (Fig 15). Whether the GFP-EDE1 and GFP-EDE1<sup>8A</sup> constructs also rescue *ede1-1*'s root growth when root length is simply measured and germination time is not taken into account remains to be tested.

When I applied oryzalin at a 150 nM concentration, the *ede1-1* mutant grew significantly shorter than wildtype, a phenotype that could be rescued by the GFP-EDE1 construct. In contrast, none of the tested GFP-EDE1<sup>8A</sup> lines was able to rescue the mutant phenotype on oryzalin. A similar scenario was seen at a higher concentration of oryzalin (Fig 15; 200 nM oryzalin).

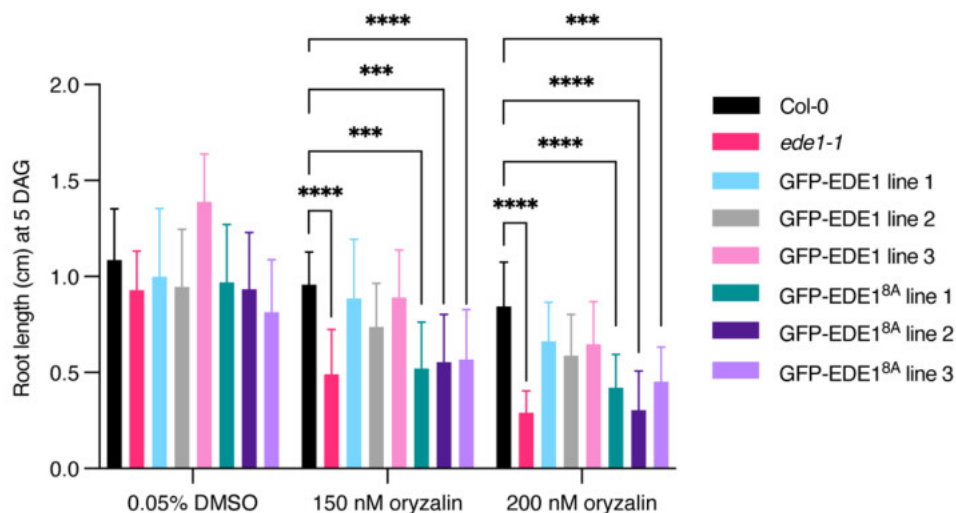


**Figure 15. A GFP-EDE1<sup>8A</sup> construct does not rescue the *ede1-1* phenotype on oryzalin.**

Root growth on 0.05% DMSO (control), 150 nM and 200 nM oryzalin plates in wildtype, *ede1-1* and *ede1-1* mutants rescued by either GFP-EDE1 or GFP-EDE1<sup>8A</sup>. Mean root length values per genotype  $\pm$  SD are shown (at least 10 seedlings per genotype were measured; \*\*\*  $P < 0.001$  and \*\*\*\*  $P < 0.0001$ ). DAG = days after germination.

I proceeded to analyze the root mitotic divisions of the *ede1-1* mutants expressing GFP-EDE1 or GFP-EDE1<sup>8A</sup> in detail. First, I decided to study the spindle mitotic array, which is clearly affected in *ede1-1* mutants where it exhibits a highly elongated shape (Lee *et al*, 2017). For that, after acquisition of confocal pictures of root tips of the different plant lines, I fitted an ellipse to RFP-TUA5-labelled spindles found in mitotic cells at metaphase. Next, I measured the following parameters: major axis, minor axis and spindle area; this approach was previously used to analyze spindle architecture (Herrmann *et al*, 2020). Plants expressing GFP-EDE1 in *ede1-1* background did not show any obvious deviation in spindle architecture from the wildtype and never exhibited *ede1-1*-like elongated spindles (Lee *et al*, 2017). However, GFP-EDE1<sup>8A</sup>-complemented *ede1-1* mutants already displayed a significantly enlarged major axis in a control condition (0.05% DMSO; Fig 16A and 16B) compared to *ede1-1* mutants rescued by GFP-EDE1 (the average major axis was  $6.955 \mu\text{m} \pm \text{SD } 0.675$  in GFP-EDE1 compared to  $7.858 \pm \text{SD } 1.093$  in GFP-EDE1<sup>8A</sup>), while the minor axis and the spindle area were not significantly different (Fig 16C and 16D). The localization of GFP-EDE1 and GFP-EDE1<sup>8A</sup> did not differ significantly in mitosis, although the signal was relatively low for both proteins as previously reported for an EDE1 reporter (J. Doonan, personal communication). Both proteins decorated spindle microtubules in a bipolar fashion as expected, since EDE1 is known to localize to microtubules minus-ends and aid microtubule-based microtubule nucleation towards the spindle midzone.

When oryzalin was applied at a concentration of 150 nM, *ede1-1* expressing GFP-EDE1<sup>8A</sup> displayed a significantly enlarged spindle major axis ( $7.396 \pm \text{SD } 0.977 \mu\text{m}$  on average in GFP-EDE1<sup>8A</sup> in comparison to  $6.286 \mu\text{m} \pm \text{SD } 0.728$  in GFP-EDE1) and conversely a significantly shortened minor axis ( $4.458 \mu\text{m} \pm \text{SD } 0.603$  in GFP-EDE1<sup>8A</sup> compared to  $5.402 \mu\text{m} \pm \text{SD } 1.471$  in GFP-EDE1; Fig 17A-C). The spindle area in *ede1-1* rescued by GFP-EDE1<sup>8A</sup>, on the other hand, was maintained when compared to *ede1-1* rescued by GFP-EDE1 (Fig 17D), similarly to control conditions. Again, extremely elongated *ede1-1*-like spindles were never observed and the localization of GFP-EDE1 and GFP-EDE1<sup>8A</sup> did not obviously differ; both proteins localized to the two poles of the spindle alongside a dark zone devoid of microtubules.

Finally, I decided to measure the duration of nuclear envelope breakdown (NEB) to anaphase onset (AO; Fig 17E). At this stage, the spindle assembly checkpoint is activated until the spindle fibers are stably attached to the sister kinetochores in a bipolar fashion and enough tension is sensed. Upon treatment with 150 nM oryzalin, *ede1-1* mutants expressing GFP-EDE1<sup>8A</sup> displayed a significant delay of this stage in comparison to the control condition (0.05% DMSO), while *ede1-1* plants rescued by GFP-EDE1 did not show a significant difference in NEB to AO when this stage was measured under control and microtubule-destabilizing conditions (Fig 17E). This is an indication that spindle microtubules in *ede1-1* mutants expressing GFP-EDE1<sup>8A</sup> are more unstable and, thus, take longer to assemble into stable attachments to kinetochores in metaphase.

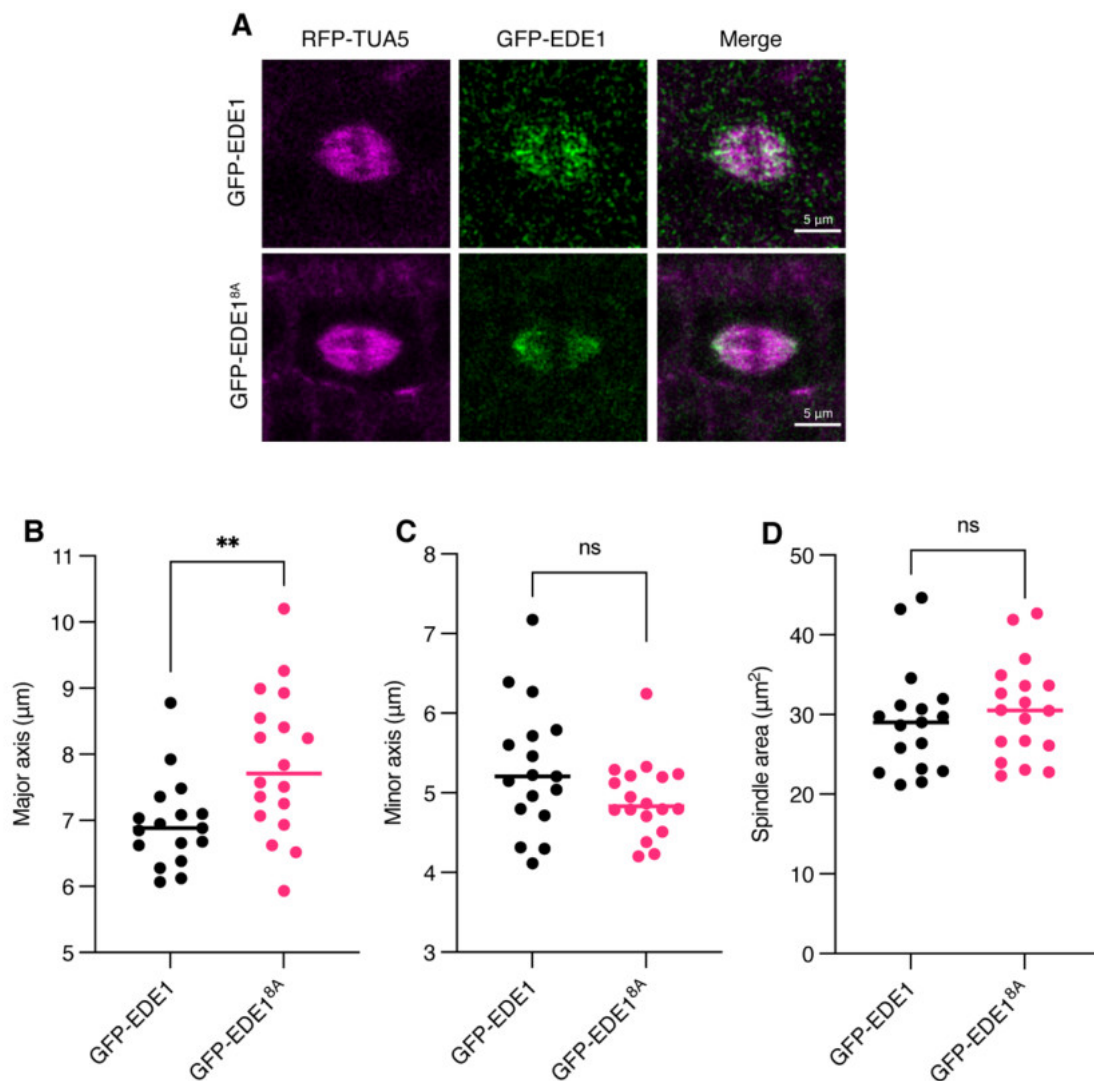


**Figure 16. Spindle architecture is affected in GFP-EDE1<sup>8A</sup>-expressing *ede1-1* mutants.**

A. Confocal microscope pictures of root mitotic divisions of plants expressing GFP-EDE1 and GFP-EDE1<sup>8A</sup> on 0.05% DMSO. GFP-EDE1 is represented in green, while RFP-TUA5 is

represented in magenta. Spindles are seen at maximum conformation before anaphase. Scale bars = 5  $\mu\text{m}$ .

B. Quantification of the major axis of a median slice of spindles at maximum conformation in GFP-EDE1- and GFP-EDE1<sup>8A</sup>-expressing *ede1-1* plants on 0.05% DMSO. Single values are plotted together with the median, which is represented as a bar. Asterisks represent significant differences in an unpaired *t* test (\*\*  $P < 0.01$ ,  $n = 17-18$ ).

C. Quantification of the minor axis of a median slice of spindles at maximum conformation in GFP-EDE1- and GFP-EDE1<sup>8A</sup>-expressing *ede1-1* plants on 0.05% DMSO. Single values are plotted together with the median, which is represented as a bar (ns = non-significant,  $n = 17-18$ ).

D. Quantification of the spindle area of a median slice of spindles at maximum conformation in GFP-EDE1- and GFP-EDE1<sup>8A</sup>-expressing *ede1-1* plants on 0.05% DMSO. Single values are plotted together with the median, which is represented as a bar (ns = non-significant,  $n = 17-18$ ).

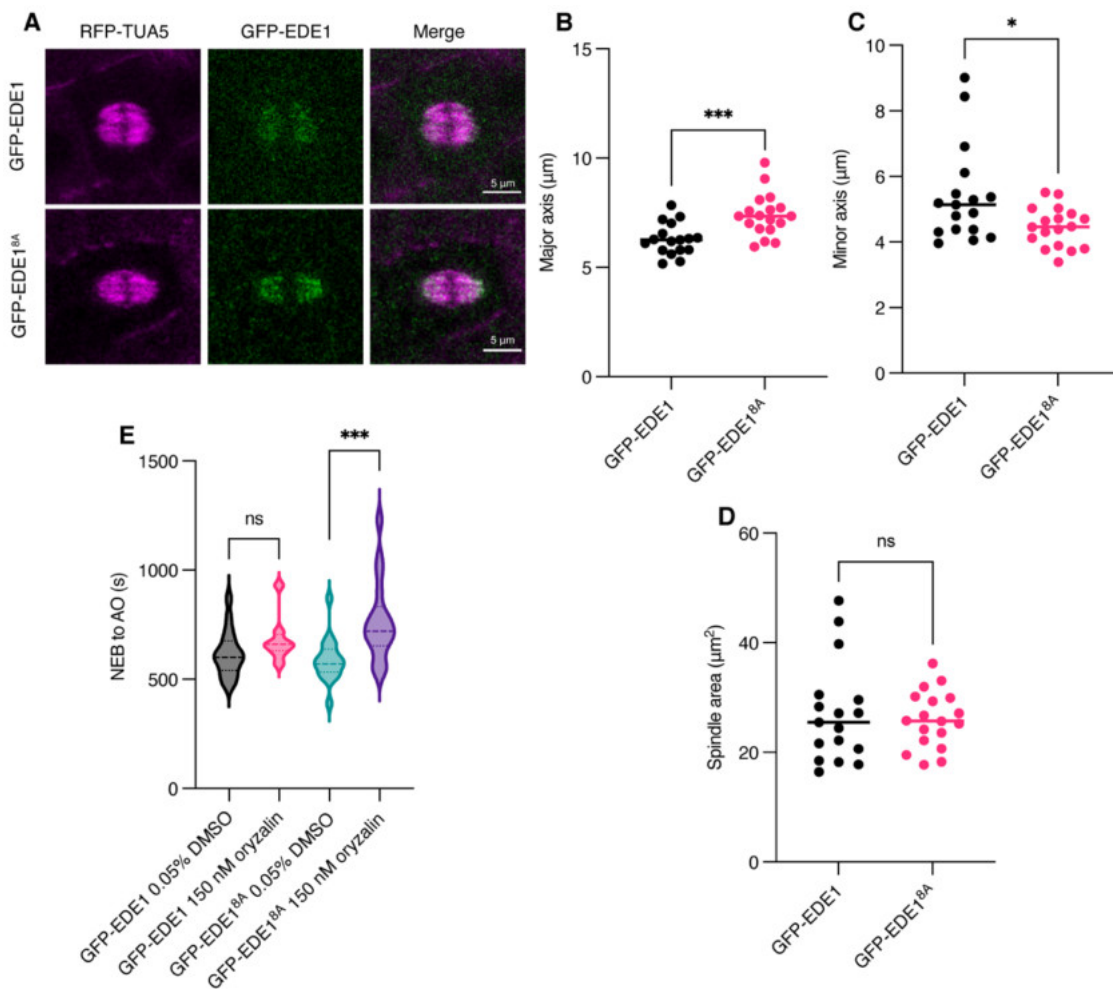


**Figure 17. Spindle architecture is affected and early spindle stages are prolonged in GFP-EDE1<sup>8A</sup>-expressing *ede1-1* mutants under microtubule-destabilizing conditions.**

A. Confocal microscope pictures of root mitotic divisions of GFP-EDE1- and GFP-EDE1<sup>8A</sup>-expressing *ede1-1* plants on 150 nM oryzalin. GFP-EDE1 is represented in green, while RFP-



TUA5 is represented in magenta. Spindles are seen at maximum conformation before anaphase. Scale bars = 5  $\mu\text{m}$ .

B. Quantification of the major axis of a median slice of spindles at maximum conformation in GFP-EDE1- and GFP-EDE1<sup>8A</sup>-expressing *ede1-1* plants on 150 nM oryzalin. Single values are plotted together with the median, which is represented as a bar. Asterisks represent significant differences in an unpaired *t* test (\*\**P* < 0.001, *n* = 17-18).

C. Quantification of the minor axis of a median slice of spindles at maximum conformation in GFP-EDE1- and GFP-EDE1<sup>8A</sup>-expressing *ede1-1* plants on 150 nM oryzalin. Single values are plotted together with the median, which is represented as a bar. Asterisks represent significant differences in an unpaired *t* test (\* *P* < 0.05, *n* = 17-18).

D. Quantification of the spindle area of a median slice of spindles at maximum conformation in GFP-EDE1- and GFP-EDE1<sup>8A</sup>-expressing *ede1-1* plants on 150 nM oryzalin. Single values are plotted together with the median, which is represented as a bar (ns = non-significant, *n* = 17-18).

E. Quantification of the duration of nuclear envelope breakdown (NEB) to anaphase onset (AO) in GFP-EDE1- and GFP-EDE1<sup>8A</sup>-expressing *ede1-1* plants on 0.05% DMSO and oryzalin conditions. Asterisks represent significant differences in an ordinary one-way ANOVA followed by Tukey's multiple comparisons test (\*\**P* < 0.001, ns = non-significant; *n* = 17-18).

## 2.3. Discussion

### 2.3.1. The CYCB1 group is a conserved regulator of mitosis and microtubule organization

It has been previously shown that the Cyclin B1 group has an essential role in mitosis in mammals, since null mutant embryos for this group arrest in G2 following only two divisions in mice (Strauss *et al*, 2018). To my knowledge, this is the most extreme phenotype known for mammal cyclin mutants. This role seems to be conserved in flowering plants, as we have also reported earlier that the CYCB1 group in *A. thaliana* is essential for cell division with CYCB1;2 playing the most central role in mitosis (Motta *et al*, 2021).

Over the past years, we have begun to understand the mechanistic role of Cyclin B-Cdk complexes in entry and progression through mitosis by regulating specific substrates. Blethrow *et al*, 2008, for instance, have identified a number of Cyclin B-Cdk1 substrates that are involved in mitotic progression. Lamin A/C phosphorylation at residues S22 and S392, for example, is required for nuclear envelope disassembly. Another example is the phosphorylation at T320 of protein phosphatase 1a, which dephosphorylates Cdk1 substrates and is, thus, a known antagonist of Cdk1. The phosphorylation of protein

phosphatase 1a at this site promotes its inhibition and, therefore, the progression of mitosis.

Interestingly, it has become clear that Cyclin B1-CDK complexes are tightly linked to microtubule dynamics in a conserved manner. For example, Cyclin B1 in humans has been found to bind MAD1 directly, which is essential for MAD1's localization to the kinetochore's corona and a robust signal of the spindle assembly checkpoint (Allan *et al*, 2020; Jackman *et al*, 2020). Also, recently, a preprint was published revealing the role of the sole Cyclin B1 in the green alga *Chlamydomonas* in microtubule dynamics, although no specific substrates were identified (Pecani *et al*, 2021).

In my thesis, I have now explored the regulation by phosphorylation of two CYCB1-CDK substrates in *A. thaliana*: GIP1 and EDE1.

### **2.3.2. The regulation of microtubule-associated proteins of the $\gamma$ TuRC by phosphorylation**

Microtubule dynamics, especially in acentrosomal flowering plants, are tightly linked to microtubule nucleation, which is carried out mainly by the  $\gamma$ TuRC. The regulation of the  $\gamma$ TuRC and its associated proteins by phosphorylation has been well documented before. For example, NEDD1, which is not part of the  $\gamma$ TuRC but binds directly to  $\gamma$ -tubulin and allows its recruitment to spindle microtubules by association with the augmin complex, has been found to be phosphorylated at several residues in humans (Gomez-Ferreria *et al*, 2012). A mutation in 23 S/T residues of NEDD1 to Ala, which was associated with an impaired ability of NEDD1 to oligomerize and interact with  $\gamma$ -tubulin, resulted in drastic spindle defects accompanied by fragmented centrosomes (Gomez-Ferreria *et al*, 2012). Another study revealed that phosphorylation of NEDD1 mediated by CDK1 at S460 induces an interaction with Polo-like kinase 1 (Plk1) and promotes its targeting to the spindle (Johmura *et al*, 2011). This interaction allows phosphorylation of HAUS8 by Plk1 and subsequent interaction of the augmin complex with microtubules (Johmura *et al*, 2011). Human GCP6, a member of the  $\gamma$ TuRC, has also been shown to be phosphorylated by Polo-like kinase 4 and the mutation of 17 residues that were predicted to be phosphorylated into Ala inhibited centriole duplication (Bahtz *et al*, 2012).

Here, I have first explored the phosphorylation regulation of GIP1, which is one of the plant homologs of MZT1 and, together with GIP2, is an essential member of the  $\gamma$ TuRC.

I have mutated the single S/T-P consensus site of GIP1 (T67), identified by mass spectrometry to be phosphorylated *in vitro*, into an Ala. Analysis of *gip1 gip2* mutants complemented with GIP<sup>T67A</sup> indicated no apparent deviation from the wildtype. An additional mutation in the two threonine residues preceding the consensus site (T65 and T66) and rescue of *gip1 gip2* also did not result in a clear change of phenotype. Thus, there are a couple of possible scenarios.

First, there might be other phosphorylation sites that were not identified in our *in vitro* kinase assays with CYCB1-CDKB2;2 complexes. Indeed, S59 was predicted to be a phosphorylation site with a score of 0.77 by the PhosPhAt database. Additionally, it has been revealed that non-proline directed multisite phosphorylation can be achieved by the action of Cks1 together with cyclin-CDK complexes after recognition of a phosphorylated consensus S/T-P site (Örd *et al*, 2019). Hence, there might be additional GIP1 phosphorylation sites *in vivo* when Cyclin-CDK co-factors are present and the initial phosphorylation event has taken place. Nevertheless, such additional secondary phosphorylation sites would also be lost with the mutation of the primary consensus S/T-P site into Ala and, therefore, this is unlikely to play a major role in the GFP-GIP1<sup>T65A</sup> or GFP-GIP1<sup>T65A;T66A;T67A</sup> dephosphomutants in the *gip1 gip2* background. The phenomenon of compensatory phosphorylation in other amino acids other than T65, T66 or T67, however, might still occur when these amino acids are mutated. This could be tested by submitting the GIP1<sup>T65A;T66A;T67A</sup> protein to *in vitro* kinase assays to potentially identify additional phosphosites, following the same procedure I described previously.

Second, although no striking phenotype was found in *gip1 gip2* rescued by GFP-GIP1<sup>T65A;T66A;T67A</sup> and the interaction of GIP1<sup>T65A;T66A;T67A</sup> with GCP3 was not affected, microtubule dynamics could be affected to a minor extent in that mutant. To test that, microtubule *in vitro* dynamics assays could be performed to analyze specific microtubule properties. In these assays, purified tubulin is added *in vitro* in an appropriate buffer system to the purified molecule of interest and parameters such as microtubule growth, shrinkage speed, catastrophe and rescue frequencies can be measured after imaging with high resolution microscopes, e.g., with total internal reflection fluorescence microscopy (TIRF; Zwetsloot *et al*, 2018). For instance,  $\gamma$ TuRC containing GIP1<sup>T65A;T66A;T67A</sup> might be less stable than the wildtype counterpart. Accordingly, the stability of microtubule minus ends could be compromised in that situation.

Alternatively,  $\gamma$ TuRCs associated with GIP1<sup>T65A;T66A;T67A</sup> might have a lower affinity towards co-factors, e.g., NEDD1, and therefore localization of those complexes could be

partially impaired. A pull-down of the dephosphomutant GFP-GIP1<sup>T65A;T66A;T67A</sup> in comparison to GFP-GIP1 *in vivo* could help reveal a difference in composition of such complexes.

Taking into consideration previous genetic analyses (Motta *et al*, 2021), it is still highly likely that GIP1 is a true substrate of CYCB1-CDKB2;2 complexes. However, the mechanism by which this happens, i.e., at which sites GIP1 gets phosphorylated *in vivo* or if phosphorylation at T67 is only relevant under certain conditions or in certain tissues remains to be elucidated.

Furthermore, if another target is responsible for a failure of a *gip2 cycb1;1 cycb1;2* triple mutant embryo (Motta *et al*, 2021) remains to be seen.

### **2.3.3. Phospho-regulation of microtubule-associated proteins of the augmin complex**

The post-translational modifications of augmin complex members seem to be finetuned by different kinases with opposing outcomes. For example, phosphorylation at residues T17, S19 and S20 of HAUS8 by Aurora-A seems to reduce microtubule binding affinity of HAUS8 (Tsai *et al*, 2011). The binding of a phosphomimic HAUS8 version (T17E, S19E, S20E and S21E) to microtubules is hence drastically reduced (Tsai *et al*, 2011).

On the other hand, as mentioned previously, HAUS8 is also known to be phosphorylated by Plk1 at several sites (Johmura *et al*, 2011). A dephosphomimic HAUS8 version with 6 mutated amino acids into Ala (HAUS8<sup>6A</sup>; S129A, T130A, S131A, S133A, S143A and S151A) is severely compromised in microtubule binding, while the respective phosphomimic version with the same amino acids mutated into aspartate binds as efficiently as the wildtype version to microtubules (Johmura *et al*, 2011). Thus, the phosphorylation of HAUS8 by Plk1 promotes its interaction with microtubules and its localization to the spindle.

Remarkably, the HAUS8<sup>6A</sup> dephosphomimic version promotes the formation of elongated spindles as judged by pole-to-pole distance, similarly to the EDE1<sup>8A</sup> I generated in my thesis. Therefore, it is tempting to speculate that a similar scenario is happening in *A. thaliana*. It remains to be tested whether a phosphomimic version of EDE1 (EDE1<sup>8D</sup>) can fully rescue the defects in spindle architecture and growth on oryzalin of *ede1-1*.

Based on the fact that GFP-EDE1<sup>8A</sup>-expressing *ede1-1* mutants displayed an elongated, abnormal spindle architecture, it is possible that the phosphorylation of EDE1 is necessary for its proper function and subsequently for a robust microtubule-based microtubule nucleation angle. Super-resolution microscopy, which can optically resolve up to approximately 10 nm (Galbraith & Galbraith, 2011), could potentially help us characterize the angle of microtubule nucleation in the mitotic divisions of these mutants. One possibility, for instance, is that the angle of nucleation in this mutant is much shallower than that of plants with an augmin complex containing a phosphorylated EDE1 and, therefore, GFP-EDE1<sup>8A</sup>-expressing *ede1-1* mutants yield an abnormally flat spindle. Another possibility, which does not exclude the first one, is that EDE1<sup>8A</sup> is binding microtubules less efficiently than a phosphorylated wildtype version. To test that, a microtubule co-sedimentation assay could be performed comparing the binding affinity of EDE1, EDE1<sup>8A</sup> and EDE1<sup>8D</sup> to microtubules.

Moreover, EDE1<sup>8A</sup>-expressing *ede1-1* mutants have a delay in duration of the early spindle stages under microtubule-destabilizing conditions. It is possible that the phosphorylated wild-type EDE1 can promote microtubule stabilization, similarly to what is known for HAUS8 and its ability to stabilize and bundle microtubules *in vitro* (Wu *et al*, 2008), while EDE1<sup>8A</sup> is less able to stabilize microtubules. It is important to note that not only the delay, but also a great increase in variance of duration of these early spindle stages in GFP-EDE1<sup>8A</sup>-expressing *ede1-1* mutants, is a hint that a stabilizing process might be impaired, similarly to what has been described in other MAP mutants. For example, *trm678* mutants, which are completely impaired in PPB formation, do not have abnormal cell division patterns but rather lose precision in their mitotic divisions as seen by a larger variance in certain parameters, such as the angle of the spindle (Schaefer *et al*, 2017). How the *trm678* mutation directly affects individual microtubule dynamics (including microtubule stability), however, is unclear.

It remains to be seen whether disrupting all of the possible 19 phosphosites of EDE1 can completely abolish its interaction with microtubules. Especially here, an important additional experiment would be to test whether the phosphomimic counterpart of EDE1 can rescue its function entirely to prove that mutation of 19 sites does not necessarily result in a non-functional protein. Still, this would not fully prove that the EDE1<sup>19A</sup> version is folding correctly. Thus, further experiments would be necessary to confirm proper folding and biological activity of such a protein version. For instance, a yeast-two hybrid assay with AUG6, its interacting augmin complex partner, could be performed to indicate EDE1 mutated in 19 amino acids has not lost all of its normal properties.

Finally, a full knockout mutant, *ede1-3*, is also available and is embryonic lethal (Pignocchi *et al*, 2009). The phenotype of *ede1-3* mutants rescued by GFP-EDE1 and GFP-EDE1<sup>8A</sup> should also be analyzed. It is possible that, in this background, the GFP-EDE1<sup>8A</sup> construct would cause a stronger phenotype, since the *ede1-1* mutant is considered weak and a truncated protein (lacking only 18 amino acids) is still produced in this background.

#### **2.3.4. The CYCB1 group likely regulates a plethora of substrates in *A. thaliana***

With the mutation of only GIP1 and EDE1 into their equivalent dephosphomimic versions (GIP1<sup>T65A;T66A;T67A</sup> in *gip1 gip2* and EDE1<sup>8A</sup> in *ede1-1*), I was not able to recapitulate a *cycb1* mutant phenotype as for instance seen in the dwarf *cycb1;1 cycb1;2* mutants (Motta *et al*, 2021). Thus, the CYCB1 group likely regulates a great number of substrates and the phenotype of *cycb1;1 cycb1;2* is highly pleiotropic, i.e., a combination of several faulty pathways. In other words, generating phosphomimic versions of single CYCB1 substrates and introducing them in a *cycb1;1 cycb1;2* mutant would most likely not rescue the *cycb1;1 cycb1;2* mutant phenotype.

On the one hand, the *cycb1;1 cycb1;2* mutant is a great tool to study the regulation of MAPs by CYCB-CDK complexes, since there is such a strong phenotype and we know relatively little about this regulation. To date, the only known cytoskeletal CDK substrates were MAP65-1 and EDE1 from *in vitro* assays and the NACK1 kinesin studies *in vivo* (Vavrdová *et al*, 2019; Pignocchi *et al*, 2009). A covalent capture of CDK phosphopeptides, as developed previously by Blethrow *et al*, 2008, is an useful tool for the identification of CDK substrates. In this study, human Cdk1 was engineered to use an analog of ATP that contains two distinct modifications. First, this ATP was modified in the adenine moiety, allowing binding to an engineered CDK; second, this ATP had a modified  $\gamma$ -phosphate that allowed the transfer of a tag to the substrates by the kinase. This tag is a phosphate mimetic called triphosphate. Peptides containing this tag were subsequently purified and phosphosites were identified by mass spectrometry. This technique could be adapted to plants and used to expand our knowledge of plant CDK substrates.

On the other hand, dissecting the regulation of different substrates by B1-type cyclins and the effect of phosphorylation on single proteins may be difficult, as seen by the lack of a clear phenotype of *gip1 gip2* expressing the GIP1<sup>T65A;T66A;T67A</sup> dephosphomutant. The

relative lack of available information on post-translational modifications *in vivo* is another complication for a study of phosphorylation regulation. For instance, in the PhosPhAt database, S8, S13, S27, T28, S66 and S104 of EDE1 were identified to be phosphorylated experimentally. Out of these sites, only S13 and S66 were mutated into Ala in the dephosphomutant GFP-EDE1<sup>8A</sup> version here-presented. Therefore, it might be necessary to submit substrates individually to *in vitro* kinase assays to identify all the phosphorylation sites. Protein expression and purification, however, is often laborious and time-consuming. *E. coli* is still the most used organism for protein expression with high yield; nevertheless, many proteins are known to be expressed in an insoluble state in this system (Gutiérrez-González *et al*, 2019). Purification of insoluble proteins and their refolding is another challenge (Singh *et al*, 2015). The emergence of other expression systems, such as the wheat germ cell-free system, may accelerate the expression of soluble eukaryotic proteins *in vitro* and allow for further advancement of our understanding of post-translational modifications (Harbers, 2014).

Here, I have been able to find a direct role of CDK phosphorylation in EDE1 function and, hence, in microtubule-based microtubule nucleation. Further experiments are necessary to narrow down the mechanism by which phosphorylation of EDE1 enables its proper functioning. Furthermore, it still remains to be seen if other CYCB members in addition to CYCB1, such as CYCB3;1 which is known to localize to spindle microtubules (Sofroni *et al*, 2020), may be responsible for phosphorylation and therefore regulation of EDE1 function.

## 2.4. Appendix

| Protein              | Position with tag | Localization probability | Peptide and phosphorylation probability   |
|----------------------|-------------------|--------------------------|---|
| AT4G09550HisGST-GIP1 | T313              | 0.996576                 | ESIPDSVTTT(0.996)PSIH   |
| AT2G44190HisGST-EDE1 | S254              | 0.921394                 | S(0.921)MEHPS(0.039)T(0.039)PA<br>INAPAPVPPPSTR   |
| AT2G44190HisGST-EDE1 | S259              | 0.864029                 | S(0.268)MEHPS(0.864)T(0.864)PA<br>INAPAPVPPPS(0.002)T(0.002)R   |
| AT2G44190HisGST-EDE1 | T260              | 0.877179                 | S(0.012)MEHPS(0.111)T(0.877)PA<br>INAPAPVPPPS(0.833)T(0.167)R   |
| AT2G44190HisGST-EDE1 | S273              | 0.833355                 | S(0.012)MEHPS(0.111)T(0.877)PA<br>INAPAPVPPPS(0.833)T(0.167)R   |
| AT2G44190HisGST-EDE1 | S288              | 1                        | FMS(1)PISSSSSSSSSSSAGDLHQ<br>LT(0.034)S(0.627)NS(0.34)PR  |
| AT2G44190HisGST-EDE1 | S291              | 0.75965                  | FMS(0.391)PIS(0.76)S(0.52)S(0.19<br>2)S(0.062)S(0.021)S(0.009)S(0.009<br>)S(0.009)S(0.009)S(0.009)S(0.009)<br>AGDLHQLTSNSPR   |
| AT2G44190HisGST-EDE1 | S292              | 0.521608                 | FMS(0.08)PIS(0.09)S(0.522)S(0.08<br>6)S(0.086)S(0.086)S(0.015)S(0.015<br>)S(0.015)S(0.003)S(0.003)S(0.001)<br>AGDLHQLTSNSPR   |
| AT2G44190HisGST-EDE1 | S293              | 0.242021                 | FMS(0.074)PIS(0.242)S(0.242)S(0.<br>242)S(0.074)S(0.074)S(0.012)S(0.0<br>12)S(0.012)S(0.012)S(0.002)SAGD<br>LHQLTSNSPR        |
| AT2G44190HisGST-EDE1 | S294              | 0.173804                 | FMS(0.174)PIS(0.174)S(0.174)S(0.<br>174)S(0.174)S(0.025)S(0.025)S(0.0<br>25)S(0.025)S(0.025)S(0.004)S(0.00<br>4)AGDLHQLTSNSPR |
| AT2G44190HisGST-EDE1 | S295              | 0.158049                 | FMS(0.024)PIS(0.158)S(0.158)S(0.<br>158)S(0.158)S(0.158)S(0.0<br>22)S(0.004)S(0.001)SSAGDLHQLT<br>SNSPR                       |
| AT2G44190HisGST-EDE1 | S296              | 0.158049                 | FMS(0.024)PIS(0.158)S(0.158)S(0.<br>158)S(0.158)S(0.158)S(0.0   |



---

|                           |      |           |  |
|---------------------------|------|-----------|--|
|                           |      |           | 22)S(0.004)S(0.001)SSAGDLHQLT<br>SNSPR   |
| AT2G44190IHisGST-<br>EDE1 | S297 | 0.0833301 | FMS(0.083)PIS(0.083)S(0.083)S(0.<br>083)S(0.083)S(0.083)S(0.083)S(0.0<br>83)S(0.083)S(0.083)S(0.083)S(0.08<br>3)AGDLHQLTSNSPR                          |
| AT2G44190IHisGST-<br>EDE1 | S298 | 0.0833301 | FMS(0.083)PIS(0.083)S(0.083)S(0.<br>083)S(0.083)S(0.083)S(0.083)S(0.0<br>83)S(0.083)S(0.083)S(0.083)S(0.08<br>3)AGDLHQLTSNSPR                          |
| AT2G44190IHisGST-<br>EDE1 | S299 | 0.232524  | FMS(0.998)PIS(0.001)S(0.003)S(0.<br>007)S(0.007)S(0.021)S(0.073)S(0.0<br>69)S(0.065)S(0.233)S(0.218)S(0.20<br>5)AGDLHQLT(0.065)S(0.018)NS(0.<br>017)PR |
| AT2G44190IHisGST-<br>EDE1 | S300 | 0.573221  | FMSPISSSSSSSSS(0.107)S(0.573<br>)S(0.319)AGDLHQLTSNSPR   |
| AT2G44190IHisGST-<br>EDE1 | S301 | 0.956855  | FMSPISSSSSSSSS(0.001)S(0.036<br>)S(0.957)AGDLHQLT(0.005)S(0.00<br>1)NSPR   |
| AT2G44190IHisGST-<br>EDE1 | T309 | 0.742757  | FMS(1)PISSSSSSSSS(0.001)S(0.00<br>1)S(0.001)S(0.001)AGDLHQLT(0.7<br>43)S(0.202)NS(0.051)PR   |
| AT2G44190IHisGST-<br>EDE1 | S310 | 0.626894  | FMS(1)PISSSSSSSSSSSAGDLHQ<br>LT(0.034)S(0.627)NS(0.34)PR   |
| AT2G44190IHisGST-<br>EDE1 | S312 | 0.994151  | FMS(1)PISSSSSSSSSSSAGDLHQ<br>LTS(0.005)NS(0.994)PR   |
| AT2G44190IHisGST-<br>EDE1 | S345 | 0.912222  | MQEGDENRPS(0.912)ET(0.088)A<br>R   |
| AT2G44190IHisGST-<br>EDE1 | T347 | 0.976782  | MQEGDENRPS(0.023)ET(0.977)A<br>R   |
| AT2G44190IHisGST-<br>EDE1 | S350 | 0.533145  | S(0.533)LDS(0.467)PFPLQQVDG<br>GK  |
| AT2G44190IHisGST-<br>EDE1 | S353 | 1         | SLDS(1)PFPLQQVDGGK   |
| AT2G44190IHisGST-<br>EDE1 | T384 | 0.999917  | LDT(1)PTTAMLPPPSR  |
| AT2G44190IHisGST-<br>EDE1 | T405 | 0.997364  | LLT(0.997)AS(0.002)AATR  |

---

|                           |      |          |                                   |
|---------------------------|------|----------|-----------------------------------|
| AT2G44190IHisGST-<br>EDE1 | S407 | 0.993578 | LLT(0.003)AS(0.994)AAT(0.004)R    |
| AT2G44190IHisGST-<br>EDE1 | S460 | 0.994449 | AFNTPT(0.001)AS(0.994)PLS(0.005)R |
| AT2G44190IHisGST-<br>EDE1 | S472 | 0.998365 | SLSS(0.002)DDAS(0.998)MFR         |

**Table S1. Mass spectrometry results of HisGST-GIP1 and HisGST-EDE1 proteins submitted to *in vitro* kinase assays.** The identification of the phosphorylation sites was obtained in collaboration with the Nakagami group at the Max Planck Institute for Plant Breeding Research and analyzed by Dr. Sara Stolze, who analyzed *in vitro* kinase assays performed by me.

## 2.5. References

- Albrecht V, Šimková K, Carrie C, Delannoy E, Giraud E, Whelan J, Small ID, Apel K, Badger MR & Pogson BJ (2010) The cytoskeleton and the peroxisomal-targeted SNOWY COTYLEDON3 protein are required for chloroplast development in Arabidopsis. *Plant Cell* 22: 3423–3438
- Allan LA, Camacho Reis M, Cioossani G, Huis in 't Veld PJ, Wohlgemuth S, Kops GJ, Musacchio A & Saurin AT (2020) Cyclin B1 scaffolds MAD1 at the kinetochore corona to activate the mitotic checkpoint. *EMBO J* 39: 1–16
- Bahz R, Seidler J, Arnold M, Haselmann-Weiss U, Antony C, Lehmann WD & Hoffmann I (2012) GCP6 is a substrate of Plk4 and required for centriole duplication. *J Cell Sci* 125: 486–496
- Bauer PM, Fulton D, Boo YC, Sorescu GP, Kemp BE, Jo H & Sessa WC (2003) Compensatory phosphorylation and protein-protein interactions revealed by loss of function and gain of function mutants of multiple serine phosphorylation sites in endothelial nitric-oxide synthase. *J Biol Chem* 278: 14841–14849
- Blethrow JD, Glavy JS, Morgan DO & Shokat KM (2008) Covalent capture of kinase-specific phosphopeptides reveals Cdk1-cyclin B substrates. *Proc Natl Acad Sci U S A* 105: 1442–1447
- Consolati T, Locke J, Roostalu J, Chen ZA, Gannon J, Asthana J, Lim WM, Martino F, Cvetkovic MA, Rappsilber J, *et al* (2020) Microtubule Nucleation Properties of Single Human  $\gamma$ TuRCs Explained by Their Cryo-EM Structure. *Dev Cell* 53: 603–617
- Cota RR, Teixidó-Travesa N, Ezquerro A, Eibes S, Lacasa C, Roig J & Lüders J (2017) MZT1 regulates microtubule nucleation by linking  $\gamma$ TuRC assembly to adapter-mediated targeting and activation. *J Cell Sci* 130: 406–419
- Dephoure N, Gould KL, Gygi SP & Kellogg DR (2013) Mapping and analysis of phosphorylation sites: A quick guide for cell biologists. *Mol Biol Cell* 24: 535–542
- Farache D, Emorine L, Haren L & Merdes A (2018) Assembly and regulation of  $\gamma$ -tubulin complexes. *Open Biol* 8: 1–8
- Galbraith CG & Galbraith JA (2011) Super-resolution microscopy at a glance. *J Cell Sci* 124: 1607–1611
- Gomez-Ferreria MA, Bashkurov M, Helbig AO, Larsen B, Pawson T, Gingras AC & Pelletier L (2012) Novel NEDD1 phosphorylation sites regulate  $\gamma$ -tubulin binding and mitotic spindle assembly. *J Cell Sci* 125: 3745–3751
- Goodson H V & Jonasson EM (2018) Microtubules and Microtubule-Associated Proteins. *Cold Spring Harb Perspect Biol* 10: 1–22

- Gutiérrez-González M, Farías C, Tello S, Pérez-Etcheverry D, Romero A, Zúñiga R, Ribeiro CH, Lorenzo-Ferreiro C & Molina MC (2019) Optimization of culture conditions for the expression of three different insoluble proteins in *Escherichia coli*. *Sci Rep* 9: 1–11
- Harbers M (2014) Wheat germ systems for cell-free protein expression. *FEBS Lett* 588: 2762–2773
- Herrmann A, Livanos P, Zimmermann S, Berendzen K, Rohr L, Lipka E & Müller S (2020) KINESIN-12E regulates metaphase spindle flux and helps control spindle size in Arabidopsis. *Plant Cell*: 1–17
- Hotta T, Kong Z, Ho CMK, Zeng CJT, Horio T, Fong S, Vuong T, Lee YRJ & Liu B (2012) Characterization of the Arabidopsis augmin complex uncovers its critical function in the assembly of the acentrosomal spindle and phragmoplast microtubule arrays. *Plant Cell* 24: 1494–1509
- Hsia KC, Wilson-Kubalek EM, Dottore A, Hao Q, Tsai KL, Forth S, Shimamoto Y, Milligan RA & Kapoor TM (2014) Reconstitution of the augmin complex provides insights into its architecture and function. *Nat Cell Biol* 16: 852–863
- Hutchins JRA, Toyoda Y, Hegemann B, Poser I, Hériché JK, Sykora MM, Augsburg M, Hudecz O, Buschhorn BA, Bulkescher J, *et al* (2010) Systematic analysis of human protein complexes identifies chromosome segregation proteins. *Science* 328: 593–599
- Jackman M, Marozzi C, Barbiero M, Pardo M, Yu L, Tyson AL, Choudhary JS & Pines J (2020) Cyclin B1-Cdk1 facilitates MAD1 release from the nuclear pore to ensure a robust spindle checkpoint. *J Cell Biol* 219: 1–17
- Janski N, Masoud K, Batzenschlager M, Herzog E, Evrard JL, Houlné G, Bourge M, Chabouté ME & Schmit AC (2012) The GCP3-interacting proteins GIP1 and GIP2 are required for  $\gamma$ -tubulin complex protein localization, spindle integrity, and chromosomal stability. *Plant Cell* 24: 1171–1187
- Johmura Y, Soung NK, Park JE, Yu LR, Zhou M, Bang JK, Kim BY, Veenstra TD, Erikson RL & Lee KS (2011) Regulation of microtubule-based microtubule nucleation by mammalian polo-like kinase 1. *Proc Natl Acad Sci U S A* 108: 11446–11451
- Kong Z, Hotta T, Julie Lee YR, Horio T & Liu B (2010) The  $\gamma$ -tubulin complex protein GCP4 is required for organizing functional microtubule arrays in *Arabidopsis thaliana*. *Plant Cell* 22: 191–204
- Lee YRJ, Hiwatashi Y, Hotta T, Xie T, Doonan JH & Liu B (2017) The Mitotic Function of Augmin Is Dependent on Its Microtubule-Associated Protein Subunit EDE1 in *Arabidopsis thaliana*. *Curr Biol* 27: 3891–3897

- Lee YRJ & Liu B (2019) Microtubule nucleation for the assembly of acentrosomal microtubule arrays in plant cells. *New Phytol* 222: 1705–1718
- Leong SL, Lynch EM, Zou J, Tay YD, Borek WE, Tuijtel MW, Rappsilber J & Sawin KE (2019) Reconstitution of Microtubule Nucleation *In Vitro* Reveals Novel Roles for Mzt1. *Curr Biol* 29: 2199-2207
- Lin TC, Neuner A, Flemming D, Liu P, Chinen T, Jäkle U, Arkowitz R & Schiebel E (2016) MOZART1 and  $\gamma$ -tubulin complex receptors are both required to turn  $\gamma$ -TuSC into an active microtubule nucleation template. *J Cell Biol* 215: 823–840
- Lindeboom JJ, Nakamura M, Hibbel A, Shundyak K, Gutierrez R, Ketelaar T, Emons AMC, Mulder BM, Kirik V & Ehrhardt DW (2013) A mechanism for reorientation of cortical microtubule arrays driven by microtubule severing. *Science* 342
- Liu P, Würtz M, Zupa E, Pfeffer S & Schiebel E (2021) Microtubule nucleation: The waltz between  $\gamma$ -tubulin ring complex and associated proteins. *Curr Opin Cell Biol* 68: 124–131
- Liu P, Zupa E, Neuner A, Böhler A, Loerke J, Flemming D, Ruppert T, Rudack T, Peter C, Spahn C, *et al* (2020) Insights into the assembly and activation of the microtubule nucleator  $\gamma$ -TuRC. *Nature* 578: 467–471
- Manning J & Kumar S (2007) NEDD1: Function in microtubule nucleation, spindle assembly and beyond. *Int J Biochem Cell Biol* 39: 7–11
- Manning JA, Shalini S, Risk JM, Day CL & Kumar S (2010) A direct interaction with NEDD1 regulates  $\gamma$ -tubulin recruitment to the centrosome. *PLoS One* 5: 1–12
- McNally FJ & Roll-Mecak A (2018) Microtubule-severing enzymes: From cellular functions to molecular mechanism. *J Cell Biol* 217: 4057–4069
- Miao H, Guo R, Chen J, Wang Q, Lee YRJ & Liu B (2019) The  $\gamma$ -tubulin complex protein GCP6 is crucial for spindle morphogenesis but not essential for microtubule reorganization in Arabidopsis. *Proc Natl Acad Sci U S A* 116: 27115–27123
- Motta MR, Zhao A, Pastuglia M, Belcram K, Komaki M, Harashima H, Komaki S, Bulankova P, Heese M, Riha K, *et al* (2021) B1-type cyclins control microtubule organization during cell division in Arabidopsis. *bioRxiv*
- Nakamura M, Ehrhardt DW & Hashimoto T (2010) Microtubule and katanin-dependent dynamics of microtubule nucleation complexes in the acentrosomal Arabidopsis cortical array. *Nat Cell Biol* 12: 1064–1070
- Nakamura M, Yagi N, Kato T, Fujita S, Kawashima N, Ehrhardt DW & Hashimoto T (2012) Arabidopsis GCP3-interacting protein 1/MOZART 1 is an integral component of the  $\gamma$ -tubulin-containing microtubule nucleating complex. *Plant J* 71: 216–225

- Örd M, Möll K, Agerova A, Kivi R, Faustova I, Venta R, Valk E & Loog M (2019) Multisite phosphorylation code of CDK. *Nat Struct Mol Biol* 26: 649–658
- Paz J & Lüders J (2018) Microtubule-Organizing Centers: Towards a Minimal Parts List. *Trends Cell Biol* 28: 176–187
- Pecani K, Lieberman K, Tajima-Shirasaki N, Onishi M & Cross FR (2021) Control of division and microtubule dynamics in *Chlamydomonas* by cyclin B/CDKB1 and the anaphase-promoting complex. *bioRxiv Cell Biol*
- Pignocchi C, Minns GE, Nesi N, Koumproglou R, Kitsios G, Benning C, Lloyd CW, Doonan JH & Hills MJ (2009) Endosperm Defective1 is a novel microtubule-associated protein essential for seed development in Arabidopsis. *Plant Cell* 21: 90–105
- Schaefer E, Belcram K, Uyttewaal M, Duroc Y, Goussot M, Legland D, Laruelle E, De Tauzia-Moreau ML, Pastuglia M & Bouchez D (2017) The preprophase band of microtubules controls the robustness of division orientation in plants. *Science* 356: 186–189
- Seltzer V, Janski N, Canaday J, Herzog E, Erhardt M, Evrard JL & Schmit AC (2007) Arabidopsis GCP2 and GCP3 are part of a soluble  $\gamma$ -tubulin complex and have nuclear envelope targeting domains. *Plant J* 52: 322–331
- Singh A, Upadhyay V, Upadhyay AK, Singh SM & Panda AK (2015) Protein recovery from inclusion bodies of *Escherichia coli* using mild solubilization process. *Microb Cell Fact* 14: 1–10
- Sofroni K, Takatsuka H, Yang C, Dissmeyer N, Komaki S, Hamamura Y, Böttger L, Umeda M & Schnittger A (2020) CDKD-dependent activation of CDKA<sub>1</sub> controls microtubule dynamics and cytokinesis during meiosis. *J Cell Biol* 219: 1–21
- Song JG, King MR, Zhang R, Kadzik RS, Thawani A & Petry S (2018) Mechanism of how augmin directly targets the  $\gamma$ -tubulin ring complex to microtubules. *J Cell Biol* 217: 2417–2428
- Strauss B, Harrison A, Coelho PA, Yata K, Zernicka-Goetz M & Pines J (2018) Cyclin B1 is essential for mitosis in mouse embryos, and its nuclear export sets the time for mitosis. *J Cell Biol* 217: 179–193
- Tian J & Kong Z (2019) The role of the augmin complex in establishing microtubule arrays. *J Exp Bot* 70: 3035–3041
- Tsai CY, Ngo B, Tapadia A, Hsu PH, Wu G & Lee WH (2011) Aurora-A phosphorylates augmin complex component Hice1 protein at an N-terminal serine/threonine cluster to modulate its microtubule binding activity during spindle assembly. *J Biol Chem* 286: 30097–30106
- Tsuchiya K & Goshima G (2021) Microtubule-associated proteins promote microtubule

- generation in the absence of  $\gamma$ -tubulin in human colon cancer cells. *J Cell Biol* 220: 1–16
- Vavrdová T, Šamaj J & Komis G (2019) Phosphorylation of plant microtubule-associated proteins during cell division. *Front Plant Sci* 10: 1–10
- Wang G, Wang C, Liu W, Ma Y, Dong L, Tian J, Yu Y & Kong Z (2018) Augmin Antagonizes Katanin at Microtubule Crossovers to Control the Dynamic Organization of Plant Cortical Arrays. *Curr Biol* 28: 1311–1317
- Wieczorek M, Urnavicius L, Ti SC, Molloy KR, Chait BT & Kapoor TM (2020) Asymmetric Molecular Architecture of the Human  $\gamma$ -Tubulin Ring Complex. *Cell* 180: 165–175
- Wu G, Lin Y-T, Wei R, Chen Y, Shan Z & Lee W-H (2008) Hice1, a Novel Microtubule-Associated Protein Required for Maintenance of Spindle Integrity and Chromosomal Stability in Human Cells. *Mol Cell Biol* 28: 3652–3662
- Zeng CJT, Lee YRJ & Liu B (2009) The WD40 repeat protein NEDD1 functions in microtubule organization during cell division in *Arabidopsis thaliana*. *Plant Cell* 21: 1129–1140
- Zwetsloot AJ, Tut G & Straube A (2018) Measuring microtubule dynamics. *Essays Biochem* 62: 725–735





**Chapter 3. Towards live cell imaging of meiosis in *Arabidopsis lyrata* and *Arabidopsis arenosa* auto- and allopolyploids**



## 3.1. Introduction

### 3.1.1. Overview of meiosis

Sexual reproduction is pervasively associated with a special kind of cell division called meiosis (Fig 1A-N; Mercier *et al*, 2015). In meiosis, the genetic material is duplicated once and cells undergo two rounds of division named meiosis I and II to form haploid gametes. The homologous maternal and paternal chromosomes pair in meiosis I and exchange physical chromosomal DNA segments, which is a process known as meiotic recombination or crossover. Recombination is widely regarded to promote genetic diversity by generating new allele combinations between the maternal and paternal allelic sets.

Meiosis I starts with prophase I, which is subdivided in several substages and is by far the longest meiotic stage (Prusicki *et al*, 2019). The first substage is leptotene, when chromosome axes assemble and the process of recombination starts. At zygotene, synapsis, which is a kind of pairing between the homologous chromosomes that is characterized by the polymerization of the synaptonemal complex (see below for details), starts. At pachytene, chromosomes are fully synapsed and recombination proceeds further. At diplotene, the synaptonemal complex dismantles, whereas chromosomes remain connected by crossovers, which will be visible in the next stage by the so-called chiasmata. Finally, at diakinesis, chromosomes condense and bivalent pairs, i.e., homologous chromosomes associated two by two, can be clearly identified.

After prophase I, homologous chromosomes align at the metaphase plate in metaphase I, still connected by chiasmata, and subsequently separate in anaphase I. In interkinesis, which includes telophase I and prophase II, two nuclei are generated and chromosomes quickly decondense. In dicotyledonous species, there is no cytokinesis at the end of meiosis I. Instead, a simultaneous cytokinesis, that is, the simultaneous formation of four cell walls between the daughter cells, takes place at the end of meiosis II (Sofroni *et al*, 2020).

In metaphase II, chromosomes align once more at the metaphase plate. This time, however, sister chromatids separate in anaphase II. In telophase II, four daughter nuclei form. Hence, by the end of meiosis, four haploid spores (in the male side, microspores; in the female side, megaspores) will form each with half of the original nuclear DNA

content. It is important to notice that sister kinetochores are fused and have a monopolar orientation in metaphase I, whereas, in metaphase II, sister kinetochores have a bipolar orientation (Hofstatter *et al*, 2021; Mercier *et al*, 2015).

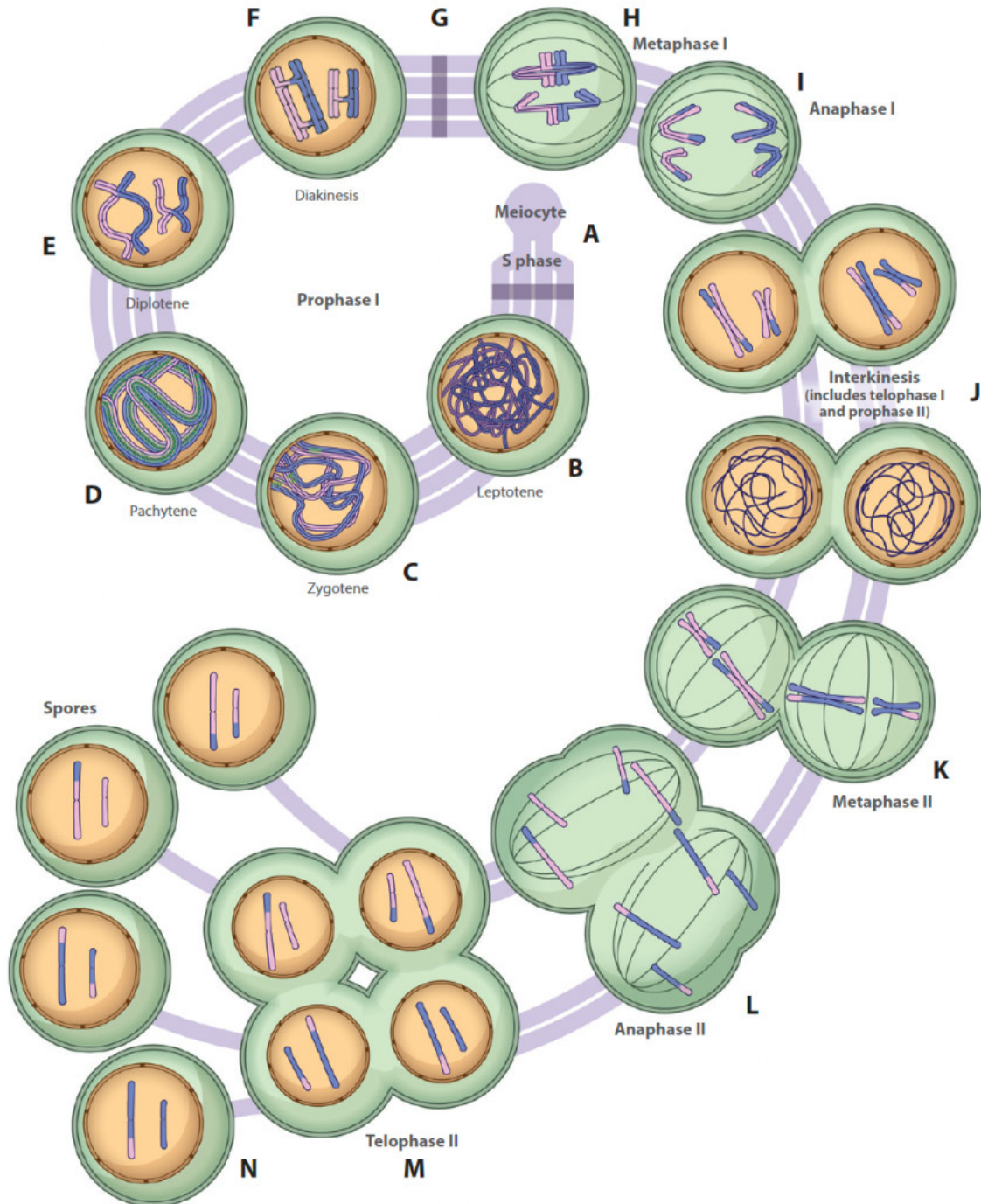


**Figure 1. A complete view of meiosis.** The figure was taken from Mercier *et al*, 2015.

A. Premeiosis includes the differentiation of cells into meiocytes and the duplication of genetic material (S-phase).

B. At leptotene, the proteinaceous chromosome axes assemble and recombination starts.

C. At zygotene, synapsis of the homologous chromosomes starts and recombination advances.

- D. At pachytene, homologous chromosomes are fully synapsed, together with the further progression of recombination.
- E. At diplotene, the synaptonemal complex is fully disassembled, but homologous chromosomes remain physically connected by chiasmata, which are the visible outcomes of crossover events.
- F. At diakinesis, chromosomes are highly condensed and are seen as pairs or bivalents connected by chiasmata.
- G. After prophase I, the nuclear envelope breakdown takes place.
- H. Metaphase I is characterized by the alignment of homologous chromosomes at the metaphase plate.
- I. In anaphase I, homologous chromosomes separate each towards one pole of the cell.
- J. Interkinesis is composed of telophase I and prophase II and comprises the formation of two daughter nuclei together with the quick decondensation of chromosomes.
- K. In metaphase II, chromosomes align once more at the metaphase plate; this time, chromosomes align individually.
- L. In anaphase II, sister chromatids separate into four daughter nuclei.
- M. In telophase II, four nuclei are established.
- N. At the end of meiosis, simultaneous cytokinesis takes place in the case of dicots, which generates four haploid spores.

### **3.1.2. The axial element and the synaptonemal complex**

During early meiosis, sister chromatids organize into chromatin loops connected to a protein axis, which is called the chromosome axis or axial element (Fig 2). This axial element is, in turn, comprised of cohesion factors, i.e., the proteins that keep sister chromatids connected throughout meiosis until anaphase II (see below for details), and other proteins that are specific to meiosis. For instance, ASY1 (ASYNAPTIC 1) and ASY3 (ASYNAPTIC 3) are well known components of the axial element in plants (Armstrong *et al*, 2002; Ferdous *et al*, 2012). Mutations in either of those components greatly reduce or abolish synapsis between homologous chromosomes, which impacts plant fertility (Ross *et al*, 1997; Ferdous *et al*, 2012). Interestingly, mutations in ASY1 or ASY3 also affect recombination, emphasizing the fact that many recombination steps are dependent on the axial element (Sanchez-Moran *et al*, 2008).

The synaptonemal complex (SC; Fig 2) is a large proteinaceous structure that forms between paired homologous chromosomes in mid-prophase I of meiosis, linking the chromosomes physically from beginning to end (Page & Hawley, 2004). It is mainly composed of the previously assembled axial element and the central elements (CEs), resembling a zip structure. The CEs polymerize between the two axial elements (from

now on referred to as lateral elements or LEs) of the homologous chromosomes. The main CE component is ZYP1, for which two homologs, ZYP1a and ZYP1b, have been identified in *Arabidopsis*. The *Arabidopsis* ZYP1 homologs have been recently described to, first, play a role in crossover assurance, i.e., the maintenance of at least one obligate crossover per bivalent for proper chromosome segregation; second, restrict the number of crossovers; third, regulate crossover interference, i.e., the observation that crossovers do not happen randomly along the chromosome length but rather influence the position of the next crossover-sensitive event (France *et al*, 2021).

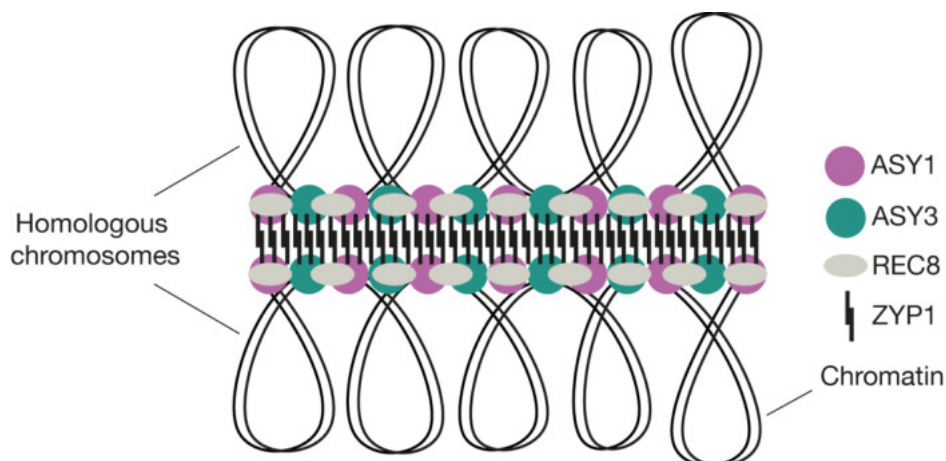


**Figure 2. A representation of the synaptonemal complex.**

The synaptonemal complex is a proteinaceous structure that forms in mid-prophase I and is characterized by the polymerization of central elements (for instance, ZYP1) between the two chromosome axes (mainly composed of ASY1, ASY3 and REC8) of homologous chromosomes, which are in these late stages known as the lateral elements.

### 3.1.3. The stepwise removal of cohesion in meiosis

As described above, homologous chromosomes separate in meiosis I, whereas sister chromatids separate in meiosis II. Hence, sister chromatids must be maintained together in meiosis I but not in meiosis II. This is enabled by a process of step-wise cohesion release: in meiosis I, sister chromatid cohesion is lost only along chromosome arms in anaphase I, whereas, in meiosis II, pericentromeric cohesion is lost in anaphase II, allowing sister chromatids to be separated (Mercier *et al*, 2015).

An important player in meiotic cohesion is RECOMBINATION 8 (REC8), which is a kleisin subunit of the cohesin complex (Cai *et al*, 2003; Chelysheva *et al*, 2005). Among others, mutations in REC8 cause a total loss of cohesion between sister chromatids as

well as a bipolar orientation of the kinetochores in metaphase I (Cai *et al*, 2003). REC8 acts together with STRUCTURAL MAINTENANCE OF CHROMOSOME 1 and 3 (SMC1 and SMC3; Fig 3) to form the core cohesin ring complex in meiosis (Liu *et al*, 2002). Another essential component of the cohesin complex is SISTER CHROMATID COHESION 3 (SCC3), since null mutants for this protein are embryonic lethal (Bolaños-Villegas *et al*, 2017). The precise nature of SCC3 function, however, is unknown. SCC3 is presumably interacting with REC8 to form the core cohesin complex, since its localization is affected in *rec8* mutants (Chelysheva *et al*, 2005). In mitosis, SCC1 takes over the role of REC8 to keep the cohesin ring complex closed and interacts with the other previously mentioned components SMC1 and SMC3 (Bolaños-Villegas *et al*, 2017; Haering *et al*, 2002).

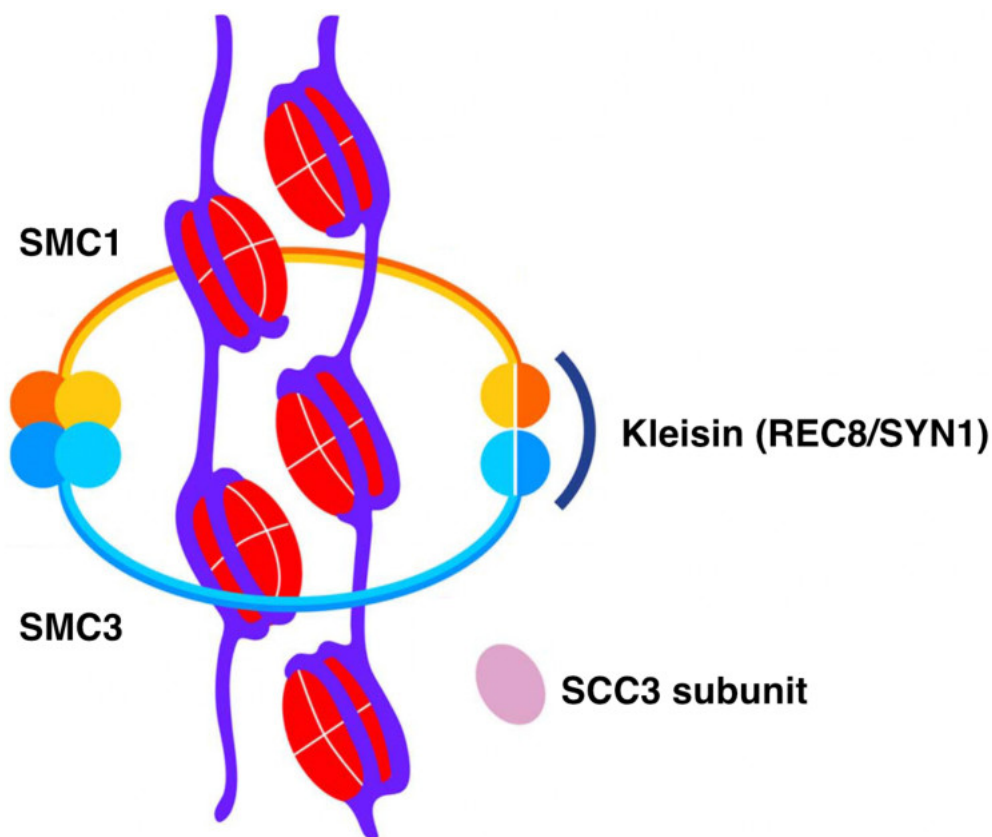


**Figure 3. The meiotic cohesin complex in *Arabidopsis*.** The figure was modified from Bolaños-Villegas *et al*, 2017.

The three core members of the cohesin ring complex In meiosis are REC8, SMC1, SMC3 and SCC3. SMC1 and SMC3 represent the hinges of the ring complex, whereas REC8 is a kleisin that keeps the whole ring closed. The SCC3 subunit may interact with the kleisin REC8.

### 3.1.4. The challenge for chromosome segregation in polyploid meiosis

Polyploidy arises as a result of whole genome duplication (WGD) events (Doyle *et al*, 2008) and can be classified in auto- and allopolyploidy. Autopolyploids contain several sets of chromosomes coming from the same species, whereas allopolyploids contain several sets of chromosomes coming from different species as a result of hybridization.

A WGD event, either in auto- or allopolyploids, provides organisms with material for evolution to happen, since it produces at least two copies of the same gene that can now evolve to perform different functions (Bomblies & Madlung, 2014). Known changes as a result of polyploidization, i.e., the process of becoming polyploid, include increases in cell size and organ size as well as increased resistance to pathogens and pests (Stebbins, 1940; Levin, 1983). Moreover, flowering plants have undergone several WGD events and many of these have been linked to an increase in diversification rate (Soltis & Soltis, 2016).

However, there are not only advantages to becoming polyploid. Many challenges to polyploid organisms begin immediately after WGD. For instance, the increase in cell size brings about dimensional problems: doubling the genome presumably doubles the space occupied by chromatin, but produces an increase of only 1.6-fold in nuclear envelope surface (Comai, 2005). This difference in dimensions may affect the interaction of chromatin and envelope-bound components because of the disproportionate changes in volume and area. Additionally, polyploidization is accompanied by major changes in gene expression, including transposon activation and duplicate gene silencing (Adams & Wendel, 2005).

Another major challenge polyploids face is chromosome segregation, both in mitosis and meiosis. For instance, polyploidy in yeast was associated with increased chromosome loss in mitosis – 30 times more often in triploid and 1000 times more often in tetraploid yeast compared to the diploid counterpart (Mayer & Aguilera, 1990). In meiosis, specifically the chromosome pairing that happens in prophase I is greatly affected by polyploidy (Bomblies *et al*, 2016).

Auto- and allopolyploids have related, but different challenges in meiosis. Both auto- and allopolyploids often have multivalent chromosome configurations in meiosis, which is the association of more than two chromosomes, as opposed to bivalent chromosome configurations (Fig 4; Hollister, 2015). This poses a problem since it is known that



multivalent formation often leads to an imbalanced chromosome segregation and aneuploid daughter cells or gametes. Allopolyploids must mainly avoid homeolog pairing, i.e., pairing between chromosomes of different species, whereas autopolyploids must ensure a balanced (mostly two-by-two) segregation. In allopolyploids, homology between homologous chromosomes is used to favor homolog bivalent formation and balanced segregation as opposed to homeolog pairing and missegregation (usually accompanied by chromosomal translocations and gene loss). In autopolyploids, this problem becomes more pronounced since multiple copies of the same homologous chromosome can be very similar or almost indistinguishable in terms of sequence and provide no specific cue for proper pairing and segregation (Bombliès *et al*, 2016).

*A. arenosa*, an outcrossing self-incompatible relative of *A. thaliana*, has been extensively used as a model to study meiotic adaptation to polyploidization. Established autotetraploid *A. arenosa* has a reduced number of crossovers per bivalent in comparison to diploids, which is thought to act in promoting a diploid-like segregation of the chromosomes in meiosis (Fig 4; Yant *et al*, 2013). Established tetraploids have more rod bivalents (one crossover per chromosome pair) and fewer ring bivalents (two crossovers per chromosome pair) in comparison to diploids. Thus, with a simple modulation of crossover rate, autotetraploids can presumably favor bivalent formation.

### **3.1.5. The adaptations to polyploid meiosis**

It is possible to generate polyploids (so-called neopolyploids) in the lab with the use of drugs such as colchicine, which binds to microtubules and promotes their disassembly. These neopolyploids often exhibit missegregation of chromosomes in meiosis (Yant *et al*, 2013). Nevertheless, autopolyploids with a stable meiosis and balanced chromosome segregation are pervasively found in nature (from here on referred to as established tetraploids or autopolyploids). Hence, established autopolyploids are assumed to have acquired adaptations to polyploid chromosome segregation that were not present in their diploid ancestors. Indeed, recent efforts to uncover these molecular adaptations in meiosis have revealed a strong differentiation of a specific set of genes in established tetraploid *A. arenosa* compared to diploid populations (Yant *et al*, 2013; Wright *et al*, 2015; Morgan *et al*, 2020). Interestingly, this set of genes includes many meiotic factors involved in axis formation, synapsis and recombination, such as *ASY1*, *ASY3*, *REC8/SYN1* and *ZYP1* (Wright *et al*, 2015). The changes in gene sequence included, for instance, a total of 13 unique amino acid polymorphisms for *ASY3* in tetraploids, i.e., these amino acid changes were never identified in diploid populations of *A. arenosa*.

*REC8/SYN1* exhibited 5 unique amino acid polymorphisms in tetraploids, of which one (D454G) was predicted to cause a loss of phosphorylation of the protein at S458.

A recent study characterized derived alleles for *ASY1* and *ASY3* that were initially identified in *A. arenosa* stable tetraploids (Morgan *et al*, 2020). These derived alleles were shown to be linked with reduced multivalent formation, reduced chromosome axis length and a larger proportion of rod-shaped bivalents in metaphase I. Hence, we are starting to understand how neopolyploids can eventually evolve to stabilize meiosis and promote balanced chromosome segregation.

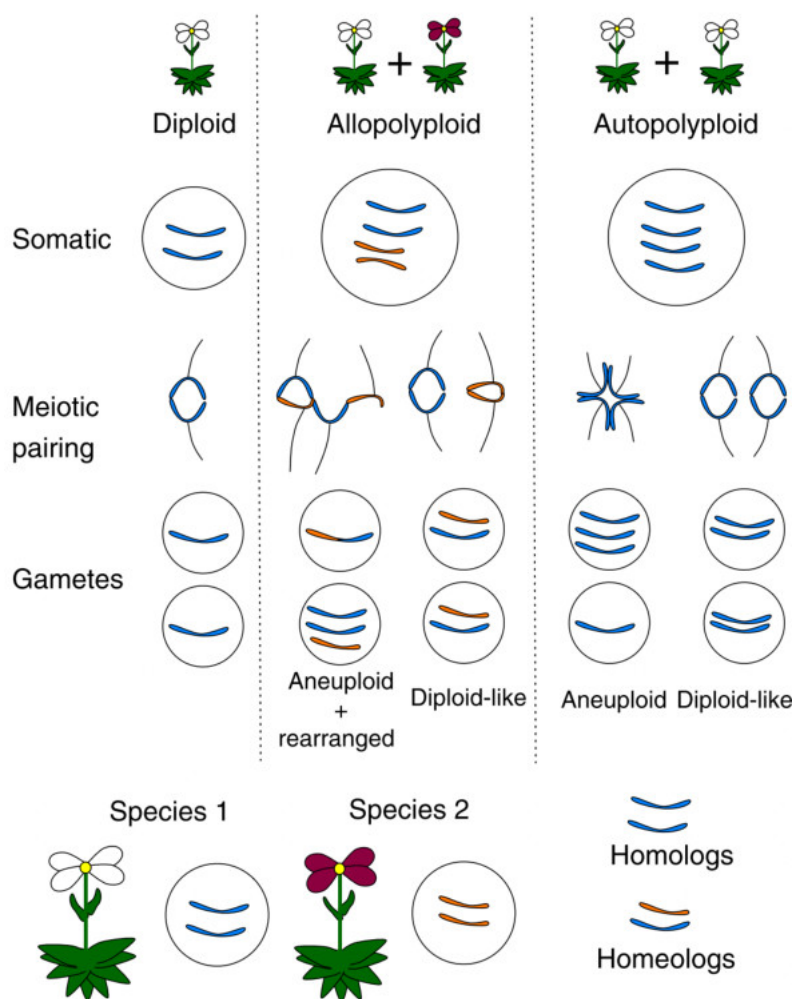


**Figure 4. Stabilization of meiosis in auto- and allopolyploids.** The picture was taken from Hollister, 2015.

Diploid plants (leftmost panel) contain two copies of each chromosome that pair and segregate in a balanced manner in meiosis, generating gametes each with one chromosome copy. Allopolyploids (central panel) contain both homolog (intra-specific) and homeolog (inter-specific) chromosomes. Stable allopolyploids exhibit a diploid-like segregation of chromosomes (avoiding pairing between homeologs) for balanced segregation. When homeolog chromosomes pair,

chromosomal translocations and gene loss can happen, which can lead to aneuploid gametes. Stable autopolyploids (rightmost panel) segregate chromosomes two-by-two in a diploid-like behavior, whereas neopolyploids present multivalent formation that can lead to gamete aneuploidy.

### 3.1.6. *A. lyrata* and *A. arenosa*: outcrossing relatives of *A. thaliana* as models for auto- and allopolyploidy

In contrast to *A. thaliana*, *A. lyrata* and *A. arenosa* are both mainly self-incompatible outcrossing species from the *Arabidopsis* genus (Fig 5). The two species have both diploid and tetraploid populations. In the case of *A. lyrata*, diploids are present in central and northern Europe in addition to northern America, while tetraploids are present mainly in eastern Austria (Schmickl & Koch, 2011). In the case of *A. arenosa*, diploids colonized the Carpathians and southeastern Europe, while the tetraploids are present in central and northern Europe (Schmickl & Koch, 2011; Kolář *et al*, 2016; Arnold *et al*, 2015). There is no recent gene flow between diploid *A. lyrata* and diploid *A. arenosa* and the two are considered well-defined species (Lafon-Placette *et al*, 2017). On the other hand, there are two known zones for hybridization between tetraploid *A. lyrata* and tetraploid *A. arenosa* (Schmickl & Koch, 2011).

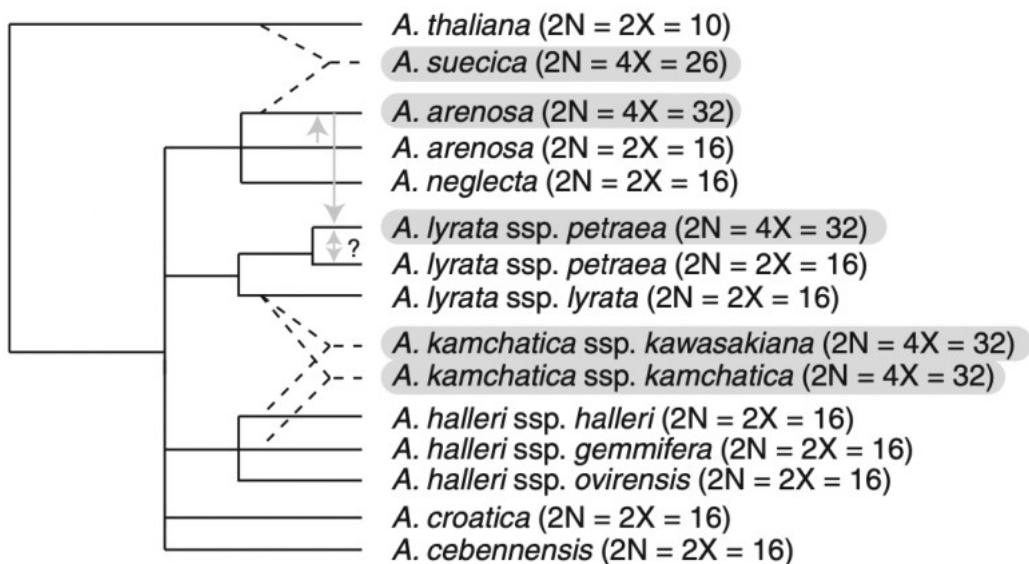


**Figure 5. Phylogenetic tree of the known *Arabidopsis* species.** This figure was taken from Bomblies & Madlung, 2014.

In gray, species that have polyploid populations are indicated. Allopolyploid species are indicated with dotted lines connecting to their parental species. Gray arrows indicate potential gene flow. Ploidy and chromosome numbers are indicated between parentheses.

A study of hybridization between *A. lyrata* and *A. arenosa* has clarified that the diploids are largely unable to produce viable hybrid seeds in both cross directions. Crosses using diploid *A. arenosa* as a female donor generated a great proportion of non-collapsed seeds; nevertheless, most of these seeds failed to germinate (Lafon-Placette *et al*, 2017). Interestingly, when tetraploid *A. lyrata* was crossed with diploid *A. arenosa* in both cross directions, seeds were fully viable. In contrast, crossing tetraploid *A. arenosa* with diploid *A. lyrata* produced largely inviable seeds. Crosses between the tetraploid populations produced mostly viable seeds as expected since the tetraploid forms are known to hybridize in nature. Hence, it is assumed that the tetraploidization of *A. lyrata* allowed gene flow between the two species and the bypass of the endosperm-based hybridization barrier between *A. lyrata* and *A. arenosa*.

### **3.1.7. State of the art of *A. lyrata* and *A. arenosa* transformation**

Up until this point, there were two studies reporting *Agrobacterium*-mediated transformation of *A. lyrata*. One study used floral dipping in *A. lyrata* (Indriolo *et al*, 2012); the second was a root-based transformation of *A. lyrata* plants in tissue culture followed by callus induction and whole plant regeneration (Fobis-Loisy *et al*, 2007). For *A. arenosa*, there was no report of transformation in the literature. Most of the studies in *A. arenosa* made use of genetic variation in the wild (autotetraploid derived alleles, see above) to study adaptation to polyploid meiosis and protein function (Wright *et al*, 2015; Morgan *et al*, 2020; Yant *et al*, 2013). In addition, the authors have made extensive use of immunolocalization and chromosome spreads to study meiosis in *A. arenosa*, which don't require stable transformation of those plants. Hence, one of the main challenges of this thesis was to confirm if *A. arenosa* plants can also be transformed by *Agrobacterium*-mediated transformation protocols and how efficient the transformation of *A. lyrata* is.

## Research aim

A complete description of the dynamics of male meiosis in *A. thaliana* has recently been produced (Prusicki *et al*, 2019). The authors followed meiosis using a reporter for microtubules (TagRFP-TUA5) and a reporter for chromosomes (REC8-GFP). Flower buds 0.4-0.6 mm in length were isolated, mounted in rich media (for details, see Prusicki *et al*, 2019) and, next, the uppermost sepal of these flower buds was removed. After that, the samples were submerged in water and observed with a confocal laser scanning microscope throughout the course of meiosis. Five parameters were analyzed in the movies: shape of the cells, microtubule conformation, nucleus position, nucleolus position, and chromosome configuration. With these parameters, 11 landmarks, i.e., pervasive meiotic cell states with a specific combination of the analyzed parameters, were identified.

By applying the above-mentioned live cell imaging technique of male meiocytes, we would like to understand the dynamics of meiosis in auto- and allopolyploids using *A. lyrata* and *A. arenosa* as models. The two species are particularly interesting for this analysis since both diploid and tetraploid populations can be found for both species and their hybridization (mainly between the tetraploids) is known to occur in nature. Furthermore, the two species possess a similar genome and chromosome number (8 chromosomes for both species), unlike other *Arabidopsis* hybrids between species that are further apart genetically. *A. suecica*, for instance, is a hybrid of *A. thaliana* and *A. arenosa* that have 5 and 8 chromosomes respectively (for more details on the phylogenetic relationships in the *Arabidopsis* genus, see Fig 5 above). As mentioned previously, homology can be used as a cue for proper chromosome pairing and segregation in meiosis. Hence, more problems in chromosome segregation would be expected in hybrids of *A. lyrata* and *A. arenosa* since homeolog chromosomes would be more similar and more likely to pair.

To follow meiotic divisions in male meiocytes of *A. lyrata* and *A. arenosa*, I generated genomic reporters using *A. lyrata* sequences to mark chromosomes and microtubules. For the tagging of chromosomes, I generated *ASY1*, *ASY3*, *REC8* and *ZYP1* reporter constructs. For the tagging of microtubules, I used a previously generated reporter construct (*RPS5Apro:TagRFP-TUA5*). Additionally, I generated CRISPR-Cas9 constructs targeting those same meiotic genes. Next, I attempted transformation of *A. lyrata* and *A. arenosa* with limited success.

## 3.2. Results

### 3.2.1. Cloning of reporter constructs

Meiosis in auto- and allopolyploids, as explained above, presents specific challenges for recombination and faithful segregation of chromosomes. Hence, describing the dynamics of meiotic progression in these organisms could help us understand the specific adaptations to polyploidy in this special division. In order to follow meiosis in diploid and polyploid *A. lyrata* and *A. arenosa* and their hybrid counterparts, I generated reporter constructs for *A. lyrata*, which has a fully sequenced and annotated genome. To date, there is no sequenced genome for *A. arenosa*. Since *A. lyrata* and *A. arenosa* are closely related species, I expected that reporters for *A. lyrata* proteins would also be able to properly localize in *A. arenosa*.

I amplified *A. lyrata* genomic sequences using primers based on the reference genome for *A. lyrata* (Table 1 and S1). Most of these sequences, however, exhibited several types of polymorphism, including single nucleotide polymorphisms (SNPs) and bigger deletions and insertions (Fig 6). The SNPs occurred mainly in exons, whereas deletions and insertions were often found in introns or other non-coding regions. To overcome this problem, I performed independent PCRs followed by independent cloning reactions. After that, individual clones were sequenced and compared. With this, I was able to detect if those differences in sequence originated as a result of faulty PCRs or were part of the native genomic sequences. This second scenario was highly likely, since there is no established homozygous line for *A. lyrata* and the plants from which genomic DNA was extracted derived from crosses between wild plants.



**Figure 6. A snapshot of an alignment of cloned *ASY1* genomic sequences with the reference genomic sequence.**

At the top, the reference sequence for *A. lyrata*'s *ASY1* can be seen (ARALYDRAFT\_894472). Exons together with their amino acid sequences are represented in magenta, whereas introns are represented by dashed lines. At the bottom, sequences obtained from cloned *ASY1* genomic sequences are aligned. Sequences of two clones (1.5 and 2.3) can be seen in the figure. A range of SNPs and deletions are highlighted in red. The purple box indicates a substitution of a Thymine (T) into a Cytosine (C) without a change in amino acid composition, since both ATT and ATC codons code for Isoleucine (Ile). The green box indicates three nucleotides that have been deleted in the two represented clones in an intronic region.

Reporter constructs were then generated using the amplified genomic sequences of *ASY1*, *ASY3*, *REC8* and *ZYP1* from *A. lyrata* (Table 1). In the case of *ASY1*, *ASY3* and *REC8*, a GFP tag was inserted at the C-terminus of the protein right before the genomic sequence encoding for a stop codon. This was chosen based on previous studies in *A. thaliana* which have shown that C-terminally-tagged reporters for these proteins are able to rescue the specific mutant phenotypes (Yang *et al*, 2020; Prusicki *et al*, 2019; Yang *et al*, 2019). *ZYP1*, on the other hand, was tagged internally, since other members of our research group have found that this protein is not completely functional when tagged at either the C- or N-terminus (S. Komaki, personal communication; Yang *et al*, 2019). Indeed, the C-terminus of *ZYP1* has recently been shown to be involved in an interaction with the lateral elements of the SC, while the N-terminus is lying in the central region of the SC and may also form crucial interactions with other SC components (Capilla-Pérez *et al*, 2021).

| Gene of interest           | Tag              | Promoter          | Terminator          |
|----------------------------|------------------|-------------------|---------------------|
| <i>ASY1</i> (genomic)      | C-terminal mEGFP | 1.723 kb upstream | 751 bp downstream   |
| <i>ASY3</i> (genomic)      | C-terminal mEGFP | 2.987 kb upstream | 1.111 kb downstream |
| <i>REC8/SYN1</i> (genomic) | C-terminal mEGFP | 371 bp upstream   | 355 bp downstream   |
| <i>ZYP1</i> (genomic)      | Internal mEGFP   | 1.373 kb upstream | 1.140 kb downstream |

**Table 1. Overview of genes of interest chosen to track meiosis in *A. lyrata* and *A. arenosa*.**

Only *A. lyrata* sequences are shown and were cloned, since there is a fully sequenced and annotated genome for this species.

Data information: kb = kilobases, bp = base pairs.

The generated reporter constructs were combined with a previously published microtubule reporter, *RPS5Apro:TagRFP-TUA5* (Prusicki *et al*, 2019; Komaki & Schnittger, 2017), since the protein sequence of this  $\alpha$ -tubulin member from *A. thaliana* was identical to the sequence of an *A. lyrata* orthologue (TUA3). The ribosomal protein (RPS5a) promoter for this reporter construct, on the other hand, was specific to *A. thaliana* and was shown to be active in both mitosis and meiosis in that species (Prusicki *et al*, 2019; Komaki & Schnittger, 2017). Hence, I assumed that this promoter would also be able to drive the expression of this gene successfully in cell divisions of *A. lyrata* and *A. arenosa*.

### 3.2.2. Cloning of CRISPR-Cas9 constructs

*A. lyrata* and *A. arenosa* mutants could be useful to assess the importance of specific meiotic factors in the adaptation to polyploid meiosis. Additionally, testing the functionality of the generated reporter constructs in their mutant backgrounds, e.g., ASY1-GFP in an *asy1* background, is common practice to validate the protein localization of the produced recombinant proteins. Therefore, I first selected suitable targets in the coding sequences of *ASY1*, *ASY3*, *SYN1* and *ZYP1* for the CRISPR-Cas9 system (Doudna & Charpentier, 2014) with the help of CRISPR-P v2.0 (<http://crispr.hzau.edu.cn/CRISPR2/>; Table 2). Based on the information provided by the CRISPR-P platform, I chose protospacer sequences with a good combination of on-score (generally above 0.8) and a small number of off-targets as well as a small off-target on-score.

With the exception of *ZYP1*, all protospacer sequences were conserved between the coding sequences of *A. lyrata* and *A. arenosa*. Hence, only one construct was designed to target individually *ASY1*, *ASY3* and *SYN1* in both species (Table 2). In the case of *ZYP1*, an additional target sequence was designed for *A. arenosa* (Table 2). Since *ZYP1* is represented by two copies in both species, which are called *ZYP1a* and *ZYP1b* in *A. thaliana*, I also selected protospacer sequences that could target both copies for both *A. lyrata* and *A. arenosa*.



| Gene               | Protospacer sequence | On-score | Exon |
|--------------------|----------------------|----------|------|
| <i>AIASY1</i>      | AATCTCGCCGATTAATTGAT | 0.5522   | 3    |
| <i>AIASY3</i>      | AAAGTGGGACTAATATCCG  | 0.8425   | 1    |
| <i>AISYN1/REC8</i> | GATCTTCGCGTGCAACGTAG | 0.8149   | 2    |
| <i>AIZYP1</i>      | TTAGCTTCTCAAGTTCAGGA | 0.7226   | 3    |
| <i>AaZYP1</i>      | GAAACTGGTGAAGGATCAGG | 0.7923   | 2    |

**Table 2. CRISPR-Cas9 target sequences using the coding sequences of *A. lyrata* and *A. arenosa* as a reference for exon position.** The protospacer sequences are shown without the protospacer-adjacent motif (PAM). The on-score was provided by the CRISPR-P v2.0 platform. Targets were chosen taking into consideration the location and score of possible off-targets.

### 3.2.3. Floral dipping of *A. lyrata* and *A. arenosa*

After generating the CRISPR-Cas9 and reporter constructs, I proceeded with plant transformations. First, I performed transformations of *A. lyrata* and *A. arenosa* using a protocol described previously by Indriolo *et al*, 2012. It is important to mention that the two species are self-incompatible and, therefore, unable to produce seeds without pollination, unlike *A. thaliana*. Hence, the compatibility of the pollen between different plants was tested in advance before floral dipping. The procedure consisted of a standard floral dipping protocol modified with the addition of vacuum infiltration for 5 min and manually pollinating the plants with cross-compatible for one week after dipping. However, this adapted floral dipping protocol did not yield any transformants.

After a first round of unsuccessful transformation of these species, I tried to modify the floral dipping protocol and extend the time of pollination of the open flower buds to increase the occurrence of transformation events (Fig 7). This was based on findings that *Agrobacterium* specifically transforms the female reproductive tissue of *A. thaliana* in flower buds that are a minimum of 6 and a maximum of 11 days away from anthesis, i.e., the opening of flower buds (Desfeux *et al*, 2000). This is due to an opening at the top of the pistil that presumably facilitates the access of *Agrobacterium* to developing ovules and megaspores and that closes off roughly three days prior to anthesis.

In this modified protocol, I first clipped all open flower buds. Next, I performed dipping of the immature closed flower buds with identical solutions to the floral dipping protocol of *A. thaliana* (for details, see the material and methods section). Vacuum infiltration at this step was found to be unessential. Following that, plants were covered and unexposed to

sunlight for 16 to 24 hours. After 5 days, I clipped all open flower buds, since these were not at the right stage for *Agrobacterium* transformation. From 6 days after dipping onwards, open flowers were hand-pollinated with cross-compatible pollen every other day for two weeks.

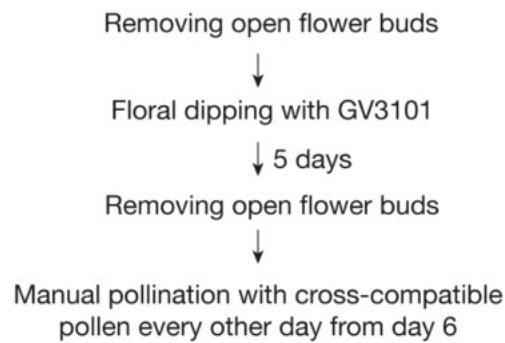


**Figure 7. The pipeline of a modified floral dipping protocol adapted to self-incompatible *A. lyrata* and *A. arenosa*.**

Initially, I performed floral dipping using the above-mentioned meiotic reporter constructs, since the screening of these transformants can be done directly by checking the signal of the labelled proteins. Indeed, I was able to recover several *A. lyrata* tetraploid transformants that contained the *REC8-GFP*, *ASY1-GFP* and *ZYP1-GFP* constructs combined with *TagRFP-TUA5* (Fig 8). However, no diploid *A. lyrata* or diploid and tetraploid *A. arenosa* transformants were ever recovered. I first screened the roots of the tetraploid *A. lyrata* transformants (Fig 8) and successfully detected the expression of the *TagRFP-TUA5* marker in root mitotic divisions, similarly to what is known for *A. thaliana* (Komaki & Schnittger, 2017).

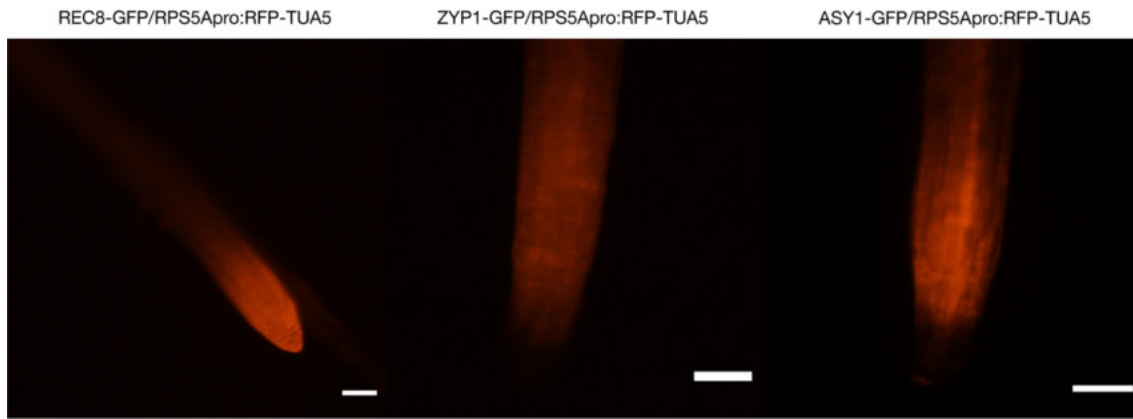


**Figure 8. *A. lyrata* (4X) transformants showed a consistent signal in the root apical meristem for microtubules (red) in mitotic divisions.**

Fluorescence stereomicroscope images of roots of *A. lyrata* seedlings. The RFP signal coincides with the root apical meristem region where mitosis is happening at a high rate. Scale bar = 50  $\mu\text{m}$ .

Next, I proceeded to check meiotic cell divisions in anthers of the tetraploid *A. lyrata* transformants (Fig 9A-D). First, the meiotic reporters *REC8-GFP* and *ZYP1-GFP* seemed not to be expressed in the meiocytes of the recovered transformants, since no signal was detected in those cells (data not shown). On the other hand, a weak signal for *ASY1-GFP* was successfully identified in meiocytes (Fig 9A, 9C and 9D). Furthermore, the reporter for *ASY1-GFP* appeared to correctly label chromosomes in early meiosis. The *TagRFP-TUA5* reporter was found to be expressed in the connective tissue surrounding the meiocytes and to label spindle microtubules in mitosis (Fig 9B), but was not active in the meiocytes themselves.

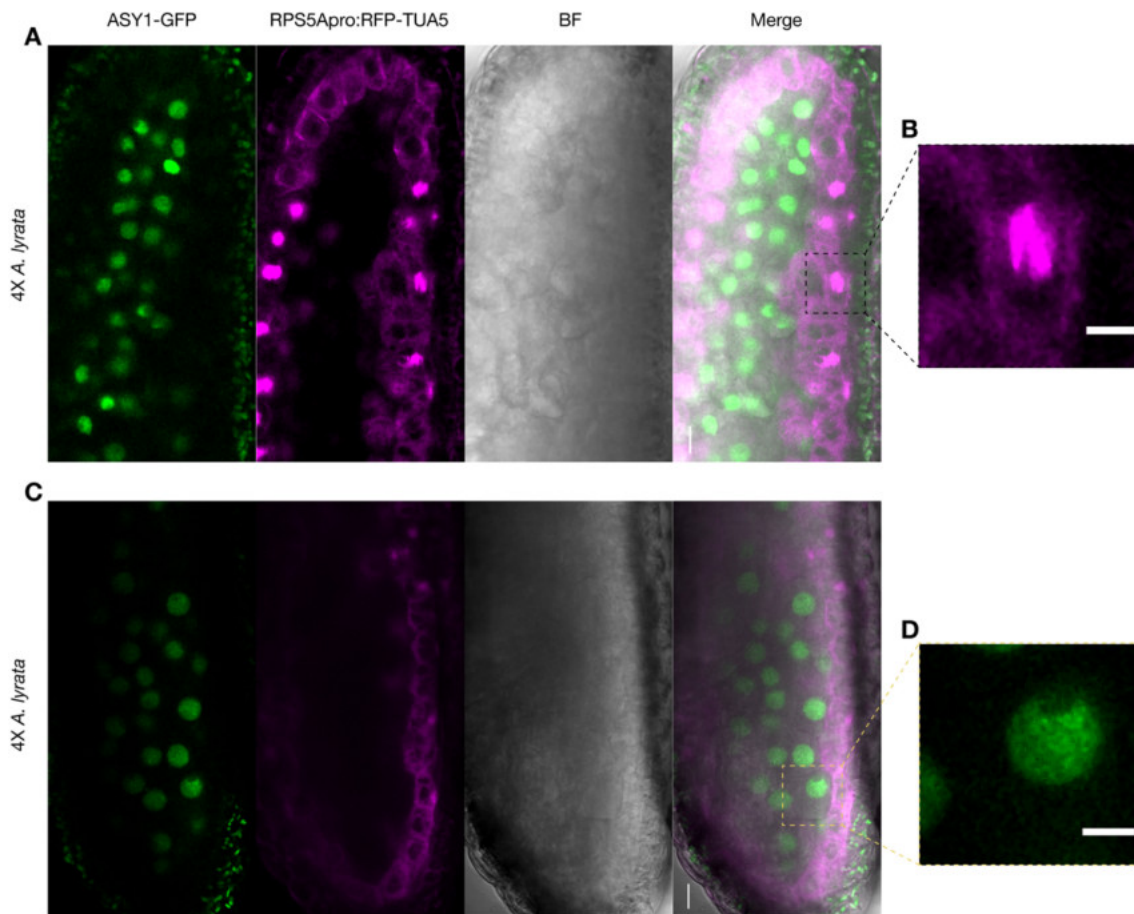


**Figure 9. Anthers of tetraploid *A. lyrata* showed chromosomes labeled by ASY1-GFP (green) and microtubules labeled by TagRFP-TUA5 (magenta).**

A. A single anther lobe is shown with meiocytes at prophase I. Tapetum cells are labeled by TagRFP-TUA5, while no signal for microtubules was found specifically in meiocytes. A dashed black square indicates a forming spindle in tapetum cells labeled by TagRFP-TUA5 and is shown in detail in (B). Scale bar = 10  $\mu\text{m}$ .

B. An early spindle stage in mitosis of a tapetum cell is shown in detail. Scale bar = 5  $\mu\text{m}$ .

C. A single anther lobe is shown with meiocytes at prophase I. Tapetum cells are labeled by TagRFP-TUA5, while no signal for microtubules was found specifically in meiocytes. A dashed yellow square indicates a meiocyte at zygotene of prophase I and is shown in detail in (D). Scale bar = 10  $\mu\text{m}$ .

D. A meiocyte at prophase I (zygotene) is shown in detail. Scale bar = 5  $\mu\text{m}$ .

BF = bright field.

Based on the finding that only a weak signal for ASY1-GFP was identified in *A. lyrata* and no signal was found for REC8-GFP, I next checked the functionality of the generated ASY1-GFP and REC8-GFP reporters in *A. thaliana* mutants (Fig 10A-B and 11A-B). In *A. thaliana*, a strong and specific localization of those two reporters to chromosomes was identified in meiosis of *asy1* and *rec8* mutants (Fig 10B and 11B). In addition, the sterility

of those mutants was successfully restored by the *A. lyrata* proteins as judged by pollen viability and seed production (data not shown). Therefore, the generated reporters were likely fully functional.

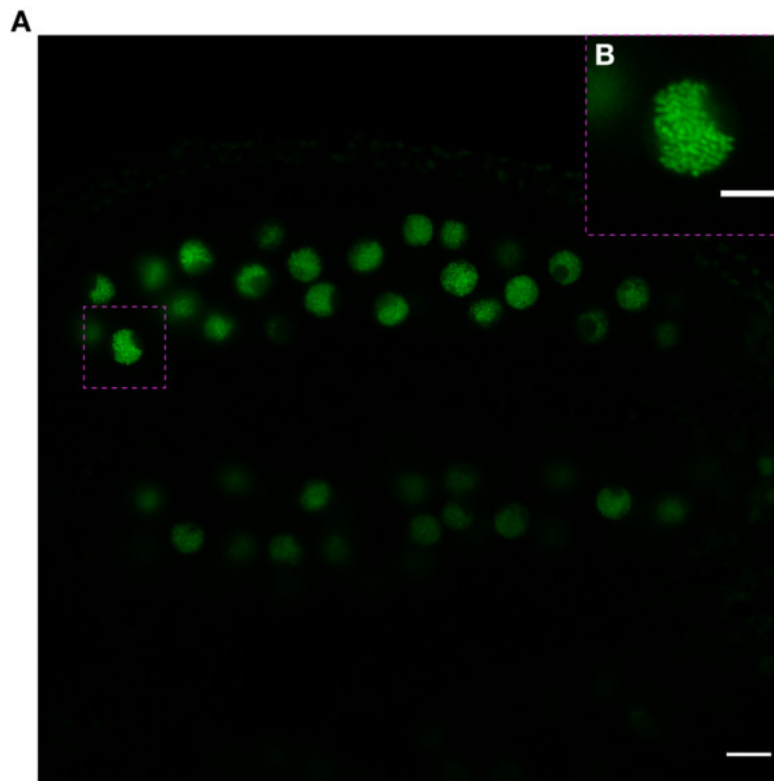


**Figure 10. The chromosomal marker ASY1-GFP construct from *A. lyrata* in the *asy1* mutant from *A. thaliana* showed a strong signal and appropriate localization.**

A. Confocal microscope image of two lobes of an anther from *A. thaliana* showing the chromosomal marker ASY1-GFP (green). Scale bar = 10  $\mu\text{m}$ .

B. A detail of a single meiocyte is shown (marked with a magenta dashed square in A). Scale bar = 5  $\mu\text{m}$ .

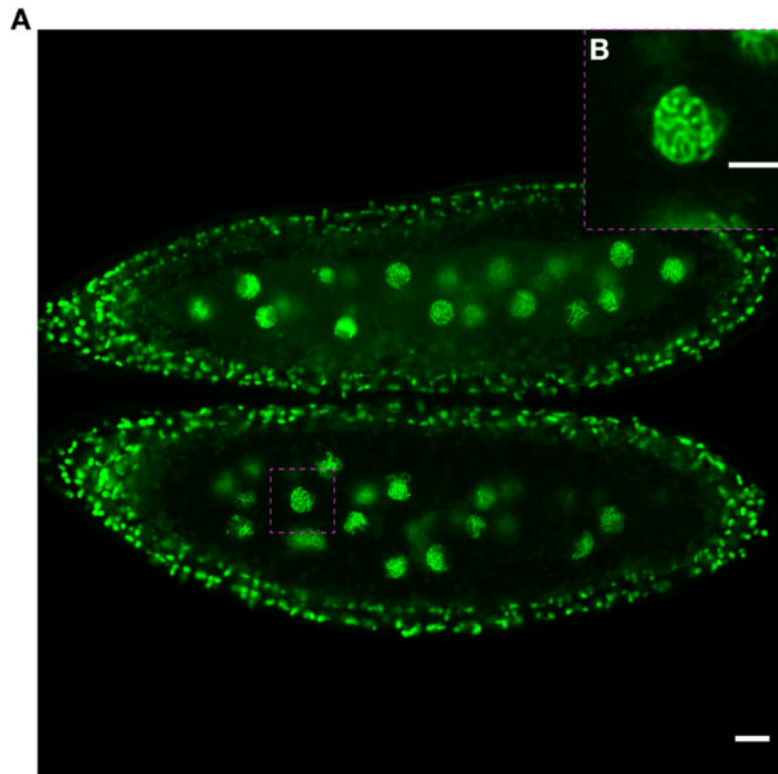


**Figure 11. The chromosomal marker REC8-GFP construct from *A. lyrata* in the *rec8* mutant from *A. thaliana* showed a strong signal and appropriate localization.**

A. Confocal microscope image of two lobes of an anther from *A. thaliana* showing the chromosomal marker REC8-GFP (green). Scale bar = 10  $\mu\text{m}$ .

B. A detail of a single meiocyte is shown (marked with a magenta dashed square in A). Scale bar = 5  $\mu\text{m}$ .

### 3.3. Discussion

Here, I have described the successful cloning of reporter and CRISPR-Cas9 constructs and transformation of tetraploid *A. lyrata*, although at a reduced efficiency. Since no reporter lines in diploid *A. lyrata* were recovered, no comparison between meiosis in diploid and autotetraploid *A. lyrata* was possible. Additionally, I did not achieve transformation of *A. arenosa*. Thus, meiosis in *A. lyrata* and *A. arenosa* hybrids could not be followed with the proper parental species controls. Therefore, with this transformation bottleneck in mind, the project was not carried out in full. With my experience as a starting point, a few changes in the reporters constructs and transformation protocol could be made.

#### 3.3.1. Self-incompatibility: a challenge for studies in *A. lyrata* and *A. arenosa*

As described above, the *A. lyrata* and *A. arenosa* plants that were used in this study were self-incompatible. This resulted in a laborious floral dipping protocol, in which plants with cross-compatible pollen had to be selected in advance to manually pollinate and generate seeds from dipped plants. However, there are known self-compatible tetraploid populations, for instance the *Arabidopsis lyrata* ssp *kawasakiana* from Japan (Mable *et al*, 2004). Self-compatible diploid *A. lyrata* populations have also been found (Mable, 2004). Thus, it would be of interest to use such self-compatible populations for transformation in the future.

The fact that a widely used inbred *A. lyrata* ecotype is inexistent also makes genetic studies more complicated, as seen with a wide variation in genomic sequences of wild plants in relation to the reference genome. Therefore, generating a self-compatible highly inbred ecotype would be desirable.

#### 3.3.2. Selecting a specific *A. lyrata* promoter could promote expression of the microtubule reporter construct in meiocytes

A reduction in the number of functional copies of meiotic genes in allopolyploids is associated with a stabilization of meiosis and prevention of non-homologous recombination (Gonzalo *et al*, 2019). Additionally, epigenetic silencing of duplicate genes has been described in allopolyploids (Adams & Wendel, 2005). Hence, the fact that I often found meiotic reporters to be inactive or weak in meiocytes could be partly due to

the polyploid background of the transformed plants, since only autotetraploid *A. lyrata* plants were recovered. There is presumably a fine regulation of meiotic gene expression in these tetraploid plants to perform stable meiotic divisions, which could include silencing of the meiotic transgenes.

Another challenge I found was the inactivity of the *RPS5Apro:TagRFP-TUA5* promoter in meiocytes. A different promoter could be used to drive expression of the microtubule reporter in meiocytes. For instance, the promoter of *ARABIDOPSIS SKP1-LIKE1 (ASK1)*; Wang & Yang, 2006) could be used, which is known to be expressed predominantly in meiosis. A second option would be the promoter of *CDKA;1*, which is known to be active in meiocytes (Sofroni *et al*, 2020). Additionally, other  $\alpha$ -tubulin homologs could be used instead of *TUA5/TUA3*, which for unknown reasons might be repressed or silenced in the meiocytes of *A. lyrata*. The selective usage of tubulin isoforms depending on the type of division is not unheard of. In maize, for instance,  $\beta$ 2-tubulin is found only in male meiocytes, but not in roots or leaves (Eun & Wick, 1998). A lack of tissue-specific gene expression information from *A. lyrata*, however, complicates this selection for new tubulin homologs.

### **3.3.3. A low transformation efficiency can be associated with the plant ecotype**

In the modified floral dipping protocol I have developed, I used the GV3101::pMP90RK *Agrobacterium* strain in the C58 chromosomal background, which is routinely used for *A. thaliana* transformation. It has been previously shown that the C24 ecotype of *A. thaliana* is highly resistant to *Agrobacterium* transformation in comparison to Col-0, with a transformation efficiency that is as low as 0–0.33% and is not dependent on bacterial strain (Ghedira *et al*, 2013). Hence, it is possible that the plants that were used here for transformation are naturally resistant to *Agrobacterium* transformation. A possible solution would be to sample *A. lyrata* and *A. arenosa* from different locations and test their specific susceptibility to *Agrobacterium* transformation.

Furthermore, *A. lyrata* and *A. arenosa* produce fewer seeds per silique compared to *A. thaliana*. For *A. lyrata*, this number has been shown to be as little as  $46.4 \pm 4.4$  seeds per silique (Yamamoto *et al*, 2019), whereas, in *A. thaliana*, there can be as many as 60 seeds in a silique (data not shown). Transforming a larger number of plants and pollinating more flowers can result in a successful transformation of both *A. lyrata* and *A.*



*arenosa* (R. Alling, personal communication), although this may be laborious and time-consuming.

### 3.3.4. Progression of meiosis in auto- and allopolyploids

A detailed report of meiosis in diploid *A. thaliana* has been recently produced (Prusicki *et al*, 2019). Comparing the dynamics of meiosis between *A. lyrata* diploids and established or newly generated tetraploids, for example, could potentially contribute to our knowledge of adaptation to polyploid meiosis. Efforts to uncover the molecular mechanism of adaptation to polyploid meiosis in *A. arenosa* have revealed specific selection acting on a number of meiotic genes (Yant *et al*, 2013; Wright *et al*, 2015).

Derived alleles for *ASY1* and *ASY3*, for instance, have been identified in wild tetraploid *A. arenosa* (Morgan *et al*, 2020). These alleles were shown to act finely in modulating multivalent chromosome formation rates, promoting a trend toward rod-shaped bivalents and regulating chromosome axis length. Hence, it would be interesting to be able to compare the localization and timing of these derived tetraploid synaptonemal complex components in comparison to their ancestral diploid counterparts.

### 3.3.5. Outlook

The stable transformation of *A. lyrata* and *A. arenosa* by floral dipping has proven difficult as reported above. On the other hand, meiotic progression could still be analyzed in allopolyploids of *A. lyrata* and *A. arenosa* with the use of immunolocalization techniques of fixed material. Indeed, many protocols are available for the immunostaining of meiocytes (Chelysheva *et al*, 2010). Furthermore, the development of super-resolution microscopy techniques, e.g., stimulated emission depletion (STED) and stochastic optical reconstruction microscopy (STORM), can allow for a nanoscale resolution of meiotic processes (Sims *et al*, 2021).

Alternatively, perhaps a more efficient transformation protocol than floral dipping could be developed. For instance, the stable genetic transformation of *A. lyrata* roots followed by regeneration of whole plants using callus induction and tissue culture has been reported (Fobis-Loisy *et al*, 2007). Since *A. lyrata* and *A. arenosa* are closely related, small changes in the root transformation protocol for *A. lyrata*, for example, could allow

for stable transformation of *A. arenosa* roots as well. Nevertheless, this remains to be tested.

Finally, a detailed description of hybrid meiosis dynamics remains to be produced. It is possible that other model systems will emerge to help us elucidate the many questions that remain regarding adaptation to auto- and allopolyploid meiosis.

### 3.4. References

- Adams KL & Wendel JF (2005) Novel patterns of gene expression in polyploid plants. *Trends Genet* 21: 539–543
- Armstrong SJ, Caryl AP, Jones GH & Franklin FCH (2002) Asy1, a protein required for meiotic chromosome synapsis, localizes to axis-associated chromatin in *Arabidopsis* and *Brassica*. *J Cell Sci* 115: 3645–3655
- Arnold B, Kim ST & Bomblies K (2015) Single geographic origin of a widespread autotetraploid *Arabidopsis arenosa* lineage followed by interploidy admixture. *Mol Biol Evol* 32: 1382–1395
- Bolaños-Villegas P, De K, Pradillo M, Liu D & Makaroff CA (2017) In favor of establishment: Regulation of chromatid cohesion in plants. *Front Plant Sci* 8: 1–12
- Bomblies K, Jones G, Franklin C, Zickler D & Kleckner N (2016) The challenge of evolving stable polyploidy: could an increase in “crossover interference distance” play a central role? *Chromosoma* 125: 287–300
- Bomblies K & Madlung A (2014) Polyploidy in the *Arabidopsis* genus. *Chromosom Res* 22: 117–134
- Cai X, Dong F, Edelmann RE & Makaroff CA (2003) The *Arabidopsis* SYN1 cohesin protein is required for sister chromatid arm cohesion and homologous chromosome pairing. *J Cell Sci* 116: 2999–3007
- Capilla-Pérez L, Durand S, Hurel A, Lian Q, Chambon A, Tauchy C, Solier V, Grelon M & Mercier R (2021) The synaptonemal complex imposes crossover interference and heterochiasmy in *Arabidopsis*. *Proc Natl Acad Sci U S A* 118: 1–11
- Chelysheva L, Diallo S, Vezon D, Gendrot G, Vrielynck N, Belcram K, Rocques N, Márquez-Lema A, Bhatt AM, Horlow C, *et al* (2005) AtREC8 and AtSCC3 are essential to the monopolar orientation of the kinetochores during meiosis. *J Cell Sci* 118: 4621–4632
- Chelysheva L, Grandont L, Vrielynck N, Le Guin S, Mercier R & Grelon M (2010) An easy protocol for studying chromatin and recombination protein dynamics during *Arabidopsis thaliana* meiosis: Immunodetection of cohesins, histones and MLH1. *Cytogenet Genome Res* 129: 143–153
- Comai L (2005) The advantages and disadvantages of being polyploid. *Nat Rev Genet* 6: 836–846
- Desfeux C, Clough SJ & Bent AF (2000) Female reproductive tissues are the primary target of *Agrobacterium*-mediated transformation by the *Arabidopsis* floral-dip method. *Plant Physiol* 123: 895–904
- Doudna JA & Charpentier E (2014) The new frontier of genome engineering with

- CRISPR-Cas9. *Science* 346: 1258096-1–1258096-9
- Doyle JJ, Flagel LE, Paterson AH, Rapp RA, Soltis DE, Soltis PS & Wendel JF (2008) Evolutionary genetics of genome merger and doubling in plants. *Annu Rev Genet* 42: 443–461
- Eun SO & Wick SM (1998) Tubulin isoform usage in maize microtubules. *Protoplasma* 204: 235–244
- Ferdous M, Higgins JD, Osman K, Lambing C, Roitinger E, Mechtler K, Armstrong SJ, Perry R, Pradillo M, Cuñado N, *et al* (2012) Inter-homolog crossing-over and synapsis in *Arabidopsis* meiosis are dependent on the chromosome axis protein AtASY3. *PLoS Genet* 8: 1–15
- Fobis-Loisy I, Chambrier P & Gaude T (2007) Genetic transformation of *Arabidopsis lyrata*: Specific expression of the green fluorescent protein (GFP) in pistil tissues. *Plant Cell Rep* 26: 745–753
- France MG, Enderle J, Röhrig S, Puchta H, Franklin FCH & Higgins JD (2021) ZYP1 is required for obligate cross-over formation and cross-over interference in *Arabidopsis*. *Proc Natl Acad Sci U S A* 118: 1–11
- Ghedira R, De Buck S, Nolf J & Depicker A (2013) The efficiency of *Arabidopsis thaliana* floral dip transformation is determined not only by the *Agrobacterium* strain used but also by the physiology and the ecotype of the dipped plant. *Mol Plant-Microbe Interact* 26: 823–832
- Gonzalo A, Lucas MO, Charpentier C, Sandmann G, Lloyd A & Jenczewski E (2019) Reducing *MSH4* copy number prevents meiotic crossovers between non-homologous chromosomes in *Brassica napus*. *Nat Commun* 10: 1–9
- Haering CH, Löwe J, Hochwagen A & Nasmyth K (2002) Molecular Architecture of SMC Proteins and the Yeast Cohesin Complex. *Mol Cell* 9: 773–788
- Hofstatter PG, Thangavel G, Castellani M & Marques A (2021) Meiosis Progression and Recombination in Holocentric Plants: What Is Known? *Front Plant Sci* 12: 1–11
- Hollister JD (2015) Polyploidy: Adaptation to the genomic environment. *New Phytol* 205: 1034–1039
- Indriolo E, Tharmapalan P, Wright SI & Goring DR (2012) The *ARC1* E3 ligase gene is frequently deleted in self-compatible Brassicaceae species and has a conserved role in *Arabidopsis lyrata* self-pollen rejection. *Plant Cell* 24: 4607–4620
- Kolář F, Fuxová G, Závěská E, Nagano AJ, Hyklová L, Lučanová M, Kudoh H & Marhold K (2016) Northern glacial refugia and altitudinal niche divergence shape genome-wide differentiation in the emerging plant model *Arabidopsis arenosa*. *Mol Ecol* 25: 3929–3949

- Komaki S & Schnittger A (2017) The Spindle Assembly Checkpoint in Arabidopsis Is Rapidly Shut Off during Severe Stress. *Dev Cell* 43: 172–185
- Lafon-Placette C, Johannessen IM, Hornslien KS, Ali MF, Bjerkan KN, Bramsiepe J, Glöckle BM, Rebernick CA, Brysting AK, Grini PE, *et al* (2017) Endosperm-based hybridization barriers explain the pattern of gene flow between *Arabidopsis lyrata* and *Arabidopsis arenosa* in Central Europe. *Proc Natl Acad Sci U S A* 114: E1027–E1035
- Levin DA (1983) Polyploidy and Novelty in Flowering Plants. *Am Nat* 122: 1–25
- Liu CM, McElver J, Tzafrir I, Joosen R, Wittich P, Patton D, Van Lammeren AAM & Meinke D (2002) Condensin and cohesin knockouts in Arabidopsis exhibit a titan seed phenotype. *Plant J* 29: 405–415
- Mable BK (2004) Polyploidy and self-compatibility: Is there an association? *New Phytol* 162: 803–811
- Mable BK, Beland J & Di Berardo C (2004) Inheritance and dominance of self-incompatibility alleles in polyploid *Arabidopsis lyrata*. *Heredity (Edinb)* 93: 476–486
- Mayer VW & Aguilera A (1990) High levels of chromosome instability in polyploids of *Saccharomyces cerevisiae*. *Mutat Res - Fundam Mol Mech Mutagen* 231: 177–186
- Mercier R, Mézard C, Jenczewski E, Macaisne N & Grelon M (2015) The molecular biology of meiosis in plants. *Annu Rev Plant Biol* 66: 297–327
- Morgan C, Zhang H, Henry CE, Franklin CFH & Bomblies K (2020) Derived alleles of two axis proteins affect meiotic traits in autotetraploid *Arabidopsis arenosa*. *Proc Natl Acad Sci U S A* 117: 8980–8988
- Page SL & Hawley RS (2004) The genetics and molecular biology of the synaptonemal complex. *Annu Rev Cell Dev Biol* 20: 525–558
- Prusicki MA, Keizer EM, van Rosmalen RP, Komaki S, Seifert F, Müller K, Wijnker E, Fleck C & Schnittger A (2019) Live cell imaging of meiosis in *Arabidopsis thaliana* - A landmark system. *Elife*: 1–31
- Ross KJ, Fransz P, Armstrong SJ, Vizir I, Mulligan B, Franklin FCH & Jones GH (1997) Cytological characterization of four meiotic mutants of Arabidopsis isolated from T-DNA-transformed lines. *Chromosom Res* 5: 551–559
- Sanchez-Moran E, Osman K, Higgins JD, Pradillo M, Cuñado N, Jones GH & Franklin FCH (2008) ASY1 coordinates early events in the plant meiotic recombination pathway. *Cytogenet Genome Res* 120: 302–312
- Schmickl R & Koch MA (2011) Arabidopsis hybrid speciation processes. *Proc Natl Acad Sci U S A* 108: 14192–14197

- Sims J, Schlögelhofer P & Kurzbauer MT (2021) From Microscopy to Nanoscopy: Defining an *Arabidopsis thaliana* Meiotic Atlas at the Nanometer Scale. *Front Plant Sci* 12: 1–17
- Sofroni K, Takatsuka H, Yang C, Dissmeyer N, Komaki S, Hamamura Y, Böttger L, Umeda M & Schnittger A (2020) CDKD-dependent activation of CDKA;1 controls microtubule dynamics and cytokinesis during meiosis. *J Cell Biol* 219: 1–21
- Soltis PS & Soltis DE (2016) Ancient WGD events as drivers of key innovations in angiosperms. *Curr Opin Plant Biol* 30: 159–165
- Stebbins GL (1940) The significance of polyploidy in plant evolution. *Am Nat* 74: 54–66
- Wang Y & Yang M (2006) The ARABIDOPSIS SKP1-LIKE1 (ASK1) protein acts predominately from leptotene to pachytene and represses homologous recombination in male meiosis. *Planta* 223: 613–617
- Wright KM, Arnold B, Xue K, Surinova M, O'Connell J & Bomblies K (2015) Selection on meiosis genes in diploid and tetraploid *Arabidopsis arenosa*. *Mol Biol Evol* 32: 944–955
- Yamamoto M, Nishimura K, Kitashiba H, Sakamoto W & Nishio T (2019) High temperature causes breakdown of S haplotype-dependent stigmatic self-incompatibility in self-incompatible *Arabidopsis thaliana*. *J Exp Bot* 70: 5745–5751
- Yang C, Hamamura Y, Sofroni K, Böwer F, Stolze SC, Nakagami H & Schnittger A (2019) SWITCH 1/DYAD is a WINGS APART-LIKE antagonist that maintains sister chromatid cohesion in meiosis. *Nat Commun* 10: 1–15
- Yang C, Sofroni K, Wijnker E, Hamamura Y, Carstens L, Harashima H, Stolze SC, Vezon D, Chelysheva L, Orban-Nemeth Z, *et al* (2020) The Arabidopsis Cdk1/Cdk2 homolog CDKA;1 controls chromosome axis assembly during plant meiosis. *EMBO J* 39: 1–19
- Yant L, Hollister JD, Wright KM, Arnold BJ, Higgins JD, Franklin FCH & Bomblies K (2013) Meiotic Adaptation to Genome Duplication in *Arabidopsis arenosa*. *Curr Biol* 23: 2151–2156

# Material and Methods

## 1. Plant methods

### 1.1. Plant growth conditions

*Arabidopsis thaliana* seeds were sown on half-strength ( $\frac{1}{2}$ ) Murashige and Skoog (MS) medium (basal salt mixture, Duchefa Biochemie) with 0.5% sucrose and 0.8% agar (plant agar, Duchefa Biochemie) and adjusted to pH 5.8 with KOH. Seeds were surface-sterilized with chlorine gas or by liquid sterilization. For the first method, 3 mL of HCl 32% was added to a beaker containing 25 mL of 13% sodium hypochlorite and seeds were left for gas sterilization between 3 hours and overnight. For the second method, a 2% bleach, 0.05% Triton X-100 solution was added for 5 min, followed by three washing steps with sterile distilled water and the addition of 0.05% agarose. Seeds were stratified at 4°C for 2 to 3 days in the dark. Plants were initially grown *in vitro* at 22°C in a 16-h light regime and then transferred to soil with a 16-h light/21°C and 8-h/18°C dark regime with 60% humidity.

### 1.2. Floral dipping of *A. thaliana*

A starter culture of *Agrobacterium tumefaciens* (pMP90RK) containing the desired plasmid was initially cultivated at 28°C overnight; always with gentamycin and additional antibiotics depending on the plasmid. The following day, this culture was centrifuged at 4000  $xg$  for 10 min and resuspended in 5% sucrose with 0.02% Silwett L-77. This mixture was carefully pipetted on immature flower buds of *A. thaliana*. Plants were then bagged in a humid environment and kept away from light for 16 to 24 hours. After harvesting the seeds, they were sown on  $\frac{1}{2}$  MS media containing the appropriate selection.

### 1.3. DNA extraction and genotyping of mutant plants

For the genotyping of T-DNA insertion lines, genomic DNA was extracted using magic buffer (50 mM Tris-HCl, pH 7.5, 300 mM NaCl and 300 mM sucrose). Small leaf fragments were cut and added to 400  $\mu$ L magic buffer containing two metal beads and subsequently shaken in a TissueLyser (QIAGEN) at 25 Hz for 2 min. After one cycle of shaking, the plates were rotated and shaken for another 2 min at 25 Hz. Next, samples

were centrifuged at 2500  $xg$  for 5 min and 100  $\mu\text{L}$  were aliquoted to fresh tubes. Samples were then diluted 10x with magic buffer before use in PCR reactions.

The genotyping was performed either using DreamTaq Green or Terra PCR Direct Polymerase. PCR reactions were assembled as the following for the first case:

| Reagent                            | Volume              |
|------------------------------------|---------------------|
| DreamTaq Green PCR Master Mix (2x) | 6.25 $\mu\text{L}$  |
| Primer 1 (10 $\mu\text{M}$ )       | 0.625 $\mu\text{L}$ |
| Primer 2 (10 $\mu\text{M}$ )       | 0.625 $\mu\text{L}$ |
| Template gDNA                      | 1.0 $\mu\text{L}$   |
| Water                              | 4.0 $\mu\text{L}$   |
| Total volume                       | 12.5 $\mu\text{L}$  |

| Temperature | Duration |
|-------------|----------|
| 95°C        | 3 min    |
| 95°C        | 30 s     |
| 55°C        | 30 s     |
| 72°C        | 1 min*   |
| 72°C        | 5 min    |

} 30-35 cycles

\* 1 min is recommended for fragments up to 2 kb. For longer products, the extension time was prolonged by 1 min/kb.

For PCRs using Terra PCR Direct Polymerase, reactions were assembled following these conditions:

| Reagent                      | Volume              |
|------------------------------|---------------------|
| Terra PCR Direct Buffer (2x) | 6.25 $\mu\text{L}$  |
| Primer 1 (10 $\mu\text{M}$ ) | 0.375 $\mu\text{L}$ |
| Primer 2 (10 $\mu\text{M}$ ) | 0.375 $\mu\text{L}$ |
| Template gDNA                | 1.0 $\mu\text{L}$   |
| Water                        | 4.5 $\mu\text{L}$   |
| Total volume                 | 12.5 $\mu\text{L}$  |



| Temperature | Duration |                |
|-------------|----------|----------------|
| 98°C        | 2 min    |                |
| 98°C        | 10 s     | } 30-35 cycles |
| 55°C        | 15 s     |                |
| 68°C        | 1 min/kb |                |
| 68°C        | 2 min    |                |

#### 1.4. Flow cytometry assay

Ten seven-day old seedlings per genotype were chopped with a fresh razorblade in homogenization buffer (45 mM MgCl<sub>2</sub>, 20 mM MOPS, 30 mM sodium citrate, 0.1% Triton X-100, pH 7.0) followed by filtration through a 15- $\mu$ m nylon mesh. Next, propidium iodide (Sigma) and RNase A (Sigma) were added to final concentrations of 50  $\mu$ g/mL and 10  $\mu$ g/mL respectively. Samples were incubated on ice for 5 min and then analyzed in a S3e Cell Sorter (Bio-Rad) with laser excitation at 488 nm. The FlowJo software was used to analyze and process the scatterplots generated by the machine.

#### 1.5. Endosperm nuclei proliferation analysis

First, flower buds were emasculated before the visible maturation and release of pollen. Then, emasculated flowers were pollinated with pollen from the corresponding genotype after 2 to 3 days. Three days after pollination, siliques were dissected and fixed in a solution of 4% glutaraldehyde in 12.5 mM cacodylate buffer, pH 6.8, followed by application of vacuum for 20 min and storage at 4°C overnight. The next day, seeds were individually mounted on microscope slides containing a 1:8:2 glycerol:chloral hydrate:water clearing solution and stored at 4°C overnight. Imaging of the slides was performed with a Zeiss LSM 780 or 880 confocal microscope with excitation at 488 nm and detection between 498 and 586 nm. Z-stacks were analyzed using the Fiji software.

#### 1.6. Root growth assays

For the oryzalin root growth assays, plants were sown on ½ MS containing either 0.5% DMSO or oryzalin. Oryzalin stocks were prepared at a 100 mM concentration in DMSO and stored at -20°C. Oryzalin was further diluted to 150 nM and 200 nM for the root growth measurements. After two days of stratification at 4°C, the plates containing the seeds were transferred to the growth chamber and root growth was recorded daily up

until five days after germination. At this timepoint, the plates were scanned and the root length was measured using the Fiji software. For the graphs, three biological replicates with at least 10 plants per genotype were measured. The average root length was measured for each single experiment and then averaged again for the final shown values.

## 2. Cloning methods

### 2.1. Amplification of genomic and coding sequence fragments

For the cloning of genomic and coding sequences, PCRs were performed using the PrimeSTAR Max DNA Polymerase (TaKaRa). Reactions were assembled as the following:

| Reagent                   | Volume       |
|---------------------------|--------------|
| PrimeSTAR Max Premix (2x) | 25 $\mu$ L   |
| Primer 1 (10 $\mu$ M)     | 1.5 $\mu$ L  |
| Primer 2 (10 $\mu$ M)     | 1.5 $\mu$ L  |
| Template DNA              | 1.0 $\mu$ L  |
| Water                     | 21.0 $\mu$ L |
| Total volume              | 50 $\mu$ L   |

Amplification of the fragments was achieved using the following PCR program:

| Temperature | Duration |                |
|-------------|----------|----------------|
| 98°C        | 5 min    |                |
| 98°C        | 10 s     | } 30-35 cycles |
| 55°C        | 5 s      |                |
| 72°C        | 5 s/kb   |                |
| 72°C        | 3 min    |                |

## 2.2. Classical restriction-based cloning

Site-directed mutagenesis was performed by PCRs with phosphorylated primers containing the desired mutations followed by self-ligation of the modified product. Phosphorylation of the primers was performed at 37°C for 20 min and the reactions were assembled as the following:

| Reagent                  | Volume   |
|--------------------------|----------|
| Oligonucleotide (100 µM) | 2.0 µL   |
| 10x reaction buffer A    | 2.0 µL   |
| ATP (10 mM)              | 2.0 µL   |
| T4 Polynucleotide Kinase | 1.0 µL   |
| Water                    | to 20 µL |

After the appropriate PCR with the phosphorylated primers, self-circularization of the PCR products was performed at 22°C for 1 hour with the following conditions:

| Reagent                  | Volume   |
|--------------------------|----------|
| Linear DNA               | 10-50 ng |
| 10x T4 DNA Ligase Buffer | 5.0 µL   |
| T4 DNA Ligase            | 5 u      |
| Water                    | to 50 µL |

Restriction digests were performed simultaneously with the dephosphorylation of plasmid DNA in order to linearize the vector and avoid self-circularization of the product in subsequent ligations. This was performed at 37°C for 15 min as following:

| Reagent                                     | Volume   |
|---|----------|
| Plasmid DNA                                 | 2 µg     |
| 10x Thermo Scientific FastDigest Buffer     | 2.0 µL   |
| FastDigest Restriction Enzyme               | 1.0 µL   |
| FastAP Thermosensitive Alkaline Phosphatase | 1.0 µL   |
| Water                                       | to 20 µL |

Blunt-ended ligation of an insert into a linearized vector was performed at 16°C overnight with the following conditions:

| <b>Reagent</b>           | <b>Volume</b>                      |
|--------------------------|------------------------------------|
| Linear vector DNA        | 20-100 ng                          |
| Insert DNA               | 1:1 to 5:1 molar ratio over vector |
| 10x T4 DNA Ligase buffer | 2.0 µL                             |
| 50% PEG 4000 solution    | 2.0 µL                             |
| T4 DNA Ligase            | 5 u                                |
| Water                    | to 20 µL                           |

Sticky-ended ligation of an insert into a linearized vector was performed at 22°C for 1 hour with the following conditions:

| <b>Reagent</b>           | <b>Volume</b>                      |
|--------------------------|------------------------------------|
| Linear vector DNA        | 20-100 ng                          |
| Insert DNA               | 1:1 to 5:1 molar ratio over vector |
| 10x T4 DNA Ligase buffer | 2.0 µL                             |
| T4 DNA Ligase            | 1 u                                |
| Water                    | to 20 µL                           |

### 2.3. Gateway cloning

First, flanking attB1 and attB2 recombination sites were added to the desired PCR products by reamplification of the fragments. Next, the BP reaction was performed to insert the desired fragment in an entry vector (either pDONR221 or pDONR223) as following:

| <b>Reagent</b>              | <b>Quantity</b> |
|-----------------------------|-----------------|
| PCR product with attB sites | 25 fmol         |
| pDONR vector                | 25 fmol         |
| Water                       | to 4 µL         |
| BP Clonase II               | 1 µL            |

BP reactions were incubated at room temperature for a minimum of 3 hours or overnight. After clones were confirmed and sequenced, the LR reaction was performed as the following:

| Reagent                                  | Quantity     |
|--|--------------|
| pDONR vector containing desired fragment | 25 ng        |
| Destination vector                       | 50 ng        |
| Water                                    | to 4 $\mu$ L |
| LR Clonase II                            | 1 $\mu$ L    |

LR reactions were incubated at room temperature for a minimum of 1 hour or overnight.

#### 2.4. Seamless ligation cloning extract (SLiCE)

The SLiCE reagents were prepared according to Zhang *et al*, 2014. Initially, vector DNA and insert DNA were designed to have an overlap of 25 bp at the 5' and 3' regions. Then, SLiCE reactions were set up as the following:

| Reagent   | Quantity                              |
|---|---------------------------------------|
| Vector DNA  | 50-200 ng                             |
| Insert DNA  | 1:1 to 10:1 in relation to vector DNA |
| 10x SLiCE Buffer (500 mM Tris-HCl, pH 7.5, 100 mM MgCl <sub>2</sub> , 10 mM ATP, 10 mM DTT) | 1 $\mu$ L                             |
| PPY SLiCE extract   | 1 $\mu$ L                             |
| Water   | to 10 $\mu$ L                         |

SLiCE reactions were incubated between 15 min and 1 hour at 37°C.

### 3. Microbiological methods

#### 3.1. Heath shock transformation of *Escherichia coli* chemically competent cells

First, chemically competent *E. coli* cells were thawed on ice for 20 to 30 min. After that, plasmid DNA was added (10 pg to 100 ng) and again this mixture was incubated on ice

for 20 to 30 min. Heat shock was then performed at 42°C for 45 s followed by putting the cells on ice for 2 min. Next, 200 µL of liquid LB (10 g/L tryptone, 10 g/L NaCl and 5 g/L yeast extract) was added and the cells were allowed to recover for 45 min to 1 hour at 37°C. After recovery, cells were plated on solid LB containing the appropriate antibiotics for selection and incubated at 37°C overnight.

### **3.2. Heat shock transformation of *Agrobacterium tumefaciens***

First, chemically competent cells were thawed on ice. After that, plasmid DNA was added (0.1 to 1 µg) and the tubes were gently flicked to mix the samples. Cells were frozen at -80°C for 10 min and subsequently thawed by incubation at 37°C in a water bath for 5 min. Next, the cells were placed on ice for 30 min. Following that, 200 µL of LB was added and the cells were either allowed to recover at 28°C for 2 hours or immediately plated on LB plates containing the appropriate antibiotics. Plates were incubated for 2 days at 28°C before colonies appeared.

### **3.3. Heat shock transformation of *Saccharomyces cerevisiae***

This section was written based on a protocol by Gietz & Schiestl, 2007. Initially, a single colony of the yeast AH109 strain was inoculated into 5 mL of liquid YPDA medium (10 g/L yeast extract, 20 g/L peptone, 20 g/L glucose monohydrate and 40 mg/L adenine hemisulfate) and grown at 28°C and 160 rpm overnight. The next day, the titer of the yeast culture was determined and the appropriate amount of yeast culture was added to fresh 2X YPDA medium (20 g/L yeast extract, 40 g/L peptone, 4% glucose, 80 mg/L adenine hemisulfate, pH 6.5) for an OD<sub>600</sub> of 0.5. The new culture was further incubated at 28°C for about 4 h until the OD<sub>600</sub> reached 2.0. The cells were harvested by centrifugation at 3,000 xg for 5 min and resuspended in 25 mL of sterile water. Next, another centrifugation step at 3,000 xg for 5 min was performed to pellet the cells. Another 25 mL of sterile water was used to resuspend the pellet and centrifugation followed with the same previous conditions. Next, the cells were resuspended in 1.0 mL of sterile water. The cell suspension was transferred to a 1.5 mL microcentrifuge tube, centrifuged for 30 s at 13,000 xg and the supernatant was then discarded. Finally, the cells were then resuspended in 1.0 mL of sterile water and 100 µL aliquots were made into 1.5 mL microcentrifuge tubes, one for each desired transformation. Centrifugation at 13,000 xg for 30 s followed and the supernatant was removed. A transformation mix for one reaction was assembled as the following table and scaled up as needed:

| Reagent                   | Quantity    |
|---------------------------|-------------|
| PEG 3350 50%              | 240 $\mu$ L |
| LiAc 1.0 M                | 36 $\mu$ L  |
| Carrier DNA (10.0 mg/mL)* | 10 $\mu$ L  |
| Water                     | 40 $\mu$ L  |
| Total volume              | 326 $\mu$ L |

\*A sample of carrier DNA was denatured in a boiling water bath for 5 min and chilled immediately on ice. Alternatively, a pre-denatured carrier DNA sample was stored at -20°C, thawed and kept on ice.

326  $\mu$ L of transformation mix were added to each transformation tube containing the cell pellet. The desired plasmid DNA was then added to each of the tubes plus water to a final volume of 34  $\mu$ L. After that, the cell pellets were resuspended by vigorous vortexing. The tubes were then placed in a water bath at 42°C and incubated for 40 min. Next, the tubes were placed on ice for 90 s, followed by centrifugation at 13,000  $xg$  and removal of the supernatant. Finally, the cells were resuspended in 100  $\mu$ L sterile water by vortexing and plated on the appropriate dropout plates. The plates were incubated at 30°C for 3 to 4 days before colonies were visible.

### 3.4. Yeast two-hybrid

After successful transformation of the desired plasmid combinations in the yeast strain and plating on double dropout media (-Leu and -Trp amino acid supplements, 6.8 g/L yeast nitrogen base, pH 5.7) for selection, three colonies per combination were dissolved in 500  $\mu$ L of sterile water and serially diluted to  $10^{-1}$ ,  $10^{-2}$  and  $10^{-3}$ . 12  $\mu$ L of the different samples, undiluted and diluted, were then dropped on double, triple (-Leu, -Trp and -His amino acid supplements, 6.8 g/L yeast nitrogen base, pH 5.7) and quadruple (-Leu, -Trp, -His and -Ade amino acid supplements, 6.8 g/L yeast nitrogen base, pH 5.7) dropout media. Growth was monitored daily and recorded when desired.

## **4. Biochemical methods**

### **4.1. SDS-PAGE**

Running gels were prepared at a standard 10% polyacrylamide concentration (3.2 mL water, 2.67 mL of 30% acrylamide/bis solution, 29:1, 2 mL of 1.5 M Tris pH 8.8, 80  $\mu$ L of 10% SDS, 80  $\mu$ L of 10% APS and 8  $\mu$ L of TEMED per single gel). The stacking gels were prepared at a 6% polyacrylamide concentration (3.4 mL water, 1 mL of 30% acrylamide/bis solution, 29:1, 417  $\mu$ L of 1.5 M Tris pH 6.8, 50  $\mu$ L of 10% SDS, 50  $\mu$ L of 10% APS, 5  $\mu$ L of TEMED per single gel). The SDS-PAGE running buffer was prepared at a 10x concentration (30 g/L of Tris base, 144 g/L of glycine and 10 g/L SDS) and further diluted to 1x before use. 5x sample buffer (0.25% bromophenol blue, 0.5 M DTT, 50% glycerol, 10% SDS and 0.25 M Tris-HCl, pH 6.8) was diluted to a 1x concentration for loading of protein samples on the gel.

### **4.2. Coomassie Brilliant Blue (CBB) staining and destaining**

After SDS-PAGE was performed, the polyacrylamide gels were stained with CBB (1 g/L Coomassie Brilliant Blue, 50% methanol and 10% glacial acetic acid) and destained with a conventional destaining solution (10% methanol and 10% glacial acetic acid).

### **4.3. Western blotting**

If protein purity or the identity of a tagged protein was to be assessed, western blots were performed. For the blotting of the proteins on a PVDF membrane, the PVDF membrane was initially wetted in methanol for 15 s, then placed in water for 2 min and finally placed in anode buffer II (25 mM Tris, 20% methanol, pH 10.4) for 5 min. A semi-dry transfer stack was assembled as the following: two pieces of filter paper were placed on anode buffer I (300 mM Tris, 20% methanol, pH 10.4) and assembled on the anode plate of a semi-dry electrophoretic transfer cell, followed by one piece of filter paper that was wetted in anode buffer II, the transfer membrane, the SDS-PAGE gel and three pieces of filter paper that were placed in cathode buffer (25 mM Tris, 20% methanol, 40 mM 6-aminocaproic acid, pH not adjusted). After that, the cathode plate of the semi-dry electrophoretic transfer cell was placed on top of the transfer stack and the blotting was subsequently performed with a constant current of 1.9 – 2.5 mA per  $\text{cm}^2$  of gel area for 30 to 60 min. After blotting was completed, blocking of the membrane was performed



with a 5% milk powder solution in TBST buffer (20 mM Tris, 150 mM NaCl, 0.1% Tween 20, pH 7.4) for 1 to 2 hours at room temperature. Next, the blocking buffer was poured off and the primary antibody solution (5% milk powder in TBST together with the appropriate antibody) was applied at 4°C overnight or at room temperature for 1 h with gentle rocking. After that, the membrane was rinsed twice with distilled water and then washed twice for 15 min with TBST. The secondary HRP-conjugated antibody solution (5% milk powder in TBST together with the appropriate antibody) was then applied and incubated on a rocker at room temperature for 30 min. After rinsing the membrane twice with distilled water, two washing steps with TBST for 20 min were performed. Finally, the SuperSignal™ West Pico PLUS Chemiluminescent substrate was used to detect the desired bands on the membrane.

#### **4.4. Protein expression**

After the desired vectors for protein expression were transformed in BL21 (DE3) *E. coli* cells, an overnight culture of the positive colonies with the appropriate antibiotics was used to inoculate an expression culture at a dilution of 1:100. This culture was incubated at 37°C until OD<sub>600</sub> between 0.4 and 0.6. Unless stated otherwise, at this point, IPTG was added at a concentration of 0.2 mM to induce protein expression and expression continued at 16°C overnight. The following day, the cultures were centrifuged at 5,000 xg at 4°C for 20 min and the cells pellets were frozen in liquid nitrogen and subsequently stored at -80°C until protein purification.

#### **4.5. Cell lysis and protein purification**

Cell pellets were initially thawed on ice for 15 min and resuspended in lysis buffer. 15-20 mL of lysis buffer were added per 100 mL of expression culture. Lysozyme was added at a concentration of 1 mg/mL and the samples were incubated with gentle rocking for 30 min at 4°C. After this step, Triton X-100 was added to a concentration of 0.2% and the samples were further incubated for 20 min at 4°C. Next, five to eight cycles of 30 s of sonication until cells were fully lysed and 20 s of rest on ice were performed. The samples were then centrifuged at 5,000 xg for 20 to 30 min at 4°C to pellet the cellular debris. The supernatant was then used for incubation with the desired affinity chromatography matrix.

For His-tagged proteins, the following protocol was employed. Initially, 100  $\mu$ L of a Ni-NTA matrix was pipetted to a 1.5 mL Eppendorf tube and briefly centrifuged at 1,200  $xg$  for 2 min. The supernatant was removed and 500  $\mu$ L of lysis buffer (PBS, pH 7.4, with 10% glycerol and 25 mM imidazole) was added. The agarose was gently mixed by inverting the tube, followed by another centrifugation step and supernatant removal. After that, the cleared lysate obtained previously was incubated with the equilibrated matrix with gentle rocking at 4°C for 60 min. Next, the agarose was washed three to five times with 500  $\mu$ L of lysis buffer. 200 to 300  $\mu$ L of elution buffer (PBS, pH 7.4, with 10% glycerol and 250 mM imidazole) was added and the samples were mixed by inversion. After 15 min of incubation on ice, samples were briefly centrifuged at 1,200  $xg$  for 2 min and the supernatant containing the purified protein was collected. The protein was further cleaned by using PD MiniTrap G-25 desalting columns and exchanged into a desired buffer composition.

For GST-tagged proteins, a similar protocol was followed. Instead of a Ni-NTA matrix, Pierce™ Glutathione Agarose was used. In addition, the composition of the lysis buffer (PBS, pH 7.4, with 10% glycerol) and the elution buffer (PBS, pH 7.4, with 10% glycerol and 10 mM L-glutathione reduced) differed.

For Strep-tagged proteins, buffer W (100 mM Tris-HCl, pH 8.0, 150 mM NaCl, 1 mM EDTA) was used for lysis and the washing steps and the elution buffer had the same composition of buffer W with 2.5 mM added desthiobiotin.

For the Cyclin-CDK complexes, where the cyclins were tagged with His and MBP and the CDKs were tagged with Strep, the two vectors were co-transformed in BL21 and the complexes were expressed and pulled down using a Ni-NTA matrix. In that case, the His-MBP-tagged cyclins served as a bait.

#### **4.6. *In vitro* kinase assays**

For identifying the phosphorylation sites of selected substrates, *in vitro* kinase assays were assembled in kinase reaction buffer (50 mM Tris-HCl, pH 7.5, 10 mM MgCl<sub>2</sub>, 0.5 mM ATP and 5 mM DTT) according to the following table:

| Reagent                | Quantity       |
|------------------------|----------------|
| Substrate              | 1 to 1.5 µg    |
| Kinase complex         | 10 to 30 ng/µL |
| Kinase reaction buffer | to 50 µL       |

Kinase reactions were incubated at 30°C for 1 h, frozen in liquid nitrogen and subsequently sent for mass spectrometry analysis.

## 5. Resources table

### 5.1. General resources table

| Reagent or resource                         | Source  |
|---|---|
| <b>Microbiological strains</b>              |   |
| <i>E. coli</i> TOP10                        | Thermo Fisher Scientific; C404010                             |
| <i>Agrobacterium tumefaciens</i> GV3101     | DNA Cloning Service   |
| <i>S. cerevisiae</i> AH109                  | Clontech; K1612-1   |
| <i>E. coli</i> BL21 (DE3) pLysS             | Thermo Fisher Scientific; C606003                             |
| <b>Commercial cloning enzymes</b>           |   |
| Gateway BP Clonase II enzyme mix            | Thermo Fisher Scientific; 11789020                            |
| Gateway LR Clonase II enzyme mix            | Thermo Fisher Scientific; 11791020                            |
| Presto™ Mini Plasmid kit                    | Geneaid; PDH300   |
| NucleoSpin® Gel and PCR Clean-up            | MACHEREY-NAGEL; 740609.250                                    |
| PrimeSTAR® Max DNA Polymerase               | TAKARA BIO; R045A   |
| Terra™ PCR Direct Polymerase Mix            | TAKARA BIO; 639270  |
| DreamTaq Green PCR Master Mix (2x)          | Thermo Scientific™; K1081                                     |
| T4 DNA Ligase                               | Thermo Scientific™; EL0011                                    |
| T4 Polynucleotide Kinase                    | Thermo Scientific™; EK0031                                    |
| FastAP Thermosensitive Alkaline Phosphatase | Thermo Scientific™; EF0651                                    |
| FastDigest SmaI                             | Thermo Scientific™; FD0663                                    |
| <b>Software</b>                             |   |
| Fiji  | <a href="https://imagej.net/Fiji">https://imagej.net/Fiji</a> |
| FlowJo                                      | <a href="https://www.flowjo.com">https://www.flowjo.com</a>   |

## 5.2. Resources table from Chapter 2

| <b>Constructs for expression in plants</b>  |  |
|---|--|
| <i>pGWB501 PRO<sub>GIP1</sub>:GFP-GIP1</i>  | Dr. Shinichiro Komaki                                      |
| <i>pGWB501 PRO<sub>GIP1</sub>:GFP-GIP1<sup>T67A</sup></i>   | Dr. Shinichiro Komaki                                      |
| <i>pGWB501 PRO<sub>GIP1</sub>:GFP-GIP1<sup>T65A;T66A;T67A</sup></i>                                 | This thesis  |
| <i>pGWB501 PRO<sub>EDE1</sub>:GFP-EDE1</i>  | Muzaffer Emre Gül  |
| <i>pGWB501 PRO<sub>EDE1</sub>:GFP-EDE1<sup>8A</sup></i>   | This thesis  |
| <i>R4pGWB501 PRO<sub>EDE1</sub>:GFP-EDE1</i><br><i>PRO<sub>RPS5A</sub>:TagRFP-TUA5</i>              | This thesis  |
| <i>R4pGWB501 PRO<sub>EDE1</sub>:GFP-EDE1<sup>8A</sup></i><br><i>PRO<sub>RPS5A</sub>:TagRFP-TUA5</i> | This thesis  |
| <b>Constructs for expression in bacteria</b>  |  |
| <i>pHGGWA HisGST:GIP1</i>   | This thesis  |
| <i>pHGGWA HisGST:GIP2</i>   | This thesis  |
| <i>pHGGWA HisGST:EDE1</i>   | This thesis  |
| <i>pHMGWA HisMBP:CYCB1;1</i>  | Dr. Hirofumi Harashima                                     |
| <i>pHMGWA HisMBP:CYCB1;2</i>  | Dr. Hirofumi Harashima                                     |
| <i>pHMGWA HisMBP:CYCB1;3</i>  | Dr. Hirofumi Harashima                                     |
| <i>pHMGWA HisMBP:CYCB1;4</i>  | Dr. Hirofumi Harashima                                     |
| <i>pCDFDuet StrepIII-CDKB2;2</i>  | Dr. Hirofumi Harashima                                     |
| <b>Constructs for expression in yeast</b>   |  |
| <i>pGAD424 GIP1</i>   | This thesis  |
| <i>pGAD424 GIP1<sup>T65A;T66A;T67A</sup></i>  | This thesis  |
| <i>pGBT9 GCP3</i>   | Muzaffer Emre Gül  |
| <b>Plant material</b>   |  |
| <i>ede1-1</i>   | NASC; <a href="#">CS9868</a> Pignocchi <i>et al</i> , 2009 |
| <i>gip1</i>   | Dr. Shinichiro Komaki; GABI_213D01                         |
| <i>gip2</i>   | Dr. Shinichiro Komaki; SALK_094257                         |
| <i>gip1<sup>-/-</sup> gip2<sup>+/-</sup></i>  | Dr. Shinichiro Komaki                                      |
| <i>gip1 gip2 pGWB501 PRO<sub>GIP1</sub>:GFP-GIP1</i>  | Dr. Shinichiro Komaki                                      |
| <i>gip1 gip2 pGWB501 PRO<sub>GIP1</sub>:GFP-GIP1<sup>T67A</sup></i>                                 | Dr. Shinichiro Komaki                                      |
| <i>gip1 gip2 pGWB501 PRO<sub>GIP1</sub>:GFP-GIP1<sup>T65A;T66A;T67A</sup></i>                       | This thesis  |

|  |             |
|--|-------------|
| <i>ede1-1</i> pGWB501 PRO <sub>EDE1</sub> :GFP-EDE1  | This thesis |
| <i>ede1-1</i> pGWB501 PRO <sub>EDE1</sub> :GFP-EDE1 <sup>8A</sup>  | This thesis |
| <i>ede1-1</i> R4pGWB501 PRO <sub>EDE1</sub> :GFP-EDE1<br>PRO <sub>RPS5A</sub> :TagRFP-TUA5               | This thesis |
| <i>ede1-1</i> R4pGWB501 PRO <sub>EDE1</sub> :GFP-EDE1 <sup>8A</sup><br>PRO <sub>RPS5A</sub> :TagRFP-TUA5 | This thesis |

### Primers used in the research

| Purpose                                       | Primer name     | Sequence                    |
|---|-----------------|-----------------------------|
| Amplification of <i>EDE1</i> genomic fragment | gEDE1_F-2       | caagaacacacgaaagagacca      |
|   | gEDE1_R         | ccccttctgttcagaaacttc       |
| Insertion of <i>Sma</i> I site in <i>EDE1</i> | gEDE1_SmaI_F    | GGGatggaggcgagaatcgg        |
|   | gEDE1_SmaI_R    | GGGttcaatcaaatttcttca       |
| Amplification of <i>GIP1</i> CDS              | GIP1_CDS_F      | GGATGGATGAGGAGGCATCTCGG     |
|   | GIP1_CDS_R      | TCAGTGTATAGATGGTGTGGTTGTG   |
| Amplification of <i>GIP2</i> CDS              | GIP2_CDS_F      | GGATGAATCAGGAAGCAGCTGAAACAG |
|   | GIP2_CDS_R      | TTAATCAACCGTAGTTGTTGTTGT    |
| Amplification of <i>EDE1</i> CDS              | EDE1_CDS_F      | GGATGGAGGCGAGAATCGGC        |
|   | EDE1_CDS_R      | TCAAACAGAAGTTGTGCACTCTTGC   |
| Genotyping of <i>gip1</i>                     | GABI_213D01_LP2 | TCGTCTCCCACTTCTCACTTCACTCTG |
|   | HIRO749         | ACAACAGTAGCTAGACTTCAGGG     |
|   | GABI_LB         | ATATTGACCATCATACTCATTGC     |
| Genotyping of <i>gip2</i>                     | SALK_094257_LP  | ATGAATCAGGAAGCAGCTGAAACAG   |
|   | SALK_094257_RP  | GGATTGAGTGGGGATGACTC        |
|   | SALK_LB1-3      | ATTTTGCCGATTTTCGGAAC        |

### 5.3. Resources table from Chapter 3

| <b>Constructs for expression in plants</b>   |                            |
|--|----------------------------|
| <i>R4pGWB501 PRO<sub>ASY1</sub>:ASY1-GFP</i> | This thesis                |
| <i>PRO<sub>RPS5A</sub>:TagRFP-TUA5</i>       |                            |
| <i>R4pGWB501 PRO<sub>ASY3</sub>:ASY3-GFP</i> | This thesis                |
| <i>PRO<sub>RPS5A</sub>:TagRFP-TUA5</i>       |                            |
| <i>R4pGWB501 PRO<sub>REC8</sub>:REC8-GFP</i> | This thesis                |
| <i>PRO<sub>RPS5A</sub>:TagRFP-TUA5</i>       |                            |
| <i>R4pWGB501 PRO<sub>ZYP1</sub>:ZYP1-GFP</i> | This thesis                |
| <i>PRO<sub>RPS5A</sub>:TagRFP-TUA5</i>       |                            |
| <i>pDe-Cas9 AIASY1</i>                       | This thesis                |
| <i>pDe-Cas9 AIASY3</i>                       | This thesis                |
| <i>pDe-Cas9 AIREC8</i>                       | This thesis                |
| <i>pDe-Cas9 AIZYP1</i>                       | This thesis                |
| <i>pDe-Cas9 AaZYP1</i>                       | This thesis                |
| <b>Plant material</b>                        |                            |
| <i>asy1<sup>-/-</sup></i>                    | Dr. Chao Yang; SALK_046272 |
| <i>rec8<sup>+/-</sup></i>                    | Dr. Chao Yang; SAIL_807B08 |

| <b>Primers used in the research</b>                     |   |   |
|---|---|---|
| <b>Purpose</b>  | <b>Primer name</b>                                      | <b>Sequence</b>                               |
| Amplification of <i>A. lyrata</i> ASY1 genomic fragment | pattB1 ASY1-lyF 2                                       | ttcgactttagactaagagagatt                      |
|   | pattB2 ASY1-lyR 2                                       | ctacacgaaagacgatgagatcacg                     |
| Insertion of SmaI site in ASY1                          | ASY1-C-term-lyF   | GGGTGAAGATACCACCTCTATCAGACA                   |
|   | SmaI  | C   |
|   | ASY1-C-term-lyR   | GGGATTAGCCTGAGATTTCTGACGCTT                   |
|   | SmaI  | G   |
|   | Amplification of <i>A. lyrata</i> ASY3 genomic fragment | pattB1 ASY3-lyF 2                             |
| pattB2 ASY3-lyR 2                                       |   | AGAAAGCTGGGTTGTTTCATAATAGAAG<br>CGAAGAGTTTCTG |

|  |                     |                              |
|--|---------------------|------------------------------|
| Insertion of SmaI site in <i>ASY3</i>                        | ASY3-C-term-lyF     | GGGTGACACTGGAGTCTCAGAATTAAT  |
|  | SmaI                | C                            |
|  | ASY3-C-term-lyR     | GGGATCATCCCTCAAACATTCTGCGAC  |
| Amplification of <i>A. lyrata REC8/SYN1</i> genomic fragment | SmaI                | A                            |
|  | SYN1-lyF            | AGTTGTGACAGTGTGGGGAC         |
| Insertion of SmaI site in <i>REC8/SYN1</i>                   | SYN1-lyR            | GGGCAGTTGCGGCTTATTAC         |
|  | SYN1-C-term-lyF     | GGGTAAGGTTTGATTTCTAAATTATAAA |
|  | SmaI                | C                            |
| Amplification of <i>A. lyrata ZYP1</i> genomic fragment      | SYN1-C-term-lyR     | GGGCATGTTGGGTCTCTTGCAATGA    |
|  | SmaI                | GA                           |
|  | ZYP1-lyF            | TTTGTGATGTGAACCTTTAGTGAGTAT  |
| Insertion of SmaI site in <i>ZYP1</i>                        | ZYP1-lyR            | G                            |
|  | ZYP1b-middle-lyF    | AAGTAATGAATGTTTCGTTTTACACA   |
|  | SmaI                | G                            |
| Insertion of SmaI site in <i>ZYP1</i>                        | ZYP1b-middle-lyR    | GGGGCACATAGACATGTTGGGGA      |
|  | SmaI                | ACT                          |
|  | ZYP1b-middle-lyF    | GGGATCTGCCTGCAGTGTCTCGTACTT  |
| AS <i>Y1</i> CRISPR-Cas9 construct                           | SmaI                | C                            |
|  | ASY1 CRISPR III lyF | ATTGAATCTCGCCGATTAATTGAT     |
|  | ASY1 CRISPR III lyR | AAACATCAATTAATCGGCGAGATT     |
| AS <i>Y3</i> CRISPR-Cas9 construct                           | ASY3 CRISPR II lyF  | ATTGAAAGTGGGACTAATATTCCG     |
|  | ASY3 CRISPR II lyR  | AAACCGGAATATTAGTCCCACCTTT    |
|  | SYN1 CRISPR I areF  | ATTGGATCTTCGCGTGCAACGTAG     |
| <i>REC8/SYN1</i> CRISPR-Cas9 construct                       | SYN1 CRISPR I areR  | AAACCTACGTTGCACGCGAAGATC     |

|   |                       |                          |
|---|-----------------------|--------------------------|
| ZYP1 CRISPR-Cas9<br>construct for <i>A. lyrata</i>  | ZYP1 CRISPR II<br>lyF | ATTGTTAGCTTCTCAAGTTCAGGA |
|   | ZYP1 CRISPR II<br>lyR | AAACTCCTGAACTTGAGAAGCTAA |
| ZYP1 CRISPR-Cas9<br>construct for <i>A. arenosa</i> | ZYP1 CRISPR I<br>lyF  | ATTGGAAACTGGTGAAGGATCAGG |
|   | ZYP1 CRISPR I<br>lyR  | AAACCCTGATCCTTCACCAGTTTC |

## 6. References

- Gietz RD & Schiestl RH (2007) High-efficiency yeast transformation using the LiAc/SS carrier DNA/PEG method. *Nat Protoc* 2: 31–34
- Pignocchi C, Minns GE, Nesi N, Koumproglou R, Kitsios G, Benning C, Lloyd CW, Doonan JH & Hills MJ (2009) Endosperm Defective1 is a novel microtubule-associated protein essential for seed development in Arabidopsis. *Plant Cell* 21: 90–105
- Zhang Y, Werling U & Edelman W (2014) Seamless Ligation Cloning Extract (SLiCE) Cloning Method. *Methods Mol Biol* 1116: 235–244



## Publications and presentations

### Publications

- B1-type cyclins control microtubule organization during cell division in *Arabidopsis*  
**Mariana Romeiro Motta**, Xin'AI Zhao, Martine Pastuglia, Katia Belcram, Farshad Roodbarkelari, Maki Komaki, Hirofumi Harashima, Shinichiro Komaki, Manoj Kumar, Petra Bulankova, Maren Heese, Karel Riha, David Bouchez, Arp Schnittger  
**EMBO reports**, e53995, December 9, 2021
- A microtubule perspective on plant cell division  
**Mariana Romeiro Motta** and Arp Schnittger  
**Current Biology**, 31, R547-R552, May 24, 2021
- The overlooked hybrid: geographic distribution and niche differentiation between *Spartina* cytotypes (Poaceae) in Wadden Sea salt marshes  
Dirk Granse, **Mariana Romeiro Motta**, Sigrid Suchrow, Klaus von Schwartzberg, Arp Schnittger and Kai Jensen  
**Estuaries and Coasts**, October 12, 2021

### Poster presentations

- Norwegian Plant Biology in Hamar, June 21-22, 2017, Hamar, Norway  
Selected for a lightning poster talk
- 2<sup>nd</sup> Biology Conference of Doctoral Candidates, May 4, 2018, Hamburg, Germany
- Hybrids – chances and challenges of new genomic combinations, June 12-14, 2019, Hamburg, Germany
- 12<sup>th</sup> International PhD School – Plant development, October 2-4, 2019, Retzbach, Germany
- 11<sup>th</sup> SALK Institute Cell Cycle Meeting, June 22-25, 2021, virtual poster presentation

## Eidesstattliche Versicherung/Declaration On Oath

Hiermit erkläre ich an Eides statt, dass ich die vorliegende Dissertationsschrift selbst verfasst und keine anderen als die angegebenen Quellen und Hilfsmittel benutzt habe.

I hereby declare, on oath, that I have written the present dissertation by my own and have not used other than the acknowledged resources and aids.

Hamburg, den 17.01.22 Unterschrift Mariana Remius Lotta

## Declaration of contributions

I hereby declare that all results shown in this thesis were obtained by my own, except from the ones indicated in the respective figure legends or resources table and in this list. Here, I summarize the contributions from the collaborators.

### Chapter 1

- Figures 3 and 4 were made based on female and male gametophytic analyses kindly performed by Dr. Xin'AI Zhao
- Figures 5 and 6 were made based on root whole mount immunolocalization studies kindly performed by Katia Belcram and Dr. Martine Pastuglia and were analyzed with the help of Dr. David Bouchez
- Figure 7A-C was made based on *in vitro* kinase assays performed by Dr. Hirofumi Harashima
- The GFP-GIP1 reporter lines in Col-0 and *cycb1;1 cycb1;2* backgrounds used in figure 7D were made by Dr. Shinichiro Komaki
- Figure EV1 was prepared based on data provided by Dr. Petra Bulankova and Dr. Karel Riha
- Figure EV2 was prepared using images provided by Dr. Manoj Kumar
- Table 2 was prepared with allele transmission data kindly provided by Dr. Xin'AI Zhao

### Chapter 2

- The phosphosites presented in figure 7 and 13 and table S1 were identified by Dr. Sara Stolze from the laboratory of Dr. Hirofumi Nakagami based on *in vitro* kinase assays performed by me
- The GFP-GIP1 and GFP-GIP1<sup>T67A</sup> in *gip1 gip2* lines used in figure 9 and 11 were generated by Dr. Shinichiro Komaki
- The HisMBP-CYCB1;1 to HisMBP-CYCB1;4 and StrepIII-CDKB2;2 proteins in figure 10 were produced using plasmids generated by Dr. Hirofumi Harashima
- Figure 12 was prepared based on a yeast-two hybrid performed by Muzaffer Emre Gül

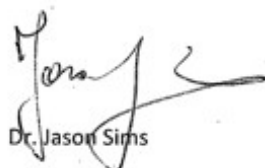
## Confirmation of correct English

Hamburg, 20<sup>th</sup> December 2021

To whom it may concern,

I am writing to confirm that the thesis submitted by Mariana Romeiro Motta has been written in correct English throughout its entire text.

Yours,



Dr. Jason Sims

Postdoctoral researcher

Developmental Biology

Institute of Plant Science and Microbiology

University of Hamburg

## Acknowledgments

First of all, I would like to thank Prof. Arp Schnittger for believing in me and supporting me throughout my time as a doctoral student. This thesis would not be possible without his support. Not only has he given me significant insights into my project, but also help with paving my career as a scientist.

Second, I want to thank Dr. Maren Heese and Dr. Susanne Stirn for carefully reading and commenting on my thesis. This dissertation would not have taken this final form without their help.

Third, I would like to thank all of the former and current lab members. I could not have asked for a more welcoming environment – I am beyond grateful for the endless help and patience with me. Besides learning how to be a better scientist, I also learned how to be a better co-worker and person. Special thanks to Fran, Óscar, Max, Stephan, Joke, Hasibe, Franzi and Lucas for making my life outside of the lab also exciting and fulfilling.

Thank you to my family for strongly supporting all of my life choices, even if it included moving away to another continent more than once, and for giving me another place to call home.

Thank you to all the friends that kept in touch remotely throughout all these years. You have been fundamental to my wellbeing.

Last, I would like to thank Marius for nurturing my soul and my stomach. This thesis would not be possible without all of those delicious lunch packages.